

INAUGURAL – DISSERTATION

zur

Erlangung der Doktorwürde

der

Gesamtfakultät für Mathematik, Ingenieur- und Naturwissenschaften

der

Ruprecht – Karls – Universität

Heidelberg

vorgelegt von

Anna Lena Emonds

aus Bonn-Duisdorf

Tag der mündlichen Prüfung :.....



Towards a Simulator Tool for Predicting Sprinting and  
Long Jump Motions with and without Running-Specific  
Prostheses: An Optimization-Based Approach

Betreuer:

Prof. Dr. Katja Mombaur

Prof. Dr. Wolfgang Potthast



# Zusammenfassung

Die Leistungen von Sprintern und Weitspringern mit Unterschenkelamputationen haben sich seit der Entwicklung spezieller Sportprothesen kontinuierlich verbessert. In den letzten Jahren gab es immer wieder Sportler mit Unterschenkelamputation, die an den Wettkämpfen der nicht-amputierten Sportler teilnehmen wollten. Aufgrund der Materialeigenschaften der Prothese gibt es Bedenken, dass diese dem Sportler einen Vorteil gegenüber nicht-amputierten Sportlern verschaffen könnte.

In dieser Arbeit untersuchen und vergleichen wir Sprint- und Weitsprungbewegungen von Sportlern mit und ohne einseitige Unterschenkelamputation mit Hilfe von präzisen Computermodellen. Ziel der Arbeit ist es, Gemeinsamkeiten und Unterschiede zwischen den Bewegungen der Sportler zu beschreiben sowie zu zeigen, dass die modell- und optimierungsbasierten Berechnungen dafür hilfreich sind.

Zur Untersuchung der verschiedenen Bewegungen haben wir subjekt-spezifische Mehrkörpermodelle für fünf Sportler (vier Sportler ohne und ein Sportler mit einseitiger Unterschenkelamputation) erstellt. Je nach Fragestellung haben die Modelle zwischen 16 (zweidimensionales Modell in der Sagittalebene) und 31 (dreidimensionales Modell) Freiheitsgrade. Für den Sportler mit Unterschenkelamputation haben wir ein drei-segmentiges Modell der Sprintprothese mit einem Rotationsfreiheitsgrad in der Sagittalebene erstellt. Die jeweilige Bewegung wird durch eine Abfolge mehrerer Phasen beschrieben, welche sich durch die Art des Bodenkontakts unterscheiden. Jede dieser Phasen wird durch eine eigene Menge gewöhnlicher Differentialgleichungen oder differential-algebraischer Gleichungen beschrieben. Wir nutzen mehrphasige Optimalsteuerungsprobleme (OSPs) mit Unstetigkeiten zur Untersuchung von Sprint- und Weitsprungbewegungen. Dabei verwenden wir drei verschiedene Formulierungen: (1) Zur Rekonstruktion der Dynamik von Sprint- und Weitsprung-Motion Capture-Aufnahmen der einzelnen Sportler formulieren wir ein Least-Squares OSP. (2) Für die Erzeugung und Vorhersage realistischer Bewegungen formulieren wir ein OSP zur Bewegungssynthese: Dieses optimiert eine Zielfunktion, welche aus einer gewichteten Kombination ausgewählter Optimalitätskriterien besteht. (3) Zuletzt formulieren wir ein inverses OSP: Dieses besteht aus einer inneren Schleife, welche ein OSP zur Synthese löst, und einer äußeren Schleife, welche die Gewichte der einzelnen Optimalitätskriterien so anpasst, dass der Abstand zwischen der Lösung der inneren Schleife und einer Referenzbewegung minimal wird.

Wir haben mit diesen drei Formulierungen zwei Sprintschritte dreier Sportler ohne und eines Sportlers mit Amputation berechnet. Dabei unterscheiden sich die Bewegungen der nicht-amputierten Sportler in einem Großteil der Variablen von der des amputierten Sportlers. Insbesondere nutzen sie unterschiedliche Aktuationsstrategien zum Rennen mit und ohne Sportprothese. Die Drehmomente im von der Amputation betroffenen Bein des amputierten Sportlers sind geringer als die in der nicht-amputierten Kontrollgruppe. In den Gelenken der oberen Extremität hingegen sind beim amputierten Sportler deutlich größere Drehmomente vorhanden. Weiterhin zeigt der Vergleich, dass die aufgrund der Prothese entstehende Asymmetrie sich im ganzen Körper widerspiegelt und auf die Gesamtbewegung auswirkt. Mithilfe der OSPs zur Bewegungsrekonstruktion (1) und -synthese (2) haben wir die letzten drei Anlaufschritte und den Weitsprung für einen Athleten ohne und einen Athleten mit einseitiger Unterschenkelamputation berechnet. In den rekonstruierten Lösungen (1) erzielt der amputierte Athlet im Vergleich zum nicht-amputierten Athleten trotz langsamerer Anlaufgeschwindigkeit eine größere Sprungweite, da sein Absprung effizienter ist. In den Lösungen der Synthese (2) erzielt hingegen der nicht-amputierte Athlet die größere Sprungweite, da er während des Absprungs eine größere Vertikalkraft erzeugt und ein besseres Verhältnis von Gewinn an vertikaler zu Verlust von horizontaler Geschwindigkeit erreicht. Abschließend haben wir unsere Idee eines Simulators zum Vergleich des amputierten Athleten mit sich selbst ohne Amputation vorgestellt. Dafür haben wir das Modell des Athleten mit Amputation aus den vorherigen Rechnungen beibehalten und durch Spiegelung des biologischen Beines eine nicht-amputierte Modellversion erstellt. Wir haben das OSP zur Bewegungssynthese (2) von Sprint und Weitsprung für beide Modellversionen berechnet. Anhand der Unterschiede zu den Lösungen, welche auf den Modellen zweier real existierender Athleten basieren, haben wir die Bedeutung des Simulators bei der Beurteilung von Vor- und Nachteil aufgrund der Nutzung der Sportprothese herausgestellt.



# Abstract

The performances of sprinters and long jumpers with below the knee amputation (BKA) have improved continuously since the development of prostheses specifically for athletic movements. In the last years, a number of athletes with BKA have attempted to compete in non-amputee competitions. Due to the specific shape and material properties of the running-specific prosthesis (RSP), concerns exist that it may give athletes an advantage over non-amputee athletes.

In this work, we investigate and compare sprinting and long jump movements of athletes with and without unilateral BKA using accurate computer models. In this context, the aim of the work is to describe similarities and differences between the athletes' movements and to show that the employed model- and optimization-based computations are useful for this purpose.

We created subject-specific multi-body models for five different athletes (four non-amputee athletes, one athlete with unilateral BKA) in order to be able to investigate the different movements. Depending on the research question, the models vary in the number of degrees of freedom (DOFs), from 16 DOFs for a two-dimensional model in the sagittal plane to 31 DOFs for a three-dimensional model. For the athlete with BKA, we created a three-segment model of the RSP with one rotational DOF in the sagittal plane. The respective motion is described by a sequence of several phases, which differ by the type of ground contact. Each of these phases is described by its own set of ordinary differential equations (ODEs) or differential algebraic equations (DAEs).

We use multi-phase optimal control problems (OCPs) with discontinuities to generate sprint and long jump motions. Three different formulations of OCPs are adopted in this work. (1) We formulate a least squares OCP to reconstruct the dynamics of sprint and long jump motion capture recordings of the individual athletes. (2) For the generation of realistic motions, which can be used for prediction, we formulate a synthesis OCP; this optimizes an objective function consisting of a weighted combination of chosen optimization criteria. (3) Last, in the study of sprint movements, we use an inverse optimal control problem (IOCP): this consists of an inner loop, in which a synthesis OCP is solved, and an outer loop, which adjusts the weights of the individual optimization criteria such that the distance between the inner loop solution and a reference movement becomes minimal.

We have successfully applied these three optimization problem formulations to the computation of two sprint steps of three athletes without and one athlete with unilateral transtibial amputation. Here, the movements of the non-amputee athletes differ from that of the amputee athlete in a large number of variables. In particular, the athletes use different actuation strategies for running with and without a RSP. We have observed lower torques in the amputee athlete in the leg affected by the amputation than in the non-amputee control group. In contrast, significantly larger torques occurred in the joints of the upper extremity in the amputee athlete. Furthermore, the comparison has shown that the asymmetry created by the RSP is reflected throughout the body and affects the entire movement.

Using the OCPs for motion reconstruction (1) and synthesis (2), we have successfully computed the last three steps of the approach and the jump of a long jump for an athlete without and an athlete with unilateral amputation. In the reconstructed solutions, the amputee athlete achieves a greater jump distance compared to the non-amputee athlete, despite a slower approach velocity, because his take-off is more efficient. In the synthesis solutions, on the other hand, the non-amputee athlete achieves the greater jump distance because he generates a greater vertical force during the take-off and achieves a better ratio of gain of vertical to loss of horizontal velocity.

Finally, we have presented our idea of a simulator tool to compare the amputee athlete with himself without amputation and have demonstrated it using the sprint and long jump movements. For this purpose, we have kept the model of the athlete with unilateral transtibial amputation from the previous studies and have created a non-amputee version of the same model by mirroring the biological leg. We have selected one objective function each for sprinting and for long jump and have solved the OCP for motion synthesis (2) for both model versions. Using the differences to the solutions based on the models of two real athletes, we have highlighted the importance of the simulator tool in the evaluation of advantages and disadvantages due to the use of the RSP.



# Acknowledgements

*It takes a village to raise a child.*

— African proverb

The first time I read this saying was during pregnancy with our first child. With a PhD thesis, it is quite similar. Therefore, I want to take this place to express my sincere thanks to my “village”.

First of all, I would like to thank my supervisor *Prof. Dr. Katja Mombaur*: for the opportunity to work on such an exciting topic and to discuss it at various conferences, and further for the constant support, helpful supervision and interesting discussions over the past years, first in Heidelberg and then also from Waterloo in Canada.

I would also like to thank my co-supervisor *Prof. Dr. Wolfgang Potthast* from the German Sport University in Cologne. I am very grateful for the fruitful discussions, the insights into research and measurements at the German Sport University and the conferences in Cologne and Tokyo.

It has been wonderful to be a part of the *Optimization, Robotics & Biomechanics (ORB)* group and I thank all my colleagues for the friendly and at the same time scientifically stimulating atmosphere. There was always someone that asked how the work was progressing or to help with problems; especially *Debora, Malin, Kevin* and *Jonas* who shared the office with me. I would also like to particularly thank *Matt* for all the explanations and help on muscle models and the RBDL muscle add-on, and valuable general tips for doing a PhD. Further thanks to *Matt, Jonas* and *Giorgos* for proofreading parts of the thesis. For the great support with all administrative issues I would like to thank *Pam, Sabine, Alex* and especially *Sarah*.

I would like to thank *Dr. Johannes Funken* from the German Sport University Cologne, who was a great help with all kinds of questions about the measurement data and enriched my work with new perspectives. I would like to thank everyone involved in the measurements of the sprint and long jump motions for the opportunity to work with these data and thus to be able to investigate physically meaningful and realistic models. In particular, I thank *Prof. Dr. Wolfgang Potthast, Dr. Johannes Funken, Prof. Dr. Steffen Willwacher, Dr. Kai Heinrich* and *Ralf Böhle* as part of the consortium of the motion studies.

I want to thank the *Simulation and Optimization* research group of *Prof. Dr. Dr. h.c. mult. Hans Georg Bock* at the Interdisciplinary Center for Scientific Computing at Heidelberg University for giving me the possibility to work with the optimal control software package MUSCOD-II.

Finally, special thanks to my family: my parents and my sisters, who have always supported me in following my interests and also very practically with childcare and food. My grandparents, who always asked whether the model could walk or jump by now. My godmother, her family and also Yannick’s family for their interest in and support of my work.

Thank you *Yannick*, for everything, your support, your encouraging words, for always being there for me! *Benjamin* and *Sophia*, watching you develop is incredibly exciting. The tirelessness with which both of you diligently ‘train’ (regardless of any efforts involved) every day since your births to discover the world – from holding your head to walking, climbing, jumping and talking – has always been a motivation for me!



# Contents

Introduction	1
<b>I Foundations of Optimization-Based Motion Studies</b>	<b>7</b>
<b>1 Overview on Analyzing Motions with and without Running-Specific Prostheses</b>	<b>9</b>
1.1 History and Characteristics of Running-Specific Prostheses . . . . .	9
1.2 Biomechanical Studies Within the Debate About Advantages and Disadvantages due to Running-Specific Prostheses . . . . .	10
1.3 Brief Introduction to Motion Capture Recordings . . . . .	11
1.4 Motion Capture Data used in this Thesis . . . . .	12
<b>2 Modeling of Human Motions with and without Below the Knee Amputation</b>	<b>15</b>
2.1 Anatomical Conventions . . . . .	15
2.2 Subject-Specific Models of Athletes with and without Below the Knee Amputation	16
2.3 Model of the Running-Specific Prosthesis . . . . .	17
2.4 Modeling of Human Motions . . . . .	18
2.5 Realistic Torque Limit Modeling by Muscle Torque Generators . . . . .	20
<b>3 Simulation of Human Motions Using Optimal Control Problem Formulations</b>	<b>23</b>
3.1 Optimal Control Problem Formulations . . . . .	23
3.2 Inverse Optimal Control Problem Formulation . . . . .	28
<b>II Optimization-Based Comparison of Sprinting Motions with and without Running-Specific Prostheses</b>	<b>31</b>
<b>4 Biomechanics and Modeling of Sprinting Motions with and without Running- Specific Prostheses</b>	<b>33</b>
<b>5 Dynamics Reconstruction of Sprinting Motions with and without Running-Specific Prostheses</b>	<b>37</b>
5.1 Analysis of the Reconstruction Quality . . . . .	38
5.2 Analysis of the Curves of Characteristic Variables . . . . .	42
5.3 Analysis of Measures Related to Effort, Energy Expenditure and Sprint Style . .	55
5.4 Summary . . . . .	59
<b>6 Synthesis of Sprinting Motions with and without Running-Specific Prostheses</b>	<b>61</b>
6.1 Comparison of Synthesized and Reference Sprinting Motions . . . . .	64
6.2 Comparison of the Synthesized Motions with Free Average Velocity . . . . .	70
6.3 Summary . . . . .	74
<b>7 Inverse Optimal Control of Sprinting Motions with and without Running-Specific Prostheses</b>	<b>77</b>
7.1 Comparison of Final and Hand-Picked Weight Solutions . . . . .	78

7.2	Interpretation of Final Weights for Sprinting with and without Running-Specific Prostheses . . . . .	79
7.3	Analysis of the Curves of Characteristic Variables . . . . .	84
7.4	Summary . . . . .	87
<b>III</b>	<b>Optimization-Based Comparison of Long Jump Motions with and without Running-Specific Prostheses</b>	<b>89</b>
<b>8</b>	<b>Biomechanics and Modeling of Long Jump Motions with and without Running-Specific Prostheses</b>	<b>91</b>
<b>9</b>	<b>Dynamics Reconstruction of Long Jump Motions with and without Running-Specific Prostheses</b>	<b>95</b>
9.1	Analysis of the Reconstruction Quality . . . . .	95
9.2	Analysis of Characteristic Variables in Long Jump . . . . .	99
9.3	Summary . . . . .	111
<b>10</b>	<b>Synthesis of Long Jump Motions with and without Running-Specific Prostheses</b>	<b>113</b>
10.1	Comparison of Reconstructed and Synthesized Long Jump Motions with and without Prostheses . . . . .	115
10.2	Comparison of Synthesized Long Jump Motions with and without Running-Specific Prostheses . . . . .	122
10.3	Summary . . . . .	125
<b>IV</b>	<b>Towards a Systematic Use of Optimization and Simulation for Performance Comparison Between Amputee and Non-Amputee Athletes</b>	<b>127</b>
<b>11</b>	<b>Comparison of the Amputee Athlete to Himself without Amputation: The Idea of a Simulator Tool</b>	<b>129</b>
11.1	Basic Structure of a Simulator Tool . . . . .	129
11.2	Sprinting Motions of the Non-Amputee and Amputee Model Versions . . . . .	133
11.3	Long Jump Motions of the Non-Amputee and Amputee Model Versions . . . . .	137
11.4	Summary . . . . .	141
<b>12</b>	<b>Conclusions and Future Work</b>	<b>143</b>
<b>A</b>	<b>Additional Figures</b>	<b>149</b>
A.1	Dynamics Reconstruction of Sprinting Motions . . . . .	149
A.2	Synthesis of Sprinting Motions . . . . .	157
A.3	Inverse Optimal Control of Sprinting Motions . . . . .	159
A.4	Dynamics Reconstruction of Long Jump Motions . . . . .	160
A.5	Synthesis of Long Jump Motions . . . . .	165
A.6	Towards a Simulator Tool: Long Jump . . . . .	167
	<b>Bibliography</b>	<b>169</b>
	<b>Figures, Tables, Acronyms</b>	<b>180</b>

# Introduction

Movement has always been a natural part of people's everyday lives. We think little about how we perform certain movements and tasks during the day. During our baby and toddler years, we have gradually learned how our body segments must work together to move safely, grasp, and discover the world. After years of training, our brain intuitively controls everyday tasks. Only when we are restricted in our mobility (e.g., by a thick winter jacket, after an operation, or due to a broken bone) or when we have to perform more complicated or new movements (e.g., in a dance course or on a difficult hiking route), we realize how important the full functionality of our body parts is in everyday life. People with disabilities often face much more difficulties, and even simple everyday tasks require concentration and practice, if not external assistance. It is not by chance that climbing stairs, opening doors and getting up from an armchair are tasks for the Cybathlon<sup>1</sup> participants in the Powered Arm Prosthesis, Powered Leg Prosthesis and Exoskeleton Races.

Competitions and championships have always existed in the history of humankind. The earliest mention of the Olympic Games in ancient times can be traced back to the year 776 BC, and it is assumed that similar competitions took place even earlier [139]. Participation in sports and competition plays a decisive role in the rehabilitation process of persons with amputations and helps them to be included in society [17]. Sports prostheses for running and jumping, named running-specific prostheses (RSPs), are of great importance in this context, as they make faster movements possible for amputees. They are a relatively new development compared to the first everyday prostheses, which can be traced back to the Roman Empire [108] (even if they are miles away from the functionality and comfort of today's prostheses). An American inventor, Van Phillips, who himself was amputated below the knee, wanted to develop a prosthesis that would enable him to run and do sports: the "FlexFoot" – inspired by the shape of a cheetah's hind leg. Recent RSPs are made of carbon fibers because it is a light, flexible, and strong material. This allows the prosthesis to store energy during contact with the ground and to return energy during decompression. Mechanically, therefore, they behave like springs and thus enable an amputee person to run [61].

Precisely due to the spring-like properties, the RSPs are always the stumbling block when it comes to the participation of amputee athletes in the competitions of non-amputee athletes like the Olympic Games. The attempts of both the double amputee sprinter Oscar Pistorius (South Africa) and the unilateral amputee long jumper Markus Rehm (Germany) to do so have each led to major discussions in public and research as well as decisions by sports courts. Considering that both clearly defeated their amputated opponents in competitions, it is understandable that they are looking for new challenges. Recently, U.S. bilateral amputee sprinter Blake Leeper put forth a similar effort to compete in the 2020 Olympics. Although meanwhile a number of studies on sprinting and long jumping in athletes with lower extremity amputations exists, the question whether the RSP provides the amputee athlete with an advantage or a disadvantage compared to non-amputee athletes cannot be easily answered and is subject of debate among researchers. Besides the direct comparison of the biomechanical properties of the movements of athletes with and without below the knee amputation (BKA), other aspects, e.g., of ethical or legal nature, are of interest when deciding whether athletes with BKA should be allowed to

---

<sup>1</sup>The Cybathlon is a biennial competition for persons with disabilities at ETH Zürich in Switzerland[115].

participate in the competitions of non-amputee athletes: from an ethical perspective, it must be discussed where reasonable lines for further technical enhancements need to be drawn to ensure that athletic competitions measure human performance and do not become contests of technology, and how athletes from poorer countries can gain access to the technology [19]. Evaluating the overall movement and stating a net advantage or disadvantage is a highly challenging task because RSPs have different influence at different phases of the movement, and sensory impairments due to the RSPs are difficult to quantify. As a consequence of the fact that only a handful of amputee athletes achieve world-class performances, and the resulting lack of statistical significance, it is not possible to draw general conclusions, but only to compare the performance and biomechanics of the individual athlete with those of a non-amputee control group. Furthermore, it is not possible to take measurements of an amputee athlete with and without an amputation in order to compare him to himself without amputation and to find out whether he could possibly reach similar top results[86, 130, 131].

At this point, computer simulations can provide a helpful complement and add new perspectives to the debate. In fact, in computer models exactly such a comparison is possible: by replacing the RSP with the corresponding part of a model of the biological leg, the matching model of an athlete without BKA to the subject-specific model of the athlete with BKA can be created. Even though this involves making assumptions about the exact segment dimensions and muscle parameters (for example, in the case of unilateral amputees, this could happen based on the measured biological leg), such a predictive simulation is as close as it can get to comparing the amputee athlete to himself without amputation. In addition, it is possible in a computer model to investigate the influence of changes, e.g., in the RSP or in muscle parameters, on the movement.

## Scope of this Thesis

The aim of this thesis is to create computer models to describe sprinting and long jump movements of athletes with and without BKA and to analyze them. The majority of biomechanical studies focuses on describing basic characteristics of a movement by recording and evaluating a large number of trials of that movement and determining the average or mean value. In contrast, the focus of this work is to describe a methodological approach that allows the comparison and analysis of movements of individual athletes based on detailed subject-specific models. In perspective, the vision is the creation of a simulator tool which, based on the exact measurement of the athlete (segment lengths, masses, muscle parameters) and possible motion capture recordings, uses predictive simulations to generate realistic movements and allows, for example, for the analysis of the movement or the comparison of the movement with and without RSP. In this work, the foundations for such a simulator tool are established without programming the final tool itself.

To this end, the first step is the development of detailed subject-specific models of the individual athletes. These are created as rigid multi-body system models consisting of 16 segments and based on the measurements of the athletes. Depending on the specific problem, the models can move exclusively in the sagittal plane (2D) or in all spatial directions (3D). The joints between the individual segments are controlled by torque actuators, whereby the number of degrees of freedom (DOFs) per joint depends on the desired accuracy of the model. For the amputee athlete, a detailed model of the RSP is created consisting of three rigid segments. The model of the RSP is realized as a spring-damper system and has one rotational DOF in the sagittal plane.

In addition to creating subject-specific models, movements are studied. The movements are simulated using various optimal control problems (OCPs). All OCPs have in common that they

minimize an objective function to be defined, taking into account the model dynamics and other constraints. Three types of OCPs are applied in this thesis:

- (i) The dynamics reconstruction OCP fits the position and joint angles of the model to measured motion capture data of the movement. This has three goals: First, the dynamics reconstruction serves to validate the model formulation for the given motion, i.e., we test whether it is possible with the model formulation to mimic the actual measured motion, or whether the model is still flawed. Second, we demonstrate that the dynamics reconstruction using a least squares OCP is a useful alternative to the standard inverse dynamics approach when reconstructing joint torques as it relies solely on joint angle measurements alone. Third, the reconstructed angles, torques, etc. serve as reference and comparison values for the following predictive simulations.
- (ii) With the help of the forward OCP, motions can be predicted based on the formulation of optimization criteria that are minimized or maximized in the objective function. Here, the selection and weighting of each optimization criterion is the crucial aspect for generating meaningful motions. In addition to predicting a motion based on a particular combination of optimization criteria, this problem formulation also allows for studying the influence of different criteria on the resulting motion.
- (iii) In order to generate the most realistic movements possible, it would be ideal to know exactly which optimization criteria an athlete minimizes or maximizes and the contribution of each criterion to the final movement. One approach to acquire this information is to solve an inverse optimal control problem (IOCP). In this approach, the criteria to be studied are combined by weights and then the solution of the forward OCP is sought by systematically and iteratively changing the weights, which are closest to the reference motion (computed in the dynamics reconstruction problem).

Using these basic building blocks, it is possible to examine and compare the sprinting and long jump movements of individual athletes.

## Contributions of this Thesis

**Human multi-body dynamics model of athletes with and without below the knee amputation and detailed model of a running-specific prosthesis** We created subject-specific rigid multi-body models of four non-amputee athletes and one athlete with unilateral BKA in different accuracies. Depending on the problem formulation, each model consists of 16 to 31 DOFs. The model of the athlete with unilateral BKA includes a detailed three-segment model of the RSP. For each actuated joint, we computed realistic torque limits based on the reconstructed motions and a Muscle Torque Generator (MTG) model.

**Reconstruction of the dynamics of recorded sprinting and long jump motions without use of force plate data** A standard approach in human motion analysis is the inverse dynamics approach which computes the dynamics of motions by combining pre-processed kinematic motion capture data, contact positions and measurements of the external ground reaction forces. However, the need of force plate data and the occurrence of high residual forces due to skin motion and wobbling masses limit the possible applications. We used a least squares OCP formulation to reconstruct the dynamics of sprinting and long jump motions with zero residual forces, based solely on kinematic data.

**Optimization-based prediction of sprinting and long jump motions for athletes with and without below the knee amputation** We synthesized sprinting and long jump motions by formulating and solving multi-phase OCPs for athletes with and without BKA. The optimization-based approach is capable of generating realistic motion sequences for sprinting at constant maximum velocity, as well as the final steps, take-off, and flight of the long jump, without having to rely on motion capture recordings. Due to the realism of the kinematic and dynamic characteristics, our approach permits the use of the resulting motions as a basis for analysis and comparison, making it a powerful tool for studying the biomechanics of sprinting and long jumping.

**Realistic parameters for the description of the individual sprint style of different athletes** We formulated an IOCP to identify the combination of optimization criteria that describes realistic human sprinting motions. With this approach, we identified the weight factors for combining the criteria separately for three non-amputee and one amputee athlete. The final best weight factors describe their individual way of sprinting and can be used to synthesize realistic motions for the individual athletes that allow for further analysis.

**Presentation of the idea of a simulator tool for comparing an athlete with below the knee amputation to himself without amputation** We illustrated the idea of a simulator tool for comparing an amputee athlete to himself without amputation using synthesized sprinting and long jump motions. For this purpose, we created a virtual twin of an existing athlete with BKA. We further generated a non-amputee model version of the amputee athlete by replacing the RSP with a copy of the left unaffected leg of the amputee model. We demonstrated the usefulness of such a simulator tool by highlighting differences between the motions of the two model versions that have not become clear from the comparison of different amputee and non-amputee athletes in the chapters before.

## Thesis Overview

This thesis is divided into four basic parts, with the first part describing the theoretical background and the remaining three parts presenting the results for sprinting, long jump, and the comparison of the amputee athlete with himself without amputation. A schematic overview of how the thesis is structured is shown in Figure I.

### I - Foundations of Optimization-Based Motion Studies

The first part gives a more in-depth introduction to the subject and the relevant methods. Chapter 1 provides a more in-depth introduction to the debate on the participation of athletes with BKA in competitions of non-amputee athletes. For this purpose, we present the history and characteristics of RSPs, as well as the results of some biomechanical studies on the topic. Since these studies are mostly based on motion capture recordings, we briefly introduce the technique used in these studies. Finally, we address the motion capture data used in this work. Chapter 2 describes in detail how the subject-specific models of the athletes as well as the RSP were created. Furthermore, we explain the basic approach of modeling human motion through multi-phase problems. Finally, we introduce “Muscle Torque Generator model” which we used in this thesis for the computation of realistic joint torque limits.

Chapter 3 is devoted to the description of the OCPs used. On the one hand, we present the three concrete formulations of the dynamics reconstruction, forward and inverse OCPs; on the other hand, we show the general solution procedure.

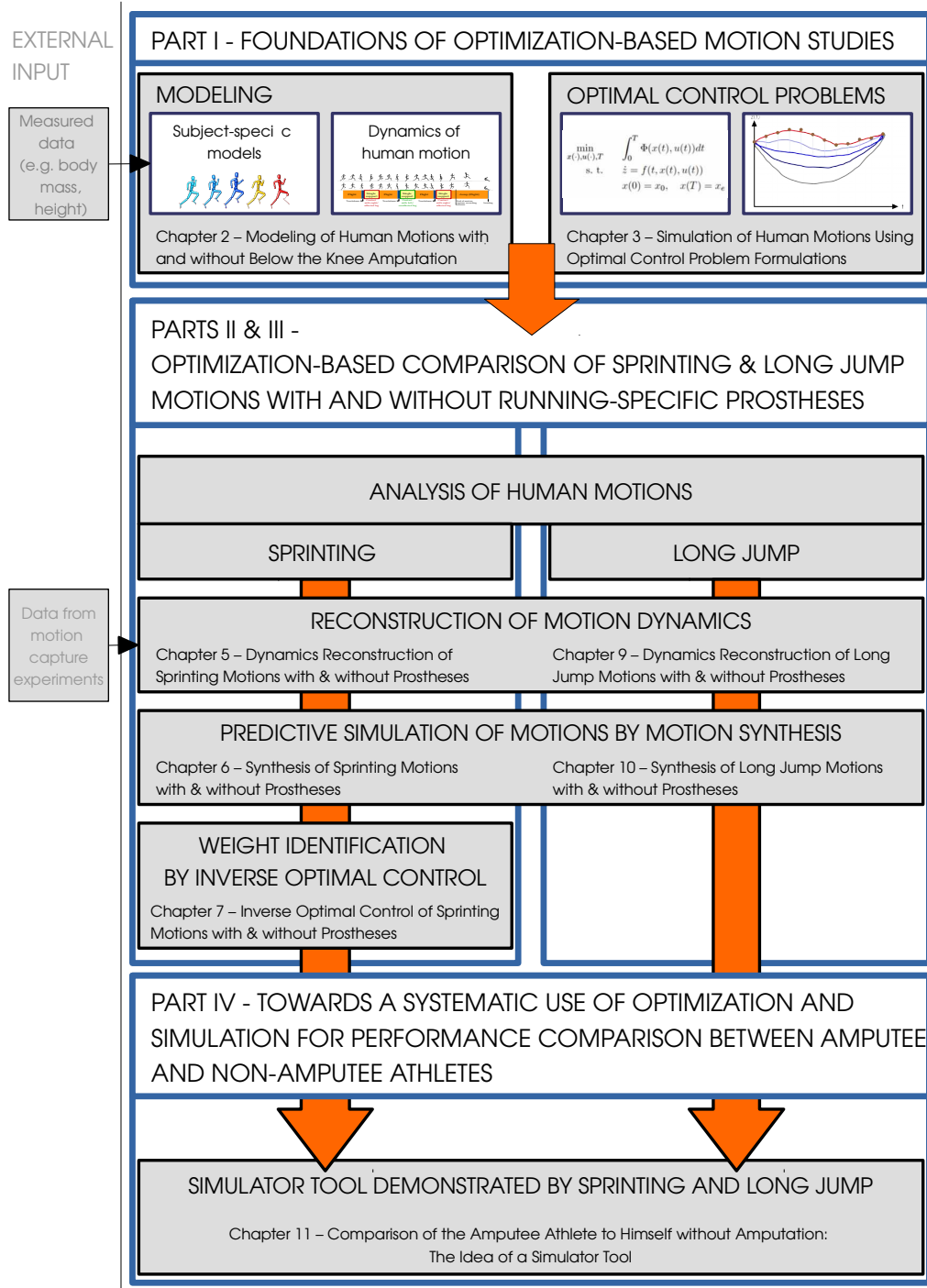


Figure I: Schematic overview of the structure of this thesis

## II - Optimization-Based Analysis of Sprinting Motions with and without Running-Specific Prostheses

The second part is dedicated to the description and analysis of sprinting with and without RSP. Chapter 4 gives a more detailed introduction to the biomechanics of sprinting with and without RSP and describes the concrete modeling of sprinting motions as a multi-phase problem.

In Chapter 5, we analyze the reconstructed sprinting motions: We start with an analysis of the reconstruction quality. In addition, we compare the curves of characteristic variables like

joint angles, joint torques, ground reaction forces or angular momentum for sprinting with and without RSP. Finally, we define measures related to effort, energy expenditure and sprint style and investigate differences between the motions of athletes with and without BKA.

Chapter 6 is concerned with the analysis of the synthesized sprinting motions. First, the constraints and objective functions for the synthesis problem are presented. Second, the resulting motions are compared to the reference motions from the dynamics reconstruction to study the similarity between the motions. In a third step, the synthesized motions of athletes with and without BKA are compared to each other.

Chapter 7 presents the results of the IOCP. After defining the concrete assignment of weights to optimization criteria, the final weight solutions are compared to the solutions of the single criteria using a similarity measure. Then, the final weight factors of the sprinting motions with and without RSP are compared to each other: We analyze both differences between the non-amputee and the amputee motions as well as the asymmetry between the weights of left and right body sides of the individual athletes.

### **III - Optimization-Based Analysis of Long Jump Motions with and without Running-Specific Prostheses**

The third part is dedicated to the description and analysis of long jump with and without RSP and considers some of the same analyses as part II.

Chapter 8 introduces the biomechanics of long jump of athletes with and without BKA. Furthermore, the phases and constraints of the long jump model are introduced.

In Chapter 9, we analyze the reconstructed long jump motions: As for the sprinting motions, we start with an analysis of the reconstruction quality and a validation of the reconstructed ground reaction forces and joint torques. To examine the differences in long jump between athletes with and without BKA, we consider characteristic parameters like jump distance, center of mass (CoM) motion, ground reaction forces and joint torques

Chapter 10 presents the results of the motion synthesis of long jump. We first introduce the specific constraints and objective functions used for the formulation of the motion synthesis problem. In a next step, we compare the synthesized motions with those of the dynamics reconstruction in order to validate the problem formulation regarding realism of the motions. Finally, we compare the long jump motion of the athlete with BKA to the one of the athlete without BKA.

### **IV - Towards a Systematic Use of Optimization and Simulation for Performance Comparison Between Amputee and Non-Amputee Athletes**

The fourth part is devoted to the vision of a simulator tool for comparing the amputee athlete to himself without amputation and to describing how this work fits into the larger picture.

Chapter 11 concretely introduces the idea of a simulator tool to compare motions of athletes with amputation to themselves without amputation. For this purpose, we present the required components and how they interact. Finally, using the concrete example of the athlete with BKA investigated in this work, we explain how the corresponding non-amputee model is created and how we would like to investigate the sprinting and long jump movements. We discuss differences between the motions of the two model versions and highlight what distinguishes the solution of the non-amputee model version to the solutions from the motion synthesis in Chapters 6 and 10 to show the strength of the simulator tool.

Finally, in Chapter 12 we conclude this work with a summary and classification in the overall picture and give an outlook on opportunities for further research.

**Part I**

**Foundations of Optimization-Based  
Motion Studies**



# 1 Overview on Analyzing Motions with and without Running-Specific Prostheses

“An Amputee Sprinter: Is he Disabled or Too-Abled?” – Under this headline, the New York Times magazine published an article on May 15, 2007, about the South African sprinter Oscar Pistorius and his efforts to participate in the Olympic Games as a bilateral transtibial amputee [81]. With this quest, the athlete has provoked a great debate, both in the scientific community and in the public, including great media attention. At the heart of the controversy is the question of whether the special sports prostheses used by athletes with below the knee amputation (BKA) for sprinting and jumping have properties that could be advantageous compared to a biological leg. To put it more pointedly: Could the athlete achieve comparable performances without the running-specific prosthesis (RSP), namely if he had two biological legs? There will probably be no final answer to this exact question, but an approximation to it is certainly possible.

## 1.1 History and Characteristics of Running-Specific Prostheses

To understand why the question of a possible advantage for athletes with amputations comes up at all, one has to look at the shape and material of modern sports prostheses. Historically, prostheses have long been rather primitive (e.g., hand hooks), comparatively heavy, and immobile. Advances in modern technologies such as microprocessors and computer chips, as well as materials research, have made today's prostheses lighter and more functional, so that people with amputations can participate in everyday life with comparatively few restrictions [108]. However, if we look specifically at leg prostheses, it quickly becomes apparent that dynamic, fast movements with hard impacts, when the foot touches the ground, are difficult and uncomfortable with everyday prostheses. In particular, the elastic and shock-absorbing properties of a biological foot are missing for running and jumping.

This situation first changed in the 1980s, when the idea of using carbon fiber reinforced polymer (CFRP) composites to design prostheses for lower limb amputees emerged. Composites are built from two or more components, combining the physical properties of each component, which allows them to closely mimic the properties of biological materials. CFRP composites have exactly the properties one would like to have for prostheses: the material is light, flexible, and strong at the same time. As described in the introduction, the first lower leg prosthesis (FlexFoot), which was made exclusively of CFRP, was developed by Van Phillips in the early 1980s. Unlike today's sprint prostheses, the FlexFoot was still composed of two parts, a J-shaped forefoot and a heel element. The combination of great flexibility and strength made more dynamic movements like running and jumping possible. Already in 1988, the FlexFoot was used for the first time at the Paralympic Games. Since the development of the FlexFoot, a number of different foot designs have been investigated, differing in particular in their shape. What modern sports prostheses have in common, however, is that they no longer contain a heel element and are essentially made of CFRP [61, 103, 120].

To be allowed to compete in competitions according to the rules of the International Paralympic Committee (IPC), athletes can only use passive devices since sport performance must be “pri-

marily being generated by the athlete’s own physical prowess” [25] and not “by automated, computer aided or robotic devices” [25]. Hence, athletes who want to compete in IPC competitions have to use purely passive devices, i.e., devices without any active control elements like microprocessors. The RSPs made of CFRP composites are such passive devices, exhibiting similar properties to a spring-damper system. If an external force acts on the RSP, for example, an athlete shifts his body weight onto the RSP, thereby generating a ground reaction force, it compresses and stores energy. If the force decreases again, for example, due to the body moving away from the RSP, the RSP can return to its initial state, releasing energy. The stiffness of the spring-like RSP is determined by the structure of the carbonfiber reinforced polymer and differs according to the type of sport desired and the athlete’s physique. Typically, higher spring stiffnesses are chosen for jumping disciplines than for running competitions [61, 103]. With the further development of modern RSPs, the performances of amputee athletes in sprinting and jumping competitions have also increased significantly and today come (rather) close to the world records of non-amputee athletes. As an example, the current best values for 100 m sprint and long jump are compared here (as of February 10, 2022):

100 m sprint	Usain Bolt (Jamaica)	NA*	9.58 s	2009/08/16
	Alan Fonteles Oliveira (Brazil)	T43 <sup>†</sup>	10.57 s	2013/07/28
	Richard Browne (USA)	T44 <sup>‡</sup>	10.61 s	2015/10/29
	Johannes Floors (Germany)	T62 <sup>†</sup>	10.54 s	2019/11/10
	Richard Browne (USA)	T64 <sup>‡</sup>	10.61 s	2015/10/29
Long jump	Michael Powell (USA)	NA*	8.95 m	1991/08/30
	Stylianos Malakopoulos (Greece)	T62 <sup>†</sup>	7.04 m	2021/06/19
	Markus Rehm (Germany)	T64 <sup>‡</sup>	8.62 m	2021/06/01

\* NA is used as an abbreviation for the non-amputee athletes.

<sup>†</sup> T43/T62 are the IPC competition classes that include athletes with bilateral BKA.

<sup>‡</sup> T44/T64 are the IPC competition classes that include athletes with unilateral BKA.

## 1.2 Biomechanical Studies Within the Debate About Advantages and Disadvantages due to Running-Specific Prostheses

Let us now return to the initial question of whether the essential factor for these performances is the spring-like property of the RSPs, for which a definite answer will be difficult to find due to the many individual aspects involved. Nevertheless, it is possible to examine the individual aspects that contribute to the answer: One building block for this is the investigation of the biomechanical differences between athletes with BKA and non-amputee athletes with comparable physical measures.

In the context of Oscar Pistorius’ attempt to compete in the Olympic Games, Brüggemann and colleagues [18] published their analysis of the biomechanics of double transtibial amputee sprinting at maximum speed compared to a control group without amputation. Due to lower joint moments at the hip and knee joints and differences in the ankle joint moments during the stance phase, they concluded that sprinting with two RSPs results in a completely different movement pattern. Together with the fact that the athlete with bilateral amputation was able to achieve an energy return of 90.7% with the RSPs (in comparison, the biological ankles were able to return 40.1% of the stored energy), the researchers reasoned that the athlete could run at maximum speed with less metabolic cost. For sprinting motions at maximum speed, the results of Weyand and co-workers [133] likewise reveal that a double amputee sprinter exhibits shorter stance phases as well as longer swing phases and applies smaller horizontal

ground reaction forces. Their conclusion that double transtibial sprinting and sprinting with biological legs are “physiologically similar but mechanically different” [133] links directly to the question formulated by Burkett et al. [19]: What is the nature of running? They point out that a sprinter should clearly run – neither bounce nor hop. Likewise, with regard to long jump with RSPs, biomechanical studies [44, 45, 136] have shown that the motion sequences differ in elementary aspects between athletes with and without BKA. From these observations the question arises, what exactly characterizes a sprinting or long jump motion; is it similar metabolic work, is it that joint angles and moments are comparable? The point-counterpoint article series (Weyand and Bundle [131] against Kram et al. [71]) clearly shows that even in the interpretation of biomechanical data alone, there are different arguments regarding a possible advantage or disadvantage of athletes with BKA compared to non-amputee athletes. Moreover, the studies mostly deal with a specific phase of the respective sprint (either sprint start, acceleration phase, or sprinting at constant maximum velocity) or long jump movement (usually take-off step). However, in order to achieve a fair overall assessment of the movements, it would be necessary to consider all phases and weigh them against each other. Here, the question arises how a weighing of the individual phases is supposed to be done. In this sense, Willwacher and colleagues [136] also conclude that an overall assessment of the movement is not possible despite their observations that athletes with BKA run up slower and jump off more efficiently.

### 1.3 Brief Introduction to Motion Capture Recordings

In order to better and fundamentally understand human motions, they must be studied in great detail. For this purpose, it is tremendously helpful if the motion can be recorded and repeatedly inspected to recognize details or different aspects. Marey [84] and Muybridge [100] were among the first researchers to study human movement patterns based on photographic images. As technology has advanced, other methods of recording human movements have become available, summarized as motion capture. Motion capture has become an important tool in many areas, as medicine (e.g., for clinical gait analysis), entertainment (e.g., for character animation), and sports (e.g., for performance improvement or injury prevention).

Nowadays, marker-based motion capture systems are the most commonly used systems. For measurements with such systems, markers are placed on the skin of the segments of interest and the movement of the markers is recorded with several cameras. The three-dimensional position of the markers is calculated using time-of-flight triangulation, for which the cameras detect the light of the markers. When using passive markers, the cameras emit infrared light beams that reflect off the markers and are then detected by the camera. Using computer models, the three-dimensional marker position is calculated to determine the underlying joint movement between adjacent segments. Marker-based motion capture systems are characterized by a high accuracy of the tracked marker positions after successful calibration. However, the application of the markers is time-consuming and complex, and movements of the skin relative to the underlying bone as well as wobbling masses pose problems. Also, the application possibilities outside a laboratory environment are limited. For further reading on the theory of motion capture systems, we refer to e.g. [12, 87, 128].

To further analyze the recorded data, a standard approach combining kinematic motion capture recordings and force plate information is the inverse dynamics analysis with the goal of computing the joint moments. A typical issue in the application of the inverse dynamics approach is the presence of high residual forces. Those are non-physical forces, which occur e.g., due to skin movement, wobbling masses or noise in the measurement data. The more dynamic and faster a motion is, the greater the forces and thus also the problem of residual forces. There

Table 1.1: Anthropometric data of the athletes with and without below the knee amputation (BKA) as used in this work. The ‘CoM position’ column gives the position of the center of mass (CoM) with respect to the origin when the floating base is situated at the origin of the coordinate system. The ‘Assignment’ column specifies if the data of the respective athlete is used for sprint or long jump computations.

Name	Height	Mass	CoM position	Assignment
Non-amputee athlete 1	1.80 m	75.4 kg	(0.3 cm, 0, 6.6 cm)	Sprint
Non-amputee athlete 2	1.83 m	71.6 kg	(0.4 cm, 0, 4.6 cm)	Sprint
Non-amputee athlete 3	1.96 m	85.2 kg	(0.5 cm, 0, 5.1 cm)	Sprint
Non-amputee athlete 4	1.83 m	84.1 kg	(0.3 cm, 0, 8.8 cm)	Long Jump
Amputee athlete	1.84 m	76.0 kg	(−0.1 cm, 0, 7.7 cm)	Sprint/ Long Jump

are various approaches to decrease the influence of the residual forces (e.g., non-zero forces at bodies or the floating base with no forces applied in experiments), e.g., a residual reduction algorithm [28] or modification of the marker post-processing [51]. A second limitation of the inverse dynamics approach is the fact that precise ground reaction force measurements are necessary, thus restricting the data capturing to the number of available force plates and indoor/laboratory conditions. Therefore, other methods which can compute the dynamic motion without force measurements and residual forces are of interest. One possibility are optimization based approaches which have been successfully used to study the dynamics of walking [41] or muscle excitations in walking and running [78, 92].

## 1.4 Motion Capture Data used in this Thesis

The sprinting and long jump motion capture data of non-amputee and amputee athletes that we use in this work were recorded within the scope of different projects at the German Sport University Cologne. All motions were recorded using marker-based motion capture techniques including a 3D camera system, force plates, collection of mechanical properties of the RSP and anthropometric data of the subjects (see Table 1.1). A detailed description of the setup can be found in [8, 135] for the sprinting motions and in [136] for the long jump motions. Data collection was not part of the thesis. All motions were recorded in an indoor sports hall using a 3D camera system (VICON TM, Oxford, UK) and force plates (Kistler Instrumente AG, Winterthur, Switzerland). Retro-reflective markers were attached to anatomical landmarks and the RSP with adhesive tape. The rotational joint of the RSP is defined by the most posterior point of the RSP which also is the point of the prosthesis’ greatest curvature [136]. The mechanical properties of the RSP and the anthropometric data of the subjects have been collected.

**Sprint running trials** For the recording of the sprint running motions, the athletes were asked to perform sprint runs on an indoor athletic track. The motion capture system includes 16 infrared cameras operating at 250 Hz and four force plates (90 cm × 60 cm) operating at 1250 Hz (non-amputee athletes) or 1000 Hz (amputee athlete) which are built into the floor of the athletic track (compare Figure 1.1 for a sketch of the setup). The motion capture data of the non-amputee athletes was recorded as part of a different project than that of the amputee athlete, which is why the force sampling rates differ. However, the exact force sampling rate is not critical in our context, as it is only used for graphical comparison. For a detailed description, we refer to [8, 135].

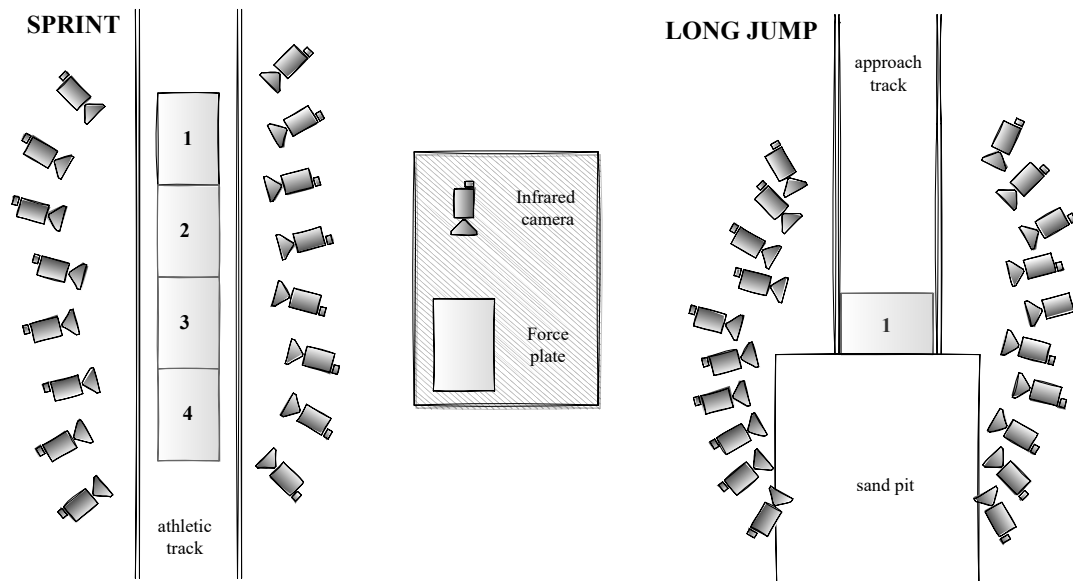


Figure 1.1: Sketch of the setup for the sprinting and long jump motion capture experiments. The position of the cameras is not exact.

**Long jump trials** For the recording of the long jump motions, the athletes were asked to perform long jumps on an indoor long jump facility including a sand pit. The motion capture system consists of 20 infrared cameras operating at 250 Hz and one force plate (90 cm × 60 cm) operating at 1000 Hz which was built into the floor below a wooden take-off board (compare Figure 1.1 for a sketch of the setup). For a detailed description, we refer to [136].

**Extraction of model joint angles from motion capture data** For each trial, the three-dimensional marker positions were saved in a c3d file (along with other information such as system settings, marker names and force plate information). To extract the subject-specific joint angles from the marker positions of the recorded movements, we use the tool PUPPETEER [38, 41]. It performs an inverse kinematics fitting procedure that maps the recorded marker positions to markers that are virtually attached to the subject-specific model of the athlete, thereby calculating the generalized coordinates of the model. For each frame, the inverse kinematics problem uses a damped Levenberg-Marquardt method, based on the description of Sugihara [126], to determine the body posture. A detailed description of PUPPETEER is given in [38].

With the PUPPETEER tool, the recorded marker positions are fitted to the virtual marker positions of the model using a least squares approach – without taking other constraints into account, such as that the foot should not penetrate the ground. Already up to this step, which serves to extract joint angles as a further reference from the recorded motion capture data, deviations from reality occur: In addition to the measurement error of the motion capture systems (system error smaller than 2 mm according to [89]), the first source of deviation is the positioning of the virtual markers on the model. The second source of deviation is the model error, since the human body actually consists of more segments and degrees of freedom (DOFs) compared to the model. In addition, as already described above, the markers move slightly with the skin, which also contributes to the model error. The third source of deviation is in the least squares fit, which minimizes the deviations, but cannot make them disappear completely.



## 2 Modeling of Human Motions with and without Below the Knee Amputation

As already mentioned in the introduction, movement is something quite natural for us as humans. Even if we do not notice this in our everyday lives, the generation of every movement is a highly complex process involving a number of components of the human body, including the brain, nerve tracts, muscles, tendons and joints. Therefore, creating a model of the human body is not a straightforward and easy task.

Each question requires a specific model, whose complexity is adapted to the question: For example, if a researcher wants to study grasping movements, a detailed model of the arm and hand is necessary; the rest of the body must not be modeled (in such detail). On the other hand, a gait analysis demands a whole body model, but the exact movement of all degrees of freedom (DOFs) of the hand is not necessary. Basic kinematic observations can already be made with very simple models (e.g., [22, 46]), while other questions can only be answered with detailed muscle models (e.g., [93, 119]). Consequently, there are models of varying levels of complexity for sprinting and long jumping in the literature. Our models are somewhere in the middle between the very simple and very detailed ones. The athletes are modeled using rigid segments connected by rotational joints. Muscular effects are considered in parts of the studies, even if no detailed muscle model was considered.

### 2.1 Anatomical Conventions

For an unambiguous description of the models and an easy-to-follow discussion of the results, some anatomical terms and conventions are introduced at this point in the same form as they will be used throughout the remainder of the work. Figure 2.1 shows the three main anatomical planes and the three principal axes. The three main body planes each divide the body: The sagittal plane divides the body into a left and a right part. The plane drawn in the figure passes exactly through the middle of the body and is called the median plane. If one looks orthogonally at the plane, one sees the lateral view of the body. In this work the models are placed in such a way that possible translational movements in the sagittal plane are forwards and backwards (along the x-axis) or up and down (along the z-axis). The transverse plane divides the body into an upper and lower part. The frontal plane separates the body into a front and rear part. Lateral movements, to the right and left, occur along the y-axis. It should be noted that we use the terms 'right' and 'left' as seen from the model.

We describe rotations of the body's limbs with respect to the three axes. Rotations around the y-axis (i.e., in the sagittal plane) are called flexion or extension, depending on the direction. We define a flexion as when the rotation results in a reduction of the joint angle (e.g., the knee is bent). The extension is always the counter movement to the flexion (e.g., the knee is stretched). Likewise, rotations around the x-axis (i.e., in the frontal plane) are called abduction or adduction. We define abduction by a movement that moves the limb away from the midline (e.g., the leg is lifted to the side). Adduction is the corresponding reverse movement (e.g., the leg is lowered back). The rotations around the z-axis (i.e., in the transverse plane) also have their own name: internal/medial rotation and external/lateral rotation. Internal or medial

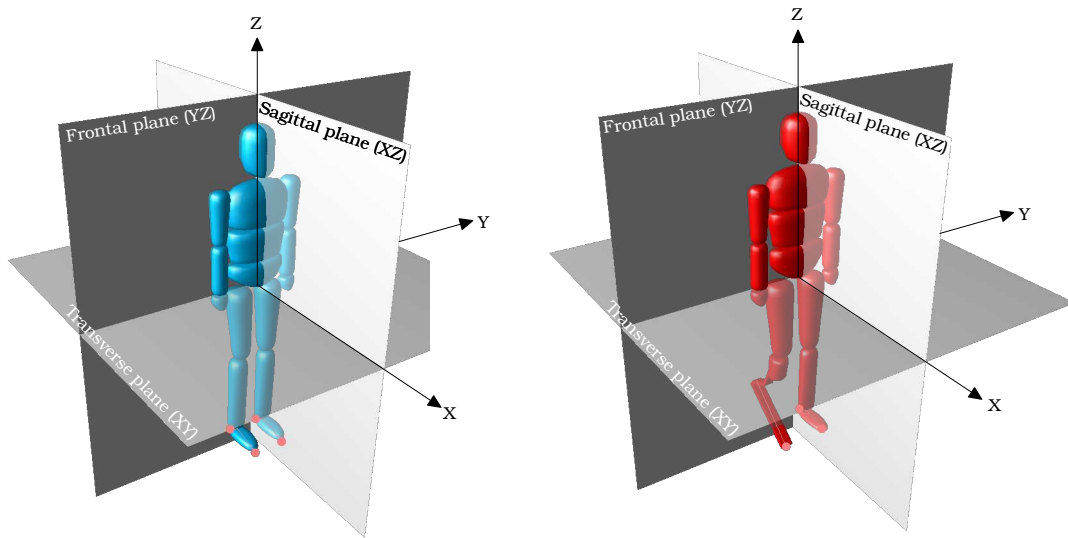


Figure 2.1: Schematic representation of anatomical planes and axes with coordinate system as defined for this thesis

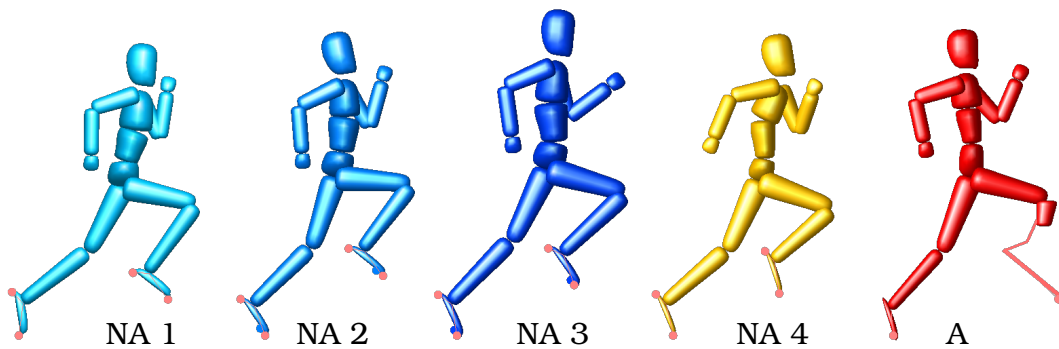


Figure 2.2: Rigid multi-body system models of amputee and non-amputee athletes with 16 segments. The non-amputee athletes labeled 1-3 (NA1, NA2, NA3) are used for the sprinting motions, the non-amputee athlete 4 (NA4) is used for the long jump motion. The model of the amputee athlete (A) is used for both sprinting and long jump studies.

rotation refers to the movement towards the midline (e.g., the straight leg rotates such that the toes point inward) while external or lateral rotation means the movement away from the midline (e.g., the straight leg rotates such that the toes point outward).

## 2.2 Subject-Specific Models of Athletes with and without Below the Knee Amputation

For the various studies of this thesis we created rigid multi-body system models that differ in the number of DOFs. All models have in common that they are composed of 16 segments (head, upper and lower arms, hands, three torso segments, thighs, shanks and feet/prosthetic device) as shown in Figure 2.2. We use the pelvic segment as floating base and the wrists are fixed for all models. The *2D model* is the most simple model with 16 DOFs as it is restricted to the sagittal plane. The three global DOFs define the position and orientation of the floating base. The rotations of the internal joints are described by the remaining thirteen DOFs. An intermediate model which we refer to as the *2D+ model* extends the simple one by a 3 DOF

Table 2.1: Degrees of freedom (DOFs) for the different models established in this work. For each model, the number of DOFs per joint is given together with the direction of the respective DOF. Here (see Figure 2.1 for the definition of the axes and planes),  
 - TX, TY, TZ denote translations along the x-, y- and z-axes and  
 - RX, RY, RZ denote rotations in the frontal, sagittal and transverse planes.

	2D model	2D+ model	3D model
Pelvis	3: TX, TZ, RY	3: TX, TZ, RY	6: TX, TY, TZ, RY, RX, RZ
Hip*	1: RY	1: RY	3: RY, RX, RZ
Knee*	1: RY	1: RY	1: RY
Ankle*	1: RY	1: RY	2: RY, RX
Prosthesis	1: RY	1: RY	1: RY
Lumbar	1: RY	1: RY	2: RY, RX
Thorax	1: RY	1: RY	2: RY, RZ
Shoulder*	1: RY	3: RY, RX, RZ	3: RY, RX, RZ
Elbow*	1: RY	1: RY	1: RY
Neck	1: RY	1: RY	1: RY
Total	16 DOFs	20 DOFs	31 DOFs

\* This joint exists twice, once on each side of the body (right and left leg or arm), except for the ankle joint of the amputee athlete.

shoulder joint. Hence, it has 20 DOFs. The *3D model* allows movements in three-dimensional space. Six global DOFs give the position and orientation of the pelvis and the remaining 25 DOFs are rotations of the internal joints around all three axes. Table 2.1 gives an overview of the DOFs present in each of the models. For each level of models, we created subject-specific models of one athlete with unilateral below the knee amputation (BKA) and of non-amputee athletes based on the de Leva data [26]. The data was extrapolated to the heights and masses of the individual athletes measured during the experiments (cf. Section 1.4 and especially Table 1.1). In the case of the athlete with unilateral BKA, a model of the prosthetic device and the remaining part of the shank replaces the below-knee segments of the right leg (cf. Section 2.3). We assume that the action of all muscles at a joint is summarized by joint torque actuators which control the rotations of the internal joints.

## 2.3 Model of the Running-Specific Prosthesis

The careful modeling of the running-specific prosthesis (RSP) is crucial for the simulations. Athletes with a BKA use carbon-fiber prostheses with a special geometry (C-shaped or J-shaped) and spring-like properties. The amputee athlete described in Section 1.4 uses Cheetah Xtreme prosthetic device (Össur, Reykjavik, Iceland). In order to create the model of the prosthetic device, a decision had to be made regarding the accuracy, just like for the whole-body models of the athletes: On the one hand, the model should be precise enough to represent the decisive characteristics, and on the other hand, it should keep the computational power within reasonable limits. As the real RSP is made from compliant material which shows an overall deformation, it does not have joints – especially no ankle joint. In our model of the RSP, this behaviour is approximated by replacing it by three rigid segments with a fixed joint between the upper ones and a rotational joint in between of the lower ones. This gives the model an

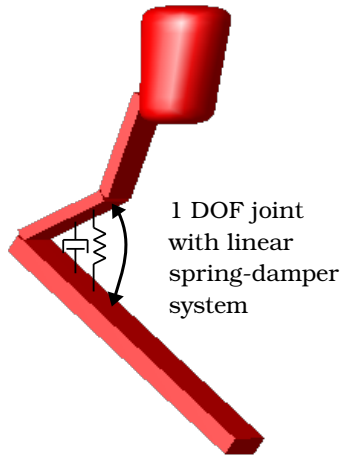


Figure 2.3: Model of the running-specific prosthesis consisting of three rigid segments. The two upper segments are coupled together at a fixed angle, while the two lower segments are connected by a 1-degree of freedom (DOF) joint. The model of the prosthetic device is attached to the remaining shank at a fixed angle and we neglect movements between the prosthetic device and the remaining limb, so there is no further model DOF at this point.

“ankle joint” on which a linear spring-damper system is acting. The point of the ankle joint is defined as the point of the prosthesis’ greatest curvature which at the same time is its most posterior point [136]. Figure 2.3 shows an illustration of the model. The joint torque  $\tau_{\text{RSP}}$  produced by the passive action of the RSP acting at the ankle joint is computed by

$$\tau_{\text{RSP}}(q_{\text{RSP}}, \dot{q}_{\text{RSP}}) = -d\dot{q}_{\text{RSP}} - k(q_{\text{RSP}} - q_{0,\text{RSP}}), \quad (2.1)$$

where  $q_{\text{RSP}}$  and  $\dot{q}_{\text{RSP}}$  denote the generalized joint angle and joint velocity of the RSP,  $d$  and  $k$  the damping and spring constants of the RSP and  $q_{0,\text{RSP}}$  the rest position of the RSP. To keep the number of variables of the optimal control problems (OCPs) as small as possible and to avoid numerical difficulties, we assume the prosthetic device to be critically damped, that is it returns to its rest position  $q_{0,\text{RSP}}$  as quickly as possible without oscillations. In this case, the damping ratio equals 1, implying that we can determine the damping constant  $d$  directly from the spring constant  $k$  and inertia matrix  $I$ . Assuming rotations in the sagittal plane (i.e., around the  $y$ -axis), the damping constant can be computed via

$$d = 2\sqrt{I_{11}k}. \quad (2.2)$$

The segment lengths and masses and the fixed angle between the upper two segments were chosen based on measurements of the real RSP (cf. Section 1.4). The shank segment of the affected leg is shortened to the length of the amputee athlete’s stump and the model of the prosthetic device is then coupled to it at a fixed angle as we neglect movements of the tibial end in the prosthesis socket.

## 2.4 Modeling of Human Motions

Human motions can be interpreted as a sequence of distinct phases. These phases are characterized by the number and type of external contacts that act on the model. For sprinting and long jump movements the model has contact with the environment only with the feet (we neglect the possible ground contact of the hands or the back after the landing in the case of the long jump). Either one (single support phase) or both feet (double support phase) can be in contact with the ground. There are also phases in which both feet do not touch the ground (flight phase). Each phase is represented by a separate set of ordinary differential equations (ODEs) or differential algebraic equations (DAEs).

If no contact occurs, the equation of motion of a rigid multi-body system is described by

$$\mathbf{M}(\mathbf{q})\dot{\mathbf{q}} + \mathbf{N}(\mathbf{q}, \dot{\mathbf{q}}) = \boldsymbol{\tau}, \quad (2.3)$$

where  $\mathbf{q}, \dot{\mathbf{q}}, \boldsymbol{\tau}$  are the generalized positions, generalized velocities and generalized forces of the model. The latter include all external forces acting on the model such as gravity and the torques due to the muscular action and the spring-damper system. The symmetric and positive definite mass matrix  $\mathbf{M}(\mathbf{q})$  is composed of the inertial properties of the system. Non-linear effects, e.g., internal Coriolis, gyroscopic and centrifugal forces, gravity and forces not caused by  $\boldsymbol{\tau}$  are stored in the vector  $\mathbf{N}(\mathbf{q}, \dot{\mathbf{q}})$ .

We model foot-ground contact using holonomic constraints rather than using a compliant contact model. During foot-ground contact we add  $m_C < n_{\text{DOF}}$  constraints  $\mathbf{g}(\mathbf{q}) = 0$  with  $\mathbf{g} : \mathbb{R}^{n_{\text{DOF}}} \rightarrow \mathbb{R}^{m_C}$ . Thus, the equation of motion reads

$$\mathbf{M}(\mathbf{q})\dot{\mathbf{q}} + \mathbf{N}(\mathbf{q}, \dot{\mathbf{q}}) = \boldsymbol{\tau} + \mathbf{G}(\mathbf{q})^T \boldsymbol{\lambda}, \quad (2.4a)$$

$$\mathbf{g}(\mathbf{q}) = 0, \quad (2.4b)$$

where  $\mathbf{G}(\mathbf{q}) = (\partial \mathbf{g} / \partial \mathbf{q}) \in \mathbb{R}^{m_C \times n_{\text{DOF}}}$  is a matrix called constraint Jacobian and  $\boldsymbol{\lambda} \in \mathbb{R}^{m_C}$  is the vector of constraint forces caused by the contact. Equation (2.4) is an index-3 DAE system. By differentiating the constraint equation (2.4b) twice and denoting the constraint Hessian of the system with  $\boldsymbol{\gamma}(\mathbf{q}, \dot{\mathbf{q}}) = -\dot{\mathbf{G}}(\mathbf{q})\dot{\mathbf{q}} \in \mathbb{R}^{m_C}$ , we can rewrite it as linear system:

$$\begin{bmatrix} \mathbf{M}(\mathbf{q}) & \mathbf{G}(\mathbf{q})^T \\ \mathbf{G}(\mathbf{q}) & \mathbf{0} \end{bmatrix} \begin{bmatrix} \ddot{\mathbf{q}} \\ -\boldsymbol{\lambda} \end{bmatrix} = \begin{bmatrix} -\mathbf{N}(\mathbf{q}, \dot{\mathbf{q}}) + \boldsymbol{\tau} \\ \boldsymbol{\gamma}(\mathbf{q}, \dot{\mathbf{q}}) \end{bmatrix}, \quad (2.5)$$

If the constraints  $\mathbf{g}$  are not redundant, the system is always solvable. To make sure that the invariants of the constraints are satisfied and assure equivalence of Eq.s (2.4) and (2.5), constraints are set at the beginning of each contact phase. The invariants of the constraints read:

$$\mathbf{g}_{pos} = \mathbf{g}(\mathbf{q}(t)) = 0, \quad (2.6a)$$

$$\mathbf{g}_{vel} = \mathbf{G}(\mathbf{q}(t)) \cdot \dot{\mathbf{q}}(t) = 0. \quad (2.6b)$$

When sprinting at maximum constant velocity and also during the last steps of the approach for a long jump, the athlete has reached a large velocity. At this stage of the movement only the ball of the foot contacts the ground. We approximate this behavior by describing the contact by a point-like, non-sliding and rigid contact. The contact event, which we also call touchdown, is modeled as an instantaneous and completely inelastic collision. This keeps the foot in contact with the ground and prevents it from bouncing back up. This approximation disregards the fast timescale effects of the real contact; nevertheless, previous research has shown that it reflects very well the actual behavior in a whole-body motion prediction context. According to this model, velocity discontinuities occur at touchdown resulting from the fact that the velocity of the contact point is instantaneously set to zero. The generalized velocities change from the velocity  $\mathbf{v}^-$  before to the velocity  $\mathbf{v}^+$  after the contact gain. The discontinuous change can be computed as

$$\begin{bmatrix} \mathbf{M}(\mathbf{q}) & \mathbf{G}(\mathbf{q})^T \\ \mathbf{G}(\mathbf{q}) & \mathbf{0} \end{bmatrix} \begin{bmatrix} \mathbf{v}^+ \\ \boldsymbol{\Lambda} \end{bmatrix} = \begin{bmatrix} \mathbf{M}(\mathbf{q})\mathbf{v}^- \\ \mathbf{0} \end{bmatrix}, \quad (2.7)$$

where  $\boldsymbol{\Lambda}$  is the impulse. In addition to the touchdown, which marks the transition from flight to contact phases and is described by a separate phase, lifting the foot means the transition

from contact to flight phases. We do not specify the timing of the phase transitions, but use switching functions which determine the transition point implicitly based on the state variables and parameters of the system:

$$c(\mathbf{q}(t_s), \dot{\mathbf{q}}(t_s), \mathbf{p}) = 0. \quad (2.8)$$

The transition from flight to contact phases happens when the  $z$ -component of the contact point position becomes zero. Lift-off events are determined by the vertical ground reaction force equaling zero. As it is not possible to derive the full equations by hand, the Rigid Body Dynamics Library RBDL which was developed by Felis at Heidelberg University [39] is used. The library is based on the dynamics algorithms developed by Featherstone [37].

## 2.5 Realistic Torque Limit Modeling by Muscle Torque Generators

Setting realistic limits for all variables is an important basis for generating natural movements and allowing meaningful analyses and conclusions to be drawn. While this is possible by hand for joint angles and, with minor restrictions, for their angular velocities by observing the range of motion, determining realistic limits for actuator torque is a more challenging task. Since we assume that the actuators summarize the activity of all muscles at a joint, box-like limits can only serve as a first approximation. The most realistic limits would be obtained by extending the model to a complete human musculoskeletal model. The muscular system is controlled by the nervous systems. The muscle type of interest for this thesis are the skeletal muscles as they are related to control of posture and locomotion. The skeletal muscles<sup>1</sup> are attached to the bony structures of the body by tendons. The contraction of a muscle moves the bones it is attached to by pulling on them and thus applies a force on the joints that the muscles spans. As muscles can only pull, they always come in so-called antagonistic pairs with one muscle contracting (agonist) and one muscle relaxing (antagonist) at the same time. However, those are not strict pairs, but one muscle can be the antagonist to more than one agonist muscle. The human body consists of a variety of muscles from rather simple ones which span a single joint of the body to complex ones which span multiple joints.

To model a complete musculoskeletal system, one would have to introduce the equations describing the dynamics of muscle contractions in addition to the equations describing the dynamics of the rigid multi-body system (see Section 2.4). Roughly speaking, muscle models describing the dynamics of muscle contractions can be divided into two main groups: Cross-bridge muscle models and Hill-type muscle models. The cross-bridge muscle models are based on the theory of Huxley [64]. They aim at describing precisely mechanical processes and chemical reactions during the muscle contractions. Hence, they are important when it comes to investigate isolated muscles. However, it is computationally intractable to solve whole body optimal control problems using Huxley models because a single muscle requires hundreds to thousands of state variables [129] to simulate a single muscle. Instead, Hill-type models [58] are used for modeling larger systems.<sup>2</sup> Hill-type models are derived by embedding experimentally measured force-velocity [58] and force-length characteristics [49] directly in the model rather than instead modeling the underlying processes that lead to the force-velocity and force-length characteristics. The force generation depends on the chemical activation of the muscle, the attachment and positioning related to the skeleton, the muscle length as well as the lengthening rate. The relationship with the last two quantities is determined by the experimentally determined parametric force-length and force-velocity curves. For muscles span-

---

<sup>1</sup>In the following simply referred to as muscles.

<sup>2</sup>We refer to publications on muscle modeling, e.g., [137, 140], for further reading.

ning a single joint, the force-length and force-velocity relationships can be directly mapped to curves describing the relationship between the torque at a specific joint and the respective joint angle and joint angular velocity. A possible modeling approach is to summarize agonist and antagonist muscle by a group muscle and compute the generated torque by Muscle Torque Generators (MTGs). A single MTG generates a torque  $\tau^M$  which can be computed by

$$\tau^M = \tau_0^M \left[ a f^A(\theta) f^V(\dot{\theta}) + f^P(\theta) \left( 1 - \beta^P \frac{\dot{\theta}}{\dot{\theta}_{max}} \right) \right]. \quad (2.9)$$

Here,  $\tau_0^M$  is the maximum active isometric torque,  $a$  is the muscle activation (varying between 0 and 1) and  $f^A(\theta)/f^P(\theta)$  and  $f^V(\dot{\theta})$  are the active/passive torque-angle and torque-velocity curves. The MTG-specific angles and velocities are denoted by  $\theta$  and  $\dot{\theta}$  and  $\beta^P$  is the non-linear normalized damping term. Finally,  $\dot{\theta}_{max}$  is the maximum angular velocity. The MTGs are implemented as an add-on to RBDL [39] and we refer to the documentation for a comprehensive description of the set-up and the data sets.

For parts of the studies presented in this thesis, a MTG model is used for the computation of realistic joint torque limits. For all investigated athletes, we first set up the MTG model with the data set which is based on the measurements of [9, 30, 65, 67, 114]. However, it appears that these data are still too weak and too stiff to model such dynamic motions as sprinting and long jump. We therefore apply the fitting routine proposed and explained in detail in [91]. By introducing additional parameters to regularize, scale, and shift the curves in the model, we can easily fit the characteristics of the model to the participant using the reconstructed dynamics (see Chapters 5 and 9). Subsequently, we apply the fitted MTG model which is capable of producing the reconstructed torques. The fitting routine is implemented in the muscle add-on to RBDL [39] using the software library IPOPT [138].

In principle, two approaches are conceivable for using the MTGs: The first option is to embed the MTGs into the dynamic equations of the model. The second option is to use the MTGs to define limits on the maximum torque that the joint torque actuators can generate. We chose the second option whenever the MTG model is used (i.e., in the motion generation OCPs).



## 3 Simulation of Human Motions Using Optimal Control Problem Formulations

Just as we do not notice the complex motions we execute in our everyday lives, we are often unaware of the various optimization problems around us. At work, transport routes, process flows, product designs, portfolios and much more are constantly being optimized. In daily life we attempt to find the best balance between work and private time, or compare offers for washing machines to determine the best price-performance ratio. Nature optimizes as well: Physical systems strive for the state of least energy and light rays move along the course of shortest time. Based on the assumption that human motions are optimal in some way [4, 5], we can generate and study sprinting and long jump motions using optimization problems.

### 3.1 Optimal Control Problem Formulations

In mathematics, the term optimization describes the minimization or maximization of a function while fulfilling constraints on the variables. In the case of dynamic systems, the variables of the optimization problem are not finite dimensional vectors but functions in time (i.e., infinite dimensional variables): The states  $\mathbf{x}(t)$  characterize the dynamic system via the equations of motion. Dynamic systems can often be manipulated by a suitable choice of input variables, which are called control variables  $\mathbf{u}(t)$ . An optimization system for such dynamic systems is called optimal control problem (OCP). The goal of the OCP is to find those state and control trajectories (and possible parameters and durations) which simultaneously minimize an objective functional  $\Phi$  and respect constraints  $\mathbf{g}_i$ ,  $\mathbf{r}^{\text{eq}}$  and  $\mathbf{r}^{\text{ineq}}$  on the variables. If the dynamic process can be subdivided into several phases, the optimal control problem is adapted accordingly. A general multi-phase OCP with discontinuities can then be formulated as follows:

$$\min_{\mathbf{x}(\cdot), \mathbf{u}(\cdot), \mathbf{p}, \mathbf{h}} \Phi(\mathbf{x}(t), \mathbf{u}(t), \mathbf{p}, \mathbf{h}) \quad (3.1a)$$

subject to:

$$\dot{\mathbf{x}}(t) = \mathbf{f}_i(t, \mathbf{x}(t), \mathbf{u}(t), \mathbf{p}), \quad t \in \mathcal{T}_i, \quad (3.1b)$$

$$\mathbf{x}(\hat{t}_i^+) = \mathbf{c}_i(\mathbf{x}(\hat{t}_i^-), \mathbf{p}), \quad i \in \mathcal{I}, \quad (3.1c)$$

$$0 \leq \mathbf{g}_i(t, \mathbf{x}(t), \mathbf{u}(t), \mathbf{p}), \quad t \in \mathcal{T}_i, \quad (3.1d)$$

$$0 = \mathbf{r}^{\text{eq}}(\mathbf{x}(\hat{t}_0), \dots, \mathbf{x}(\hat{t}_k), \mathbf{u}(\hat{t}_0), \dots, \mathbf{u}(\hat{t}_k), \mathbf{p}), \quad \hat{t}_0, \dots, \hat{t}_k \in \mathcal{T}, \quad (3.1e)$$

$$0 \leq \mathbf{r}^{\text{ineq}}(\mathbf{x}(\hat{t}_0), \dots, \mathbf{x}(\hat{t}_k), \mathbf{u}(\hat{t}_0), \dots, \mathbf{u}(\hat{t}_k), \mathbf{p}), \quad \hat{t}_0, \dots, \hat{t}_k \in \mathcal{T}. \quad (3.1f)$$

It is based on a general dynamic system with  $N$  Phases on the time interval  $\mathcal{T} = [t_0, t_f] \in \mathbb{R}$  (with  $t_f = t_N$ ). The system is described by the piecewise continuous state variables  $\mathbf{x}(t) : \mathcal{T} \rightarrow \mathbb{R}^{n_x}$  and controlled by the controls  $\mathbf{u}(t) : \mathcal{T} \rightarrow \mathbb{R}^{n_u}$  and finite dimensional parameters  $\mathbf{p} \in \mathbb{R}^{n_p}$ . The subintervals  $\mathcal{T}_i = [t_{i-1}, t_i]$  define the timings for phase changes and all phase indices are added to the set of phase indices  $\mathcal{I} = \{1, \dots, N\}$ . The system dynamics on each subinterval is given by a set of ordinary differential equations (ODEs) with right hand sides  $\mathbf{f}_i : \mathbb{R} \times \mathbb{R}^{n_x} \times \mathbb{R}^{n_u} \times \mathbb{R}^{n_p} \rightarrow \mathbb{R}^{n_x}$ . The discontinuities in the state variables at phase switches are

formalized by switching functions  $c_i : \mathbb{R}^{n_x} \times \mathbb{R}^{n_p} \rightarrow \mathbb{R}^{n_x}$ . The constrained infinite dimensional optimization problem minimizes the objective functional  $\Phi : \mathcal{X} \times \mathcal{U} \times \mathbb{R}^{n_p} \times \mathbb{R}^{n_h} \rightarrow \mathbb{R}$  (with  $\mathcal{X}$  and  $\mathcal{U}$  denoting the sets of all state and control trajectories, respectively) while respecting the path constraints  $\mathbf{g}_i : \mathbb{R} \times \mathbb{R}^{n_x} \times \mathbb{R}^{n_u} \times \mathbb{R}^{n_p} \rightarrow \mathbb{R}^{n_{g_i}}$ ,  $i \in \mathcal{I}$  as well as the equality and inequality constraints  $\mathbf{r}^{\text{eq/ineq}} : (\mathbb{R}^{n_x})^k \times (\mathbb{R}^{n_u})^k \times \mathbb{R}^{n_p} \rightarrow \mathbb{R}^{n_r}$  (with  $r = r_{\text{eq}} + r_{\text{ineq}}$ ).

Usually the objective function (3.1a) of an OCP is given in the most general form as a Bolza type objective function:

$$\Phi(\mathbf{x}(t), \mathbf{u}(t), \mathbf{p}, \mathbf{h}) = \sum_{i=1}^N \int_{t_{i-1}}^{t_i} \Phi_{L_i}(t, \mathbf{x}(t), \mathbf{u}(t), \mathbf{p}) dt + \sum_{i=1}^N \Phi_{M_i}(t_i, \mathbf{x}(t_i), \mathbf{p}). \quad (3.2)$$

This objective function is composed of two parts, the Lagrange type and the Mayer type objective function. The former (first summand) is evaluated by integration along the trajectories for all times in the interval  $\mathcal{T}_i$ . The latter (second summand) is only calculated at the end of the interval  $\mathcal{T}_i$ . By suitable reformulations, the two types can be transformed into each other, so that ultimately one of the two ways of defining objective functions would be sufficient. However, the formulation of concrete conditions such as minimization of energy (Lagrange type) or total time (Mayer type) is simplified by the possibility of choosing between them.

### 3.1.1 Dynamics Reconstruction Using Optimal Control Problems

For the reconstruction of the full dynamics of motions we employ an OCP formulation that merely takes reference kinematics (cf. Section 1.4) without any force plate information. The advantage of this approach is the ability to determine all joint angles with zero residual error as well as ground reaction forces solely by introducing a proper constraint that ensures ground contact. We express the multi-phase least squares OCP as follows:

$$\min_{\mathbf{x}(\cdot), \mathbf{u}(\cdot), \mathbf{p}} \sum_{k=0}^m \frac{1}{2} \left( \|W(q_k^{MC} - q(\hat{t}_k))\|_2^2 + \gamma_u \|\mathbf{u}(\hat{t}_k)\|_2^2 \right) \quad (3.3a)$$

subject to

$$\dot{\mathbf{x}}(t) = f_i(t, \mathbf{x}(t), \mathbf{u}(t), \mathbf{p}), \quad t \in [\hat{t}_i, \hat{t}_{i+1}], \quad (3.3b)$$

$$\mathbf{x}(\hat{t}_i^+) = c_i(\mathbf{x}(\hat{t}_i^-), \mathbf{p}), \quad i = 0, \dots, m-1, \quad (3.3c)$$

$$\mathbf{g}(t, \mathbf{x}(t), \mathbf{u}(t), \mathbf{p}) \geq 0, \quad t \in [\hat{t}_i, \hat{t}_{i+1}], \quad (3.3d)$$

$$\mathbf{r}^{\text{eq}}(\mathbf{x}(0), \dots, \mathbf{x}(\hat{t}_{m-1}), \mathbf{p}) = 0, \quad (3.3e)$$

$$\mathbf{r}^{\text{ineq}}(\mathbf{x}(0), \dots, \mathbf{x}(\hat{t}_{m-1}), \mathbf{p}) \geq 0. \quad (3.3f)$$

The generalized positions  $\mathbf{q}(t) \in \mathbb{R}^{n_{\text{dof}}}$ , the generalized velocities  $\dot{\mathbf{q}}(t) \in \mathbb{R}^{n_{\text{dof}}}$  and the joint torques  $\boldsymbol{\tau}(t) \in \mathbb{R}^{n_{\text{actuated}}}$  form the differential state vector  $\mathbf{x}(t) \in \mathbb{R}^{2n_{\text{dof}} + n_{\text{actuated}}}$ . As controls  $\mathbf{u}(t) \in \mathbb{R}^{n_{\text{actuated}}}$ , we use the derivatives of the joint torques  $\mathbf{u}(t) = \dot{\boldsymbol{\tau}}(t)$ . All equations of the OCP are evaluated at discrete points in time  $\hat{t}_i$ ,  $i = 0, \dots, m-1$  where the number of points is chosen separately for each phase. The individual phase durations are fixed to values that are prescribed by the kinematic reference motion. We set them manually by carefully reviewing the animation sequences. For all variables (states  $\mathbf{x}$ , controls  $\mathbf{u}$  and parameters  $\mathbf{p}$ ), the path constraints (3.3d) define the upper and lower bounds, which are set generously in the case of the problem so that the model can easily follow the kinematic reference. Further constraints that specify proper ground contact dynamics and kinematic conditions (e.g., touchdown and lift-off events) are formulated in the non-linear point constraint equations (3.3e) and (3.3f).

Equation (3.3a) defines the objective function which is made up of two terms: the actual least squares term and a regularization term. The former computes the deviation among generalized coordinates  $q(\hat{t}_k)$  of the model and coordinates of the kinematic reference  $q_k^{MC}$ . The diagonal weight matrix  $W \in \mathbb{R}^{n_{dof} \times n_{dof}}$  balances the different orders of magnitude such that a proper reproduction of the reference movement is obtained. The motion capture sampling rate might not correspond with the OCP solver nodes. This problem is addressed by a spline interpolation of the reference motion which then is evaluated at the respective nodes. The regularization term inhibits too heavy oscillations in the controls and thus also in the joint torques. Nevertheless, the least squares term is the dominant component of the objective function if the weighting factor  $\gamma_u$  is chosen appropriately. The full multi-phase dynamics as described in Section 2.4 is incorporated in Eq.s (3.3b) and (3.3c).

### 3.1.2 Motion Synthesis Using Optimal Control Problems

Movements which optimize a basic optimization criterion or a combination of basic criteria are computed as solutions of a multi-phase OCP of the form:

$$\min_{\mathbf{x}(\cdot), \mathbf{u}(\cdot), \mathbf{p}, \mathbf{h}} \Phi(\mathbf{x}(t), \mathbf{u}(t), \mathbf{p}, \mathbf{h}) \quad (3.4a)$$

subject to:

$$\dot{\mathbf{x}}(t) = f_i(t, \mathbf{x}(t), \mathbf{u}(t), \mathbf{p}), \quad t \in \mathcal{T}_i, \quad (3.4b)$$

$$\mathbf{x}(\hat{t}_i^+) = c_i(\mathbf{x}(\hat{t}_i^-), \mathbf{p}), \quad i \in \mathcal{I}, \quad (3.4c)$$

$$\mathbf{g}_i(t, \mathbf{x}(t), \mathbf{u}(t), \mathbf{p}) \geq 0, \quad t \in \mathcal{T}_i, \quad (3.4d)$$

$$\mathbf{r}^{\text{eq}}(\mathbf{x}(\hat{t}_0), \dots, \mathbf{x}(\hat{t}_m), \mathbf{u}(\hat{t}_0), \dots, \mathbf{u}(\hat{t}_m), \mathbf{p}) = 0, \quad (3.4e)$$

$$\mathbf{r}^{\text{ineq}}(\mathbf{x}(\hat{t}_0), \dots, \mathbf{x}(\hat{t}_m), \mathbf{u}(\hat{t}_0), \dots, \mathbf{u}(\hat{t}_m), \mathbf{p}) \geq 0. \quad (3.4f)$$

It calculates the optimal states  $\mathbf{x}(t) = [\mathbf{q}(t), \dot{\mathbf{q}}(t), \boldsymbol{\tau}(t)]^T$ , controls  $\mathbf{u}(t) = \dot{\boldsymbol{\tau}}(t)$ , phase durations  $\mathbf{h} = [h_0, \dots, h_{n_{\text{ph}}-1}]$  (with  $n_{\text{ph}}$  being the number of phases) and parameters  $\mathbf{p}$ . The spring constant and the damping constant of the running-specific prosthesis (RSP) could also be included as free parameters in this problem formulation. However, we have decided to set the values to the ones obtained from the reconstruction. The system dynamics and the different types of constraints are formulated in Eq.s (3.4b)–(3.4f), analogously to Eq.s (3.3b)–(3.3f) (see Section 3.1.1 for a description of the individual equations).

Equation (3.4a) is a placeholder for the mathematical formulation of a linear combination of basic optimization criteria with weighting factors  $\gamma$ :

$$\Phi = \sum_{j=1}^{n_M} \left( \gamma_j \varphi_{M_j}(t_f, \mathbf{x}(t_f), \mathbf{p}) \right) + \sum_{k=1}^{n_L} \left( \gamma_{k+n_M} \sum_{i=1}^N \int_{t_{i-1}}^{t_i} \varphi_{L_k}(t, \mathbf{x}(t), \mathbf{u}(t), \mathbf{p}) dt \right). \quad (3.5)$$

It is a combination of  $n_M$  objective functions of Mayer type and  $n_L$  objective functions of Lagrange type. Mayer type objective functions formulate basic optimization criteria which are assessed at the end of a phase. Optimization criteria that are evaluated along the complete solution history are expressed with Lagrange type objective functions. The weight factors allow for the study of different combinations of basic criteria and for balancing the importance of the respective criteria. Three approaches are particularly promising for the identification of meaningful criteria: if there are already solutions of the reconstruction of the dynamics (see Section 3.1.1) for the motion, one can use them to draw conclusions about possibly good criteria for

the generation of it. Second, biomechanical studies of kinematic or dynamic characteristics of the motion can be helpful. An overview of the state of research in sprinting and long jump with and without amputation is given in each of the introductory chapters on the movements (cf. Chapters 4 and 8) – with a particular focus on possible optimization criteria. Finally, other possible criteria have been shown to be useful in predictive simulations for creating realistic human movements. For example, simulations of human walking [40], running [94, 121] and platform diving [70] could be generated using torque minimization, torque derivative minimization or/and head stabilization terms when other performance-related criteria were introduced into the optimization as constraints or additional objective functions. In a study on three-dimensional human walking [40], minimizing angular momentum was also a significant component of the objective function. With a minimization of torques-approach, Mombaur [94] confirmed the experimental results comparing a double transtibial amputee athlete and a non-amputee athlete of Brüggemann and co-workers [18] and showed that double transtibial sprinting could be generated with lower joint torques. Mombaur gives in [95] a detailed list of optimization criteria, on which human movements might be based and which therefore might be suitable for predictive simulations. The concrete basic optimization criteria for the study of sprinting and jumping motions are described in Chapters 6 and 10.

### 3.1.3 Numerical Solution of Optimal Control Problems

In order to determine the optimal inputs and state functions, the OCP must be solved. Two basic approaches can be distinguished: indirect and direct methods. The main difference is how the methods handle the infinite dimensionality of states and controls. Indirect methods (based on the Pontryagin maximum principle) transform the OCP into a boundary value problem by calculating first order optimality conditions and solving it. For the solution with direct methods, however, the state and control functions must be appropriately discretized and parameterized (“first-discretize-then-optimize”). Thus, the OCP is transformed into a finite dimensional non-linear optimization problem. For the discretization of the state trajectories, direct collocation or shooting methods are suitable. A method for direct multiple shooting was introduced by Bock and Plitt [15].

**Discretization of controls** To realize the control discretization, a time grid

$$t_0 < t_1 < \dots < t_{m-1} < t_m = T \quad (3.6a)$$

and subintervals

$$I_j = [t_{j-1}, t_j] \text{ for } j = 1, \dots, m \quad (3.6b)$$

are defined in a first step. On each subinterval, the control function is then replaced by a finite dimensional parameter vector

$$\mathbf{u}(t) \approx \mathbf{u}(t; \mathbf{q}_{j-1}) = \xi(t, \mathbf{q}_{j-1}) \quad (3.7)$$

through base functions  $\xi$  and parameters  $\mathbf{q}_j \in \mathbb{R}^{k_u n_u}$ . As base functions, piecewise constant ( $k_u = 1$ ), piecewise linear ( $k_u = 2$ ) or even more complicated discretizations ( $k_u \geq 2$ , e.g., splines) can be selected. Since more complicated base functions are also associated with more variables in the optimization problem, we use piecewise constant base functions,

$$\xi(t, \mathbf{q}_j) = \mathbf{q}_j, \quad (3.8a)$$

or piecewise linear base functions,

$$\xi(t, \mathbf{q}_j) = \mathbf{q}_j^1 + \frac{t - t_{j-1}}{t_j - t_{j-1}} (\mathbf{q}_j^2 - \mathbf{q}_j^1) \quad \text{with} \quad \mathbf{q}_j = [\mathbf{q}_j^1, \mathbf{q}_j^2]^T. \quad (3.8b)$$

**Parameterization of differential states using multiple shooting** The shooting methods are based on the idea of converting the boundary value problem into an initial value problem which then can be solved with standard solvers for ODEs. In contrast to the single shooting method, where a sole initial value problem is defined over the entire time horizon, the multiple shooting method defines  $m$  initial value problems of the form

$$\dot{\mathbf{x}}(t) = \mathbf{f}(t, \mathbf{x}(t), \xi(t, \mathbf{q}_{j-1})), \quad j = 1, \dots, m, \quad t \in I_j, \quad (3.9a)$$

$$\mathbf{x}(t_{j-1}) = \mathbf{s}_{j-1}, \quad (3.9b)$$

is formulated on the subintervals  $I_j$ . In principle, these subintervals do not have to correspond to the intervals for the control discretization; they could also be subsets of the respective other grid. For numerical reasons, however, identical grids are used for the discretization of the controls and the states in practice, which is why we directly adopt this formulation. The grid time points  $t_0, \dots, t_m$  are called multiple shooting nodes. The parameterization of the problem is achieved via the initial values  $\mathbf{s}_j \in \mathbb{R}^{n_x}$ . In practice, it is helpful to choose meaningful rather than random initial values due to numerical considerations. Measured motions could be used for instance. The solution of the initial value problem is denoted by  $\eta(t_j; t_{j-1}, \mathbf{s}_{j-1}, \mathbf{q}_{j-1})$ . Since the initial value problems are solved independently on each interval, the solution is not necessarily continuous over the entire time interval. Therefore, additional  $m$  continuity conditions which demand equality of the end point of a subinterval and the start point of the subsequent subinterval, are introduced:

$$\eta(t_j; t_{j-1}, \mathbf{s}_{j-1}, \mathbf{q}_{j-1}) - \mathbf{s}_j = \mathbf{0}, \quad j = 1, \dots, m, \quad t \in I_j. \quad (3.10)$$

**Discretization of path and point constraints** We use a simple approach to discretize the path and point constraints by evaluating them solely at the multiple shooting nodes. Then it holds:

$$\mathbf{g}(\mathbf{s}_j, \mathbf{q}_j) \geq \mathbf{0}, \quad j = 1, \dots, m-1, \quad (3.11a)$$

$$\mathbf{r}(\mathbf{x}(\hat{t}_0), \dots, \mathbf{x}(\hat{t}_k)) \geq \mathbf{0}, \quad \hat{t}_0, \dots, \hat{t}_k \in [t_0, T]. \quad (3.11b)$$

**Free parameters and phase durations** Problems with free parameter vectors or free phase durations can always be converted into problems with fixed parameter vectors or phase durations by using suitable transformations.

**Solution of the discretized optimal control problem** As a result of the discretization we get a large scale non-linear programming problem (NLP). After introducing an vector  $\mathbf{y}$  grouping together all the variables of the OCP (parameterized states, discretized controls, parameters, phase durations),

$$\mathbf{y} = [\mathbf{s}_0, \mathbf{q}_0, \dots, \mathbf{s}_{m-1}, \mathbf{q}_{m-1}, \mathbf{s}_m, \mathbf{q}_m, \mathbf{p}, d_1, \dots, d_N], \quad (3.12)$$

the OCP can be written in the following general and compact form:

$$\min_{\mathbf{y}} F(\mathbf{y}) = \Phi_M(\mathbf{s}_m), \quad (3.13a)$$

$$\text{subject to: } \mathbf{h}(\mathbf{y}) = \mathbf{0}, \quad (3.13b)$$

$$\mathbf{g}(\mathbf{y}) \geq \mathbf{0}. \quad (3.13c)$$

We want to illustrate the basic idea of the solution based on this general formulation: For the solution, we use a Sequential Quadratic Programming (SQP) method, which solves a NLP iteratively; for one iteration step  $\mathbf{y}_k$  the large NLP is replaced by a quadratic programming problem (QP) problem. Its solution then determines the next iteration step  $\mathbf{y}_{k+1}$ , whereby a sequence of the form

$$\mathbf{y}_{k+1} = \mathbf{y}_k + \alpha \delta \mathbf{y}_k, \quad (3.14)$$

with the step direction  $\delta \mathbf{y}_k$  and the step length  $\alpha \in \mathbb{R}$  is obtained. A line search method is used as globalization strategy for determining the step length  $\alpha > 0$ . The step direction  $\delta \mathbf{y}_k$  is the solution of the following quadratic problem:

$$\min_{\delta \mathbf{y}_k} \nabla F(\mathbf{y}_k)^T \delta \mathbf{y}_k + \frac{1}{2} \delta \mathbf{y}_k^T \mathbf{B}(\mathbf{y}_k) \delta \mathbf{y}_k, \quad (3.15a)$$

$$\text{subject to: } \mathbf{h}(\mathbf{y}_k) + \nabla \mathbf{h}(\mathbf{y}_k)^T \delta \mathbf{y}_k = \mathbf{0}, \quad (3.15b)$$

$$\mathbf{g}(\mathbf{y}_k) + \nabla \mathbf{g}(\mathbf{y}_k)^T \delta \mathbf{y}_k \geq \mathbf{0}. \quad (3.15c)$$

The Hessian matrix  $\mathbf{B}$  of the Lagrangian function is usually approximated in practice, e.g., by a constant Hessian matrix, using the Gauss-Newton approximation or the (limited-memory) Broyden-Fletcher-Goldfarb-Shenno (BFGS) update method. This determination of the step direction  $\delta \mathbf{y}_k$  and SQP methods in general is motivated by applying the Newton method to the first-order optimality conditions (KARUSH-KUHN-TUCKER (KKT) conditions) of non-linear constrained optimization problems. Due to the multiple shooting approach and the chosen control discretization, the KKT matrix is sparse and very structured. Special condensing techniques make use of these structures and thus create much smaller and more compact QP problems [15] which can be solved by standard QP solvers, e.g., QPOPT [48].

For a complete and detailed description of the theory of OCPs and their solutions, we refer to the relevant textbooks, e.g., [47, 102].

All OCPs of this thesis are solved using the software package MUSCOD-II [15, 77], developed at the Interdisciplinary Center for Scientific Computing at Heidelberg University which has implemented the above described methods and procedures to solve OCPs. The large NLP resulting from the control discretization and state parameterization is solved by a specially tailored SQP method including condensing for the QP subproblems.

## 3.2 Inverse Optimal Control Problem Formulation

For the identification of optimization criteria in sprinting and long jump motions with and without RSPs, we make use of an inverse optimal control problem (IOCP). We establish potential basic optimization criteria and combine them into an objective function (3.4a) using weight factors. The central idea of the IOCP approach is then to determine the corresponding weights, which generate movements that are as similar as possible to the recorded reference movement. This is done by formulating a problem with an inner loop where the motion synthesis OCP (3.4) is computed and an outer loop where the weights are identified based on a

parameter estimation problem.

IOCP formulations have been mainly used for questions in robotics, e.g., navigation [2], arm movements [3], collaborative manipulation tasks [82] or transferring human motions on robots [23, 24, 96, 97]. Two main solution strategies exist: one can keep the bi-level formulation [23, 96, 97, 109] or achieve a one-level formulation by replacing the lower-level OCP (3.4) with its optimality conditions [2, 7, 52]. To compute the optimal weight factors  $\boldsymbol{\gamma}$  in this thesis, we apply a bi-level IOCP formulation consisting of two nested optimization problems:

$$\begin{aligned} \min_{\boldsymbol{\gamma}} \frac{1}{N_{\hat{\mathbf{x}}} N_{\hat{t}}} \sum_{i=0}^{N_{\hat{\mathbf{x}}}-1} w_i^2 \sum_{j=0}^{N_{\hat{t}}-1} \left( \Lambda(x_i^{(\boldsymbol{\gamma})}(\hat{t}_j)) - \hat{x}_{i,j} \right)^2 \\ + \frac{1}{N_h} \sum_{i=0}^{N_h-1} w_{i+N_{\hat{\mathbf{x}}}}^2 \left( h_i^{(\boldsymbol{\gamma})} - \hat{h}_i \right)^2 \end{aligned} \quad (3.16a)$$

such that  $\mathbf{x}^\gamma(t)$  and  $\mathbf{s}$  are determined by solving

$$\begin{aligned} \min_{(\mathbf{x}, \mathbf{u}, \mathbf{p}, \mathbf{h})} \Phi(\mathbf{x}(t), \mathbf{u}(t), \mathbf{p}, \mathbf{h}, \boldsymbol{\gamma}) \\ \text{s.t. constraint (3.4b)–(3.4f)}. \end{aligned} \quad (3.16b)$$

The reference data  $\hat{\mathbf{X}} = (\hat{x}_{i,j})_{i=0,\dots,N_{\hat{\mathbf{x}}}-1, j=0,\dots,N_{\hat{t}}-1}$  comprises  $N_{\hat{\mathbf{x}}}$  generalized position histories, which are evaluated at discrete points in time  $\hat{t}_j, j = 0, \dots, N_{\hat{t}} - 1$ . The latter are relative time points within each phase to make different phase durations possible. As reference data, we use the solutions of the dynamics reconstruction OCP as defined in Section 3.1.1 and discussed in Chapter 5 for 2D sprinting.

The bi-level IOCP formulates a parameter estimation problem for the unknown weights  $\boldsymbol{\gamma}$  on the upper level and a multi-phase OCP on the lower level. For a description of the latter, we refer to the previous section (Section 3.1.2). For balancing the different orders of magnitude and achieving a custom weighting in the parameter estimation problem, we introduce scaling factors  $w_i, i = 0, \dots, N_{\hat{\mathbf{x}}} + N_s - 1$  into the calculation of the differences between the reference curves and times and their calculated counterparts. Optimal solutions for a specific set of weights  $\boldsymbol{\gamma}$ , i.e., the solutions to the inner OCP are denoted by a superscript  $(\boldsymbol{\gamma})$ . The function  $\Lambda$  is introduced to project the state vector  $\mathbf{x}$  onto only a part of the vector which is necessary if reference data exists or should be used only for some part (e.g., only position variables  $\mathbf{q}$ ). The upper level optimization problem is solved using the derivative free method BOBYQA [110] of the NLOpt library [66]. The inner OCP problem is solved by MUSCOD-II [15, 77].



## **Part II**

# **Optimization-Based Comparison of Sprinting Motions with and without Running-Specific Prostheses**



## 4 Biomechanics and Modeling of Sprinting Motions with and without Running-Specific Prostheses

The Oxford Learner's Dictionary defines the verb 'to sprint' as 'to run [...] a short distance very fast'. Sprint races in common athletics competitions include 100 m-, 200 m- and 400 m-distances and consist of start, acceleration, constant velocity phases. For the 200 m- and 400 m-distances, the race also includes sprinting around curves. In addition, although not part of the actual race, the deceleration phase after crossing the finish line is crucial to finish the race safely. Running a short distance as fast as possible requires mobilizing all the strength for this short period of time. At this point, it becomes clear why the use of a running-specific prosthesis (RSP) with spring-like properties raises questions regarding comparability with non-amputee sprinters.

It is reasonable to assume that a sprinter in a competition will challenge himself to his own performance capabilities in terms of muscle strength, fatigue and velocity in order to complete the distance in the shortest possible time. In the literature, running velocity is commonly considered the product of step length and frequency [1, 63]. However, it is not clear which of the two criteria is decisive for maximum sprinting velocity. Salo et al. [116] reported that in elite sport it strongly depends on the individual athlete whether he achieves a high pace by a high step frequency, a large step length or a combination of both criteria. If one now considers sprinting movements with RSPs, it is evident that step length and step frequency must play a decisive role here as well: Weyand and Bundle [131] have observed higher step frequencies for bilateral transtibial amputee sprinting, which they attribute to short swing times due to the light carbon fiber prostheses. With regard to the step lengths of amputee athletes, Hobara and colleagues [63] found that they were shorter compared to non-amputee sprinters and consequently differences in performance could be observed. In another study on unilateral amputee sprinters, Hobara et al. [62] identified differences in the stiffness control between the two legs. In studies of the sprint start [27, 111], the authors found that the maximal step frequency is attained almost immediately in elite sprinting, while the step length increases gradually over the first steps. These findings suggest that for each running situation (start, acceleration, sprinting at maximum speed, curve sprinting, deceleration) there exists a specific combination of optimization criteria upon which the current movement is based. Indeed, various studies comparing amputee and non-amputee sprinters show that RSPs influence performance in sprint start [125, 127, 134] and curve sprinting [43]. Taboga and colleagues [127] as well as Strutzenberger and co-workers [125] found lower horizontal ground reaction forces during the first steps of the sprint race in the group of amputee athletes compared to non-amputee athletes. Willwacher et al. [134] attributed the reduced sprint start performance of the amputees to impairments in the transmission of force to the starting block due to the RSP. Yet, these results also mean that when assessing advantage or disadvantage due to the RSP, all phases of the motion to be judged must be analyzed and balanced.

Since the human body is a sophisticated and complex system, both with and without artificial limbs, it is quite conceivable that other criteria play a role in the generation of movement. Weyand and co-workers [132] have shown that fast and slow runners produce comparably

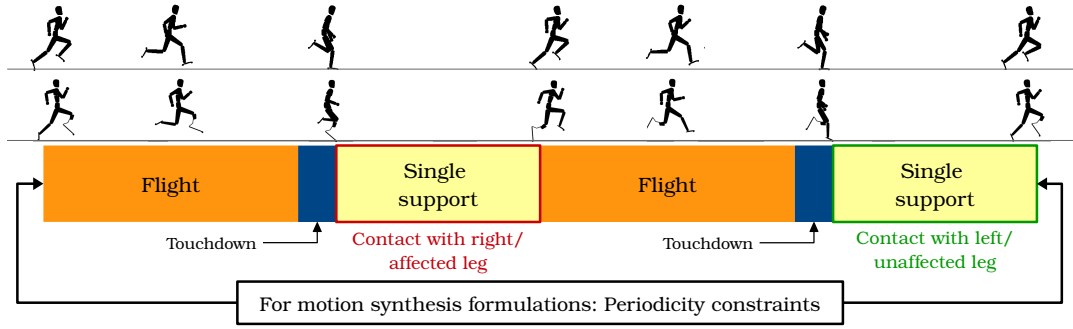


Figure 4.1: Phase description of the sprinting model. We model two full steps of sprinting at constant average velocity, each consisting of three phases.

large vertical impulses and thus also similar mean flight times. These are, however, caused by different combinations of the applied force and the stance time. Faster speeds are achieved by applying large forces in short contact times. Furthermore the angular momentum seems to play an essential role in sprinting. According to a study by Kugler and Janshen [73], the positioning of the body and thus the angular momentum are the decisive factors for the driving forces during the sprint start. Hinrichs [59] also points out the importance of the inverse relationship between upper and lower body angular momentum. Willwacher et al. [135] show that an insufficient compensation of angular momentum between upper and lower body leads to high free moments during the maximum velocity phase of sprinting. According to Mero and colleagues [88], an optimal combination of biomechanical variables (e.g., mechanisms of force production) and external factors (e.g., ground conditions, athletic shoes) is crucial for performance in sprinting competitions.

In this part, we analyze and compare the sprinting motions of amputee and non-amputee athletes based on the whole-body models described in Chapter 2 with respect to their kinematic and dynamic characteristics. As a basis we consider two steps at constant speed, i.e., after the sprinters have finished accelerating and reached their sprinting velocity. In order to be able to compare the movements, we have defined the footfall patterns sequence and the sequence of phases (compare Figure 4.1): The first step (called “Right Step” or “Affected step”) starts with the release of the left foot from the ground and ends with the release of the right foot/RSP from the ground. Therefore, it includes first a flight phase, then the touchdown of the right foot/RSP and the subsequent contact phase (“right contact”). The second step (also referred to as the “Left step” or “Unaffected step”) reflects the same phase sequence for the other side of the body and ends when the left foot comes off the floor. For a subset of problems, more precisely for all motion generating problems, periodicity constraints are inserted at the beginning and end of the two steps. Due to the one-sided amputation, we do not assume symmetry between the right and left side, so no periodicity is required after the first step. Within the framework of the optimal control problems (OCPs) from Chapter 3, the conditions for a physically correct ground contact are formulated by (in)equality constraints. Thus, the following conditions are introduced for the modeling of sprinting motion using the notation of ‘LH’ and ‘RH’ as the left and right hallux contact points, respectively:

**Gain of ground contact** As can also be seen in Figure 4.1, the touchdown is modeled as a separate transition phase. It is triggered when the  $z$  coordinate of the respective contact point touches the ground, i.e., when it becomes zero:

$$P_z^{LH/RH}(x(t)) = 0, \quad t \in \{t_1, t_4\}. \quad (4.1)$$

---

Furthermore, it must be guaranteed that the contact foot is firmly anchored to the floor and does not lift off again or travel along the floor. A possible formulation for this limits the vertical speed of the contact point:

$$-V_z^{LH/RH}(x(t)) \geq 0, \quad t \in \{t_1, t_4\}. \quad (4.2)$$

**During ground contact** To ensure that the contact point remains firmly on the ground throughout the contact phase, the vertical force is restricted to always be positive:

$$F_z^{LH/RH}(x(t), u(t)) \geq 0, \quad t \in \mathcal{T}_2 \text{ (right contact) or } t \in \mathcal{T}_5 \text{ (left contact)}. \quad (4.3)$$

**End of ground contact** Each contact phase ends and simultaneously each flight phase begins with the lifting of the corresponding foot, which occurs as soon as the vertical ground reaction force at the corresponding contact point vanishes:

$$F_z^{LH/RH}(x(t), u(t)) = 0, \quad t \in \{t_0, t_3, t_6\}. \quad (4.4)$$

Additional constraints might be added for the different OCPs, depending on what the solutions aims for.

Based on this modeling, we applied all three problem formulations as presented in Chapter 3 to human sprinting movements. In this part, we will examine the results and analyze the movements in detail, both in terms of differences between reconstructed and simulated movements and in terms of those between non-amputee and amputee athletes.

First, we will present the dynamics reconstruction (Chapter 5). Subsequently, generated motions based on ten different optimization criteria will be analyzed and compared with the reconstructed solutions (Chapter 6). Finally, the weighting of these criteria is examined by means of an inverse optimal control problem (IOCP) (Chapter 7), where the goal is to find out the combination of criteria underlying the actually measured motion.



## 5 Dynamics Reconstruction of Sprinting Motions with and without Running-Specific Prostheses

As a basis for reconstructing the dynamics of sprinting movements, we selected one motion capture trial of an amputee athlete and one motion capture trial for each of three non-amputee athlete. The details of the motion capturing which was not part of this work and the extraction of the reference positions and joint angles are described in Section 1.4. The dynamics reconstruction was done first in the sagittal plane with a *2D model* and then in all three dimensions with a *3D model* (cf. Section 2.2). For each athlete, we thus created a subject-specific multi-body model based on the total heights and masses given in Table 1.1 with varying number of degrees of freedom (DOFs) depending on whether it was used in two or three dimensions. For all athletes and both two-dimensional and three-dimensional cases, the least squares optimal control problem (OCP) was formulated as described in Section 3.1.1, using the respective motion capture trial as a reference.

The following analysis brings together the results and discussions presented in [33, 35, 68] and adds cross-cutting observations. In the following analysis we will first examine the kinematic precision and a validation of the reconstructed solutions for both the two-dimensional and three-dimensional models (Section 5.1). We will conduct the subsequent discussion of the characteristic variables for sprinting based on the solutions of the three-dimensional solution, splitting it into a sagittal plane part (which complies with reconstructed solutions of the two-dimensional models) and a part discussing frontal and transversal plane motions (Sections 5.2 and 5.3). We summarize the crucial findings in the concluding section and discuss for which questions the three-dimensional models provide additional insights (Section 5.4).

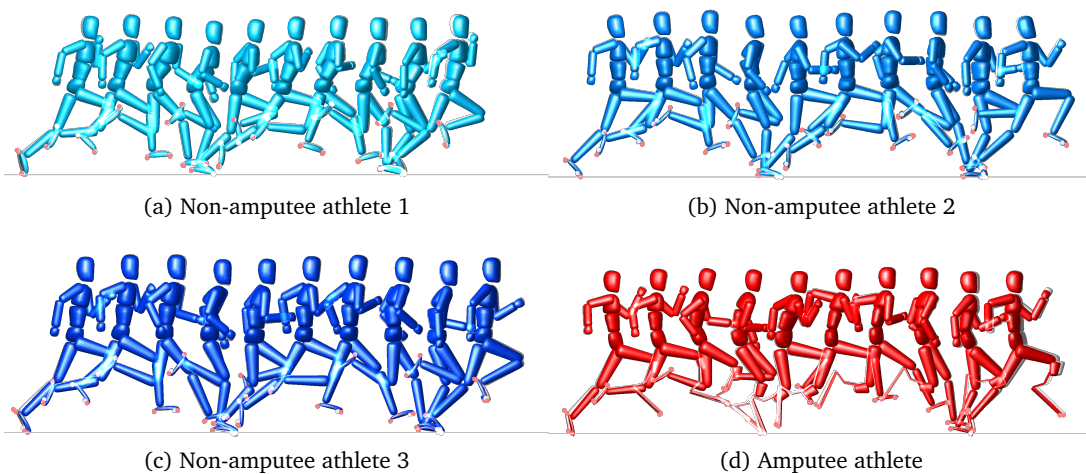


Figure 5.1: Animated sequences visualize the solutions of the sprinting dynamics reconstruction optimal control problem using the 3D models. The colored models show the reconstructed sprinting motions, the grey models in the background show the respective reference movements.

Table 5.1: Rotational and translational root-mean-square errors (RMSEs) between reconstructed and reference motions for the reconstructed sprinting motions. The results are given for the 2D and 3D models of three non-amputee athletes (NA1, NA2, NA3) and one amputee athlete (A). The upper row gives the RMSEs for the translational degrees of freedom (DOFs), the lower row the ones for the rotational DOFs.

	NA1		NA2		NA3		A	
	2D	3D	2D	3D	2D	3D	2D	3D
Trans (cm)	0.898	0.359	0.672	0.479	1.677	0.417	1.791	0.712
Rot (rad)	0.006	0.010	0.009	0.004	0.024	0.005	0.034	0.010

As a reminder, we refer to the point of greatest curvature of the running-specific prosthesis (RSP) when we address the ‘prosthetic ankle joint’ or the ‘ankle of the prosthetic leg’, respectively, in the following analysis.

Figure 5.1 shows both the reconstructed (solutions of the OCP; colored models) and the reference movements (grey models in background). The animated sequences are generated using the 3D models.

## 5.1 Analysis of the Reconstruction Quality

To evaluate the quality of the dynamic reconstruction, we consider three things: first, we examine the precision of the kinematic reconstruction, that is, how well the reconstructed positions and joint angles reproduce those of the reference motions. Then, we use the measured ground reaction forces and literature values for the joint torques to validate the reconstructed solution.

### 5.1.1 Kinematic Precision of the Reconstructed Solutions

For each DOF, we computed the root-mean-square error (RMSE) between the reconstructed and the reference motions via

$$RMSE = \sqrt{\frac{1}{n_q m_n} \left( \sum_{k \in \mathcal{I}_{DOF}} \sum_{j=0}^{m_n} (q_k^{OCP}(\hat{t}_j) - q_k^{MC}(\hat{t}_j))^2 \right)}, \quad (5.1)$$

where  $q_k^{OCP}$  and  $q_k^{MC}$  are the reconstructed and reference generalized positions of the respective DOF, respectively. We distinguish between translational and rotational DOFs which is taken care of by introduction of the set of indices  $\mathcal{I}_{DOF}$ . We normalize by the number of multiple shooting nodes  $m_n$  and the number of DOFs  $n_q = |\mathcal{I}_{DOF}|$ . The RMSEs are listed in Table 5.1 for both 2D and 3D models.

The solution of the least squares OCP matches the reference motions very well, with RMSEs of less than 1.8 cm for the translational and less than 0.035 rad ( $\approx 2^\circ$ ) for the rotational DOFs. At this point it must be noted again that the above mentioned errors only refer to the deviations between reconstructed motion and reference motion; additional errors to the real motion are caused by measurement errors and the transfer of the motion capture data to the respective model. As already described in Section 1.4, the reference motion can be non-physical to a certain extent, for example, the foot can penetrate the ground. In the OCP we exclude such non-physical behavior with the help of the constraints. The resulting necessary displacements lead to deviations in the individual generalized joint positions and make up the main part of the RMSEs. Relative to the motion range of the generalized positions, the RMSEs are in a

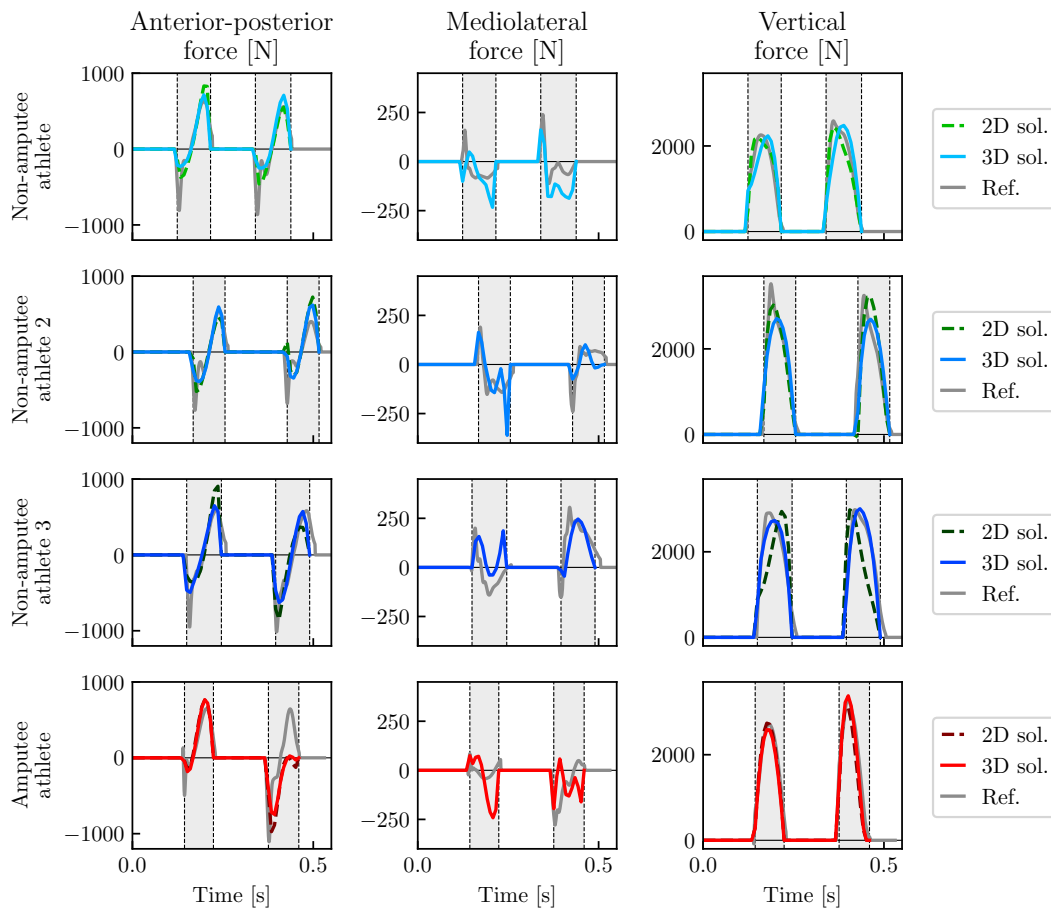


Figure 5.2: Anterior-posterior (TX), mediolateral (TY) and vertical (TZ) ground reaction forces of the reconstructed two-dimensional and three-dimensional sprinting motions. For each athlete (first row: non-amputee athlete 1, second row: non-amputee athlete 2, third row: non-amputee athlete 3, fourth row: amputee athlete), we compare the computed forces (labeled ‘2D sol.’ for the reconstruction using the 2D model and ‘3D sol.’ for the one using the 3D model) and the filtered measured forces (labeled ‘Ref.’). The grey regions show contact phases where the first contact occurs with the right/affected leg and the second contact with the left/unaffected leg as shown in the phase order in Fig. 4.1.

very good order of magnitude. It is noticeable that the RMSE for the 3D model is on average smaller than for the 2D model. We attribute this to the fact that in the two-dimensional case the motion capture data had to be projected onto the sagittal plane, which possibly resulted in slightly less physical reference movements. This is particularly evident in the joints of the upper extremity and spine, since the upper body moves more in the transversal and frontal planes during sprinting than the lower body. Overall, however, the curves of the 2D and 3D models correspond in the sagittal plane. For sake of completeness, we show the RMSEs for the individual joints for all four athletes in the appendix (Figures A.1 and A.2). In the appendix, we further give diagrams with the generalized positions of both the reconstructed and the reference motions for the 2D and 3D models of all four athletes (Figures A.3 and A.4).

### 5.1.2 Validation of Reconstructed Ground Reaction Forces

Figure 5.2 compares the ground reaction forces, which once come from the OCP reconstruction (for both the 2D and the 3D model) and once from the filtered force plate data. Each row shows

the ground reaction forces of one athlete, ordered as NA1, NA2, NA3, A from top to bottom and forces in x-, y- and z-directions from left to right. Overall, the curves of the ground forces correspond well: In the case of the anterior-posterior forces (TX), all models first generate a braking force and then a propulsion force. The timings of the transition between the braking and the propulsive component also match. The models generate parabolic vertical forces (TZ), which is consistent with the measured curves and the literature [22, 46]. However, there are also three observations where the models cannot reproduce the measured data completely:

1. The model of the non-amputee athlete 2 does not show the measured strong increase in vertical force (TZ).
2. The forward component of the anterior-posterior ground reaction forces (TX) is partly over- or underestimated, especially during the second contact. In the case of the amputee model, the propulsive component could not be reconstructed at all during the second contact phase (unaffected foot).
3. In the case of the mediolateral ground reaction forces (TY) the reconstruction follows only roughly a similar course as the measured data.

As an explanation for this deviation of the models from the measured data, we can think of three reasons: It is possible that artifacts in the measurements lead to these deviations. Furthermore, it is a plausible assumption that our rather simple modeling of the ground contact by a foot model with one fixed contact point per foot is responsible for such deviations, since the contact point moves along the hallux for real sprinting movements. This might be especially the case for the third item in the above list of observations. Furthermore, it cannot be excluded that the regularization term in the objective function (3.3a) contributes to the first and second effect. We have introduced the weight factor  $\gamma_u$  for regularization. Thus, the goal of this contribution to the objective function is to eliminate peaks in order to produce a smoother solution. Although the weighting factor  $\gamma_u$  was chosen with great care to avoid a strong influence on the solution, this regularization term still assumes that a (given) motion is executed in the most efficient way.

### 5.1.3 Validation of Reconstructed Joint Torques

Our modeling approach summarizes the action of all muscles at a joint by torque actuators; thus, the individual contributions of the antagonist and agonist muscles cannot be calculated. Therefore, all computed torques are net torques. With our approach to reconstruct the dynamics of motions, these external net joint torques can be calculated without residual forces from the kinematic data alone. To show that this approach produces realistic torques, we compare the calculated torques of the non-amputee athletes with those obtained for non-amputee sprinting in the literature [14, 118, 124]. As far as we know, there are no publications yet that have measured the torques of sprinters with unilateral below the knee amputation (BKA). Therefore, we will qualitatively compare the calculated torques of the amputee athlete with those for bilateral below-knee amputee sprinting [18]. The computed torques for both the non-amputee and amputee athletes are shown in the diagrams of Figures 5.3 (sagittal plane) and 5.4 (frontal and transversal planes).

Bezodis and colleagues [14] and Stafilidis and Arampatzis [124] have studied sprinting movements for velocities ranging from  $9.06 \text{ m s}^{-1}$  to  $10.37 \text{ m s}^{-1}$ . Using a standard inverse dynamics approach, they calculated the sagittal moments of the legs during the stance phase of the sprinting motion. We compare their data with the calculated torques obtained for the contact phase. Except for the peak at the beginning of the contact phase, which Bezodis et al. [14] describe,

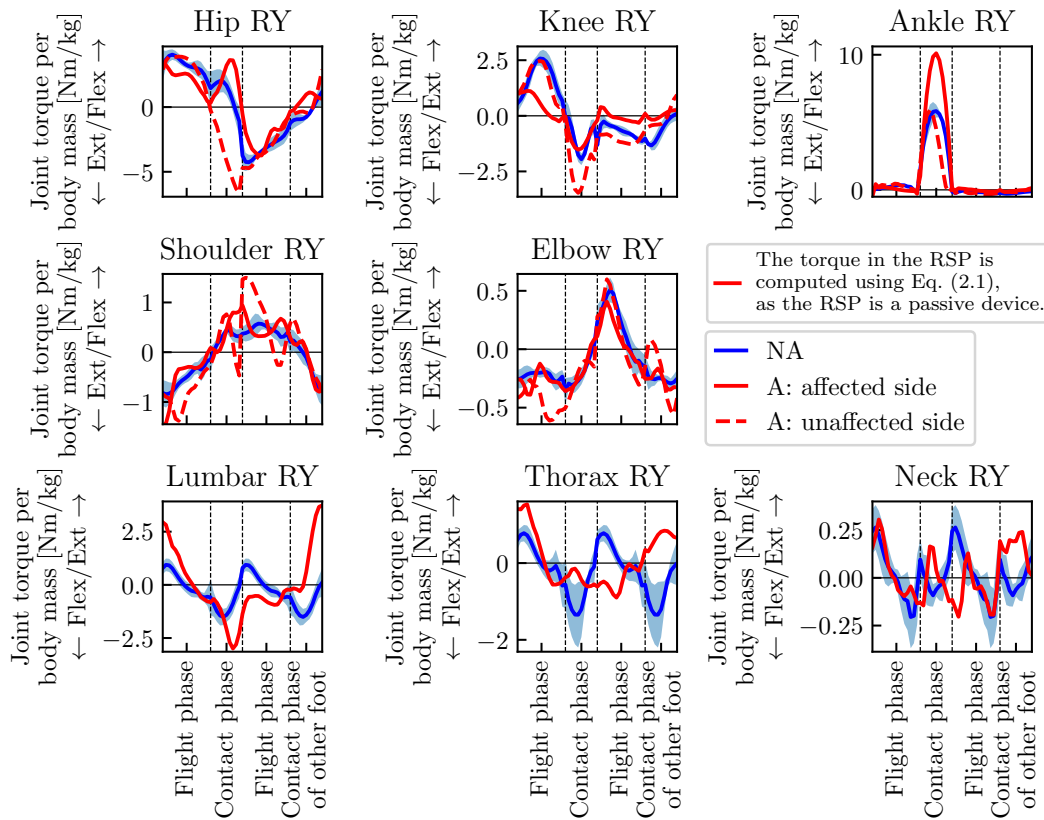


Figure 5.3: Sagittal plane joint torques of the amputee athlete (‘A’) and the non-amputee reference group (‘NA’) for the reconstructed sprinting motions. Phase durations are scaled for comparability and joint torque values are normalized by body mass. The abbreviations ‘Flex’ and ‘Ext’ denote the directions of flexion and extension, respectively.

both the magnitude and the trend from external flexion to external extension torques are consistent for the hip joint torques. For the knee joints, our calculations yield values of  $1 \text{ N m kg}^{-1}$  for the maximum extension torque and  $3 \text{ N m kg}^{-1}$  for the maximum flexion torque. They thus cover a comparable range to the torques specified in [14, 124] ( $\pm 2.5 \text{ N m kg}^{-1}$  as maximum values for extension and flexion torque). For the ankle joint we have calculated peak external flexion torques of approximately  $5 \text{ N m kg}^{-1}$ . These torques, as well as the course of the curve, are consistent with the results in the literature provided. Stafilidis and colleagues[124] further reported transversal and frontal moments for knee and ankle joints. Our models have only one DOF per knee (RY) and two DOFs per ankle (RY, RZ); hence, we can only compare the transversal ankle moment where the order of magnitude matches the data reported by Stafilidis et al. However, their data suggests that the remaining moments are rather small and we do not lose much by the simplifications of the model. In addition to comparable torques during the contact phase, Schache and colleagues[118] also calculated torques during the swing phase for sprinting at  $(8.95 \pm 0.70) \text{ m s}^{-1}$  in all three planes. These are comparable to the swing phase torques calculated with our approach.

The comparison of the torques of the affected leg of the one-sided amputee with the values reported by Brüggemann and colleagues[18] for athletes with bilateral below-knee amputation shows that these torques are of the right order of magnitude for the amputee sprinter as well. It is noticeable, however, that although the order of magnitude fits in the hip joint, the curves differ significantly. This can probably be explained by differences between unilateral

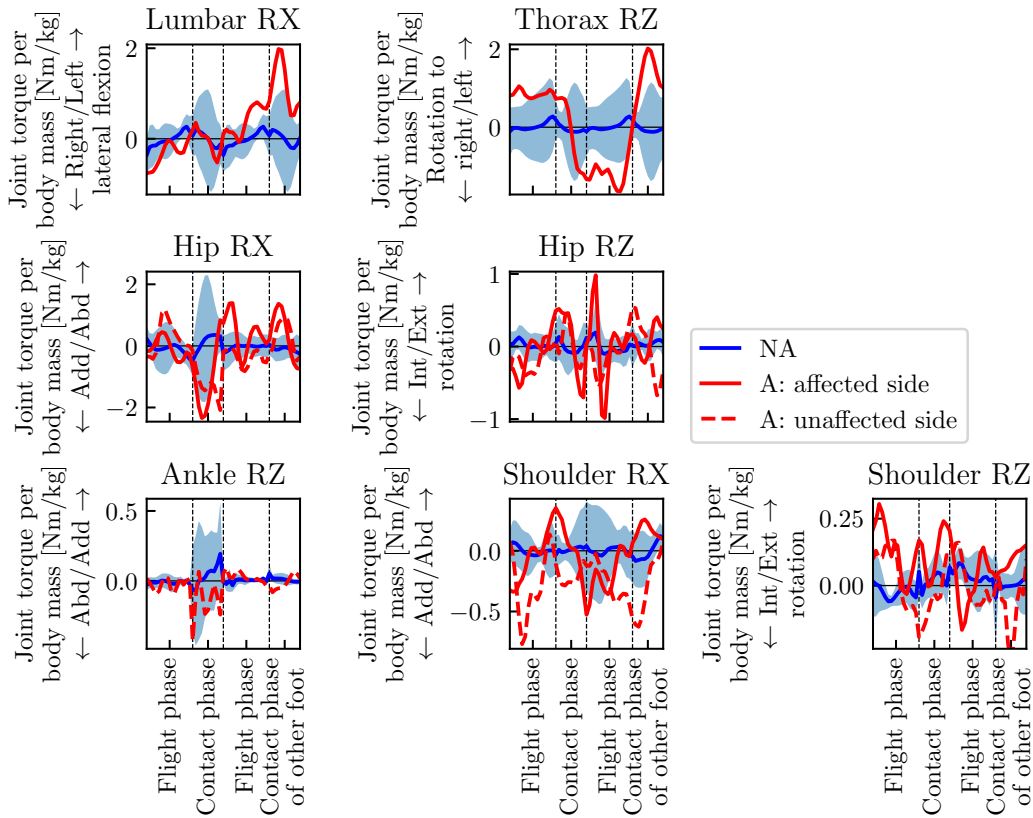


Figure 5.4: Frontal and transversal plane joint torques of the amputee athlete ('A') and the non-amputee reference group ('NA') for the reconstructed sprinting motions. Phase durations are scaled for comparability and joint torque values are normalized by body mass. The abbreviations 'Abd', 'Add', 'Int' and 'Ext' stand for 'Abduction', 'Adduction', 'Internal' and 'External', respectively.

and bilateral amputee sprinters in terms of lower limb weight and leg stiffness[86]. It is also noteworthy that the maximum flexion torque in the prosthetic ankle joint of the unilateral amputee is approximately  $11 \text{ N m kg}^{-1}$  according to our calculations. Brüggemann et al.[18] have estimated a value of approximately  $6.5 \text{ N m kg}^{-1}$  for bilateral amputees. Of course, it should be noted that in the two studies, both the actual prosthesis models used and the modeling of the prostheses in the computer models differ. The difference may also be due to the lower limb asymmetry of the unilateral amputee.

In summary, a further analysis is reasonable, since the fit errors are rather small, the calculated ground reaction forces correspond to those measured and the calculated torques are also comparable to literature values.

## 5.2 Analysis of the Curves of Characteristic Variables

We did not set the spring and the damping constants  $k$  and  $d$  of the RSP to a certain value for the solution of the OCP. The spring constant was a free parameter and the damping constant was computed based on the value of the spring constant using Eq. (2.2). The reconstructed values differ slightly between the 2D and 3D models: they are found to be

- $k = 2851.5 \text{ N m rad}^{-1}$  and  $d = 5.78 \text{ N m s rad}^{-1}$  in the case of the 2D model and

Table 5.2: Phase durations for the sprinting motions of the amputee athlete and the non-amputee reference group. The phase numbering corresponds to the order shown in Figure 4.1.

Phase	Non-amputee athletes	Amputee athlete
First flight phase	$(0.147 \pm 0.012) \text{ s}$	0.144 s
First contact phase (with right/affected leg)	$(0.092 \pm 0.002) \text{ s}$	0.080 s
Second flight phase	$(0.149 \pm 0.012) \text{ s}$	0.152 s
Second contact phase (with left/unaffected leg)	$(0.093 \pm 0.002) \text{ s}$	0.084 s

- $k = 2649.4 \text{ N m rad}^{-1}$  and  $d = 5.57 \text{ N m s rad}^{-1}$  in the case of the 3D model.

The individual phase durations differ between the athletes. The phase durations are set to fixed values in the OCP, which were determined by manually registering the touchdown and take-off times in the animated reference sequences. The measurement data of the force plates were used for verification. Table 5.2 shows the phase durations of the amputee athlete and the control group of non-amputee athletes. While the flight phases are of comparable length, the amputee athlete has significantly shorter contact times. This means that the total time for one step is shorter for the amputee than for the non-amputee reference group. This means that the amputee athlete has a higher step frequency. Since the individual phase durations of the athletes do not coincide, we have normalized each phase for all diagrams comparing amputee and non-amputee sprinting.

Instead of comparing the individual values and curves of the three non-amputee athletes to the amputee athlete, we want to use the mean and standard deviation of the three of them. It is an intuitive assumption that non-amputee athletes show a symmetrical gait. Furthermore, it is not a priori clear that the right side of the amputee's body has to be compared with the right side of the non-amputees just because they coincide coincidentally. It thus might be a good idea to compute mean values of both steps of the three athletes, taking into account the phase shift for joints involved in both body sides.

**Symmetry analysis of kinematics and dynamics** We start our analysis with studying the (a)symmetry between the two steps, both for the non-amputee group and the amputee athlete. Figure 5.5 depicts the absolute differences in the generalized positions between the two sprinting steps. For the computation of the differences, we subtracted the curves of the positions and joint angles of the second step from the first step, taking into account the phase shift for right and left joints. Hence, the results show one airborne and one contact phase. For the non-amputee athletes, we show the individual curves (dotted lines) along with the mean and standard deviation (solid line with shaded region around this line). Figure 5.5 depicts the absolute differences in the generalized positions. A value close to zero means great symmetry; we can thus consider the graphs as a measure of the symmetry of the sprinting motion. As expected, the diagrams clearly reveal the inter-limb asymmetry of the amputee athlete. If we look at the figures as a whole, it is immediately apparent that the values of the non-amputee group of reference athletes are much closer to zero than those of the amputee athlete. Therefore, the non-amputee athletes run in a much more symmetric style than the amputee athlete. Since the absolute deviations between the two steps are also rather small for the mean value of the reference group of the non-amputee athletes, our above assumption is justified.

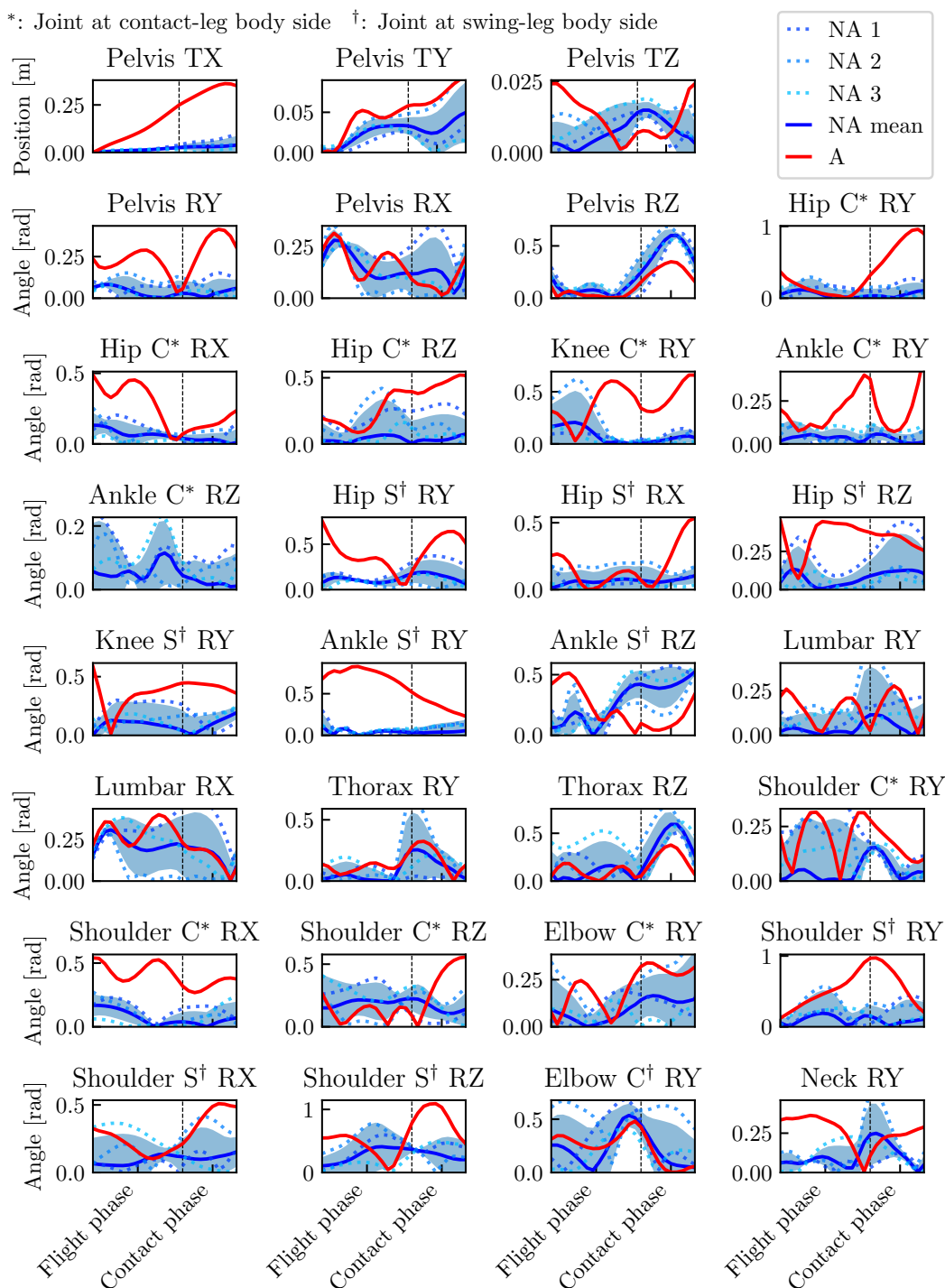


Figure 5.5: Amount of asymmetry in the generalized positions between the two steps of the amputee athlete (‘A’), the non-amputee reference group (‘NA mean’) and the three individual non-amputee athletes (‘NA1’, ‘NA2’, ‘NA3’). The differences were calculated by subtracting the second step trajectories from the first step trajectories, taking into account shifts between left and right side joints. We show the absolute differences such that a value of 0 describes a perfectly symmetric motion. Phase durations are scaled for comparability.

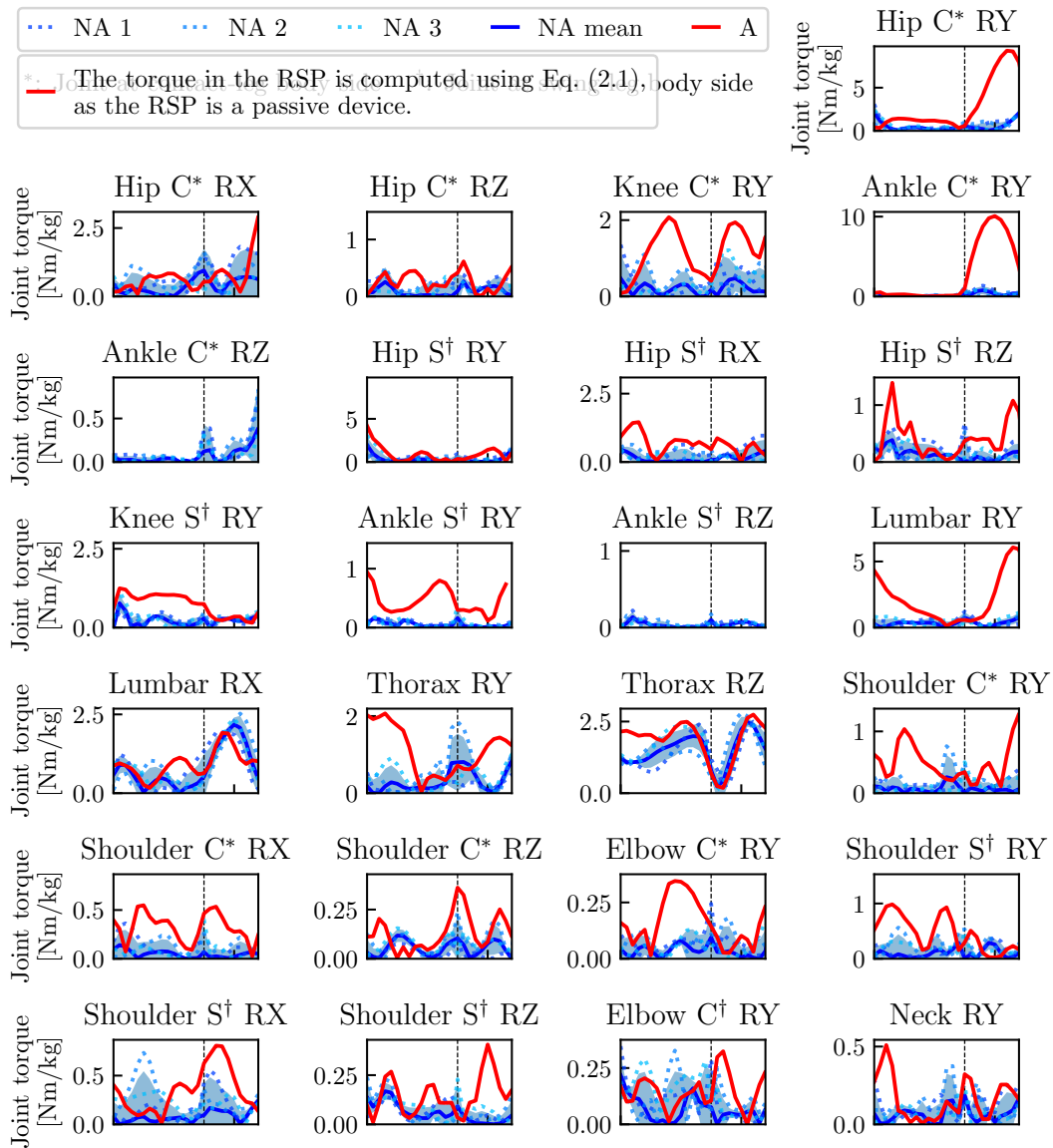


Figure 5.6: Amount of asymmetry in the joint torques between the two steps of the amputee athlete (‘A’) and the non-amputee reference group (‘NA mean’) and the three individual non-amputee athletes (‘NA1’, ‘NA2’, ‘NA3’). The differences were calculated by subtracting the second step trajectories from the first step trajectories, taking into account shifts between left and right side joints. We show the absolute differences such that a value of 0 describes a perfectly symmetric motion. Phase durations are scaled for comparability. Joint torques are normalized by body mass. The joint torque in the prosthetic ankle is passively produced and computed via Eq. (2.1).

Nevertheless, it is interesting that the non-amputee athletes also show considerable asymmetries between the two steps. The large standard deviation regions for some joint angles indicate that the three athletes in the non-amputee reference group do not run as symmetrically as one might expect in view of the comparatively symmetrical human body. This is probably due to individual differences in mass, length and muscle strength of the different body segments and the fact that most people have a ‘strong side’. In comparison with the amputee athlete, the difference in the forward movement and the segments of the lower extremity is particu-

larly striking. Let us first look at the translational DOFs of the floating base segment which is the pelvis segment: The absolute differences are about three and a half times larger for the amputee athlete than for the mean of the non-amputee athletes. At the end of the step, the amputee athlete has a difference of about 30 cm in the forward direction distance (Pelvis TX). This means that the pelvic segment of the amputee athlete covers a greater distance during the step following contact with the RSP than in the other step. If we add the step length information from Table 5.3, we notice that the difference in step length is only half of this value (15 cm). This observation fits in with the fact that the step following the prosthetic contact has a flight duration that is 8 ms longer. There is a considerable difference in how the amputee athlete aligns his overall position in terms of foot contact points compared to the non-amputee athletes.

We find symmetry values that are more than twice as large for comparing the rotational DOFs of the amputee athlete with those of the non-amputee reference group. Here, the differences between the two steps are especially pronounced in the joints of the legs and arms. The sagittal plane motion of the hips and the motion of the knees during contact differ a lot between the steps with prosthetic and biological leg contacts. The asymmetry in the arms which are on the body side opposite to the affected leg (labeled ‘swing-side’) suggests that the amputee employs his arms for inter-limb asymmetry compensation.

Figure 5.6 shows the absolute differences in the joint torques between the two steps. The torque in the prosthetic ankle is computed via Eq. (2.1) and is passively produced. If we consider all joints together, the amount of asymmetry in the torques of the amputee athlete is three times as big as in the ones of the non-amputee athletes. For almost all joints, it is significantly larger compared to the control group. In addition to the fundamentally different actuation strategy of amputee athletes compared to non-amputee sprinters (which e.g., has already been described in studies for bilateral transtibial amputee sprinters [18, 133]), the unilateral amputee athlete thus also has to adapt the actuation pattern for each of his steps, depending on whether the next contact will occur with the prosthetic or biological foot. Such an actuation strategy with very different and sometimes large torques (see sections on torques in Sections 5.2.1 and 5.2.2) could potentially increase the risk of fatigue or injury in affected joints.

Although, we found some non-negligible asymmetry in non-amputee sprinters as well, we consider the argument that it would be somewhat arbitrary to compare the right side of the amputee with the right sides of the non-amputee athletes as more decisive. Hence, the curves of the left side of the body were shifted in such a way that the contact phases of the corresponding side of the body were superimposed. For the non-amputee athletes, we then computed the mean and standard deviation of both legs and all three athletes which are represented by a solid line and shaded regions around it. In the analysis, we will never refer to the individual non-amputee athletes, but always to this mean value when referring to the non-amputees or the non-amputee control group. For the amputee athlete, we show the curves for both body sides, if necessary (which is in the case of the hip, knee, ankle, shoulder and elbow joints). The curves of the side not affected by the amputation are represented by a dashed and all other ones by a solid line.

**Ground reaction forces and center of mass movement** With regard to the analysis of sprinting movements, the ground reaction forces and the center of mass (CoM) movement are interesting. They are shown in Figure 5.7. For the non-amputees, the propulsive and braking components are similarly large, indicating a forward movement at approximately constant speed. This is also evident in the forward velocity of the CoM (see CoM velocity TX). The situation is significantly different for the amputee athlete: During contact with the RSP, the driving component is significantly stronger than the backward driving component, so that he

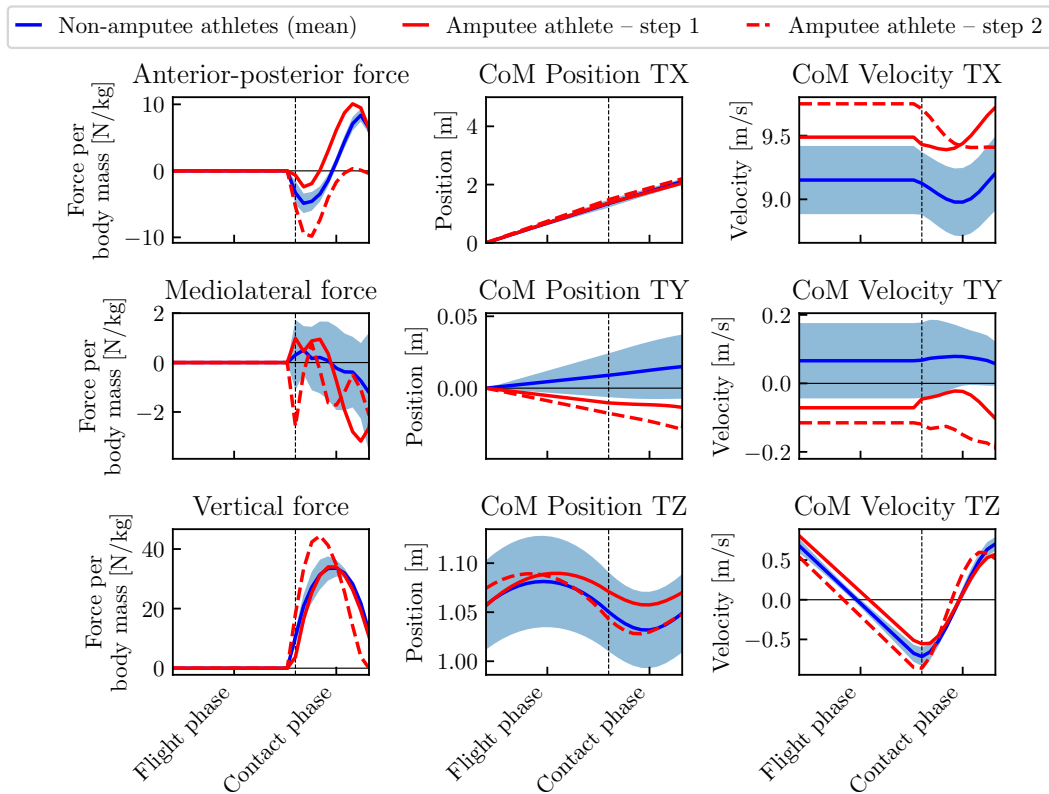


Figure 5.7: Ground reaction forces, center of mass (CoM) positions and velocities of the amputee athlete ('A') and the non-amputee reference group ('NA') for the reconstructed sprinting motions. Phase durations are scaled for comparability.

gains forward velocity through contact. For contact with the biological leg, the opposite is true: there is no propulsive force, which is also clearly evident in the loss of velocity of the forward component of the CoM (see CoM velocity TX). Part of this behavior may be due to the problem formulation, since it is possible that at the end of the time horizon an unfavorable part of the objective function dominates, which promotes this behavior of CoM velocity and force. This is also indicated by the premature flattening towards zero of the vertical ground reaction force at the end. Here it would be interesting to analyze a further flight phase following the second step. Nevertheless, it can be clearly stated that the vertical ground reaction forces of both legs of the amputee athlete are higher than those of the non-amputee athlete. Of particular interest is the increased ground reaction force in the amputee's biological leg, which is  $10 \text{ N kg}^{-1}$  (30%) higher than that of the non-amputee athletes, since it could be assumed that the amputee uses his RSP during the first step to achieve the same running speeds with less effort. In fact, however, the amputee applies more force in less time (remember: phase durations are normalized) to run at comparable speeds. As described above, the amputee's forward velocity increases during contact with the prosthetic leg. However, during this phase he may generate less vertical speed than the reference group of non-amputee sprinters. Interestingly, the course of the horizontal CoM position is rather similar for both steps of the amputee athlete and also for the non-amputee reference group. In the vertical component of the CoM, the amputee's CoM is always higher than the average of the non-amputee athletes, probably due to the geometry of the RSP, which promotes "tip-toe" running.

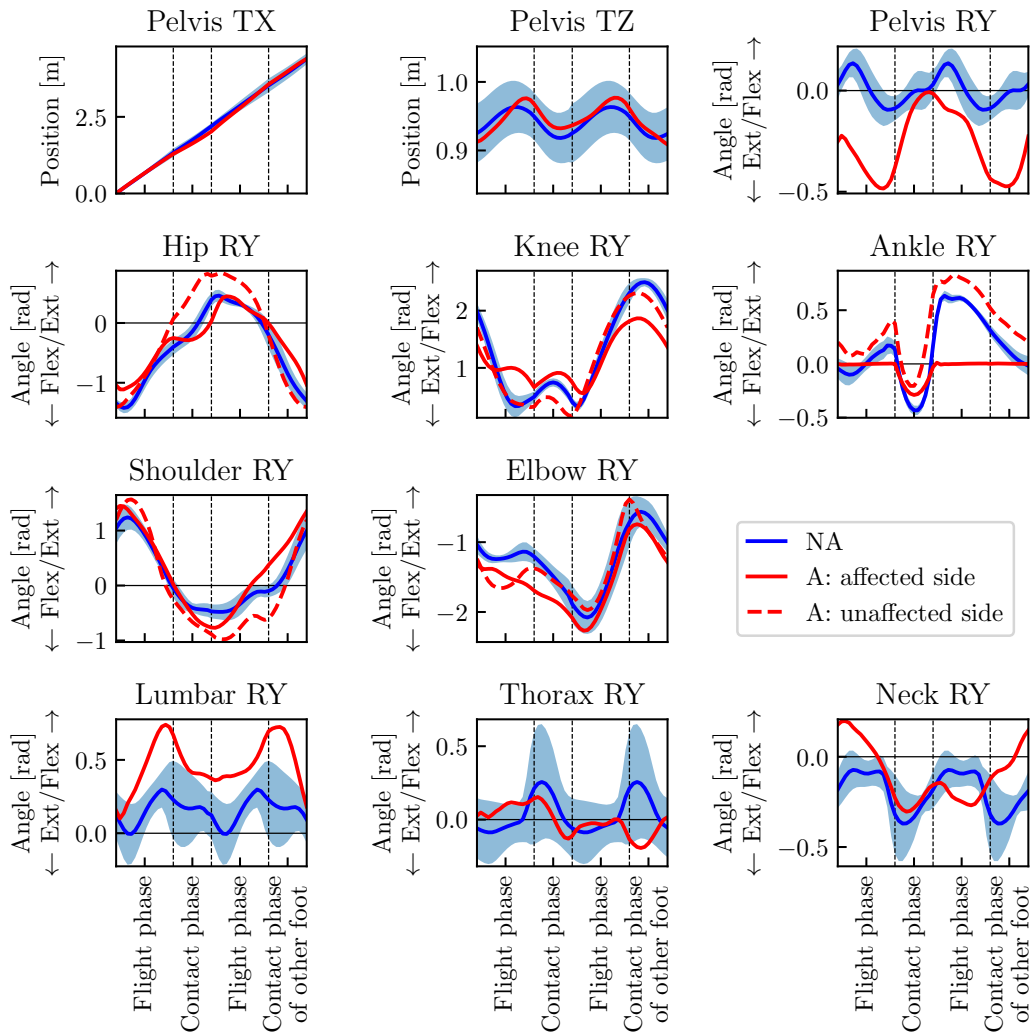


Figure 5.8: Sagittal plane generalized positions of the amputee athlete ('A') and the non-amputee reference group ('NA') for the reconstructed sprinting motions optimal control problem. Phase durations are scaled for comparability. The abbreviations 'Flex' and 'Ext' denote the directions of flexion and extension, respectively.

### 5.2.1 Sagittal Plane Movements

**Overall position and joint angles** Figure 5.8 shows the curves of the pelvis positions and the joint angles in the sagittal plane. As we have seen, the total duration of a step is shorter in the case of the amputee athlete than in the control group. For the distance he covers during this time in the forward direction (see diagram 'Pelvis TX'), the amputee's line is within the standard deviation of the non-amputee control group. Therefore, it follows that the amputee athlete runs at a faster velocity. His average running velocity is  $9.55 \text{ ms}^{-1}$ , while that of the non-amputee athletes is  $(9.14 \pm 0.33) \text{ ms}^{-1}$ . The vertical motion over the course of the sprinting is likewise similar for all athletes (compare diagram 'Pelvis TZ'). Nevertheless, it is noticeable that the curve of the amputee athlete is almost always slightly above the mean value of the non-amputee reference group.

As one might have expected, the greatest differences between amputee and non-amputee sprinters are found in the joints of the legs (hip, knee, ankle). The differences between the

side affected by the amputation and the side not affected also become very clear. In the hip, amputee and non-amputee athletes show a similar range of motion, both in terms of flexion and extension of the joint. The amputee actually moves the unaffected hip in a similar way to the non-amputee athletes, but with a greater range of motion. The course of movement on the side of the amputation also looks similar. However, it is noticeable that the maximum extension is reached much later: While for the non-amputee athletes the maximum extension is reached at the end of the contact phase, it is reached on the affected side of the amputee at a later point in time, around the middle of the flight phase. The differences in the knee and ankle joints are even more pronounced, as they are evident in both legs. In the case of the amputee athlete, we find significantly less flexion and extension in the knee on the affected side. On the non-affected side, especially the flexion during the contact phase is significantly lower than in the non-amputee control group. Brüggemann et al. have already observed such reduced knee flexion in bilateral amputee sprinters [18]. The significant difference in flexion of the ankle joint and prosthetic ankle must be considered with caution, as a direct comparison is not possible due to the geometric differences between the RSP and the biological foot.

Similar differences between the unilateral amputee athlete and the non-amputee athletes can also be seen in the joints of the arms. The range of motion in the shoulder joints of the amputee athlete is significantly greater than in the non-amputee comparison group. This greater range of motion may indicate the need to compensate for the asymmetry between the two legs, particularly in terms of weight and stiffness, and to make increased use of the arms to reach sprinting velocity.

Finally, if we look at the spinal joints, it is noticeable that the amputee athlete mainly moves the lower spine (pelvis, lumbar) and neck more, but shows very little movement in the upper body (thorax). In the non-amputee reference group, the movements are more strongly distributed over all joints. Overall, it appears that the amputee athlete has a more upright running style.

**Joint torques** Figure 5.3 shows a comparison of the joint torque curves of the amputee athlete and the non-amputee control group over time. For better comparability, the torques were normalized using the total body mass. Significant differences in the torques in amputee and non-amputee sprinting are apparent. Apart from the joint torques of the hip joint during the contact phase, the joint torques of the affected leg of the amputee athlete are generally (significantly) lower than those of the control group. It is interesting that the hip torque remains a flexing torque during contact, while the non-amputee hip torque already turns into an extension torque within the phase. This may be necessary to bring the body forward during contact and compensate for the different geometry of the affected leg and the small flexion torque in the knee joint. One possible explanation for this significantly lower torque in the amputee's knee could be the fact that the knee is affected by the amputation as well. Nevertheless, studies [44, 45] suggest that athletes with an amputation below the knee use a strategy that makes optimal use of the spring-like properties of the RSP by reducing external sagittal plane knee moments. The RSP is a passive component. This means that in our model there is no torque actively generated by torque actuators (cf. Section 2.3). Therefore, we calculated the passive torque acting on the RSP using Eq. (2.1) and included it into the diagram by a green line. We use the results of the OCPs for the spring and damping constant. It is noticeable that the torque generated by the RSP is approximately twice as high as the torque in the biological ankles (both for the amputee athlete and the non-amputee control group). If we look at the geometry of the RSP, this can be quickly understood: large torques are produced by similar ground reaction force profiles due to the long lever arm resulting from the length of the RSP. The torques applied by the torque actuators in the biological leg of the amputee athlete are on average clearly larger than those of the non-amputee control group, especially in the knee

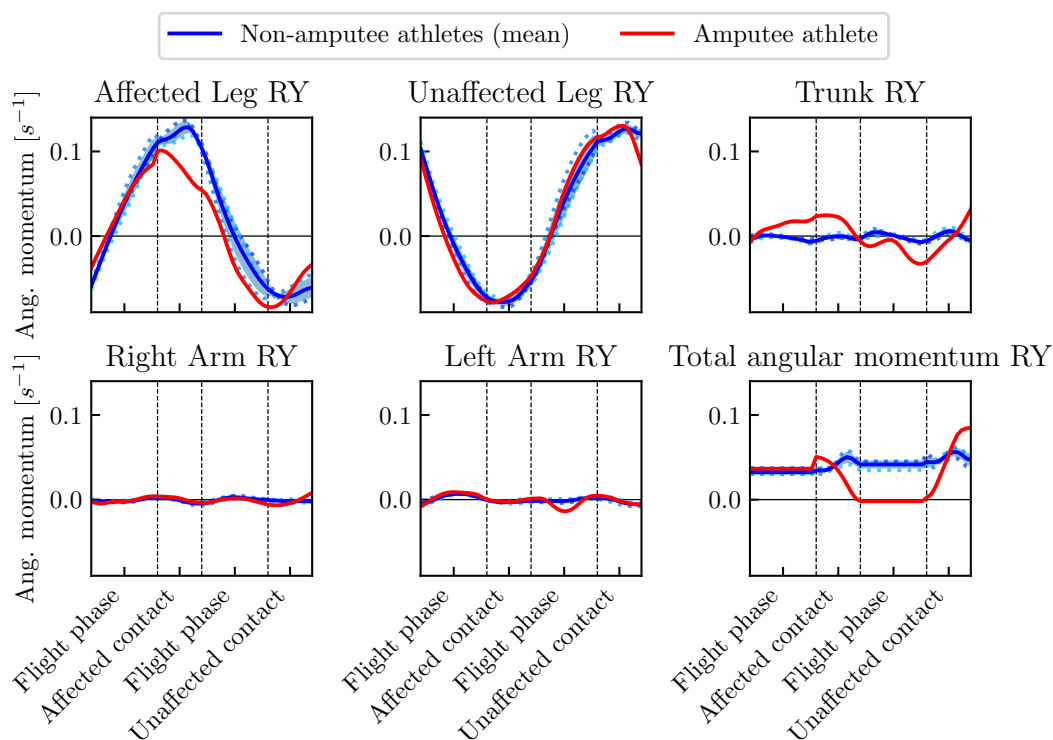


Figure 5.9: Sagittal plane angular momentum about center of mass of the amputee athlete (‘A’) and the non-amputee reference group (‘NA’) for the reconstructed sprinting motions. Phase durations are scaled for comparability and angular momentum values are normalized by body mass and body height squared.

joint. In the latter, the peak flexion torque of the amputee athlete more than doubles the one of the non-amputee control group. In addition, the hip shows a clearly different course: Instead of a flexion torque, an extension torque acts here during the contact phase.

In the joints of the arms, a similar course is shown overall for both amputee and non-amputee sprinting. It is noticeable that the amputee athlete’s torques are on average greater than those of the non-amputee control group. In the spinal joints, we observe larger torques for the amputee athlete as well.

**Angular momentum about center of mass** Figure 5.9 shows the contributions of the different body parts (legs, arms, trunk) to as well as the total angular momentum with respect to the center of mass for rotations in the sagittal plane (RY). The values have been normalized by body mass and body height squared for better comparability. Again, even at first glance considerable differences between the amputee athlete and the non-amputee reference group are visible. Let us first consider the total angular momentum of non-amputee athletes: Their courses correspond to the angular momentum observations in a publication by Hinrichs[59], although the absolute numbers differ due to the different running velocities (Hinrichs investigated slower running movements). It is noticeable that arms and trunk move around an angular momentum of zero, but the angular momentum of the two legs is counter-rotating. The contact leg always has a larger angular momentum, so that a total angular momentum is generated that does not oscillate around zero. As Hinrichs[59] also describes, the reason for this is that the legs, especially the feet, actually perform a circular movement and thus have a positive angular momentum. This is particularly interesting in view of the fact that the

individual components of the amputee's angular momentum behave differently. For the biological leg, we actually find a movement comparable to that of the non-amputee athlete. In other words, he rolls the biological foot in a similar circular motion. For the prosthetic leg, the angular momentum during contact is on the one hand significantly lower, and on the other hand the course during contact of the biological foot is also different. This can probably be attributed to the asymmetry caused by the lighter RSP and difficulties of a circular movement with the RSP. Nevertheless, the contribution of the legs cannot completely explain the entirely different course of the total angular momentum. Therefore, we consider the angular momentum of the arms and the trunk. As far as the arms are concerned, it can be stated that the greatest deviations occur during the flight phase following contact with the affected leg. Apart from that, the course is similar to that of the non-amputee athletes. It is mainly the torso's angular momentum that differs significantly. Instead of circling around zero within each step, the angular momentum is greater than zero during the first two phases and less than zero during the last two phases. This demonstrates that the amputee athlete must use his arms and trunk in a significantly different way to achieve stability when running and to compensate for inter-limb asymmetry.

### 5.2.2 Frontal and Transversal Plane Movements

**Overall position and joint angles** Figure 5.10 shows the diagrams of the overall position and the joint angles in the frontal and transversal planes. All diagrams show clear differences between amputee and non-amputee sprinting and also between the two sides of the body. Let us first look at the overall position of the sprinters: While the non-amputee athletes tend to move to the left on average, the amputee athlete shifts his body to the left in the first step and then to the right in the second step during sprinting. He thus seems to make a much stronger compensatory movement to counterbalance the inter limb asymmetry. The comparison with the CoM movement shows, however, that the amputee moves it over the two steps altogether to the right, i.e., to the affected side. In the non-amputee sprinters, the rotations of the floating base segment in the frontal and transverse planes are close to 0 rad. In the case of the amputee athlete, they are significantly larger and also change to a much greater extent over the course of the two steps. In absolute terms, however, these values are also a few degrees. Nevertheless, the curve in the frontal plane is particularly interesting because it also indicates that the amputee rotates significantly more around the sagittal axis (x-axis), which is again attributable to inter-limb weight asymmetry. This stronger rotation is also reflected in the spinal joints, which likewise have significantly higher values in the amputee sprinter. Since these compensate for the rotations of the pelvis segment, it can be assumed that this is necessary in order to maintain an upright upper body and, in particular, a steady head looking to the front.

If we now look at the motion of the amputee's leg and arm joints, it is noticeable that these angles are also significantly larger than in the non-amputee control group. For the leg joints, the mean value of the non-amputee comparison group lies between  $-0.121$  rad to  $0.035$  rad (corresponding to approximately  $-7^\circ$  to  $2^\circ$ ), for the arm joints between  $-0.085$  rad to  $0.205$  rad (corresponding to approximately  $-5^\circ$  to  $11.75^\circ$ ) – although the standard deviations are relatively large. Nevertheless, for the amputee athlete, the values are usually outside or on the edge of the standard deviations. If we now compare the affected (right) and unaffected (left) sides of the amputee (solid vs. dashed line), we must note that the signs for these rotations are defined in exactly the opposite way, so for a qualitative comparison we must mirror one of the two lines on the x-axis in thought. On both axes considered, the movement of the hip is significantly greater on the side with amputation than on the other: This shows that the amputee has to move them in a significantly different way to be able to sprint with the RSP. In contrast, the arm on the unaffected side shows greater values for shoulder movement around the sagittal

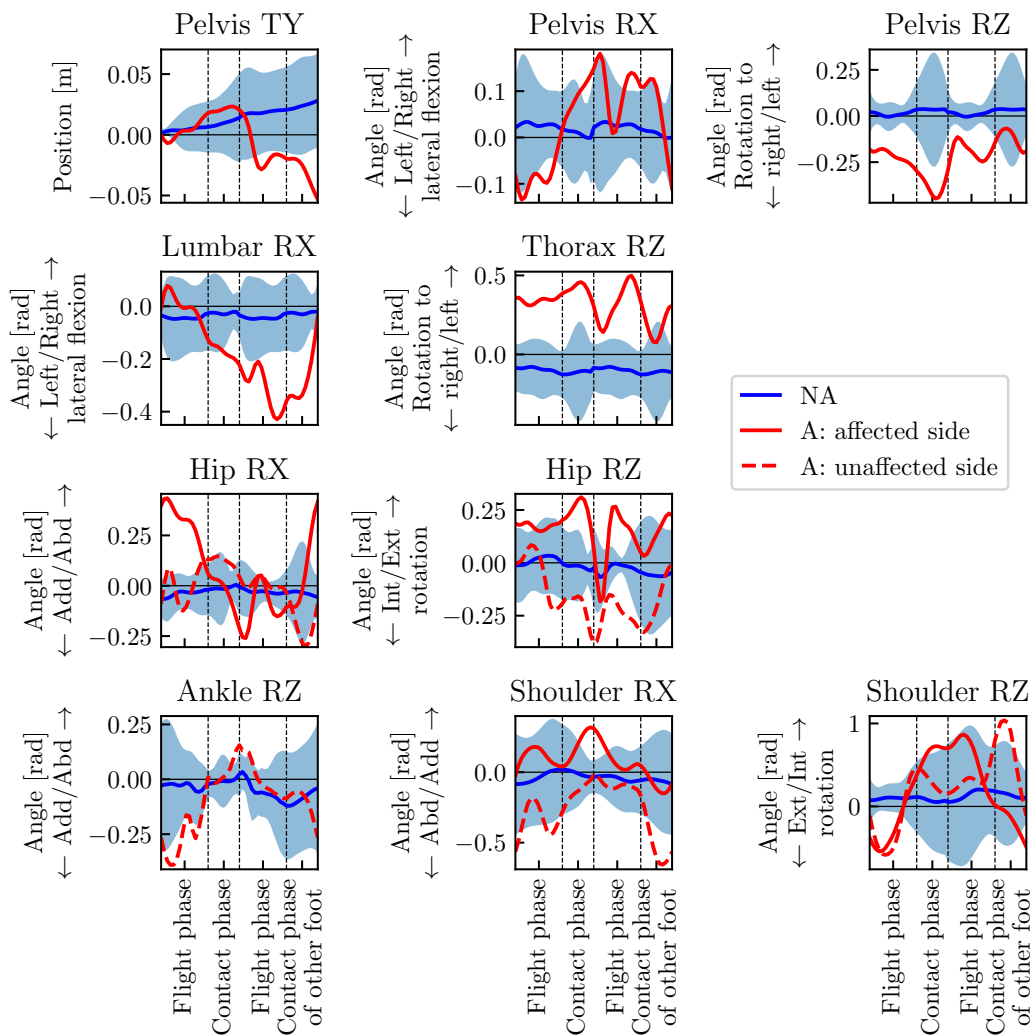


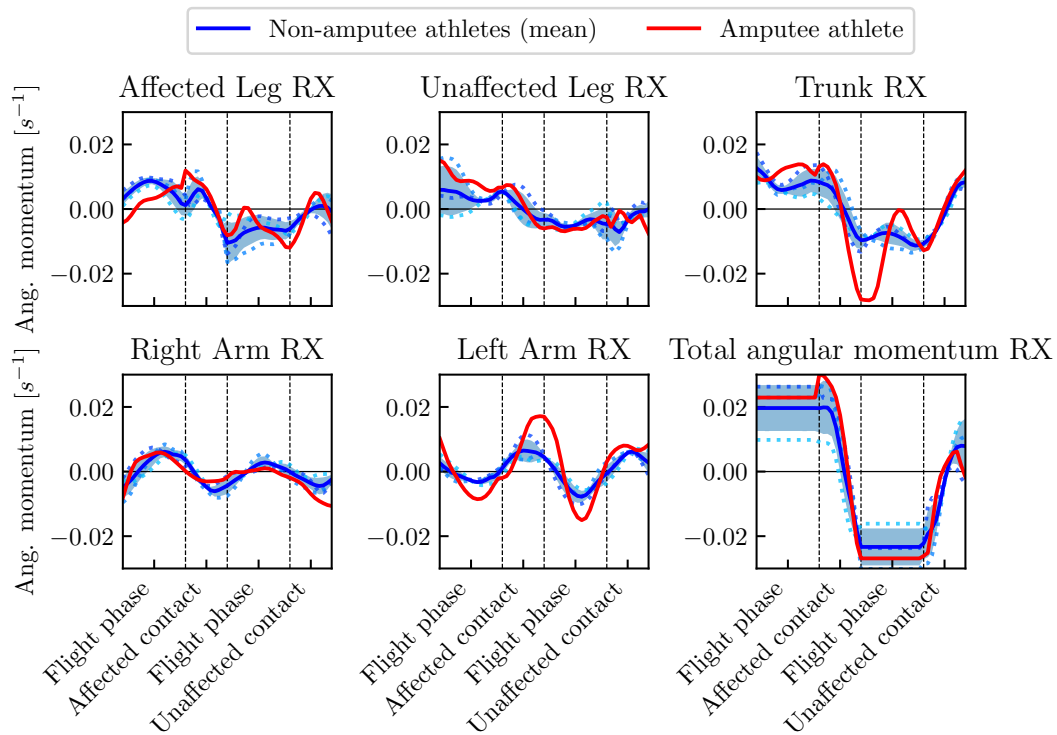
Figure 5.10: Frontal and transversal plane generalized positions of the amputee athlete ('A') and the non-amputee reference group ('NA') for the reconstructed sprinting motions. Phase durations are scaled for comparability. The abbreviations 'Abd', 'Add', 'Int' and 'Ext' stand for 'Abduction', 'Adduction', 'Internal' and 'External', respectively.

axis (RX), indicating that the arms are used for counterbalancing in amputee sprinting.

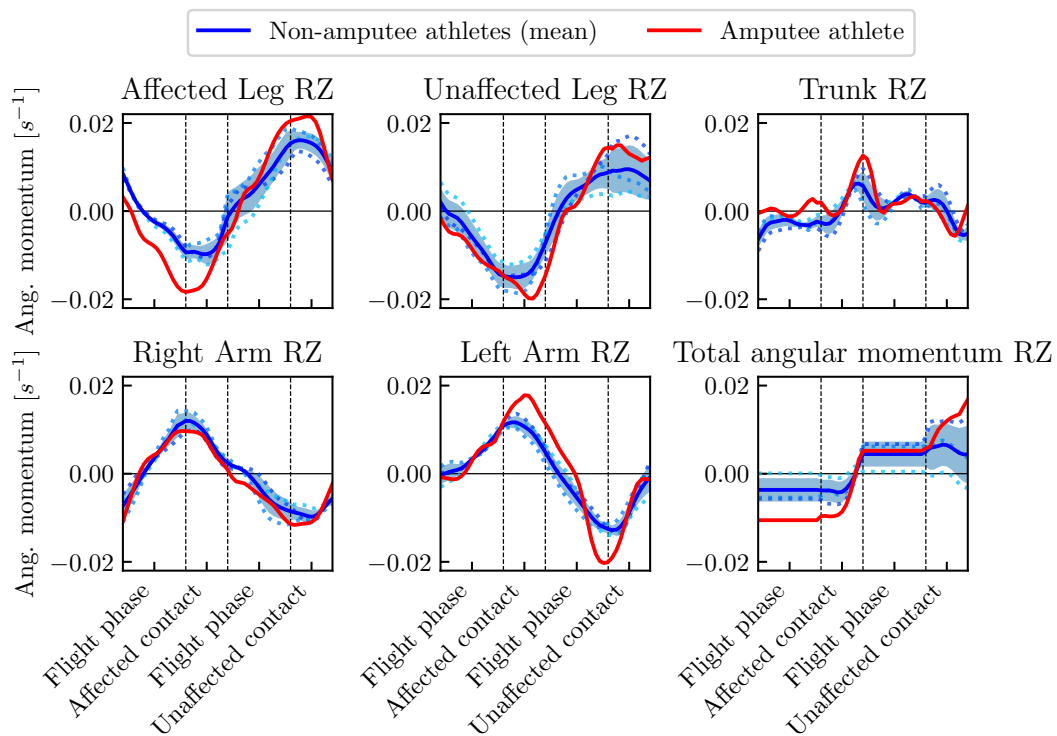
**Joint torques** The joint torques of the frontal and transversal planes are visualized in Figure 5.4. They are normalized by body mass for better comparability. Overall, it can be seen that the torques of the frontal and transverse planes are smaller than those of the sagittal plane. The course of the torques supports the statements we have already made when considering the corresponding joint angles. The joint torques of the amputee athlete are overall significantly higher than those of the non-amputee control group. For all joints, the mean value of the non-amputee athletes is close to zero, between  $-0.5 \text{ N m kg}^{-1}$  to  $0.4 \text{ N m kg}^{-1}$ . Considering the hip rotation torques, we can clearly observe differences between the affected and the unaffected leg of the amputee athlete. In addition to the fact that the torques of the biological leg of the amputee athlete are on average larger than the ones of the non-amputee athlete, we see more oscillation implying permanent adjustment of the torques for stabilizing the sprinting motion. It is noticeable that the spinal moments of the amputee are further significantly greater than

those of non-amputee athletes, especially in the phases following contact with the RSP. It appears, therefore, that the amputee athlete must apply greater torque after prosthetic contact and also during contact with the unaffected leg to compensate for the weight asymmetry between the two legs. The torque curves of the legs and arms do not differ greatly between the two sides of the body taken into account the opposite signs for the two of them.

**Angular momentum about center of mass** Figure 5.11 shows the frontal and transversal plane contributions to the angular momentum about CoM. In addition to the mean and standard deviation of the non-amputee control group, the individual contributions of the three non-amputee athletes are given. The contributions in the frontal and transversal plane to the angular momentum are in total significantly smaller than those in the sagittal plane. Similarly to the sagittal plane angular momentum, we find comparable histories for the biological leg angular momenta in the frontal and transversal planes, but differences in those of the affected leg. In the frontal plane, the total impulse for all athletes is around zero, which indicates an overall periodic movement in this plane. However, while the individual components of the non-amputee athletes also show relatively even courses, differences are noticeable for the components of the amputee athlete: There is a frequent change in the angular momentum of the affected leg which implies recurring adjustments of this leg. Further prominent differences are found in the contribution of the trunk and left arm (on the side of the body not affected by the amputee). At the end of the contact phase with the RSP and in the subsequent flight phase, the torso angular momentum of the amputee is significantly greater. In particular, the spinal segments and the arm opposite the amputation thus seem to compensate for the lift-off of the prosthetic leg, which is significantly lighter than the biological leg. This is also reflected in the angular momentum of the transversal plane: Here, the relatively periodic total angular momentum around zero is made possible by the opposite arm compensating for the greater angular momentum of the affected leg compared to the non-amputee reference group. The larger rotations of the prosthetic leg are possibly caused by the fact that the RSP is modeled as a fixed device with only one rotational DOF in the sagittal plane.



(a) Frontal plane angular momentum



(b) Transversal plane angular momentum

Figure 5.11: Angular momentum about center of mass of the amputee athlete (A) and the non-amputee reference group (NA) for the reconstructed sprinting motions. Phase durations are scaled for comparability and angular momentum values are normalized by body mass and body height squared. The abbreviations stand for non-amputee athletes and amputee athlete, respectively.

### 5.3 Analysis of Measures Related to Effort, Energy Expenditure and Sprint Style

After the qualitative comparison of the results based on the graphs, we want to examine the sprinting movements of the amputee athlete and the non-amputee control group with a second approach. For this purpose, we have calculated relevant measures regarding effort, energy consumption and sprint style. With regard to the next step of trying to create new sprinting motions using OCPs as described in Section 3.1.2, it is of great interest to find out which variables sprinters may maximize or minimize. For the description of the measures, the following conventions should be noted: All torques, forces and angular momenta were normalized based on the individual body mass  $M$  and body height  $H$  in the latter case of the athletes and then labeled  $\tau_i^* = \frac{\tau_i}{M}$ ,  $f_{ap/ml/v}^* = \frac{f_{ap/ml/v}}{M}$  and  $l_y^* = \frac{l_y}{M \cdot H^2}$ . The total time is denoted by  $T$  and the horizontal distance covered by the floating base by  $D$ . The measures can then be formulated as follows:

- Average over absolute and squared joint torques (normalized by distance):

$$\frac{1}{TD} \int_0^T |\tau_i^*| dt \text{ and } \frac{1}{TD} \int_0^T (\tau_i^*)^2 dt .$$

- Average over absolute and squared joint torque derivatives (normalized by distance):

$$\frac{1}{TD} \int_0^T |\dot{\tau}_i^*| dt \text{ and } \frac{1}{TD} \int_0^T (\dot{\tau}_i^*)^2 dt .$$

- Absolute mechanical work of each joint (normalized by distance):

$$\frac{1}{D} \int_0^T |\tau_i^* \dot{\phi}_i| dt .$$

- Average over joint powers (normalized by distance):

$$\frac{1}{TD} \int_0^T (\tau_i^* \dot{\phi}_i) dt .$$

- Relative contact time:  $t_{\text{contact}}/t_{\text{step}}$ .
- Step frequency (with: one step = one flight phase + one contact phase):  $f_{\text{step}}$ .
- Step length:  $d_{\text{step}}$ .
- Average horizontal forward velocity of the floating base segment:  $\overline{v_{h,\text{pelvis}}}$ .
- Anterior-posterior, mediolateral and vertical change of momentum:

$$\int_0^T f_{ap}^* dt \text{ and } \int_0^T f_{ml}^* dt \text{ and } \int_0^T f_v^* dt .$$

- Mean anterior-posterior and vertical force:  $\overline{f_{ap}^*}$ ,  $\overline{f_{ml}^*}$  and  $\overline{f_v^*}$ .
- Vertical peak force:  $(f_v^*)_{\text{max}}$ .

- Average over absolute and squared angular momentum with respect to the CoM:

$$\frac{1}{T} \int_0^T |l_{x,y,z}^{*,C}| dt \text{ and } \frac{1}{T} \int_0^T \left( l_{x,y,z}^{*,C} \right)^2 dt .$$

We distinguished the different components of the angular momentum  $l_{x,y,z}^C$  in each plane, where  $C$  is a placeholder for arms, legs or trunk. In addition, the values were computed for the total angular momentum.

- Average over absolute and squared head orientation in the sagittal plane:

$$\frac{1}{T} \int_0^T |\varphi_{\text{head}}| dt \text{ and } \frac{1}{T} \int_0^T \varphi_{\text{head}}^2 dt$$

with  $\varphi_{\text{head}} = q_{\text{pelvis\_RY}} + q_{\text{lumbar\_RY}} + q_{\text{thorax\_RY}} + q_{\text{head\_RY}}$ .

- Average over absolute and squared head angular velocity in the sagittal plane:

$$\frac{1}{T} \int_0^T |\dot{q}_{\text{head}}| dt \text{ and } \frac{1}{T} \int_0^T (\dot{q}_{\text{head}})^2 dt .$$

Wherever possible the absolute and the squared values were calculated, because the combination of both quantities can give information about whether the curve has single peaks. Furthermore, whenever reasonably possible, the results are given separately for each joint and the sum over all joints is calculated. For the joint powers such a sum is meaningless, because in the numerical calculation positive and negative values will cancel each other out. In reality, however, a negative joint power value does not mean an energy gain. The integrals were calculated numerically using the information at the multiple shooting nodes. The computed measures are listed in Table 5.3.

In order to compare sprinting with and without RSP and to draw conclusions about possible optimization criteria, we systematically go through the measures. First of all we look at the joint torque values: For both the absolute and the squared values, the sum of all torques is smaller in the case of the amputee sprinter than in the case of the non-amputee athletes. Therefore, in the solution of the OCP, the amputee athlete must apply less active torque per body mass and distance covered. For the individual joints, however, there are cases where the amputee has to generate less torque (knee of affected leg, ankle of unaffected leg) as well as more torque (arms, spinal segments, knee of unaffected leg) or where the torque is comparable to that of the non-amputee athletes (biological leg). This confirms the observations made when examining the torque diagrams.

Next, we look at the derivatives of the torques. Here it is noticeable that the sum over all joints provides values of a comparable order of magnitude, but that there are significant differences for almost all of the individual joints. It is remarkable that the values for both knee joints and the joint in the upper back (“Thorax”) are (significantly) smaller for the amputee athlete than for the non-amputee athletes. For the remaining joints, the values for the amputee athlete are (significantly) larger. We conclude from this that the rate of change in torque for the two groups as a whole differs little. The fact that both the absolute and squared values in both knee joints are (significantly) smaller for the amputee athlete than in the non-amputee control group shows that the rate of change in the torques in these joints is very low for the amputee.

The comparison of the absolute mechanical work between amputee and non-amputee sprinters is another interesting aspect: In the leg affected by the amputation, the amputee athlete produces significantly less work in the sagittal plane. In the hip joint it is about 70 % and in the

Table 5.3: Measures of sprinting with and without running-specific prosthesis (RSP) applied to the results of the sprinting dynamics reconstruction. Criteria for which the calculated value for the amputee athlete (A) is significantly lower than the value for the non-amputee control group (NA) are highlighted in red. The opposite is true for criteria highlighted in blue. The abbreviations ‘R’ and ‘L’ refer to the right (affected) or left (unaffected) body side.

	NA	A - R	A - L	NA	A - R	A - L
Joint	Absolute torques [ $\text{N kg}^{-1}$ ] normalized to total body mass [kg] and traveled distance [m]			Squared torques [ $\text{N}^2 \text{m kg}^{-2}$ ]		
Hip RY	0.542 ± 0.063	0.436	0.649	1.698 ± 0.266	1.097	2.486
Hip RX	0.132 ± 0.017	0.152	0.136	0.140 ± 0.041	0.171	0.136
Hip RZ	0.043 ± 0.009	0.065	0.053	0.013 ± 0.005	0.034	0.019
Knee RY	0.248 ± 0.027	0.099	0.309	0.389 ± 0.065	0.087	0.582
Ankle RY	0.226 ± 0.018	-	0.178	0.930 ± 0.089	-	0.632
Ankle RZ	0.019 ± 0.003	-	0.014	0.005 ± 0.001	-	0.002
Shoulder RY	0.097 ± 0.010	0.104	0.149	0.055 ± 0.012	0.070	0.137
Shoulder RX	0.039 ± 0.012	0.041	0.064	0.012 ± 0.007	0.011	0.026
Shoulder RZ	0.016 ± 0.003	0.026	0.022	0.002 ± 0.001	0.004	0.003
Elbow RY	0.055 ± 0.004	0.052	0.073	0.016 ± 0.002	0.014	0.030
Lumbar RY	0.161 ± 0.020	-	0.259	0.182 ± 0.054	-	0.500
Lumbar RX	0.106 ± 0.006	-	0.113	0.078 ± 0.007	-	0.106
Thorax RY	0.134 ± 0.026	-	0.129	0.144 ± 0.080	-	0.104
Thorax RZ	0.174 ± 0.007	-	0.237	0.161 ± 0.013	-	0.281
Neck RY	0.028 ± 0.011	-	0.026	0.006 ± 0.004	-	0.004
Sum	3.434 ± 0.299	-	3.386	7.090 ± 0.727	-	6.539
Joint	Absolute torque derivatives [ $\text{N kg}^{-1} \text{s}^{-1}$ ] normalized to total body mass [kg] and traveled distance [m]			Squared torque derivatives [ $\text{N}^2 \text{m kg}^{-1} \text{s}^{-2}$ ]		
Hip RY	8.03 ± 1.30	10.98	9.62	617 ± 252	1105	711
Hip RX	4.93 ± 0.55	8.55	6.26	218 ± 64	512	284
Hip RZ	2.76 ± 0.34	5.40	4.05	79 ± 56	304	107
Knee RY	7.11 ± 0.86	4.56	6.66	472 ± 167	228	442
Ankle RY	7.10 ± 0.83	-	7.60	986 ± 238	-	1094
Ankle RZ	2.36 ± 1.10	-	2.22	89 ± 79	-	52
Shoulder RY	2.68 ± 0.36	2.78	4.18	71 ± 23	64	114
Shoulder RX	1.60 ± 0.20	1.72	2.12	26 ± 16	20	34
Shoulder RZ	1.04 ± 0.30	1.30	1.52	27 ± 31	11	22
Elbow RY	1.52 ± 0.17	1.39	1.92	26 ± 10	13	27
Lumbar RY	5.69 ± 0.30	-	7.54	243 ± 32	-	439
Lumbar RX	4.30 ± 0.59	-	4.66	147 ± 41	-	173
Thorax RY	5.22 ± 1.33	-	3.72	290 ± 153	-	99
Thorax RZ	3.97 ± 0.28	-	4.82	125 ± 19	-	195
Neck RY	1.99 ± 0.49	-	1.96	40 ± 20	-	26
Sum	99.5 ± 3.9	-	105.5	6070 ± 269	-	6078
Joint	Absolute mechanical work [ $\text{J kg}^{-1} \text{m}^{-1}$ ] normalized to total body mass [kg] and traveled distance [m]			Joint powers [ $\text{W kg}^{-1} \text{m}^{-1}$ ]		
Hip RY	1.67 ± 0.14	1.18	2.23	2.54 ± 0.40	0.75	1.98
Hip RX	0.19 ± 0.06	0.25	0.19	0.08 ± 0.21	0.13	-0.04
Hip RZ	0.07 ± 0.02	0.12	0.08	-0.05 ± 0.03	-0.00	-0.01
Knee RY	1.28 ± 0.05	0.28	1.41	-2.05 ± 0.18	-0.43	-2.15
Ankle RY	0.96 ± 0.10	-	0.88	-0.42 ± 0.21	-	-1.01
Ankle RZ	0.02 ± 0.01	-	0.02	-0.00 ± 0.02	-	-0.02
Shoulder RY	0.35 ± 0.05	0.38	0.67	0.03 ± 0.07	0.19	0.38
Shoulder RX	0.04 ± 0.02	0.05	0.14	-0.01 ± 0.02	0.00	0.10
Shoulder RZ	0.04 ± 0.01	0.07	0.08	0.03 ± 0.01	-0.03	0.02
Elbow RY	0.16 ± 0.02	0.13	0.23	0.11 ± 0.08	0.10	-0.03
Lumbar RY	0.27 ± 0.05	-	0.60	-0.05 ± 0.09	-	-0.39
Lumbar RX	0.11 ± 0.01	-	0.14	0.04 ± 0.01	-	0.07
Thorax RY	0.28 ± 0.14	-	0.12	0.15 ± 0.12	-	0.12
Thorax RZ	0.30 ± 0.03	-	0.40	0.22 ± 0.11	-	0.11
Neck RY	0.06 ± 0.02	-	0.03	0.05 ± 0.04	-	0.02
Sum	10.61 ± 0.45	-	9.68	-	-	-

Table 5.3: Measures of sprinting with and without running-specific prosthesis (RSP) applied to the results of the sprinting dynamics reconstruction (cont.)

	NA	A	NA	A	NA	A
	Right step (pros. leg)		Left step (biol. leg)		Average for both steps	
Rel. cont. time	0.39 ± 0.03	0.36	0.39 ± 0.04	0.36	0.39 ± 0.04	0.36
Step frequency [Hz]	4.20 ± 0.31	4.46	4.15 ± 0.27	4.24	4.17 ± 0.29	4.35
Step length [m]	2.20 ± 0.09	2.11	2.21 ± 0.08	2.27	2.20 ± 0.08	2.19
Average vel. [ $\text{m s}^{-1}$ ]	9.11 ± 0.30	9.03	9.17 ± 0.37	10.06	9.14 ± 0.30	9.54
Anterior-posterior change of momentum [ $\text{N s kg}^{-1}$ ]	0.10 ± 0.08	0.31	0.10 ± 0.10	-0.32	0.10 ± 0.09	-0.00
A.-p. mean force [ $\text{N kg}^{-1}$ ]	0.38 ± 0.31	1.49	0.38 ± 0.41	-1.46	0.38 ± 0.37	0.02
Mediolateral change of momentum [ $\text{N s kg}^{-1}$ ]	-0.04 ± 0.07	-0.06	0.00 ± 0.11	-0.09	-0.02 ± 0.10	-0.08
ML. mean force [ $\text{N kg}^{-1}$ ]	-0.16 ± 0.30	-0.29	0.03 ± 0.44	-0.41	-0.06 ± 0.39	-0.35
Vertical change of momentum [ $\text{N s kg}^{-1}$ ]	2.30 ± 0.22	1.87	2.37 ± 0.07	2.18	2.34 ± 0.17	2.02
Vert. mean force [ $\text{N kg}^{-1}$ ]	9.57 ± 1.04	8.93	9.77 ± 0.54	9.92	9.67 ± 0.83	9.43
Vert. peak force [ $\text{N kg}^{-1}$ ]	33.2 ± 3.4	34.0	35.3 ± 1.9	44.4	34.2 ± 3.0	39.2
		NA	A	NA	A	
		Absolute values		Squared values		
Angular momentum arms RY [ $10^{-3} \text{ s}^{-1}$ ]	-0.90 ± 0.21	-1.41	0.020 ± 0.004	0.34		
Angular momentum legs RY [ $10^{-3} \text{ s}^{-1}$ ]	42.65 ± 2.59	26.11	2.11 ± 0.32	1.38		
Angular momentum trunk RY [ $10^{-3} \text{ s}^{-1}$ ]	-1.22 ± 0.28	-0.26	0.020 ± 0.003	0.21		
Angular momentum total RY [ $10^{-3} \text{ s}^{-1}$ ]	40.53 ± 2.39	24.44	1.88 ± 0.28	1.30		
Angular momentum arms RX [ $10^{-3} \text{ s}^{-1}$ ]	0.16 ± 0.49	-0.88	0.02 ± 0.01	0.14		
Angular momentum legs RX [ $10^{-3} \text{ s}^{-1}$ ]	-1.05 ± 1.17	0.33	0.13 ± 0.09	0.06		
Angular momentum trunk RX [ $10^{-3} \text{ s}^{-1}$ ]	-0.50 ± 0.72	-0.25	0.08 ± 0.02	0.08		
Angular momentum total RX [ $10^{-3} \text{ s}^{-1}$ ]	-1.40 ± 2.15	-0.79	0.44 ± 0.20	0.56		
Angular momentum arms RZ [ $10^{-3} \text{ s}^{-1}$ ]	-0.23 ± 0.74	0.72	0.24 ± 0.04	0.21		
Angular momentum legs RZ [ $10^{-3} \text{ s}^{-1}$ ]	1.22 ± 1.35	-1.49	0.36 ± 0.07	0.15		
Angular momentum trunk RZ [ $10^{-3} \text{ s}^{-1}$ ]	-0.03 ± 0.37	0.41	0.01 ± 0.01	0.19		
Angular momentum total RZ [ $10^{-3} \text{ s}^{-1}$ ]	0.96 ± 0.86	-0.37	0.03 ± 0.02	0.14		
		NA	A	NA	A	
		Absolute values		Squared values		
Head orientation [rad]	0.09 ± 0.02	0.10	0.010 ± 0.004	0.02		
Head velocity [ $\text{rad s}^{-1}$ ]	3.62 ± 0.79	2.68	26.60 ± 15.98	10.06		

knee joint less than 25 % of the corresponding values for the non-amputee athletes. Again, two approaches provide an explanation: First, it can be assumed that the capabilities of the residual leg are also reduced by the amputation, especially in the knee joint, which is the joint closest to the location of amputation. On the other hand, however, these numbers also support the assumption that transtibial amputee sprinters use a strategy to increase the loading of the RSP by reducing the loading of the biological structures of the residual leg. While the absolute mechanical work in the prosthetic leg is thus reduced compared to the non-amputee control group for the sagittal plane motion, the situation is different in the biological leg. Here the amputee athlete produces 30 % more mechanical work in the hip joint and 11 % more mechanical work in the knee joint. For all planes, the amputee produces significantly more mechanical work in the shoulder and spinal joints (values 1.27–3.5 times as large as for non-amputee sprinting).

Hence, it seems that an increased mechanical work in the hip of the unaffected leg and the upper body is needed to compensate for inter-limb asymmetries.

The differences in joint power are also immediately apparent. In the sagittal plane, both hip joint values of the amputee athlete are significantly lower than those of the non-amputee comparison group (affected leg: 29 %, unaffected leg: 78 %). Hence, less power is generated in the hip of the amputee athlete. The knee of the affected leg of the amputee athlete absorbs less energy than the unaffected knee and the knees of the non-amputee athletes. However, less energy is absorbed in the ankle of non-amputee athletes than in the biological ankle of the amputee athlete. It appears that the amputee athlete partially compensates for the lower energy production in the hip joints and the higher energy loss in the ankle by work of the upper body.

Since the values of total contact times, step frequency, step length and average velocity do not add any new insights to the discussion already carried out in Section 5.2, we will now move on to the analysis of the measures related to the ground reaction forces. In particular, significant differences between the amputee athlete and the non-amputee control group were found in the anterior-posterior component of the ground reaction forces and the change of momentum induced by them. For sprinting movements, a change of momentum close to zero would be expected, since braking and propulsive contributions should more or less compensate each other. For the non-amputee sprinters, we find values of around  $0.11 \text{ N s kg}^{-1}$  for the individual steps and the average of both steps which is slightly above the expected value of 0. For sprinting with RSP, we see significant deviations when considering the individual steps: During contact with the RSP the value is well above zero, for contact with the biological leg it is well below zero. This means that for the former the propulsive contribution clearly dominates and for the latter the braking contribution. Interestingly, the change of momentum averaged over both steps is close to zero. Of course, at this point it must be noted that the reconstruction of the horizontal component of the ground reaction force did not work completely (cf. discussion in Section 5.1). As previously discussed in Section 5.2, the amputee athlete seems to generate velocity during prosthetic contact. The anterior-posterior mean forces support this observation as well. Overall, this significant difference between the two legs of the amputee athlete, and also in comparison to the non-amputee athletes, cannot be explained entirely by weaknesses in the modeling and reconstruction.

Finally, we look at the measures related to the overall posture and its change during sprinting, namely angular momentum about CoM, head orientation and velocity. First, we consider the integral over the angular momentum values. For perfectly symmetric sprinting, they should be close to zero for the frontal and transversal planes (RX, RZ). For both planes, the total angular momentum values of the amputee athlete are closer to zero than those of the non-amputee control group. If we look at the individual components, we notice that this does not apply to them on average. In other words, the amputee athlete runs more periodically overall and his overall rotation in the frontal and transverse planes is smaller than in the non-amputee athletes. However, the movements of the individual components (arms, legs, upper body) in these two planes are much more irregular. This reflects the inter-limb asymmetry due to the RSP. In the sagittal plane, the total angular momentum of the amputee and also that of the legs is significantly lower. Overall, less rotation is found in the amputee sprinting movement than in non-amputee sprinting.

## 5.4 Summary

We reconstructed both the two-dimensional and three-dimensional kinematics and dynamics of two steps of sprinting at maximum velocity for three non-amputee and one unilateral am-

putee athlete from kinematic motion capture data (position and joint angles computed from marker coordinates). The consistency of the results with additionally measured ground reaction force data as well as joint torques from the literature shows that the proposed least squares OCP formulation is a valid method for computation of the dynamics of motion capture recordings without need of force plate data. Hence, it represents a valuable alternative to classical inverse dynamics approaches for computing the dynamics, which can also be used, for example, when the force data set is erroneous or no force plates are available. Furthermore, the least squares approach has the advantage of fitting to all markers in a balanced manner, avoiding unintended error propagation along the kinematic chain.

We found significant differences between sprinting with and without RSP, both in the considered curves for angles, torques, forces and angular momentum as well as in the actuation patterns and the investigated measures. By considering the curves for all thirteen joints, a more differentiated picture emerges than if we had considered only the legs and the CoM motion. For example, we found that the torques and mechanical work in the leg affected by the amputation of the amputee athlete were sometimes significantly smaller than in the non-amputee control group; however, the corresponding magnitudes in the joints of the upper body, i.e., arms and trunk, were mostly larger in comparison. In general, a comparison between athletes with and without BKA naturally raises the question of which criteria are useful for this purpose e.g., whether it makes sense to use measures related to efficiency for comparison, since the goal of a sprinter is to run as fast as possible rather than as efficiently as possible. This chapter provides a comprehensive overview of possible criteria, ranging from curve trajectories of characteristic variables to numerical values of defined measures. We will come back to this question in the chapter on the comparison of the amputee athlete with himself without amputation in the planned simulator tool (Chapters 11).

We would like to emphasize another major difference between sprinting with and without RSP in this summary, as we will return to it throughout the upcoming chapters: Although the movements of all four athletes show certain asymmetries between the two steps, these are much more pronounced in the athlete with BKA. However, while asymmetries between the two legs are expected, inter-limb asymmetry has actually been shown to affect the entire body and thus the entire movement. For instance, the amputee athlete compensates for the inter-limb asymmetry mainly with his upper body, i.e., the arms and the torso, as shown, among others, by the comparatively large torques in the corresponding joints. We consider this observation so important for two reasons that we highlight it again in the summary: First, larger torques in individual joints carry a higher risk of abrasion, fatigue, and injury in those joints. On the other hand, the asymmetry shows that unilateral amputees have to adapt their actions in each step to the conditions of the current contact leg<sup>1</sup>. In our opinion, this asymmetry, which is also evident in the strong trunk movement, has an overall destabilizing effect on movement.

With these observations and results, the reconstruction of the dynamics of recorded sprinting movements establishes a solid basis: based on the successfully reconstructed movements (for both the 2D and 3D models), we can assume that the models are valid as a formulation of sprinting at maximal velocity. While the results also provide a valuable contribution standing on their own (as the reconstruction succeeds without the presence of measured force data) we would like to go one step further to get closer to the goal of comparing the amputee athlete to himself without amputation in the computer model. To this end, in the following two chapters we examine movements generated based on minimization or maximization of one or more optimization criteria.

---

<sup>1</sup>And this also shows the decisive difference to the studies on bilateral transtibial amputees: They are again a symmetrical system in themselves and consequently can also use their RSPs consistently, which could possibly be advantageous due to their spring-like properties, especially for longer races.

## 6 Synthesis of Sprinting Motions with and without Running-Specific Prostheses

We start this chapter on the synthesis of sprinting motions by revisiting the results of the sprinting reconstruction, which we discussed in the previous chapter. Especially concerning the motion of the trunk and the arms, we observed important differences among both the frontal and transversal planes in the reconstructed motions. Nevertheless, for the predictive simulations in this and the following chapter, we will restrict them to the 2D models, which move purely in the sagittal plane. The reasons are primarily practical, but can also be justified by the observations of the dynamics reconstruction results: Since no reference motion is given anymore when generating motions, in a three-dimensional model it is not a priori prohibited that the individual segments intersect each other. Therefore, it would be necessary to introduce additional conditions into the problem formulation which prevent this pairwise penetration<sup>1</sup>. Together with the already existing complexity of a three-dimensional model and the intention to introduce realistic bounds on the joint torques by a Muscle Torque Generator (MTG) model, the problem would become very complex and thus computationally intense. In this work, we are interested in straight sprinting steps at maximum velocity, which essentially occur in the forward direction. In addition, although the observations in the frontal and transverse planes showed differences, the corresponding variables were of a much smaller order of magnitude than those in the sagittal plane. Therefore, while these differences are relevant to a more sophisticated and detailed consideration, we chose to limit ourselves to the 2D model in favor of realistic torque limits and a trade-off between knowledge gained from a more accurate model and computational time.

Hence, for the investigation of how different optimization criteria influence the resulting sprinting motions, we established the two-dimensional rigid body models of the two-dimensional dynamics reconstruction (see Chapter 5). A detailed description of the used *2D model* is given in Section 2.2. The optimal control problem (OCP) which we use to simulate the sprinting motions is the motion synthesis OCP described in Section 3.1.2. The analysis in this chapter is based on results given in [32]. Additional sprinting synthesis results can be found in [69].

**Constraints to the optimal control problem** For the motion synthesis problem, the contact constraints (4.1)–(4.4) are extended by the so called ‘friction cone’ conditions. The friction cone is a polyhedral convex cone satisfying

$$\|f_t\| < \mu \|f_n\|, \quad (6.1)$$

where  $f_t$  and  $f_n$  are the tangential and normal contact forces acting between two objects (cf. Figure 6.1). As long as the contact forces stay within the friction cone, the contact will remain fixed. If the contact forces are at the left/right edge of the friction cone, the object will start left/right sliding. The friction coefficient  $\mu$  depends on the materials of the two objects which are in contact: Object pairs with a large friction coefficient will stick together more easily than object pairs with a small friction coefficient (this becomes also clear from the fact that the opening width of the cone is determined by the arcustangens of  $\mu$ ). As an example, steel

---

<sup>1</sup>We will describe one possible way of introducing such constraints in Chapter 10.

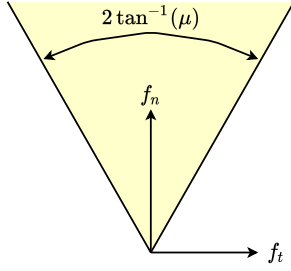


Figure 6.1: Visualization of the friction cone condition

with an oil film has a (kinetic) friction coefficient of 0.06, whereas rubber on asphalt has a (kinetic) friction coefficient of 1.05 [29]. As both running shoes and the running-specific prostheses (RSPs) as well as the tartan running tracks are designed to provide secure non-sliding contact, we set the friction coefficient to 1. The friction cone condition is formalized by two constraints acting on the ground reaction forces via

$$\mu F_z^{LH/RH}(x(t), u(t)) - F_x^{LH/RH}(x(t), u(t)) \geq 0, \quad t \in \mathcal{T}_2 \text{ or } t \in \mathcal{T}_5, \quad (6.2a)$$

$$\mu F_z^{LH/RH}(x(t), u(t)) + F_x^{LH/RH}(x(t), u(t)) \geq 0, \quad t \in \mathcal{T}_2 \text{ or } t \in \mathcal{T}_5, \quad (6.2b)$$

where  $F_x^{LH/RH}$  and  $F_z^{LH/RH}$  are the horizontal and vertical ground reaction forces produced at the left or right contact point, respectively. They are formulated as inequality constraints within the respective contact phase. At the end of a phase, they collapse to the equality constraints

$$F_z^{LH/RH}(x(t), u(t)) = 0, \quad t \in \{t_0, t_3, t_6\}, \quad (6.3a)$$

$$F_x^{LH/RH}(x(t), u(t)) = 0, \quad t \in \{t_0, t_3, t_6\}, \quad (6.3b)$$

due to the lift-off condition (4.4). As the equality constraints are numerically easier to solve, we thus use this formulation at the end of contact phases.

In addition to these ground contact constraints, we formulate constraints introducing limits on the joint torques based on the MTGs described in Section 2.5. More specifically, we formulate two constraints for each joint torque, one for the maximum possible value and one for the minimum possible value.:

$$\tau_i - \tau_{\text{EXT/FLEX}}^M(a, \theta_i, \dot{\theta}_i, \boldsymbol{\alpha}) \geq 0, \quad (6.4a)$$

$$-\tau_i + \tau_{\text{FLEX/EXT}}^M(a, \theta_i, \dot{\theta}_i, \boldsymbol{\alpha}) \geq 0. \quad (6.4b)$$

The maximum possible torques  $\tau_{\text{EXT/FLEX}}^M$  which can be generated by extension or flexion, respectively, are calculated using the MTGs via Eq. (2.9) (see Section 2.5). The indices ‘‘EXT’’ and ‘‘FLEX’’ denote extension and flexion torques, whereby the choice of the signs depends on the definition of the joint angles. Since we are interested in the calculation of the upper and lower limits for the torques, we set the activation of the muscles to the maximum value  $a = 1$ . We use the values calculated by means of the fitting routine described in Section 2.5 for the parameter  $\boldsymbol{\alpha}$ . The fit routine was performed using the reconstructed solutions from Chapter 5 to determine the parameters of the individual athletes. The constraints are imposed as inequality constraints at each multiple shooting node of the OCP.

Finally, additional constraints are imposed for two reasons:

1. to extract parameters as step length or step frequency by equality constraints in the respective phases, and
2. to avoid unwanted behavior such as the foot penetrating the ground while swinging forward in flight.

---

**Formulation of objective functions from basic optimization criteria** Eight criteria form the basic objective functions, from which the objective function (3.5) is composed as a linear combination. By a suitable choice of the weighting factors  $\gamma$  different combinations can be realized and an adaptation to different orders of magnitude or importance can be achieved. Three criteria are formulated as objective functions of Mayer type as they are evaluated at the end of a phase. The remaining five criteria are represented by Lagrange type objective functions, as they are calculated over the entire phase. In the following, the basic criteria and the formulation of the concrete basic objective functions are presented:

1. *Maximize Average Velocity*: The objective function of Mayer type computes the average velocity as fraction of the distance covered by the pelvis  $x_{\text{pelvis}}$  and the total time  $t_f$ :

$$\varphi_{M_1}(t_f, \mathbf{x}(t_f), \mathbf{p}) = -p_{\text{vel}} = -\frac{x_{\text{pelvis}}(t_f)}{t_f}. \quad (6.5a)$$

2. *Maximize Step Frequency*: Step frequency is the inverse of the time required to complete a full step, i.e., one flight and one contact phase. We chose to evaluate it at the end of the contact phases. Hence the Mayer type objective function is evaluated twice, once for each step:

$$\varphi_{M_2}(t_f, \mathbf{x}(t_f), \mathbf{p}) = -(p_{\text{freq},R} + p_{\text{freq},L}) = -\left(\frac{1}{t_R} + \frac{1}{t_L}\right). \quad (6.5b)$$

3. *Maximize Step Length*: Step length is chosen to be the distance between the contact points of the two feet, measured from the lift-off of one foot to the touchdown of the other foot. Its maximization is formulated as objective function of Mayer type:

$$\varphi_{M_3}(t_f, \mathbf{x}(t_f), \mathbf{p}) = -(p_{\text{length},R} + p_{\text{length},L}). \quad (6.5c)$$

4. *Maximize Vertical Ground Reaction Force Over Contact Time*: As discussed in the introduction, Weyand and colleagues [132] have observed that high class sprinters generate large ground reaction forces within a short contact phase. We translate this finding into an objective function of Lagrange type by maximizing the fraction of vertical ground reaction force  $f_v$  and contact phase duration  $p_c$ :

$$\varphi_{L_4}(t, \mathbf{x}(t), \mathbf{u}(t), \mathbf{p}) = -\left(\frac{f_{v,R}}{p_{c,R}} + \frac{f_{v,L}}{p_{c,L}}\right). \quad (6.5d)$$

Apparently, this objective function is only assessed during the contact phases and not during the flight phases.

5. *Minimize Torques Squared*: In order to investigate a criterion that correlates with effort, we introduce a Lagrange type objective function which minimizes the squared joint torques:

$$\varphi_{L_5}(t, \mathbf{x}(t), \mathbf{u}(t), \mathbf{p}) = \|\boldsymbol{\tau}(t)\|_2^2. \quad (6.5e)$$

6. *Minimize Torque Derivatives Squared*: We apply the Lagrange type objective function that formalizes the minimization of the squared joint torque derivatives both as a single criterion and as a regularization term. In the latter case, the weight factor is chosen to be

sufficiently small.

$$\varphi_{L_6}(t, \mathbf{x}(t), \mathbf{u}(t), \mathbf{p}) = \|\dot{\boldsymbol{\tau}}(t)\|_2^2 = \|\mathbf{u}(t)\|_2^2. \quad (6.5f)$$

7. *Minimize Angular Momentum Squared*: The angular momentum of the spinal segments around the center of mass (CoM) should be (near) zero during the sprinting to produce an upright motion. Therefore, an objective function of Lagrange type is formulated, which measures and minimizes the deviation of this angular momentum from zero:

$$\varphi_{L_7}(t, \mathbf{x}(t), \mathbf{u}(t), \mathbf{p}) = \|\mathbf{l}_{CoM}^{torso}(\mathbf{q}(t), \dot{\mathbf{q}}(t))\|_2^2. \quad (6.5g)$$

Since we are considering only sprinting in the sagittal plane, just the angular momentum around the frontal axis is used.

8. *Head Stabilization*: To avoid uncontrolled nodding and wobbling of the head, we formulate, if necessary, a Lagrange-type objective function for head stabilization:

$$\varphi_{L_8}(t, \mathbf{x}(t), \mathbf{u}(t), \mathbf{p}) = \|\theta_{\text{head,abs}}\|_2^2. \quad (6.5h)$$

However, this objective functions is never used as a single criterion.

Based on these eight criteria, we have defined eight composite objective functions by appropriately choosing the weighting factors  $\gamma$ : Seven of them ( $\Phi_1, \dots, \Phi_7$ ) investigate the influence of a main criterion on the resulting sprinting motion (these are named after the main contribution criterion). In these, only small terms have been added to the objective function to regularize the controls and stabilize the head. This addition of small terms is also necessary because some of the criteria do not yield a unique solution, so that the added terms then choose the solution. The last objective function ( $\Phi_8$ ) combines two main criteria, namely maximizing step length and step frequency. So this last objective function aims to investigate the influence of maximizing the product of step length and frequency, which is commonly accepted as a way to calculate speed. Therefore, we expect results similar to the solution for the objective function *Max. average velocity*. The exact composition of the objective functions with the concrete weighting factors is summarized in Table 6.1. For each of these objective functions and each of the two athletes (amputee and non-amputee), we synthesized one sprinting motion at fixed average velocity and one sprinting motion at free average velocity. Figure 6.2 shows some exemplary animated sequences of the optimized motions (for the criteria *Max. Average Velocity*, *Max. Step Length* and *Min. Torques Squared*). The animated sequences for the remaining criteria are shown in Figure A.5 in the appendix.

## 6.1 Comparison of Synthesized and Reference Sprinting Motions

For the evaluation of the optimization criteria, we first compare the generated solutions (denoted by superscript  $S$ ) with the respective solutions of the motion capture reconstructions (denoted by superscript  $M$ ) from Chapter 5, separately for the non-amputee and the amputee athlete. Due to the large number of solutions (16 generalized positions for each of eight different objective functions and one reference movement, both for the amputee and non-amputee athlete), a graphical or tabular comparison as in the previous chapters appears to be clearly too confusing and space-consuming. Therefore, our goal is to combine both temporal and postural differences into a single measure of similarity. Of course there is the difficulty that the different quantities (positions, joint angles, times) have different units and very different orders of magnitude. There is no clear way how such a similarity measure should be defined

Table 6.1: Weight factors for the formulation of objective functions for sprinting from basic optimization criteria

	Name	$\gamma_1$	$\gamma_2$	$\gamma_3$	$\gamma_4$	$\gamma_5$	$\gamma_6$	$\gamma_7$	$\gamma_8$
$\Phi_1$	Max. Average Velocity	1	0	0	0	0	$10^{-9}$	0	10
$\Phi_2$	Max. Step Frequency	0	1	0	0	0	$10^{-9}$	0	10
$\Phi_3$	Max. Step Length	0	0	1	0	0	$10^{-9}$	0	10
$\Phi_4$	Max. Force over Time	0	0	0	1	0	$10^{-6}$	0	100
$\Phi_5$	Min. Torques Squared	0	0	0	0	1	$10^{-5}$	0	$10^4$
$\Phi_6$	Min. Torque Deriv.s Squared	0	0	0	0	0	1	0	$10^7$
$\Phi_7$	Min. Angular Momentum	0	0	0	0	0	$10^{-9}$	1	100
$\Phi_8$	Max. Step Length & Frequency	0	1	1	0	0	$10^{-9}$	0	10

and how the different orders of magnitude should be weighted against each other. We have chosen the weighting based on the respective relative sizes, but also taking into account psychophysics studies. Temporal and postural distances were weighted in a ratio of 1:1 ( $\omega^T = 1$ ). The similarity measure then reads

$$d(\mathbf{q}^S(t), \mathbf{q}^M(t), t_f^S, t_f^M) = \sum_{j=1}^4 \omega^T d_j^T(t_f^S, t_f^M) + \sum_{k=1}^4 d_j^P(\mathbf{q}^S(t), \mathbf{q}^M(t)). \quad (6.6)$$

We define the temporal similarity measure per phase by comparing the computed and the reference phase durations normalized by the respective reference phase duration via

$$d_j^T(t_f^S, t_f^M) = \frac{|t_{f,j}^S - t_{f,j}^M|}{t_{f,j}^M}. \quad (6.7a)$$

The index  $j$  specifies the respective phase,  $j \in \{\text{flight phase 1, contact phase 1, flight phase 2, contact phase 2}\}$ . The postural similarity measure is defined based on the root-mean-square error (RMSE) as

$$d_k^P(\mathbf{q}^S(t), \mathbf{q}^M(t)) = \frac{1}{\theta_r} \sqrt{\frac{1}{n_q m} \left( \sum_{k \in \mathcal{I}_{DOF}} \sum_{j=0}^m (q_k^S(t_j) - q_k^M(t_j))^2 \right)}. \quad (6.7b)$$

The differences between recorded and computed positions and joint angles are computed at corresponding relative time points of each phase. We distinguish the contributions of the overall position, legs, arms and spinal joints by introduction of a set of indices  $\mathcal{I}_{DOF}$  which contains the indices of each group. The number of degrees of freedom (DOFs) is given by  $n_q = [2, 6, 4, 4]$ . The number of function evaluations  $m$  is given by the number of multiple shooting points as they define the corresponding relative time points per phase. Since the range of motion varies greatly between different joints, we have normalized the value for each rotational group with the maximal range of motion  $\theta_r = \max_{k \in \mathcal{I}_{DOF}} (\max(q_k^M) - \min(q_k^M))$  present in the reference data. In this way, we avoid that different ranges severely interfere with the result. From the definitions of temporal ( $d_j^T$ ) and postural ( $d_j^P$ ) distances it is clear that a small value for the similarity measure means that the two movements are very close. A value of zero would mean a perfect match of the movements. The similarity measure values are given in Figure 6.3 with the left diagram showing the postural similarity, the middle diagram showing

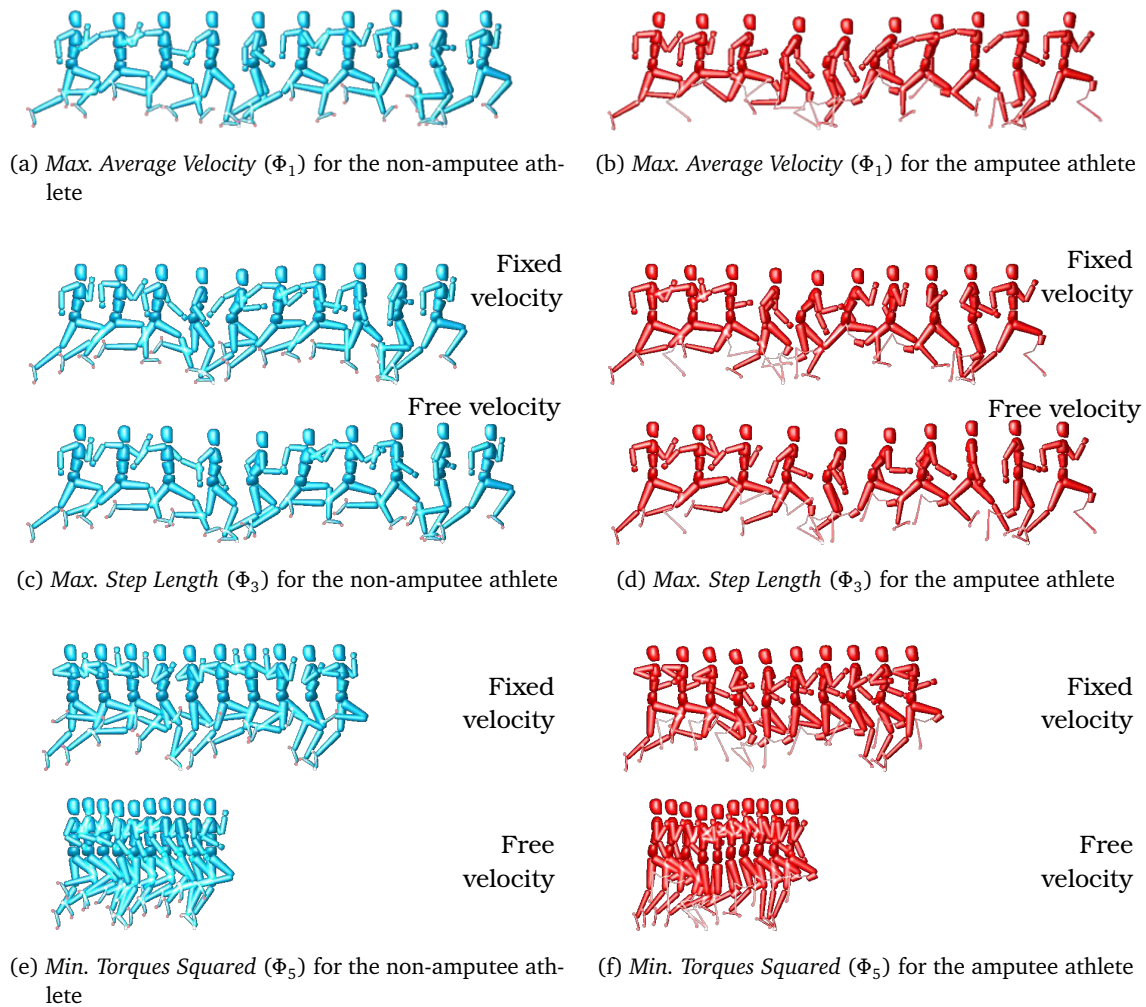


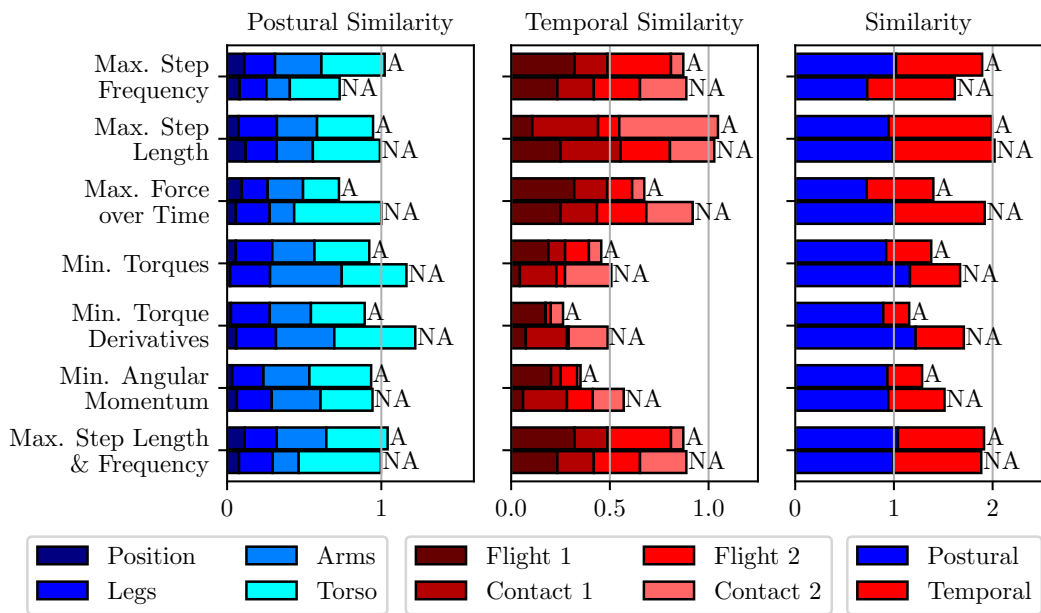
Figure 6.2: Animated sequences of some exemplary optimized sprinting motions for the amputee and the non-amputee athletes

the temporal similarity and the right diagram showing the combination of both postural and temporal similarity.

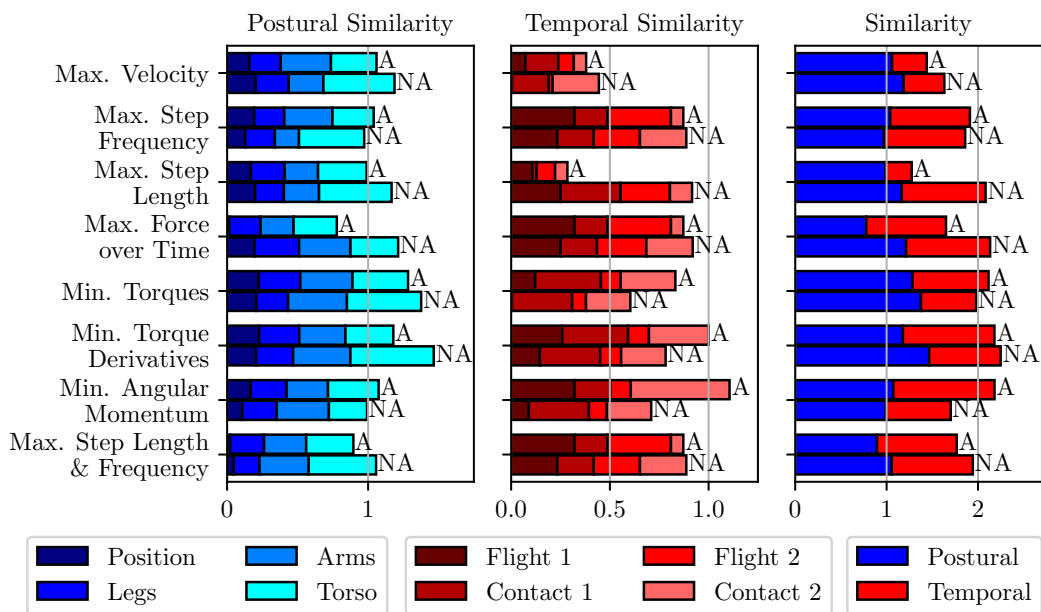
We first consider the solutions where the average velocity was fixed (Figure 6.3a). In terms of overall similarity (with the chosen weighting), we can rank the similarity measures from low to high as follows:

- | non-amputee athlete (NA)                   | amputee athlete (A)                        |
|--|--|
| 1. <i>Min. Angular Momentum</i>            | 1. <i>Min. Torque Derivatives Squared</i>  |
| 2. <i>Max. Step Frequency</i>              | 2. <i>Min. Angular Momentum</i>            |
| 3. <i>Min. Torques Squared</i>             | 3. <i>Min. Torques Squared</i>             |
| 4. <i>Min. Torque Derivatives Squared</i>  | 4. <i>Max. Force Over Time</i>             |
| 5. <i>Max. Step Length &amp; Frequency</i> | 5. <i>Max. Step Frequency</i>              |
| 6. <i>Max. Force Over Time</i>             | 6. <i>Max. Step Length &amp; Frequency</i> |
| 7. <i>Max. Step Length</i>                 | 7. <i>Max. Step Length</i>                 |

For both athletes, the objective function *Min. Angular Momentum* is among the best two overall similarity values. Hence, it seems that angular momentum control is an important factor



(a) Similarity measures of sprinting for fixed average velocity



(b) Similarity measures of sprinting for free average velocity

Figure 6.3: Similarity measures computed for the solutions of the sprinting motion synthesis optimal control problems with fixed and free average velocity. For the two diagrams on the left, we have further subdivided the similarity measure into individual components, namely contributions of the overall position, arms, legs and torso in the case of the postural measure and contributions of the four phases in the case of the temporal measure. For the right diagram, we combined postural and temporal measures. The abbreviations ‘NA’ and ‘A’ stand for the non-amputee and the amputee athlete, respectively.

in sprinting motions. The other two minimizing objective functions *Min. Torques Squared* and *Min. Torque Derivatives Squared* are among the best four similarity measures for both athletes. This result is rather counterintuitive, since the explosiveness and dynamics of a sprinting move-

ment suggests maximizing optimization criteria. In addition, the goal of a sprinter is to push himself to the limits without regard to energy efficiency. Two considerations help to understand these results: Firstly, we are looking at the OCP solutions at a fixed average velocity, which is therefore fixed. This implies that the average kinematic translational energy is already fixed as well. It is exactly that needed to maintain the prescribed velocity. The two objective functions then achieve solutions that maintain the velocity the most efficient and dynamic way (see also earlier studies on sprinting with RSPs[94]). If the average velocity is left free to choose, the situation changes significantly (see Figure 6.3b). The second observation is that for a numerically complex problem like the two sprinting steps, the initial values for the variables must be good enough. Therefore, we start all OCPs from the reconstructed solution. If we now have an optimization criterion like *Max. Step Length*, which can only be achieved by long steps, the solution may have to move far away from the starting motion. In the case of the minimizing objective functions examined here, minima can be achieved by different combinations of the individual joint torques. Thus, it is possible that the solutions do not have to move as far away from the start values to reach the termination criterion as the maximizing objective functions. To exclude this behavior, a sensitivity analysis with respect to the initial value would be helpful. A look at the temporal similarity values supports this observation, because especially for the three minimizing criteria the temporal values are very close to the reference values. They are the top three objective functions for both the non-amputee and amputee athlete. The objective function *Max. Step Length* has the worst similarity measures for both athletes. This is easily explainable since for larger steps more time is needed. It is noticeable that the order of the postural similarity measures differs significantly (again ranking from low to high similarity values):

non-amputee athlete (NA)	amputee athlete (A)
1. <i>Max. Step Frequency</i>	1. <i>Max. Force Over Time</i>
2. <i>Min. Angular Momentum</i>	2. <i>Min. Torque Derivatives Squared</i>
3. <i>Max. Step Length</i>	3. <i>Min. Torques Squared</i>
4. <i>Max. Step Length &amp; Frequency</i>	4. <i>Min. Angular Momentum</i>
5. <i>Max. Force Over Time</i>	5. <i>Max. Step Length</i>
6. <i>Min. Torques Squared</i>	6. <i>Max. Step Frequency</i>
7. <i>Min. Torque Derivatives Squared</i>	7. <i>Max. Step Length &amp; Frequency</i>

For the non-amputee athlete, we find *Max. Step Frequency* and *Max. Step Length* among the best three objective functions. Average sprinting velocity is commonly defined as the product of step frequency and step length, hence the fact that both criteria have high postural similarity measures indicates that the non-amputee athlete indeed tries to run as fast as possible. The objective function *Max. Step Length & Frequency* ranks fourth in terms of postural similarity of the non-amputee athlete. Hence, it seems that the non-amputee reference athlete aims to achieve both high step frequencies and large step lengths with a stronger focus on the step frequency for his optimal way of sprinting. We assume that different weight factors balancing step frequency and step length might yield even higher similarities. A systematic way to identify weight factors matching recorded reference motions is described in Section 3.2 with results presented in Chapter 7.

We now consider the solutions where the average velocity was free (Figure 6.3b). In terms of overall similarity (with the chosen weighting), we can rank the similarity measures from low to high as follows:

non-amputee athlete (NA)	amputee athlete (A)
1. <i>Max. Average Velocity</i>	1. <i>Max. Step Length</i>
2. <i>Min. Angular Momentum</i>	2. <i>Max. Average Velocity</i>
3. <i>Max. Step Frequency</i>	3. <i>Max. Force Over Time</i>
4. <i>Max. Step Length &amp; Frequency</i>	4. <i>Max. Step Length &amp; Frequency</i>
5. <i>Min. Torques Squared</i>	5. <i>Max. Step Frequency</i>
6. <i>Max. Step Length</i>	6. <i>Min. Torques Squared</i>
7. <i>Max. Force Over Time</i>	7. <i>Min. Angular Momentum</i>
8. <i>Min. Torque Derivatives Squared</i>	8. <i>Min. Torque Derivatives Squared</i>

As already briefly mentioned, the picture is significantly different for the solutions with freely adjustable average velocity: For both athletes the objective function *Max. Average Velocity* is among the two best criteria. This objective function can obviously only be formulated if the average velocity is not fixed. Furthermore, it is noticeable that the maximizing criteria perform significantly better when the average velocity is not fixed, while the minimizing objective functions show rather lower similarity values on average. In contrast to the solutions with fixed average velocity, a comparable picture emerges when considering the individual position or temporal similarity measures. The main reason for this is that without fixing the average velocity no translation energy level is given, so that significantly lower torques are possible. However, these are connected with lower average velocities, which can, among other things, also lead to greater deviations in posture and phase durations. At this point it is interesting to take a look at the average velocities of the individual solutions, which is given in Table 6.2.

As would be intuitively expected, our model generates slow average velocities for the minimizing objective functions and high average velocities for the maximizing objective functions. For most objective functions, these velocities are smaller or comparable to the fixed average velocity of the motion capture recordings, which were also used as average velocities for the fixed velocity solutions. However, three (non-amputee athlete) or four (amputee athlete) solutions have significantly higher average velocities ( $11.13 \text{ m s}^{-1}$  to  $14.96 \text{ m s}^{-1}$ ). At this point, it should be noted that we are investigating the phase of sprinting at maximum velocity, i.e., exactly the phase in which the highest velocities are reached. Analyses of the fastest non-amputee 100 m sprinters have shown that they run after 60 m to 70 m at an average velocity of  $12.34 \text{ m s}^{-1}$  [72, 83]. This value fits the calculated average velocities for the objective function *Max. Step Length*. The remaining faster average velocities are about  $1 \text{ m s}^{-1}$  to  $2.5 \text{ m s}^{-1}$  larger, i.e., our model seems to be able to run faster than the fastest human so far, despite the fitted torque limits. Here, two aspects can contribute to the explanation: On the one hand, the movements are computed as a whole; all variables are thus selected by the OCP at any time in such a way that they fulfill the objective functions optimally. On the other hand, it is possible that limitations of our models, which are rather simple in some points (such as the restriction to the sagittal plane, the neglect of aerodynamic drag, the simple foot model and the heuristic fitting routine instead of actual measurements), allow higher average velocities. A detailed comparison with motion capture recordings of sprinters with average velocities of about  $12.3 \text{ m s}^{-1}$  would be useful.

If we now compare the average velocities between the non-amputee and amputee athletes, no clear trend can be identified. For the majority of the objective functions, the difference is very small, the deviations from one another being less than 8%. For three objective functions, differences in average velocities are more pronounced: *Max. Step Length*, *Max. Step Frequency*, *Max. Force Over Time*. For the first and last one, the average velocities are greater in the case of the amputee athlete. It is particularly interesting that the amputee athlete runs on average  $1.1 \text{ m s}^{-1}$  slower than the non-amputee athlete. It has been shown that leg stiff-

Table 6.2: Average velocities of the solutions of the different sprinting motion synthesis optimal control problems

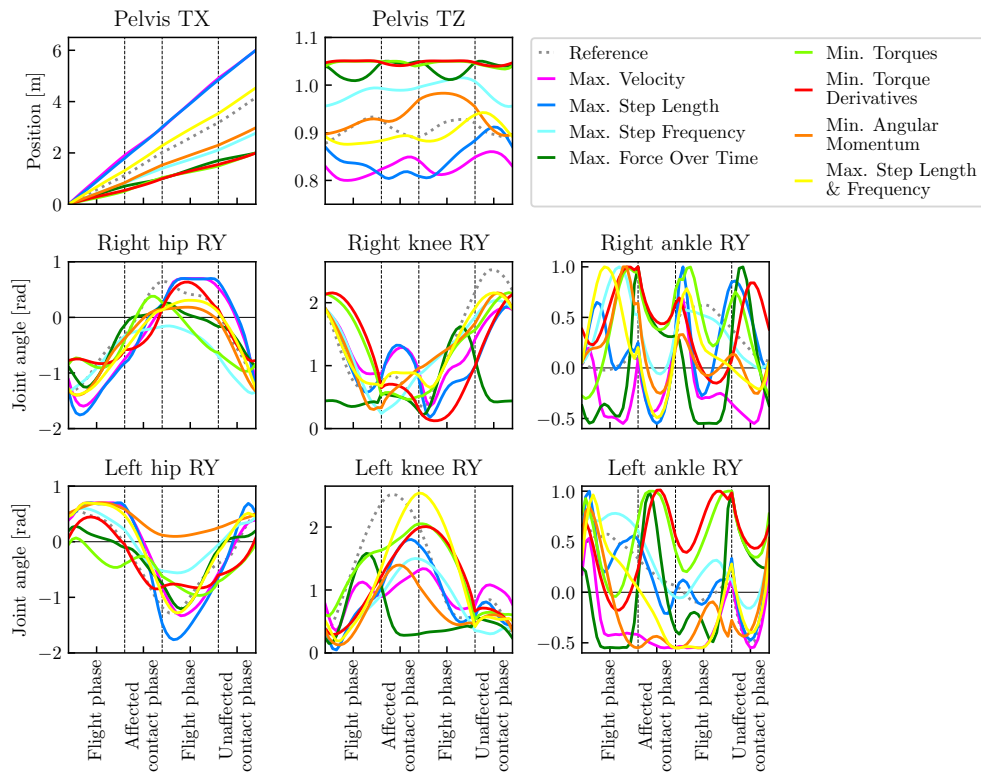
	Non-amputee athlete	Amputee athlete
Fixed velocity (reconstructed from reference athletes, cf. Chapter 5)	9.52 m s <sup>-1</sup>	9.54 m s <sup>-1</sup>
<i>Max. Average Velocity</i>	14.96 m s <sup>-1</sup>	14.67 m s <sup>-1</sup>
<i>Max. Step Length</i>	11.13 m s <sup>-1</sup>	12.73 m s <sup>-1</sup>
<i>Max. Step Frequency</i>	8.15 m s <sup>-1</sup>	7.05 m s <sup>-1</sup>
<i>Max. Force Over Time</i>	4.35 m s <sup>-1</sup>	13.08 m s <sup>-1</sup>
<i>Min. Torques</i>	4.18 m s <sup>-1</sup>	4.01 m s <sup>-1</sup>
<i>Min. Torque Deriv.s</i>	3.84 m s <sup>-1</sup>	4.14 m s <sup>-1</sup>
<i>Min. Angular Momentum</i>	5.84 m s <sup>-1</sup>	5.88 m s <sup>-1</sup>
<i>Max. Step Length &amp; Frequency</i>	13.34 m s <sup>-1</sup>	13.65 m s <sup>-1</sup>

ness and stride frequency are related to each other in running, either directly[36] or via contact time length[98]. However, studies on sprinters with unilateral below the knee amputation (BKA)[50, 62, 86] have shown that the fixed stiffness of the RSP and the associated differences to the biological leg restrict the ability to regulate the stiffness of the entire leg affected by the amputation and thereby achieving top speed. Our simulation seems to confirm these results: When required to maximize step frequency, the amputee model can only generate slower average velocities. Nevertheless, for other objective functions the amputee model is able to generate higher average velocities than the non-amputee model. This result is in accordance with observations that running velocity is not only determined by step frequency[50, 62, 86], hence amputee athletes might adjust other parameters to achieve high velocities (compare the ranking of similarity measures: *Max. Velocity* and *Max. Step Length* are the best two objective functions for the amputee athlete in terms of overall similarity for free average velocities, *Max. Step Frequency* is only the fifth best; for the non-amputee athlete, it is the third best objective function).

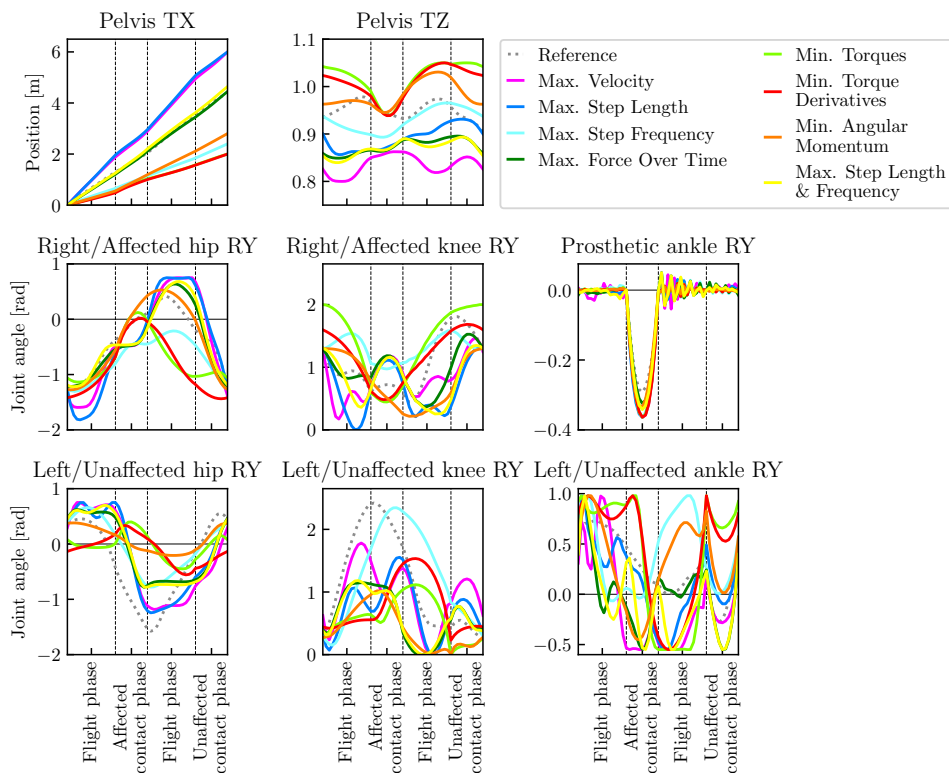
Considering all motions, the highest average velocity is achieved with the objective function *Max. Average Velocity* for the non-amputee athlete. For the same objective function, the amputee athlete also achieves his highest average velocity; however, it is 0.29 m s<sup>-1</sup> slower than the one of the non-amputee athlete. This could indicate that above a certain velocity the RSP actually prevents the amputee from running faster. Further investigation would be necessary.

## 6.2 Comparison of the Synthesized Motions with Free Average Velocity

Finally, in order to be able to further classify these observations, we now examine the kinematics and dynamics of the generated movements at free average velocity and compare them with the reference movement from the reconstruction (see Chapter 5). The overall position, leg joint angles and torques of the non-amputee and the amputee athlete are shown in Figures 6.4 and 6.5, respectively. When looking at the position in space ('Pelvis TX/TZ') it is noticeable that the generated movements are distributed around the reference value; some cover a greater distance, others a shorter one. It is interesting that for both athletes, the forward distance traveled for the objective functions *Max. Average Velocity* and *Max. Step Length*



(a) Non-amputee athlete



(b) Amputee athlete

Figure 6.4: Overall position and leg joint angles of the non-amputee and amputee athletes for eight synthesized motions with free average velocity. The dotted gray lines give the solutions from the dynamics reconstruction.

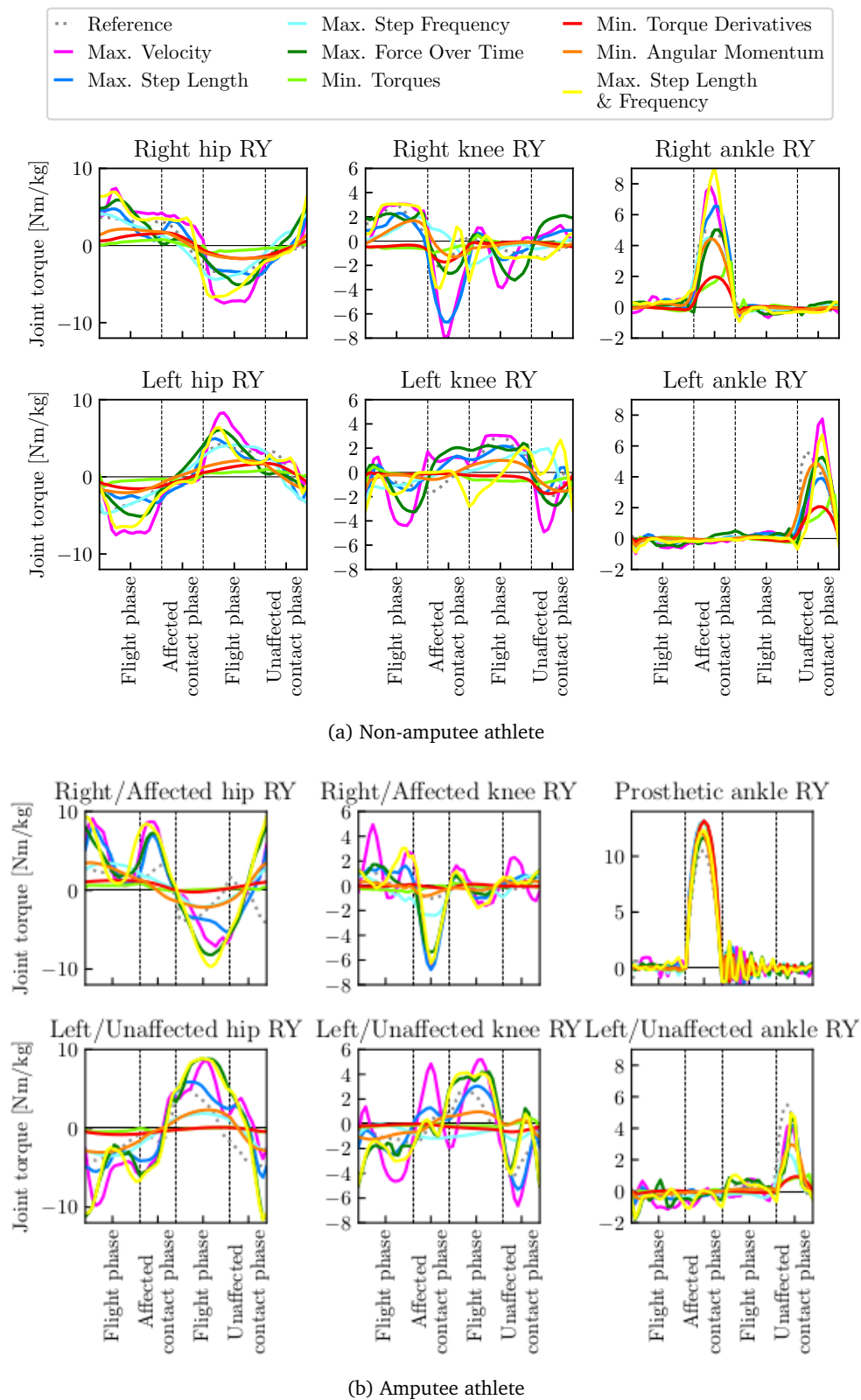


Figure 6.5: Leg joint torques of the non-amputee and amputee athletes for eight synthesized motions with free average velocity. The dotted gray lines give the solutions from the dynamics reconstruction. The given torque in the prosthetic ankle is computed via Eq. (2.1), as the RSP is a passive device.

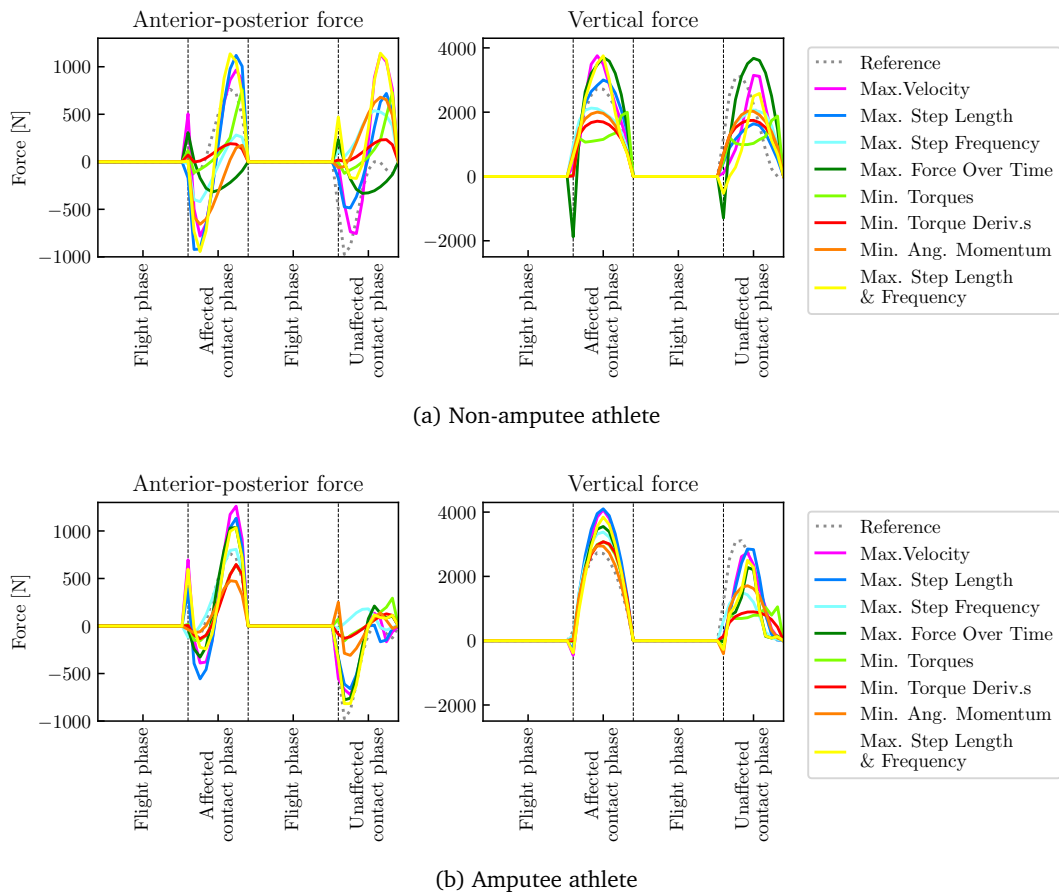


Figure 6.6: Ground reaction forces of the non-amputee and amputee athletes for eight synthesized motions with free average velocity. The dotted gray lines give the solutions from the dynamics reconstruction.

are almost identical. For both athletes, the objective function *Max. Step Length & Frequency*, which combines step length and frequency, is very close to the reference movement. As expected, the distance traveled is significantly shorter with the objective functions minimizing torque (derivative). In the case of the amputee athlete, a striking feature of these is the significant lowering of the vertical position during contact with the RSP. This is necessary to maximize the flexion of the prosthetic ankle joint and makes sense since the spring properties of the RSP are thus optimally exploited. Conversely, less torque is required in the other joints. However, the strong utilization of the RSP can also be seen in the other objective functions. In all generated movements, the RSP is flexed more than in the actual reference movement. As a result, the passive device also generates more torque than the reconstructed torque. In the biological ankle, the exact opposite is evident: The torque (actively generated here) is lower than the reconstructed torque. The ground reaction forces shown in Figure 6.6 show the same: During prosthetic contact, the forces for all objective functions are greater than those of the reconstruction; during biological contact, they are smaller for all. This behavior means that the model of the amputee athlete makes significantly more efficient use of the RSP than in reality. One reason for this could again be the idealization of the OCP solution: Since the OCP solves the movement as a whole, there is also knowledge of the overall movement and environment at all times, so that, for example, the foot can be perfectly positioned for a touchdown. This is not possible for a real person.

For both sprinters, the majority of the generated motions show significantly greater flexion in

the knee during the contact phases. Correspondingly, the torques during this phase are also significantly higher. This is interesting because – as discussed in the analysis of the reconstruction results – there is a presumption that unilateral amputee athletes intentionally stiffen their knee in order to make optimal use of the spring properties of the RSP. Our simulation supports this hypothesis on the one hand, since it shows that even with limits on torque that are adapted to the athlete’s capabilities, more flexion and greater torque in the knee would indeed be possible during this phase. On the other hand, our model makes significantly better use of the RSP than the real amputee athlete in the measurements. Thus, the simulations suggest that it is not necessarily necessary to stiffen the knee in order to fully exploit the RSP.

### 6.3 Summary

We successfully computed realistic sprinting steps of one athlete with and one athlete without BKA, based on seven combinations of optimization criteria for sprinting at fixed average velocity and eight combinations of optimization criteria for sprinting at free average velocity. We compared the resulting motions to the reference motions from the previous chapter based on a similarity measure and identified the best (combinations of) criteria. It has been shown that especially maximization of step length, step frequency or average speed yield realistic movements with small similarity measure values. In the upcoming chapter, in which an inverse optimal control problem (IOCP) is considered to identify the optimization criteria underlying the reference movements, we have included the maximization of step length and step frequency as criteria to be able to analyze the individual behavior of each athlete. On the other hand, in the chapter comparing the amputee athlete with himself without amputation in the suggested simulator tool, we also decided to use an objective function that mainly maximizes the average velocity. In addition, by examining the different objective functions, it became clear that angular momentum control seems to play an important role in the movement of the athlete with BKA, which we will further investigate in the upcoming chapter.

Compared to the reference motions, however, some differences have been noticed that show further possible research directions: First, for some objective functions (namely those that maximize optimization criteria), rather large average velocities occur. This is – as explained earlier – presumably mainly due to the fact that the OCP computes the motion as a whole and thus can take the optimal position at any time in all DOFs and compute the optimal actuation pattern. This is not equally possible in reality. Here, the results of the IOCP in the next chapter will provide further insight, as it is likely that athletes do not optimize a single criterion, but a combination with weight factors to be determined. Another issue that could be explored further regarding the large velocities is whether the torques actually correspond to the torques possible for the athlete at each time point. Compared to the initial work on motion generation [69], the introduction of a MTG model to compute the limits represented a significant improvement. Nevertheless, further investigations are possible: a sensitivity analysis with respect to the individual variables could provide interesting insights here. Another research question with respect to velocities is raised by the observation that the amputee athlete runs faster than the non-amputee athlete only up to a certain velocity and then this behavior reverses. Here, further research would be interesting to compare our results, which suggest that the RSP may have a more hindering effect above a certain velocity threshold, with those of Grabowski et al. [50], which assume that the RSP fundamentally hinders force production and thus top speeds. In this context, there is also another issue raised by the results presented here: Compared to the measured reference movements, the amputee athlete makes better use of the RSP, but also shows greater knee flexion. With the current calculations it is not yet possible to explain exactly what the cause of this behavior is and where the discrepancy between

observation and simulation comes from. Finally, in the previous chapter, we discussed how the inter-limb asymmetry of the amputee athlete affects the motions. Here, we have not concentrated our analysis on investigating symmetry and asymmetry in the motions of amputee and non-amputee athlete. This will be done in more detail in the next chapter where we further subdivide the optimization criteria with respect to joints of left and right body sides and to left and right steps.



## 7 Inverse Optimal Control of Sprinting Motions with and without Running-Specific Prostheses

After having examined different optimization criteria and their effects on the generated sprinting motions in the previous chapter (Chapter 6), we are now interested in identifying which combinations of optimization criteria underlie realistic sprinting motions and whether they differ for sprinting with and without running-specific prosthesis (RSP). This chapter gives an extended version of the results presented in [34]. Additional results using fixed average velocities, less subjects and box limits for the torques (in contrast to the here applied limits based on Muscle Torque Generators (MTGs)) are published in [31]. To get closer to an answer to these questions, we choose the formulation of an inverse optimal control problem (IOCP), whose general formulation and solution are described in Section 3.2. On the inner level we use the identical problem formulation as in the previous chapter (Chapter 6), i.e., we adopt all constraints, limits and initial values. Only the selection of the basic criteria and composition of the overall objective function differ. When selecting the objective functions, we have oriented ourselves on those of the pure motion generation problem. In addition to the weight factors  $w_i$  which are the optimization variables of the outer problem and thus need to be of a comparable magnitude, we introduced constant scaling factors  $s_i$  to compensate for different orders of the individual criteria; they are given in Table 7.1. As we are not only interested in the identification of criteria which underlie the sprinting motions, but also want to examine differences which occur due to the inter-limb asymmetry of the unilateral amputee athlete, we further split the criteria, e.g., in right and left side contributions. The objective function then has five main contributing criteria (which are possibly subdivided):

$$\begin{aligned} \Phi(\mathbf{w}; \mathbf{x}(t), \mathbf{u}(t), \mathbf{p}, \mathbf{h}) &= \varphi_{L_A}(\gamma_0, \dots, \gamma_{10}; t, \mathbf{x}(t), \mathbf{u}(t), \mathbf{p}) + \varphi_{L_B}(\gamma_{11}; t, \mathbf{x}(t), \mathbf{u}(t), \mathbf{p}) \\ &+ \varphi_{L_C}(\gamma_{12}; t, \mathbf{x}(t), \mathbf{u}(t), \mathbf{p}) \\ &+ \varphi_{M_A}(\gamma_{13}, \gamma_{14}; t_f, \mathbf{x}(t_f), \mathbf{p}) + \varphi_{M_B}(\gamma_{15}, \gamma_{16}; t_f, \mathbf{x}(t_f), \mathbf{p}), \end{aligned} \quad (7.1)$$

where the individual components are:

- Minimization of Torque Derivatives Squared (based on Eq. (6.5f))<sup>1</sup>:

$$\begin{aligned} \varphi_{L_A}(\gamma_0, \dots, \gamma_{10}; t, \mathbf{x}(t), \mathbf{u}(t), \mathbf{p}) &= \gamma_0 s_0 u_{\text{right hip}}^2(t) + \gamma_1 s_1 u_{\text{left hip}}^2(t) \\ &+ \gamma_2 s_2 u_{\text{right knee}}^2(t) + \gamma_3 s_3 u_{\text{left knee}}^2(t) \\ &+ \gamma_4 s_4 u_{\text{right ankle}}^2(t) + \gamma_5 s_5 u_{\text{left ankle}}^2(t) \\ &+ \gamma_6 s_6 (u_{\text{thorax}}^2(t) + u_{\text{lumbar}}^2(t) + u_{\text{head}}^2(t)) \\ &+ \gamma_7 s_7 u_{\text{right shoulder}}^2(t) + \gamma_8 s_8 u_{\text{left shoulder}}^2(t) \\ &+ \gamma_9 s_9 u_{\text{right elbow}}^2(t) + \gamma_{10} s_{10} u_{\text{left elbow}}^2(t). \end{aligned} \quad (7.2a)$$

<sup>1</sup>In the case of the amputee athlete, the weight  $\gamma_4$  for the right ankle joint torque derivative is set to zero, as no active torque acts in the prosthetic ankle.

- Head Stabilization (based on Eq. (6.5h)):

$$\varphi_{L_B}(\gamma_{11}; t, \mathbf{x}(t), \mathbf{u}(t), \mathbf{p}) = \gamma_{11} s_{11} \|\theta_{\text{head,abs}}\|_2^2. \quad (7.2b)$$

- Minimization of Trunk Angular Momentum about center of mass (CoM) Squared (based on Eq. (6.5g)):

$$\varphi_{L_C}(\gamma_{12}; t, \mathbf{x}(t), \mathbf{u}(t), \mathbf{p}) = \gamma_{12} s_{12} \|\mathbf{l}_{CoM}^{torso}(\mathbf{q}(t), \dot{\mathbf{q}}(t))\|_2^2. \quad (7.2c)$$

- Maximization of Step Frequency (based on Eq. (6.5b)):

$$\varphi_{M_A}(\gamma_{13}, \gamma_{14}; t_f, \mathbf{x}(t_f), \mathbf{p}) = \gamma_{13} s_{13} P_{\text{freq},R} + \gamma_{14} s_{14} P_{\text{freq},L}. \quad (7.2d)$$

- Maximization of Step Length (based on Eq. (6.5c)):

$$\varphi_{M_B}(\gamma_{15}, \gamma_{16}; t_f, \mathbf{x}(t_f), \mathbf{p}) = \gamma_{15} s_{15} P_{\text{length},R} + \gamma_{16} s_{16} P_{\text{length},L}. \quad (7.2e)$$

The initial values for the 17 weight factors  $\gamma$  are chosen based on the results of the motion synthesis study described in Chapter 6 and given in Table 7.1. The initial step size for the BOBYQA algorithm was set to 0.5. The IOCPs identified a set of optimal weights for the three non-amputee and the amputee athlete with which motions are synthesized that are close to the reference motions. The optimal weights are given in Table 7.1, together with the mean value for the three non-amputee athletes.

## 7.1 Comparison of Final and Hand-Picked Weight Solutions

In Chapter 6, we chose the weight factors for combining the single optimization criteria into an objective function by hand. The IOCP approach which we use here is far more systematic. Therefore, we start the analysis of the IOCP solutions by comparing the best weight solutions with the ones produced by hand-picked combinations of weights. For this comparison, we apply the similarity measure (6.6) of the previous chapter consisting of a postural and a temporal part. The similarity measures are shown in Figure 7.1. The upper eight bars give the values for the eight objective functions investigated in Chapter 6 for the non-amputee athlete 1 (left side of diagram) and the amputee athlete (right side of diagram). The remaining four bars give the best weight similarity values for the three non-amputee athletes and the amputee athlete. We added dashed vertical lines to the diagrams that show the postural and temporal similarity measures of the best weight solutions. For all four athletes, the best weight similarity measures are much smaller than the ones for solutions with hand-picked weight combinations. The former are thus closer to the reference motions. In the case of the non-amputee athletes, both postural and temporal values are significantly smaller; the similarity improves by at least 15 % if we take all three athletes into account. If we only compare the non-amputee athlete 1 for whom the similarity measures with the hand-picked combinations of weights are computed, it even improves by almost 50 %. The overall similarity measure is improved by at least 10 % individually and by 35 % on average for the best weight solutions of the amputee athlete. In this case, however, there are individual criteria for which the postural similarity measure is a bit worse (*Max. Step Length, Max. Force over Time, Max. Step Length & Frequency*). In summary, the IOCP approach provides weights that can be used to compose objective functions that are closer to the reference motion.

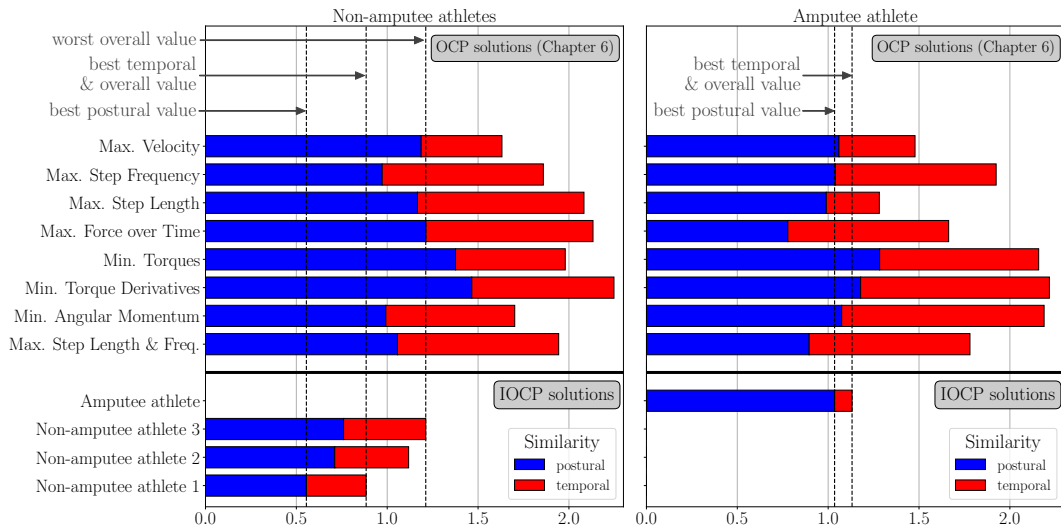


Figure 7.1: Postural and temporal similarity measures comparing the best weight inverse optimal control problem solutions with the solutions by hand-picked combinations of weights (Chapter 6) for three non-amputee athletes and one amputee athlete

Figure 7.2 shows the movements in animated sequences, graphically representing the similarity of the solutions. The sequences were created at the same relative time points of the motion. The colored models show the best weight IOCP and the grey models the reference motions. We directly notice that the best weight motions have similarities to the reference motions and coincide in key features. However, at the same time we see differences especially in the second step, which will be discussed in Section 7.3 in more detail. It is also noticeable that the model of the non-amputee athlete 1 remains behind the reference data and the models of the non-amputee athlete 2 and the amputee athlete remain in front of the reference data. This suggests that the velocity may be too low for the former and too high for the latter. We will also address this observation in Section 7.3.

## 7.2 Interpretation of Final Weights for Sprinting with and without Running-Specific Prostheses

After the previous section has shown that the IOCP method is a significant improvement over hand-picked weight combinations in terms of the similarity of the calculated solutions to the reference movements, we will now in a next step take a closer look at the best weights. The calculated best weights for each of the three non-amputee athletes and the amputee athlete are given in Table 7.1. In addition, we calculated the mean of the best weights of the non-amputee athletes for each criterion. We will focus in particular on two questions during the discussion:

1. For which optimization criteria do the best weights found for the amputee athlete differ significantly from those of the non-amputee athletes?
2. Are there any optimization criteria for which the best weights for the left and right body sides differ significantly?

Thus, while the first question focuses on differences between non-amputee and amputee sprinting, the second question considers the aspect of asymmetry due to unilateral below-knee amputation, which we have also addressed in the previous two chapters.

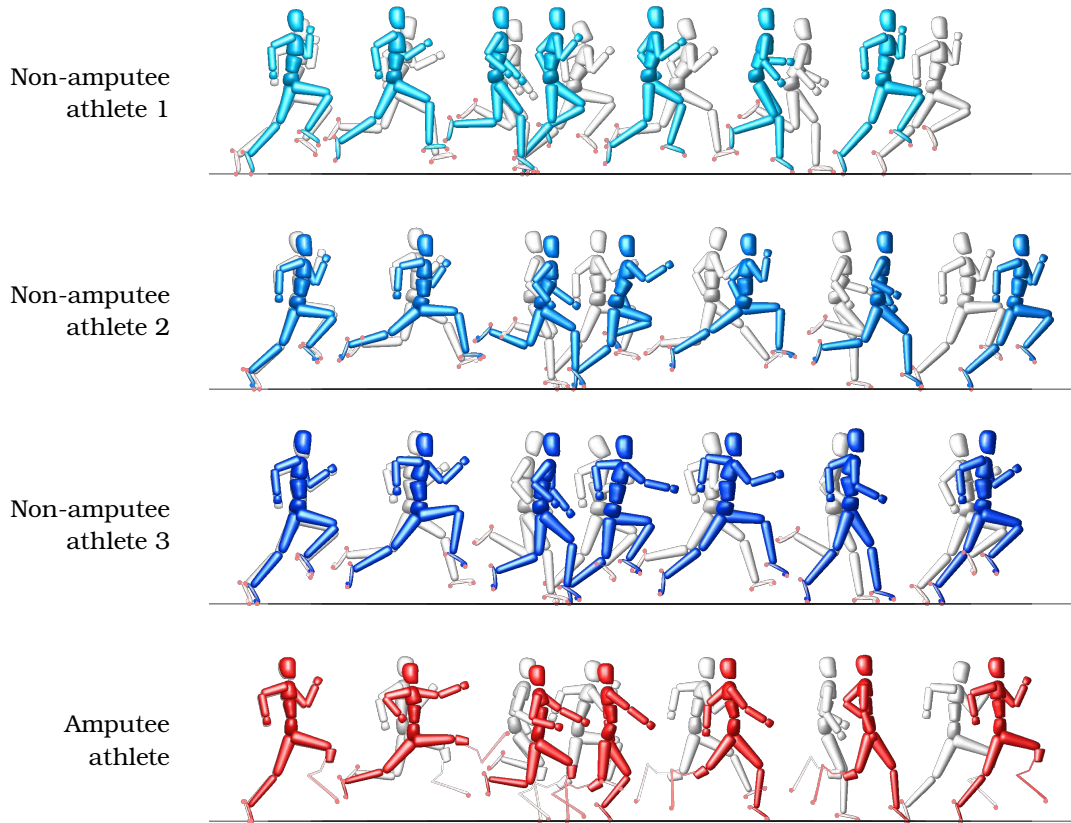


Figure 7.2: Animated sequences of the best weight inverse optimal control problem solutions (colored models) and the reconstructed reference motions from Chapter 5 (grey models). The snapshots have been taken at identical relative times in the motion.

### 7.2.1 Differences in Best Weights Between Athletes with and without Below the Knee Amputation

When looking at the identified best weights in Table 7.1 we immediately notice that there are clear differences between the weights of the amputee athlete and the group of non-amputee athletes. We first consider the weight factors associated with a minimization of the joint torque derivatives ( $\gamma_0 - \gamma_{10}$ ). The first weight factor  $\gamma_0$  (minimization of right hip torque derivative) is fixed to 1 for all athletes due to numerical reasons (usage of BOBYQA algorithm). Most of the remaining ten weights related to torque derivative minimization are equal ( $\gamma_3, \gamma_7, \gamma_8, \gamma_{10}$ ) or larger ( $\gamma_1, \gamma_6, \gamma_9$ ) for the amputee motion than the one of the non-amputee group. In the case of the amputee athlete, the weight factor  $\gamma_4$  is zero since the RSP is a passive device and only active torque derivatives have been considered in the objective functions. Only two weights are smaller:  $\gamma_2$  (right/affected knee) and  $\gamma_5$  (left/unaffected ankle). A greater minimization of the torque derivatives means that changes in torque are suppressed more resulting in smoother torques and an actuation pattern with less abrupt changes. As becomes also clear in the next section (see Figure 7.4), the torques themselves, nevertheless, can have similar orders of magnitude. Interestingly, the values connected to the right knee (circa one third of the value of the control group) and the left ankle (circa three quarters of the value of the control group) are much smaller in the case of the amputee athlete. Hence, it seems that the amputee athlete needs an actuation pattern with the possibility of sudden changes in the knee of the affected leg and the ankle of the unaffected leg for sprinting. This observation still holds for the knee weight if we compare the amputee athlete with non-amputee athlete 1 whose

Table 7.1: Scaling factors, initial and optimal weight factors for the base optimization criteria of the inverse optimal control problem. The abbreviations ‘NA’ and ‘A’ denote the non-amputee and amputee athletes, respectively.

	Scaling factors $\sigma_i$	Initial weights	Final Weights $\gamma_i$				
			NA 1	NA 2	NA 3	mean NA	A
$\gamma_0^*$	$10^{-9}$	1.000	1.000	1.000	1.000	1.000	1.000
$\gamma_1$	$10^{-9}$	1.000	1.029	1.004	1.006	$1.013 \pm 0.014$	1.280
$\gamma_2$	$10^{-9}$	1.000	1.027	0.998	1.014	$1.013 \pm 0.015$	0.391
$\gamma_3$	$10^{-9}$	1.000	0.999	1.000	1.004	$1.001 \pm 0.003$	0.990
$\gamma_4$	$10^{-8}$	1.000	0.988	0.969	0.993	$0.983 \pm 0.013$	-
$\gamma_5$	$10^{-8}$	1.000	1.000	0.998	1.983	$1.327 \pm 0.568$	0.982
$\gamma_6$	$10^{-9}$	0.900	1.001	0.997	1.007	$1.002 \pm 0.005$	1.110
$\gamma_7$	$10^{-9}$	0.900	0.902	0.897	0.872	$0.891 \pm 0.016$	0.897
$\gamma_8$	$10^{-9}$	0.900	0.896	0.893	0.884	$0.891 \pm 0.006$	0.834
$\gamma_9$	$10^{-9}$	0.900	0.862	0.901	0.890	$0.884 \pm 0.020$	1.210
$\gamma_{10}$	$10^{-9}$	0.900	0.889	0.909	0.873	$0.890 \pm 0.018$	0.903
$\gamma_{11}$	1	10.00	10.04	10.00	9.96	$10.00 \pm 0.04$	10.01
$\gamma_{12}$	0.05	0.500	0.497	0.527	0.461	$0.495 \pm 0.033$	1.101
$\gamma_{13}$	1	0.000	1.067	-0.004	0.008	$0.357 \pm 0.615$	-0.024
$\gamma_{14}$	1	0.000	0.155	-0.007	-0.162	$-0.005 \pm 0.159$	-0.064
$\gamma_{15}$	0.1	1.000	0.996	1.039	0.930	$0.988 \pm 0.055$	1.171
$\gamma_{16}$	0.1	1.000	0.911	0.466	0.759	$0.712 \pm 0.226$	1.050

\* The weight  $\gamma_0$  is fixed to 1.000 for the BOBYQA algorithm.

reference motion’s average velocity is closest to the average velocity in the amputee athlete’s reference motion. This is no longer the case for the weight related to the left/unaffected ankle, where the values are quite close to each other; this is probably due to the fact that the standard deviation of the mean value of the non-amputee group is very large, since the identified best weight in the case of non-amputee athlete 3 is twice as large as in the case of the other two non-amputee athletes. As expected the weight factor  $\gamma_{11}$  related to the gaze stabilization does not differ significantly between non-amputee and amputee sprinting confirming the idea that it is not a decisive criterion, but mainly added for supporting an upright head posture.

While the objective functions, which are weighted using the weight factors discussed so far, are numerically and general motion inspired, the remaining five weight factors correspond to criteria which are more specifically introduced for synthesizing sprinting motions: The weight factor  $\gamma_{12}$  belongs to the minimization of the upper body’s angular momentum with respect to the CoM. We observe a significant difference between non-amputee and unilateral amputee sprinting here. The weight factor of the amputee athlete is more than twice as large as the one of the non-amputee controls. Again, a smaller weight factor is accompanied by more freedom, which means that the angular momentum of the amputee athlete is significantly more controlled. As we also noted in the dynamics reconstruction chapter (Chapter 5), angular momentum control plays a major role in amputee sprinting and is clearly different from non-amputee sprinting.

Last, we consider the weight factors  $\gamma_{13} - \gamma_{16}$ , which are associated with the optimization criteria of maximizing step frequencies and step lengths of right and left steps. Again, large differences between non-amputee and amputee sprinters are apparent. First of all, however,

it should be pointed out that the standard deviations for the group of non-amputee athletes are very large for the weights other than  $\gamma_{15}$ , especially for those belonging to step frequency maximization. Therefore, we will again compare the weight of the amputee with both the mean of the non-amputee athletes and the weight for non-amputee athlete 1, who has a comparable average speed in the reference movement as the amputee athlete (non-amputee athletes 2 and 3 run significantly slower). When comparing with the mean value, it is noticeable that the signs of the weights differ in the step frequency maximization: The weights in the amputee sprinter have a negative sign, which means that the step frequencies are actually minimized rather than maximized. In the group of non-amputee athletes, on the other hand, the step frequency plays a crucial role only during the first step, as the weight becomes zero for the second step. The difference becomes even more obvious if we compare only with non-amputee athlete 1. It is further interesting that for all athletes, the pattern is recognizable that the weight for the second step ( $\gamma_{14}$ ) is smaller than that for the first step ( $\gamma_{13}$ ). Here, it would be exciting to investigate the reverse step order to rule out that this behavior has numerical reasons. The weights related to step length maximization are larger in the case of the amputee athlete compared to the non-amputee athletes ( $\gamma_{15}$ : 20% larger than non-amputee athletes,  $\gamma_{16}$ : 50% larger than non-amputee athletes). The trend for these two weights, too, is that the weight for the second step is lower than the one for the first step for all athletes. As with the weights belonging to the step frequency, an investigation with reversed step order would be interesting to exclude effects of problem formulation (e.g., periodicity after two steps).

### 7.2.2 Differences in Best Weights Between Left and Right Body Sides

To get closer to answering the second question, we formulate a measure of the asymmetry of the weights between the left and right sides of the body. It calculates an asymmetry value by normalizing the difference of the weights between right and left half of the body with respect to the mean value of right and left body sides:

$$asymmetry = \frac{\gamma_r - \gamma_l}{0.5(\gamma_r + \gamma_l)} \cdot 100, \quad (7.3)$$

with  $\gamma_{r/l}$  being the weight related to the right/left body side. The computed asymmetry values are given in Table 7.2. A positive value indicates that the weight related to the right side of the body is larger than the one related to the left side of the body. If we first take a look at the asymmetry values for the non-amputee athletes, we notice that the non-amputee athletes 1 and 2 are more symmetric than non-amputee athlete 3. This is mainly due to the fact that the weights related to step frequency maximization differ greatly for this specific athlete yielding an asymmetry value of -221.93. Even though the asymmetry for almost all athletes seems to be greatest at step frequency, this value is very striking. Since the non-amputee athlete 3 also has the worst values for similarity (cf. Figure 7.1) and we furthermore have already noted in the discussion of symmetry for the reconstructed solutions in Chapter 5 that he has the most asymmetric running style, we would like to ignore this value in the discussion. Instead, we will again focus on the mean of the non-amputee athletes and on non-amputee athlete 1, who is most similar to the amputee athlete in stature and average velocity of the reference movement. For the non-amputee athletes, the weights for minimizing the torque derivatives in the joints are relatively symmetrical, and the asymmetry values are small. The exception is the weight belonging to the ankle joint. However, also here the comparatively large value comes from the non-amputee athlete 3. Significant asymmetries show up in the non-amputee athletes in the weights for step frequency and step length. In particular, for the non-amputee athletes 2 and 3, the inverse relationship of step length and step frequency can be found due to the opposite

Table 7.2: Asymmetry values computed for the individual joints of the best weight solutions for the three non-amputee athletes and the athlete with below the knee amputation

Weights	NA 1	NA 2	NA 3	mean NA	A
$\gamma_0, \gamma_1$ (hip)	-2.83	-0.38	-0.57	$-1.26 \pm 1.39$	-24.59
$\gamma_2, \gamma_3$ (knee)	2.75	-0.19	0.96	$1.17 \pm 1.47$	-86.75
$\gamma_4, \gamma_5$ (ankle*)	-1.28	-3.02	-66.59	$-23.63 \pm 57.83$	
$\gamma_7, \gamma_8$ (shoulder)	0.72	0.43	-1.36	$-0.07 \pm 1.94$	7.29
$\gamma_9, \gamma_{10}$ (elbow)	-2.99	-0.87	1.90	$-0.66 \pm 3.03$	29.04
$\gamma_{13}, \gamma_{14}$ (step frequency)	149.29	-54.66	-221.93	$-42.44 \pm 44.45$	-92.13
$\gamma_{15}, \gamma_{16}$ (step length)	8.92	76.09	20.21	$35.07 \pm 23.22$	10.97
Sum of absolute values	168.89	135.65	313.53	$104.30 \pm 193.01$	250.77

\*As  $\gamma_4 = 0$  in the case of the amputee athlete, we cannot compute the asymmetry value in this case. Due to the clearly different geometry between prosthetic and biological ankle and the resulting intrinsic asymmetry in this joint, the calculated asymmetry value would further not be meaningful.

signs. Overall, it appears that asymmetries in the non-amputee athletes arise primarily from changes in step length and step frequency.

This is completely different for the amputee athlete. All asymmetry values related to minimization of torque derivatives are significantly larger than in the non-amputee athletes. If we take the absolute values of the asymmetries for the amputee athlete, they are 0.3 to 123 times the values of the non-amputee athletes' mean and 0.6 to 31.5 times those of the non-amputee athlete 1. The sum of the absolute values is 2.4 times or 1.5 times larger for the amputee athlete than for the non-amputee reference group or non-amputee athlete 1, respectively (and that, although the sum for the non-amputee cases includes the asymmetry value of the ankle joint, which could not be calculated for the amputee athlete). The asymmetry values are particularly large for the weights, which are associated with minimizing the torque derivatives in the leg joints ( $\gamma_1 - \gamma_4$ ) and maximizing the step frequency ( $\gamma_{13}, \gamma_{14}$ ). Let us first discuss the weights related to the torque derivatives in the leg joints: The weights of the affected leg of the amputee athlete (right leg) are larger than those of the unaffected (left) leg by a factor of circa 1.3 (hip) and 2.5 (knee). As a comparison, the deviations for the non-amputee athletes are at a maximum factor of 0.03 (both for hip and knee joints). Hence, huge and sudden changes in the torques of the unaffected leg are less restricted for the amputee athlete such that less smooth torque histories are possible. It appears that the torques of the biological leg are needed to compensate the inter-limb asymmetry and balance actions of the RSP, e.g., resonating effects due to the spring-like properties.

The asymmetry value related to the step frequency is relatively large for all four athletes. Compared to the other final weights, the weights related to step frequency maximization are rather small. Nevertheless, the difference due to the inter-limb weight asymmetry is clearly visible, since the step frequency is also related to the ability to bring the legs forward quickly, which in turn depends on the weight of the leg, among other things. At this point, however, we would again like to point out that we observed the overall trend that the weights for step length and step frequency become smaller in the second step and that one cause could lie in the problem formulation.

Table 7.3: Comparison of the reference data and the best weight inverse optimal control problem solution for the four athletes regarding total time of the two steps, distance covered by the pelvis segment during the two steps and average velocity. The abbreviations ‘NA’ and ‘A’ denote non-amputee and amputee athletes, respectively.

	Reference data			IOCP solution		
	Total time	Distance	Velocity	Total time	Distance	Velocity
NA 1	0.438 s	4.15 m	$9.49 \text{ m s}^{-1}$	0.405 s	3.60 m	$8.88 \text{ m s}^{-1}$
NA 2	0.516 s	4.54 m	$8.79 \text{ m s}^{-1}$	0.543 s	5.10 m	$9.38 \text{ m s}^{-1}$
NA 3	0.490 s	4.56 m	$9.30 \text{ m s}^{-1}$	0.526 s	4.73 m	$8.98 \text{ m s}^{-1}$
A	0.460 s	4.38 m	$9.52 \text{ m s}^{-1}$	0.474 s	4.89 m	$10.32 \text{ m s}^{-1}$

### 7.3 Analysis of the Curves of Characteristic Variables

As already mentioned in the consideration of the similarity measures, it is of course also interesting to see which of the generalized positions correspond well with the reference motion, which ones show stronger deviations and how the torques of the individual joints compare to the reference ones from the reconstructed solution. In Figure 7.2, we have noticed that the best weight solutions remain behind the reference data for non-amputee athlete 1 and in front of the reference data for non-amputee athlete 2 and the amputee athlete. To further investigate what this visual observation means for the average velocities of the individual athletes in the best weight IOCP solutions compared to those of the reference motions, we summarize the total times of the two steps, the distances covered by the pelvis segment during the two steps and the average velocities of both the reference data and the final weight IOCP solution for all four athletes in Table 7.3. The values indeed confirm the plausible assumption that the average velocity of the best weight solution of the non-amputee athlete 1 is below that of the reference data (likewise for the non-amputee athlete 3, even if this is not so clear from the observation of the animated sequences). For the non-amputee athlete 2 and the amputee athlete, the average velocities of the best weight solutions are above those of the reference data. Except for the non-amputee athlete 3, this is due to the fact that the distance covered by the pelvis segment is significantly smaller or larger than in the reference. In the mean of the three non-amputee athletes these individual differences actually cancel each other out and both the total time and the distance covered as well as the average velocity are comparable. Thus, at this point there is still potential to improve the best weights of the IOCP solutions by giving more weight to the deviations in the forward component of the pelvis segment in the IOCP formulation.

In addition, we display the root-mean-square errors (RMSEs) both the generalized positions and the joint torques. Figure 7.3 shows a comparison of the generalized positions of the best weight IOCP (blue line: mean of non-amputee athletes; blue shaded areas: standard deviation of non-amputee athletes; red line: amputee athlete) and the reference motions (grey dashed line: mean of non-amputee athletes; grey shaded areas: standard deviation of non-amputee athletes; grey dotted line: amputee athlete). It further gives the phase durations for both groups. Figure 7.4 illustrates the joint torques in the same way. The individual RMSEs between the reference data and the best weight IOCP solutions can be found in Figure A.6 in Appendix A.3 for reference purposes. We first examine the phase durations: For both the non-amputee group and the amputee athlete the best weight IOCP solutions match the phase durations of the reference motions very well. This is in accordance with the small temporal similarity measures. Hence, the IOCP procedure was able to identify solutions with realistic

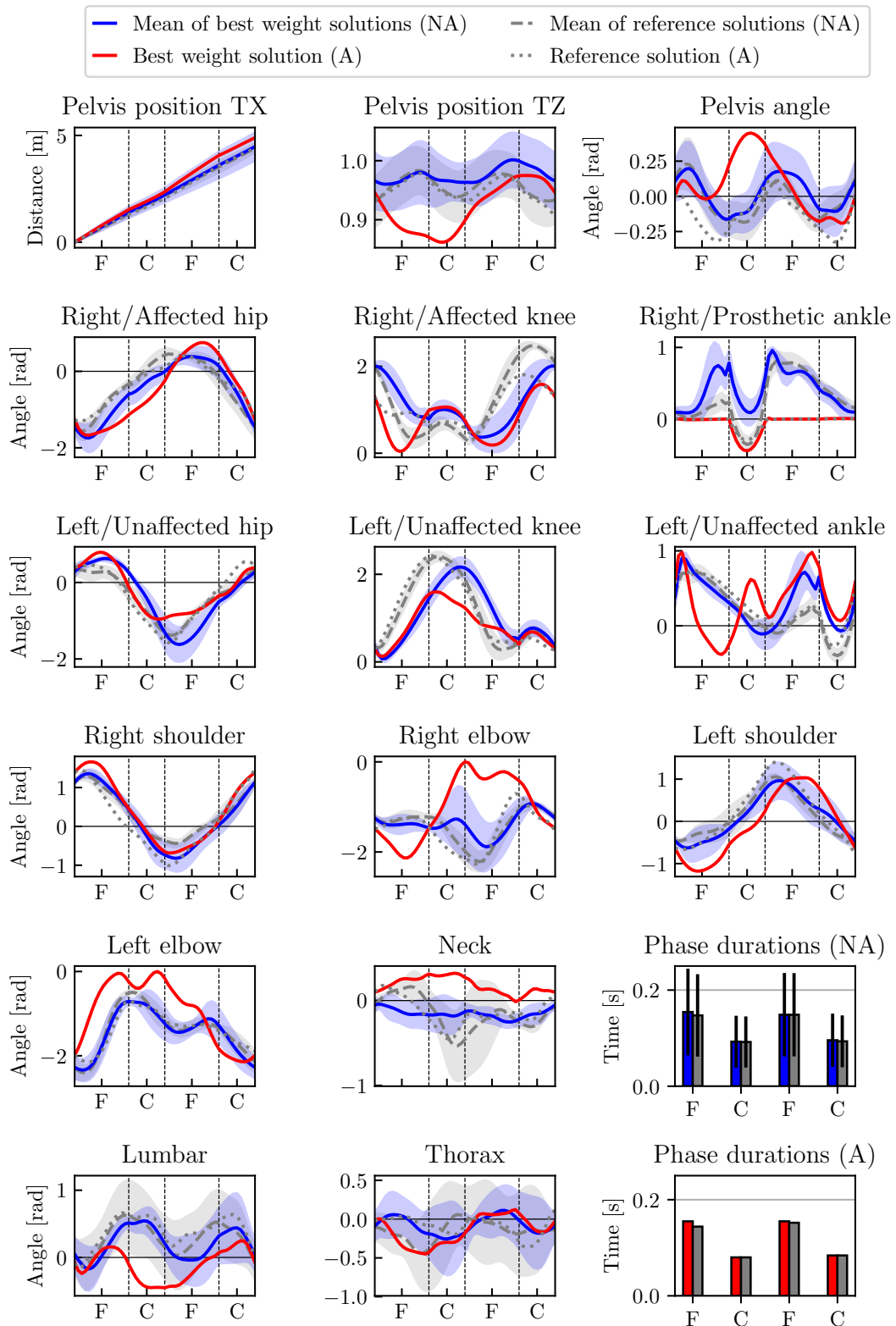


Figure 7.3: Generalized positions of the best weight inverse optimal control problem solutions and the reconstructed reference motions from Chapter 5 for the non-amputee reference group (NA) and the amputee athlete (A). Phase durations are scaled except in the diagram entitled 'Phase durations'.

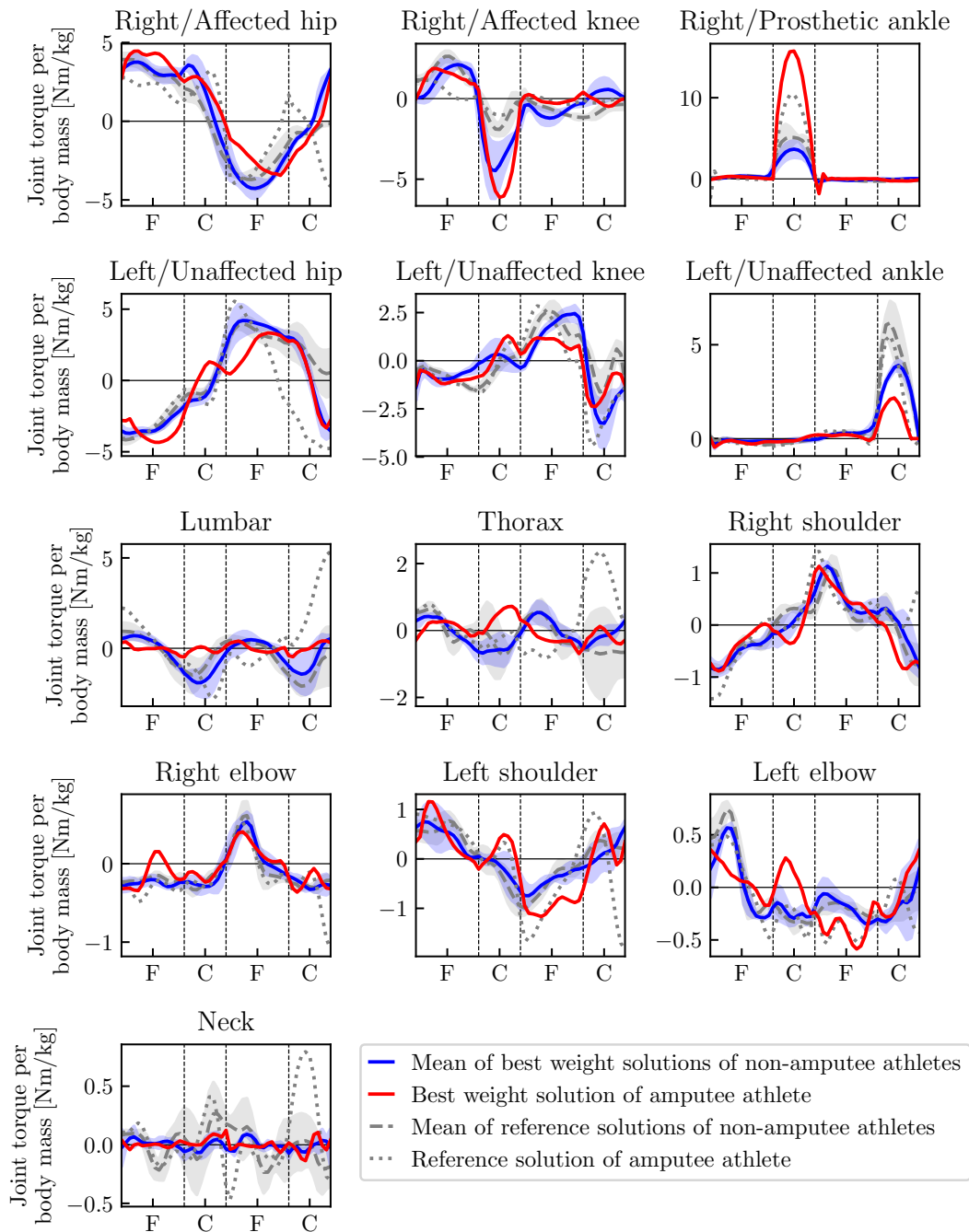


Figure 7.4: Joint torques of the best weight inverse optimal control problem solutions and the reconstructed reference motions from Chapter 5 for the non-amputee reference group (NA) and the amputee athlete (A). Phase durations are scaled and joint torques are normalized by individual body mass. The reference joint torques are the ones from the two-dimensional dynamics reconstruction described in Chapter 5.

phase durations. If we now consider the generalized positions, it is directly noticeable that the deviations between the best weight and the reference motions are larger, albeit still small enough. While the IOCP procedure has delivered motions where the forward distance is closely tracked for the non-amputee athletes, it is larger for the amputee athlete when compared to the reference motion. We clearly see the effect of the larger weights related to step length

maximization. Also in vertical motion, the best weight IOCP and the reference motion match better in the non-amputee group than in the amputee athlete. In the latter, a severe lowering during contact with the RSP can be observed, which makes sense if one wants to load the RSP to the maximum, but cannot be recognized in the reference motion. The fact that the RSP is used more strongly is also evident in the angular course of the ankle joint. However, to achieve this stronger flexion in the ankle, the model also needs a strong knee flexion, which is not observed in unilateral amputee athletes (but which we have already discussed in the synthesized solutions in Chapter 6). In the literature [44, 45], intentional stiffening of the knee is indeed described as a strategy to make optimal use of the RSP. In line with these observations, the amputee athlete also shows a completely different actuation pattern in the leg affected by the amputation than in the reconstructed solution. The flexion torque of the best weight IOCP solution in the knee is more than five times larger than the reconstructed torque. Several explanations are possible here: it could be that the amputee athlete could actually make even better use of his RSP with a change in actuation strategy. It is also possible that the MTGs model overestimates the actual capabilities of the knee joint affected by the amputation. Furthermore, it is conceivable that the fact that an optimal solution is calculated, is actually exploited at this point to the extent that all variables are optimally chosen at all times of the movement, but these choices are not achievable in reality. It is interesting to note at this point that the respective flexion torque of the best weight IOCP motion in the knee of the non-amputee group is also significantly larger than in the reference motion, while the respective torque in the ankle is smaller (for both contact phases). In the biological leg of the amputee athlete, the torques in the knee and ankle in the best weight solution are actually significantly smaller than the reconstructed values. Again, the question is whether swapping the step sequence would reproduce the results.

If we come back to the joint angles, it can also be seen in the arm and spinal joints that the deviations are greater in the amputee athlete compared to the non-amputee group. Especially for the elbows, the lumbar and the neck the deviations are significant. Here also the asymmetry of the unilateral amputee athlete is again clearly evident. While the torques of the arms nevertheless match rather well, the spinal joints show significant differences between reconstructed and best weight IOCP torques.

Overall, these observations indicate that there is likely more room for improvement in the amputee athlete's weights so that they better reflect the actuation strategies for legs and spine found in the real athlete.

## 7.4 Summary

We identified individual best weight factors for three non-amputee and one unilateral amputee athlete based on an IOCP approach. The results demonstrate the great potential of the approach as we found smaller similarity values for all athletes compared to the solutions computed with combinations of optimization criteria with hand-picked weight factors. Hence, a more systematic approach in identifying weight factors indeed results in a closer description of reality. However, it should be noted that the success of the IOCP still depends on at least reasonably good initial values and that the calculations take much longer compared to the synthesis with a fixed objective function, since an optimal control problem (OCP) has to be solved in each step (instead of once). Furthermore, the approach naturally considers only the selected objective functions, so it cannot be excluded that criteria are missing; but this is also the case for the simple motion synthesis problem. Although we assume that we have included the most important criteria in the analysis, also based on the preliminary work in the previous two chapters, it is possible that there are other criteria that contribute to the movement.

This assumption could provide part of the explanation for why differences to the reference movements still exist: Most noticeable were differences in the leg joints and the fact that the model of the amputee athlete utilizes the RSP better than the real athlete does in the measured data. Here, another careful look is needed to identify the causes. Besides possibly still missing criteria, further adjustments of the problem formulation would also be possible: the IOCP could, for example, be extended by a fit to the ground reaction forces. Improvements of the models might also be necessary, e.g., with respect to the foot-contact model, in order to describe the rolling of the foot more realistically. Another adjustment screw would be an even more individual weighting of the separate deviations in the joint angles and phase durations in the IOCP. The last suggestion, however, leads the idea of a more systematic approach a bit into absurdity, since it then comes down to heuristic trial and error. However, based on specific observations such as the significant differences in average velocities due to deviations in the forward motion of the pelvis segment, readjustment of the weights in the IOCP formulation may actually be beneficial.

In comparing the results of athletes with and without below the knee amputation (BKA), we have focused in particular on asymmetry in this chapter. It has also been shown in the weight factors that the amputee athlete shows a significantly more asymmetrical way of sprinting. Of particular interest here is also the observation that the asymmetry of the weights does not show up solely in the weights associated with the leg joints, but impacts all weight factors. Thus, inter-limb asymmetry actually affects the entire body and movement as a result. All three problem formulations we have discussed in this part (dynamics reconstruction, motion synthesis, IOCP) have thus been able to contribute different aspects in the analysis of the asymmetry. This example shows well the justification of all three formulations, which support each other, each opening new perspectives and thus contributing to the overall picture. Therefore, it is logical that all three problem formulations also play a role in the planned simulator tool that we introduce in Chapter 11.

The three chapters in this part have examined sprinting by athletes with and without BKA from different perspectives and provided interesting insights. However, one big question that cannot be answered with these results (besides a few minor areas of improvement) is: which differences between sprinting with and without RSP are actually due to the different models and can therefore be attributed to the RSP, and which differences are due to the fact that we are comparing different athletes who may differ in individual physique and training level? We will return to this question in Chapter 11, in which we will compare the sprinting movements of the amputee athlete with those from a model of the amputee athlete without amputation.

## **Part III**

# **Optimization-Based Comparison of Long Jump Motions with and without Running-Specific Prostheses**



## 8 Biomechanics and Modeling of Long Jump Motions with and without Running-Specific Prostheses

As with the sprint, the long jump consists of several phases: the approach from a standing position, the take-off, the jump and the landing in the sand pit. And in the long jump, too, the goal of the movement in competition is clearly defined, namely to achieve the greatest possible jumping distance. In a review article on the biomechanics of the long jump [79], Linthorne names the decisive factors for this: a fast approach, a good take-off technique and consequent take-off position with correct placement of the take-off foot and proper flight and landing techniques. The biomechanics of all long jump phases have been studied in detail for non-amputee athletes (see e.g., [6, 10, 53, 55, 75, 76, 79, 101]).

During the approach, the first objective is to achieve the greatest possible forward speed and then, towards the end, to get into a good position for the correct placement of the foot on the take-off board and the take-off. Most of the approach is quite standardized and it is only during the final steps that long jumpers use visual control to get into a good position for the take-off step with the help of step length adjustment [54, 56, 74].

Next, the technique of the take-off step is relevant: Since the jump itself has similarities to the projectile motion, many parameters are already fixed at the time of take-off. Therefore, both high vertical and horizontal velocities and an optimal take-off angle of the center of mass (CoM) are important. Since the athlete ideally comes into the final step already with a high forward velocity, the goal is to produce a high vertical velocity during this final step without losing too much of the already existing forward velocity. For this, the ground contact duration as well as the ground reaction force exerted are crucial [6], with more successful long jumpers applying greater forces in shorter times [13]. Long jumpers typically use a technique during the take-off step called “pivoting”, which is described in the literature as follows: The take-off leg acts as a rigid pivot arm that allows rotation of the CoM about the fixed ground contact point established by the take-off foot [76]. Even though a large take-off velocity is more significant than the take-off angle for the jump distance according to Linthorne and colleagues [80], the latter has also been studied in terms of what the optimal angle is. They proposed a formula for predicting the optimal take-off angle based on the optimal angle of the projectile motion and the take-off parameters and showed that it is individual for each athlete [80]. Nevertheless, take-off angles between  $15^\circ$  to  $27^\circ$  can be observed for successful long jumpers [10, 20, 53, 75, 76, 101]. If one considers not only the body’s CoM, but also the contribution of the individual body segments, movement of the arms in particular is of great importance: According to Lees and colleagues [76], an explosive lifting of the arms and the free leg at the end of the step is important for a successful jump. Ashby and Delp [11] have shown in computer simulations of the standing long jump that arm movements increase the take-off velocity of the CoM and thus the jump distance.

To achieve an optimal landing position, the maneuvering of the body during the airborne phase plays a crucial role. This is closely related to a proper control of the angular momentum: In this context, approach run and take-off contribute to the total angular momentum in about the same order of magnitude [60]. During the latter, ground reaction forces produce a forward

rotation about the transverse axis with respect to the CoM [13]. In this regard, the work of Ramey [113] suggests that successful long jumpers rotate forward during the jump. Herzog [57] describes an upright posture and appropriate arm and leg movement to control and stabilize this forward angular momentum. Various authors [16, 112, 113] examine the influence of different jumping techniques (hitch kick, hang, sail) on landing efficiency and describe differences due to angular momentum control. The importance of considering angular momentum is also shown in computer simulations by Chow and Hay [21], which show too large jump distances when angular momentum about the transverse axis is neglected.

As for the sprint, the fact that the prosthetic device may have different influence during different phases of a movement is also shown by long jump studies comparing amputee and non-amputee elite athletes. Nolan and colleagues collected kinematic data of athletes with and without below the knee amputation (BKA) between 1998 and 2004. They published their results in a series of publications (e.g., [104, 105, 106, 107]). At that time, many amputee athletes were jumping off their biological leg, which is also reflected in the measurement data. Compared to today's top athletes, the athletes also achieved significantly shorter jump distances (1 m to 2 m less) [42]. The researchers observed that the amputee athletes approached more slowly, but that those who use their biological leg for take-off applied a comparable technique compared to the non-amputee athletes. Because of the relationship between approach velocity and jump distance described earlier, the amputee athletes achieved shorter jump distances. When comparing which leg the amputee long jumpers used for take-off, they found that the athletes using their biological leg could not control their downward velocity at touchdown like non-amputee athletes. Nevertheless, the longest jump distance (world record distance at this time) in the study [105] was achieved by one of the athletes jumping with their biological leg.

Today, the vast majority of unilateral amputee athletes jump off their running-specific prostheses (RSPs). Nolan and colleagues [107] observed that unilateral amputee athletes reduce the range of motion in the hip and knee during take-off to use their RSPs as a kind of "spring-board". In a comparison of three long jumpers with unilateral BKA and seven non-amputee long jumpers, Willwacher et al. [136] found that the amputee athletes started slower but took off more efficiently. Further, they observed that the prosthetic foot was better at storing energy than the biological foot. Nevertheless, the researchers point out that with these observations it is not possible to make a statement regarding advantage or disadvantage related to the overall movement (consisting of the different phases). Unlike non-amputee long jumpers, amputee long jumpers move mainly within the sagittal plane during the take-off step [45]. As also shown by Nolan et al. [107], Funken and colleagues [44] describe that unilateral amputee athletes stiffen their knee during the take-off step and reduce the range of motion to use the RSP as an efficient spring.

This part deals with the analysis of long jump movements of amputee and non-amputee athletes regarding kinematic and dynamic characteristics. Due to the numerical limitations, we consider the last three steps before the jump as well as the actual jump. Once again - as in the analysis of the sprint running - we have specified a step pattern and thus a sequence of phases for better comparability (and selected the motion capture trials accordingly): The first and second steps are identical in sequence and phases to the two steps of the investigated sprinting motion (compare Figure 4.1). The third step starts with the release of the left foot and ends with the right foot/RSP jumping off the board. The examined movement is finished by a flight phase (compare Figure 8.1); in the case of the motion capture recordings, the final point is determined by the length of the recording, as the latter ends during the flight phase; therefore, the landing itself could not be reconstructed. For the motion synthesis problems, the entire jump is considered, so that the phase ends when ground is touched. Just as in the mod-

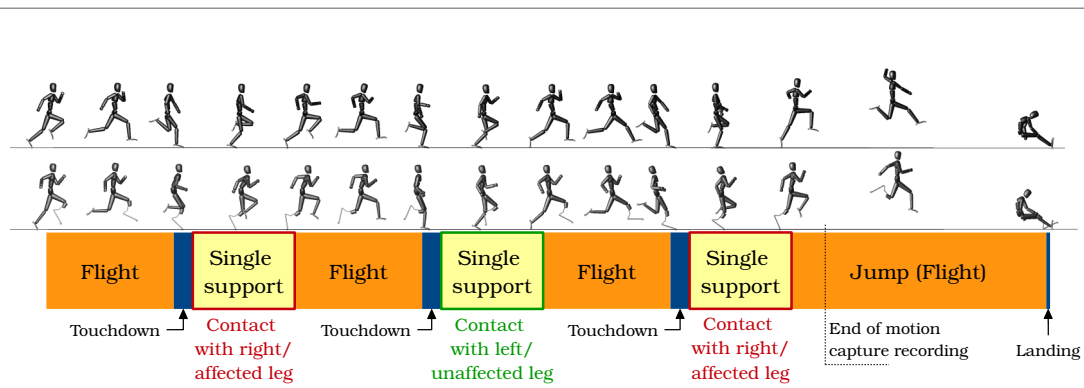


Figure 8.1: Phase description of the long jump model. We model the three last steps of the long jump approach, each consisting of three phases, and the jump itself.

eling of sprinting movements, conditions are formulated to ensure physically correct contact of the feet with the ground. Since the long jump phases are composed of the same components as the phases of the sprint model, the conditions for contact are identical as well. Therefore, we just refer to the respective equations:

- Gain of ground contact: Eq.s (4.1), (4.2)
- During ground contact: Eq. (4.3)
- End of ground contact: Eq. (4.4)

Unlike for the previous contact gain events, the touchdown on landing at the end of the jump is not modeled by a separate transition phase. Instead, constraints are formulated at the end point of the jump flight phase. We further discuss these constraints as well as additional constraints added for the motion synthesis problem at the beginning of Chapter 10.

Based on this modeling, we applied the dynamics reconstruction and motion synthesis optimal control problems to human long jump motions. In this part, we will discuss the resulting long jump motions in details. Thereby we investigate differences between non-amputee and amputee long jump as well as differences between reconstructed and synthesized solutions. We start with the presentation of the dynamics reconstructions of the long jump motions of the 2D+ and 3D models (Chapter 9) and a comparison of the two of them. We then discuss the generated long jump motions for the 2D+ models in Chapter 10.



# 9 Dynamics Reconstruction of Long Jump Motions with and without Running-Specific Prostheses

The dynamics of two long jump trials, one for an amputee athlete and one for a non-amputee athlete, was reconstructed using the least squares optimal control problem (OCP) formulation (see Section 3.1.1) in three dimensions. For each of the two athletes, we established a subject-specific 3D model (named *3D model*), see Section 2.2) based on the anthropometric data of Table 1.1.

## 9.1 Analysis of the Reconstruction Quality

As in Chapter 5, we start with an analysis of the reconstruction quality taking into account the root-mean-square errors (RMSEs) between the solution of the OCP and the reference motion, the comparison of the reconstructed ground reaction forces with the measured ones and the comparison of the reconstructed torques with published data.

### 9.1.1 Kinematic Precision of the Reconstructed Solutions

Table 9.1 gives the RMSEs for each of the two athletes. As for the sprinting trials, the reconstructed solution matches the reference data very well, with less than 1.9 cm of error for the translational DOFs and less than 0.053 rad ( $\approx 3^\circ$ ) of error for the rotational ones. As said before, these errors only concern the quality of the reconstruction, additional errors might stem from measurement errors and the transfer of the measurement data onto the respective model. In the long jump reconstruction, too, the main cause of the errors can be found in the fact that the reference movement during the contact is possibly non-physical. For example, the ground might be penetrated or contact times might not fit exactly. For sake of completeness, we show the diagrams comparing the generalized positions of both reference and reconstructed motions as well as the RMSEs of the individual joints for both athletes in the appendix (Figures A.7 and A.8).

Table 9.1: Rotational and translational root-mean-square errors (RMSEs) between reconstructed and reference motions for the long jump. The results are given for one non-amputee and one amputee athlete. The upper row gives the RMSEs for the translational degrees of freedom (DOFs), the lower row the ones for the rotational DOFs.

	Non-amputee athlete	Amputee athlete
Trans (cm)	1.460	1.897
Rot (rad)	0.053	0.030

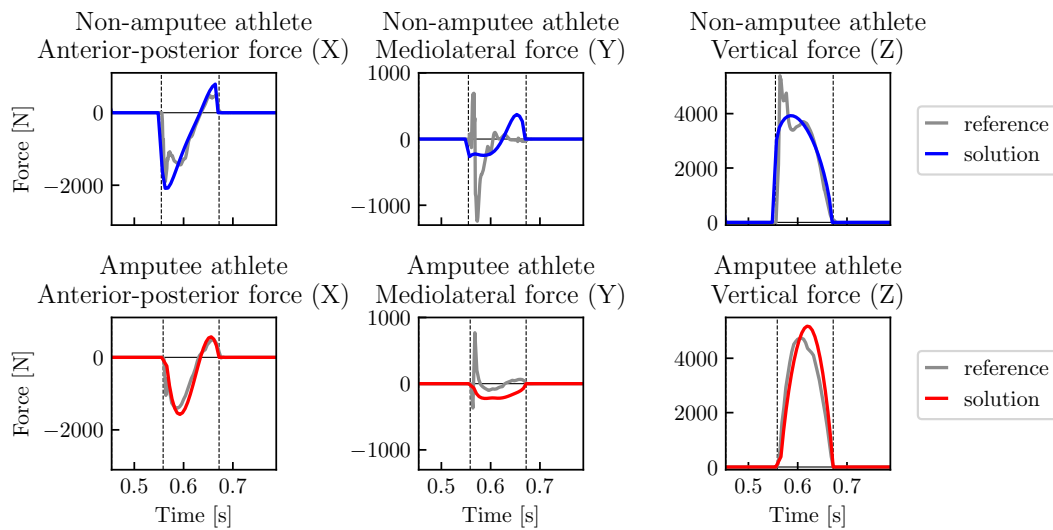


Figure 9.1: Anterior-posterior (TX), mediolateral (TY) and vertical (TZ) ground reaction forces of the amputee and the non-amputee athlete for the reconstructed three-dimensional long jump motions. As the measurements included only one force plate (below the take-off bar), we only consider the last contact phase. For each athlete (first row: non-amputee athlete, second row: amputee athlete), we compare the computed forces and the raw measured forces.

### 9.1.2 Validation of Reconstructed Ground Reaction Forces

As a second and a third measure of the reconstruction quality, we compare the ground reaction forces with the measured data from force plates and the reconstructed joint torques with data from literature [45, 99, 123]. In each case, only data for the last contact phase which is the take-off phase, is available. Figure 9.1 shows the anterior-posterior (X), mediolateral (Y) and vertical (Z) ground reaction forces of the last contact phase. The upper row gives the forces of the non-amputee athlete and the lower row the ones of the amputee athlete. For both athletes and all three components of the ground reaction force, we see good overall agreement between the measured and reconstructed forces except for some peaks and artifacts in the data. Let us now go through the diagrams from left to right to describe the individual deviations:

1. For the anterior-posterior force (X), the expected sequence of braking and propulsive force is generated in both models. For the non-amputee athlete, both the braking and the propulsive components are slightly overestimated. Nevertheless, we find the agreement sufficient, but mention this point specifically here so that it is taken into account in the later comparison of magnitudes related to the anterior-posterior force.
2. For the mediolateral force (Y), the reconstructed forces do not show the strong peaks found in the measured data. Since we only show the unfiltered raw force measurement data here and it cannot be ruled out that the peaks are (partly) due to noise, we additionally take a look at the filtered ground reaction forces from the literature [45] for comparison. This shows that the curve for the amputee athlete is just a bit too large, but otherwise fits the measured data. For the non-amputee athlete, however, even the filtered measurement data still shows a peak in the lateral direction, which is not reconstructed in our model. However, the magnitude is also consistent here.
3. For the vertical force (Z), our models both calculate parabolic curves, with the force curve of the non-amputee athlete showing a significantly stronger increase at the beginning. Even though the curve still does not exactly reconstruct the sharp increase and

the associated two-peak structure, this shows that the non-amputee model calculates a different force profile than the amputee model and thus at least comes close to the measured data. For the amputee athlete, the force is a little too large.

All deviations can be partly explained by the fact that we use a comparatively simple foot contact model with a single fixed contact point at the tip of the foot. Furthermore, it is possible that the prescribed start time of the ground contact does not exactly match the one in the motion capture recordings. Another building block to explain this is the rigidity of the model and the instantaneous touchdown, which make it difficult to replicate the fast time scale actions (e.g., the sharp peak in the vertical force of the non-amputated athlete) (cf. [122]). However, the latter could also be due to the fact that the number of shooting nodes is limited (since the problem would otherwise become numerically too large and the computation time too long): During the last contact phase, the frequency of the shooting nodes is 185.2 Hz, while the frequency of the force plate is 1000 Hz. This means that the force curve is formed from 20 measurement points in the reconstructed and 108 measurement points in the measured data.

### 9.1.3 Validation of Reconstructed Joint Torques

Figure 9.2 shows the joint torques of the take-off leg during the last contact phase for both athletes. The joint torque in the prosthetic device (Right/Affected ankle RY) is passively produced and computed via E Eq. (2.1) with the reconstructed spring constant  $k = 3150 \text{ N m rad}^{-1}$  (see next section).

We compare the joint torques of the non-amputee athlete to the data reported by Funken et al. [45], Muraki et al. [99] and Shimizu et al. [123] and those of the amputee athlete to the data reported by Funken et al. [45]. Funken and colleagues [45] reported the three-dimensional moments of three unilateral amputee and seven non-amputee athletes during take-off. Muraki and co-workers [99] analysed the motions of eleven non-amputee athletes and computed the sagittal plane joint torques during take-off. Shimizu and Ae [123] studied twelve non-amputee athletes and reported the joint torques in the sagittal plane as well as the hip abduction/adduction torque during take-off. Basically, when comparing both the amputee and the non-amputee athlete, we find that the reconstructed torques fit well with those from the literature with respect to the rough curve shapes and the timing. Furthermore, it can be seen for all torques that the values are slightly larger in the case of our reconstruction and that the curves are a bit smoother, i.e., smaller fluctuations as in the literature curves tend not to be reproduced.

We first highlight the most important differences between the reconstructed torques of the non-amputee athlete and the values reported in the literature for non-amputee athletes: For the hip extension/flexion torque (RY), the reconstructed torque does not follow the double-peak course as shown at the beginning of the contact phase in the literature data. Also, the oscillation back and forth between extension and flexion torque as in the data of Funken et al. [45] and Muraki et al. [99] is not reproduced. Instead, there is a transition from extension to flexion torque after about 75 % of the stance duration. This fits with the data of Shimizu and Ae [123] (as well as those of Funken et al. [45], considering the final transition to the flexion moment). Overall, the variations between the torques of the three publications taken for comparison are already so large that we consider the deviations of our torques to be unproblematic. For the other hip torques (RX and RZ), it is again apparent that the reconstruction smoothes the curves, because the back and forth between abduction and adduction (RX) or external and internal rotation (RZ) is not precisely reproduced. Nevertheless, it can also here be stated that both the magnitude and the basic course (from abduction to adduction (RX) or from external rotation to internal rotation (RZ)) fit the literature values. The smoothing is probably caused

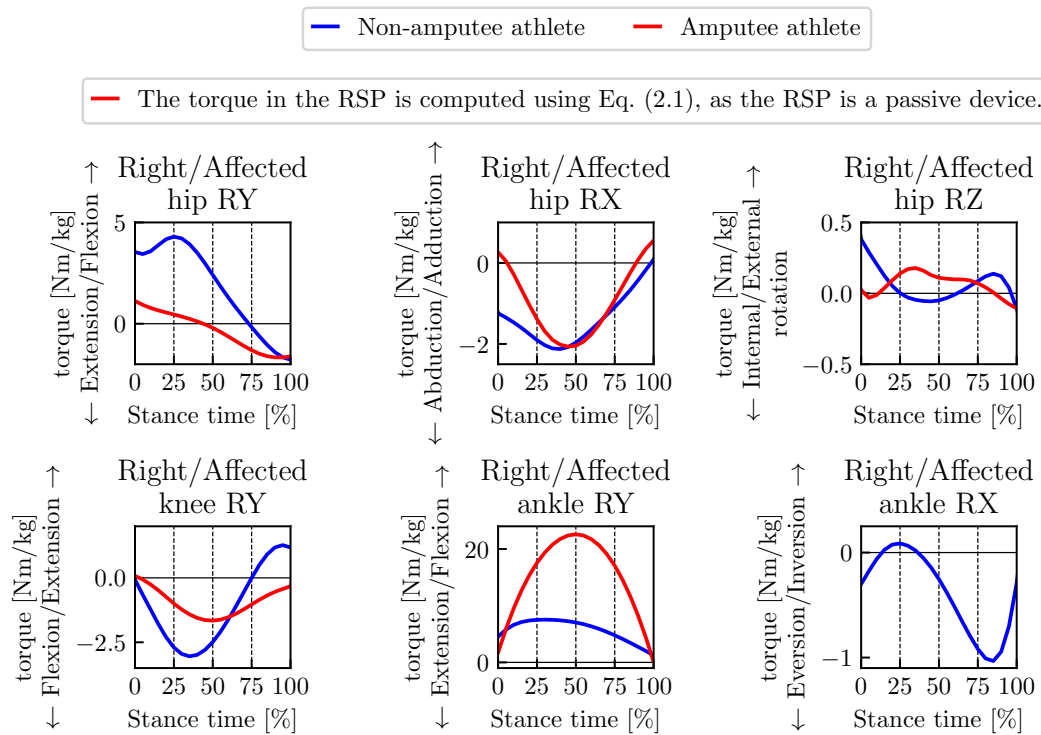


Figure 9.2: Stance leg joint torques of the non-amputee (‘NA’) and the amputee (‘A’) athlete during the last contact phase of the reconstructed three-dimensional long jump motions. The individual phase durations are given in percent of the total stance time and the joint torques are normalized by body mass. The joint torque in the prosthetic ankle is passively produced and computed via Eq. (2.1).

by the fact that the OCP can compute the optimal solution at any point (with the knowledge of prior and following time points) which is not possible for a real athlete and that we added a regularization term which – despite being small – contributes to a smoothing. While the knee and ankle extension/flexion (RY) torques match the literature data well, there is a difference for the ankle inversion/eversion torque (RX): The peak in the eversion moment appears only at the end of the stance phase while it is at the beginning of the stance phase in the the data reported by Funken et al. [45].

The comparison of the reconstructed torques of the amputee athlete with the literature values [45] also shows a generally consistent picture. For the torques of the sagittal plane (RY), the deviation in the torque calculated for the running-specific prosthesis (RSP) is particularly noticeable: It has a significantly larger peak value in the reconstructed solution. Possibly the cause of the different magnitudes lies in different assumptions about the prosthesis model, e.g., the length of the lower rigid segment that acts as a lever arm. Furthermore, a difference in the hip torques for flexion/extension (RY) and abduction/adduction (RX) is apparent: In the literature, a hip flexion torque (RY) is reported for the whole stance phase and the RX torque alters between abduction and adduction. In our reconstructed solution, we see a transition from flexion to extension in the RY torque and the RX torque remains mainly in the abduction region. We assume that these torques describe an optimal way of achieving the required joint positions for our model. The reconstructed internal/external rotation hip torque (RZ) fits well with the literature values, being slightly larger in comparison. Since the reference values include only three athletes, it cannot be ruled out that smaller deviations in the reconstructed torques are merely due to differences in modeling, e.g., the fact that Funken et

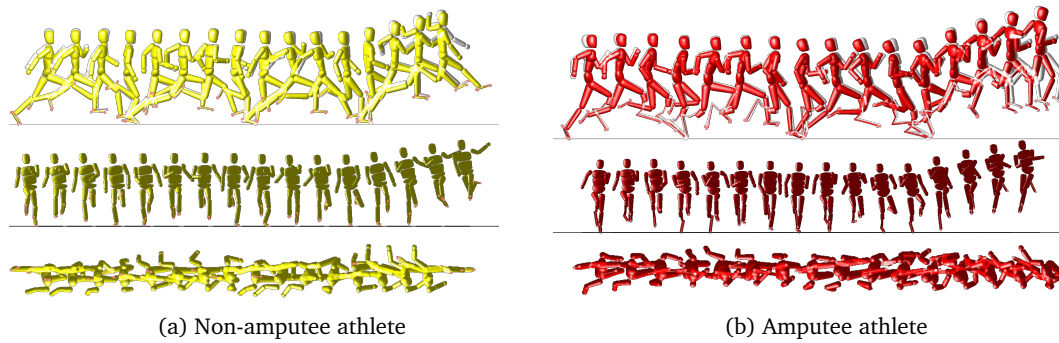


Figure 9.3: Animated long jump sequences visualize the solutions of the dynamics reconstruction optimal control problem. The upper row shows the sagittal plane view, the middle row shows the motion from front view, the lower row shows the motion from top view. The colored models show the reconstructed sprinting movements. For the sagittal plane view, the grey models in the background show the respective reference movements.

al. [45] calculated torques in all three planes for all leg joints.

In conclusion, the three measures that we applied to judge the reconstruction quality show that the solutions seem to be valid and allow for further analysis.

## 9.2 Analysis of Characteristic Variables in Long Jump

The reconstructed motions (solutions of the OCP as colored models) and the reference motions (joint angle trajectories based on PUPPETEER fit as grey models) are shown in Figure 9.3. The motion capture recordings ended during the jump (see Figure 8.1).

In the following, we will examine characteristic variables such as phase durations, joint angles, joint torques, forces and angular momenta in terms of differences between the non-amputee and the amputee athlete. As the motion capture recordings ends during the jump, we omit the last flight phase for the analysis and only consider the last three steps before take-off.

As in the dynamics reconstruction of the sprinting motions (Chapter 5), we did not set the spring and damping constants  $k$  and  $d$  of the prosthetic device, but the spring constant was a free parameter to be determined by the OCP. The damping constant can then be computed via Eq. (2.2). With this approach, we reconstructed them as

- $k = 3150 \text{ N m rad}^{-1}$  and  $d = 6.07 \text{ N m s rad}^{-1}$  for the 3D model.

The spring constants differs from the one computed for the the sprinting reconstruction: In the case of the long jump the spring constant is higher than in sprinting, which means that the spring is stiffer. As described in the introduction, different stiffnesses are chosen for different sports disciplines with stiffer RSPs being usually used in jump movements. Therefore, the result is reasonable.

In Table 9.2, we list the individual phase durations of the non-amputee and the amputee athletes. We find great differences in these individual phase durations. The difference in the phase duration of phase 7 which is the phase describing the actual jump is not relevant as it is determined by the cut-off of the motion capture data. However, we should keep in mind that the motion capture recording of the amputee athlete captured 0.065 s more of the jump than that of the non-amputee athlete when comparing this phase.

When considering the first two steps, it is noticeable that the contact time of the amputee athlete with the prosthetic device is significantly shorter than the one with the biological leg

Table 9.2: Phase durations of the modeled phases for the amputee and the non-amputee athlete for the reconstructed long jump motions. The phase numbering corresponds to the order shown in Figure 8.1: 1 - first flight phase, 2 - first right contact phase, 3 - second flight phase, 4 - left contact phase, 5 - third flight phase, 6 - second right contact phase (take-off), 7 - fourth flight phase (jump, truncated by end of motion capture recording). The abbreviations 'NA' and 'A' stand for the non-amputee and the amputee athlete, respectively.

phase	1	2	3	4	5	6	7
NA	0.136 s	0.088 s	0.144 s	0.086 s	0.110 s	0.108 s	0.116 s
A	0.156 s	0.072 s	0.128 s	0.084 s	0.126 s	0.106 s	0.187 s

and those of the non-amputee athlete. A contact time of only 0.072 s (Amputee athlete, phase 2) appears to be fairly short; however, we have already noticed during the reconstruction of the sprinting movements that the contact phase with the RSP is significantly shorter than that with the biological leg and the contact phases of the non-amputee athletes. The take-off contact phase is for both athletes remarkably longer than the previous contact phases. However, the actual phase duration of the take-off contact phase did not differ between the two athletes. It is also noticeable that the flight phases following contact with the biological leg (phases 1 and 5) are of longer duration and those following contact with the RSP (phase 3) of shorter duration compared to the non-amputee athlete.

### 9.2.1 Estimated Jump Distance and Take-Off Angle

As the motion capture recordings stop during the jump, we cannot directly extract the jump distance from the recordings. Therefore, we follow the approach of Willwacher et al. [136] to compute the jump distance based on the parameters at take-off. For this, we assume a parabolic flight curve of the center of mass (CoM) after take-off with the start point defined by the horizontal and vertical CoM positions at take-off  $p_x^{CoM}(t_{take-off})$  and  $p_z^{CoM}(t_{take-off})$ . Then, the jump distance is the distance from the horizontal position of the contact point at lift-off  $p_x^{RH}(t_{take-off})$  to the intersection of the ground and the CoM flight parabola. The parabolic flight curves are defined as:

$$p_x^{CoM}(t) = p_x^{CoM}(t_{take-off}) + v_x^{CoM}(t_{take-off}) t, \quad (9.1a)$$

$$p_z^{CoM}(t) = p_z^{CoM}(t_{take-off}) + v_z^{CoM}(t_{take-off}) t + \frac{1}{2} g t^2, \quad (9.1b)$$

where  $v_x^{CoM}(t_{take-off})$  and  $v_z^{CoM}(t_{take-off})$  denote the horizontal and vertical CoM velocities at take-off. Equation (9.1b) is used to compute the time of flight  $t_{flight}$  by setting the vertical position to zero, i.e.,  $p_z^{CoM}(t = t_{flight}) = 0$ . Subsequently, the jump distance  $d_{jump}$  is calculated via Eq. (9.1a) by inserting the time of flight  $t_{flight}$ , i.e.

$$d_{jump} = p_x^{CoM}(t_{flight}) - p_x^{RH}(t_{take-off}). \quad (9.2)$$

The take-off angle is computed from the CoM velocities at take-off by

$$\beta_{take-off} = \arctan\left(\frac{v_z^{CoM}(t_{take-off})}{v_x^{CoM}(t_{take-off})}\right). \quad (9.3)$$

Based on these definitions, we compute the following values for the reconstructed solutions:

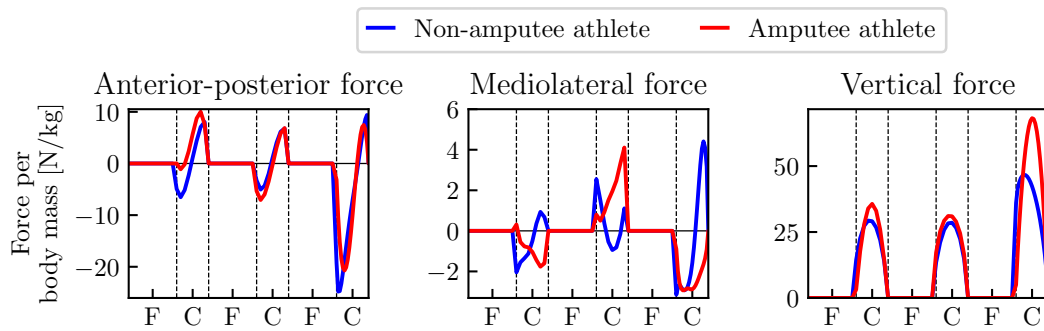


Figure 9.4: Ground reaction forces of the amputee and the non-amputee athlete for the reconstructed long jump motions. The abbreviations ‘F’ and ‘C’ on the x-axis denote flight and contact phases, respectively. The phase order is as shown in Figure 8.1. Phase durations are scaled for comparability. Ground reaction forces are normalized by body mass.

- a jump distance of 8.29 m with a take-off angle of  $20.25^\circ$  for the amputee athlete and
- a jump distance of 7.58 m with a take-off angle of  $16.38^\circ$  for the non-amputee athlete.

Thus, based on the estimated distance, the amputee athlete jumps about 71 cm longer than the non-amputee athlete. Even if we consider in the discussion that the formula for the jumping distance does not represent flight and landing technique and the amputee athlete might lose a bit more there than the non-amputee athlete (because the handling of the RSP is probably a bit more difficult when landing), the difference is still clear. From this comparison of the jump distance of two individual athletes alone, it is certainly not possible to draw any conclusions regarding the influence of the RSP. In particular, we have no information about the level and training status of the two athletes at the time of the measurements. In the following, we thus intend to look at other characteristic variables in order to determine differences in the movements that may explain the different jump distances.

A first clue is provided by the take-off angle. It is greater by  $3.87^\circ$  for the amputee compared to the non-amputee athlete. As already described in the introduction to long jump, the take-off angle is relevant in so far as one could calculate the optimal take-off angle for a given take-off height for the simplified description of the long jump as a projectile motion. For a jump height of zero, the optimal angle  $\beta_{\max}$  for maximizing distance would be  $45^\circ$  and for all angles  $0^\circ \leq \beta \leq 45^\circ$ , distance would increase with angular size. Although this consideration is a major simplification, it explains quite clearly one of the factors contributing to the greater jump distance of the amputee athlete.

### 9.2.2 Ground Reaction Forces

Figure 9.4 shows the anterior-posterior (TX), mediolateral (TY) and vertical (TZ) components of the ground reaction forces over the last three steps for the non-amputee and the amputee athlete. The forces are normalized by body mass. Table 9.3 gives measures related to the ground reaction forces. For each component, we computed the change of momentum and the mean force as defined in Section 5.3. In addition, we computed the vertical peak force values.

When comparing the curves and values for the non-amputee and amputee athlete, several differences are apparent. We begin by examining the graph of the mediolateral force: During the third-last contact phase, the forces of both athletes have a significant component in medial direction. While the force curve of the non-amputee athlete transitions to the lateral region, the

Table 9.3: Measures related to the ground reaction forces for the three contact phases of the reconstructed long jump motion of the non-amputee and the amputee athlete. The measures are computed as defined in Section 5.3.

	Non-amputee athlete	Amputee athlete
THIRD-LAST CONTACT PHASE		
Anterior-posterior change of momentum	$-0.027 \text{ N s kg}^{-1}$	$0.266 \text{ N s kg}^{-1}$
Anterior-posterior mean force	$0.21 \text{ N kg}^{-1}$	$4.14 \text{ N kg}^{-1}$
Mediolateral change of momentum	$-0.054 \text{ N s kg}^{-1}$	$-0.061 \text{ N s kg}^{-1}$
Mediolateral mean force	$-0.57 \text{ N kg}^{-1}$	$-0.96 \text{ N kg}^{-1}$
Vertical change of momentum	$1.973 \text{ N s kg}^{-1}$	$1.672 \text{ N s kg}^{-1}$
Vertical mean force	$23.19 \text{ N kg}^{-1}$	$24.04 \text{ N kg}^{-1}$
Vertical peak force	$29.33 \text{ N kg}^{-1}$	$35.67 \text{ N kg}^{-1}$
SECOND-LAST CONTACT PHASE		
Anterior-posterior change of momentum	$-0.001 \text{ N s kg}^{-1}$	$-0.104 \text{ N s kg}^{-1}$
Anterior-posterior mean force	$0.43 \text{ N kg}^{-1}$	$-0.79 \text{ N kg}^{-1}$
Mediolateral change of momentum	$0.027 \text{ N s kg}^{-1}$	$0.141 \text{ N s kg}^{-1}$
Mediolateral mean force	$0.38 \text{ N kg}^{-1}$	$1.95 \text{ N kg}^{-1}$
Vertical change of momentum	$1.878 \text{ N s kg}^{-1}$	$2.061 \text{ N s kg}^{-1}$
Vertical mean force	$22.61 \text{ N kg}^{-1}$	$25.47 \text{ N kg}^{-1}$
Vertical peak force	$28.52 \text{ N kg}^{-1}$	$31.07 \text{ N kg}^{-1}$
LAST CONTACT PHASE – TAKE-OFF PHASE		
Anterior-posterior change of momentum	$-0.976 \text{ N s kg}^{-1}$	$-0.760 \text{ N s kg}^{-1}$
Anterior-posterior mean force	$-8.19 \text{ N kg}^{-1}$	$-7.06 \text{ N kg}^{-1}$
Mediolateral change of momentum	$-0.055 \text{ N s kg}^{-1}$	$-0.247 \text{ N s kg}^{-1}$
Mediolateral mean force	$-0.38 \text{ N kg}^{-1}$	$-2.34 \text{ N kg}^{-1}$
Vertical change of momentum	$4.169 \text{ N s kg}^{-1}$	$4.918 \text{ N s kg}^{-1}$
Vertical mean force	$36.72 \text{ N kg}^{-1}$	$46.69 \text{ N kg}^{-1}$
Vertical peak force	$46.68 \text{ N kg}^{-1}$	$68.16 \text{ N kg}^{-1}$

curve of the amputee athlete is only in the medial region. During the second-last contact phase, the force of the non-amputee athlete transitions from lateral to medial direction, while the one of the amputee athlete is completely in lateral direction. Here, the non-amputee athlete applies the larger forces as the absolute values of the mediolateral change of momentum and mean force are larger compared to the amputee athlete. During the last contact phase the forces of the two athletes are in medial direction and of comparable magnitude at the beginning of the contact phase. While the curve of the amputee athlete remains in this direction, the curve of the non-amputee athlete transitions to the lateral direction.

More interesting, however, are the anterior-posterior and vertical force components. Here, too, there are clear differences, which also depend on the respective contact phase. During the contact phases with the RSP (third-last and last contact), the braking components of the horizontal force of the amputee athlete are smaller compared to the non-amputee athlete. This

is also reflected in the corresponding values for the change of momentum, because the amputee athlete has either a positive instead of a negative value (third-last contact) or a smaller value in absolute numbers (last contact) which means that the braking component is less pronounced. During the third-last contact phase, the mean force value for the amputee athlete is clearly positive, i.e., the propulsive component is larger than the braking component and the amputee athlete accelerates. In contrast, the non-amputee athlete has a much smaller positive mean force value, which indicates that he accelerates less. During the last contact phase, the mean values are both negative, but the value of the non-amputee athlete is larger in absolute terms. Thus, he decelerates more. In addition, the amputee athlete is able to generate a larger vertical force during each of the contact phases with the RSP (third-last contact: approximately 22 % larger peak force; last contact: approximately 46 % larger peak force). For the last contact phase, also the mean force is larger for the amputee than the non-amputee athlete while for the third-last contact phase the mean force values are close to each other. If we now consider the vertical change of momentum, we find that for the amputee athlete it is smaller by 15 % during the third-last contact phase and larger by 18 % during the last contact phase compared to the non-amputee athlete. For both athletes, it can be seen that lower peak values were calculated in all three force components during contact with the left (biological in the case of the amputee athlete) leg. This is plausible since long jumpers usually take off with their strong leg; therefore, the second-last contact occurs with the “weaker” leg. Compared to the third-last contact vertical peak force value, the vertical peak force of the second-last contact is smaller by 3 % for the non-amputee and by 13 % for the amputee athlete. If one compares directly the vertical peak forces of non-amputee and amputee athlete during the second-last contact phase, it appears that the force of the amputee athlete is slightly larger (by 9 %). Hence, the amputee athlete seems to generate slightly larger vertical forces than the non-amputee athlete, independent of the use of a RSP.

Two observations in particular are interesting: First, that in the case of the reconstructed long jump steps – exactly opposite to the observations for the reconstructed sprinting steps – the amputee athlete exploits the RSP more (and generates larger (vertical) forces compared to the non-amputee athlete) and generates lower forces in the biological leg in return (cf. Figure A.9 in the appendix, where we compare the force trajectories of the third-last and second-last steps with the corresponding steps of the reconstructed sprinting motion). Second, the amputee athlete can generate a much larger vertical force during the last contact than the non-amputee athlete. Even if we take into account that he might perform at a higher level (by e.g., 10 % based on the peak forces of the biological legs during the second-last contact phase) and that the vertical force was slightly overestimated by the reconstruction compared to the force plate measurements (by 9 %), it is still a hint that the amputee athlete exploits his RSP for an efficient take-off.

### 9.2.3 Motion of the Center of Mass

Figure 9.5 shows the curves related to the CoM motion over the last three steps for the non-amputee and the amputee athletes. Table 9.4 gives the horizontal and vertical CoM velocities at touch-down and lift-off as well as the corresponding change in CoM velocity for each of the three contact phases.

Again, we focus on the horizontal and vertical components as they are more decisive for the performance analysis<sup>1</sup>. When comparing the forward motion of the CoM, it is noticeable that

<sup>1</sup>In the mediolateral direction, it is particularly noticeable that amputee and non-amputee athletes move in opposite directions and that the variation of the amputee athlete is less pronounced. However, it cannot be clearly determined whether this was possibly only the case in the specific trials. Interestingly, the movement during the last contact phase is then very similar, albeit shifted.

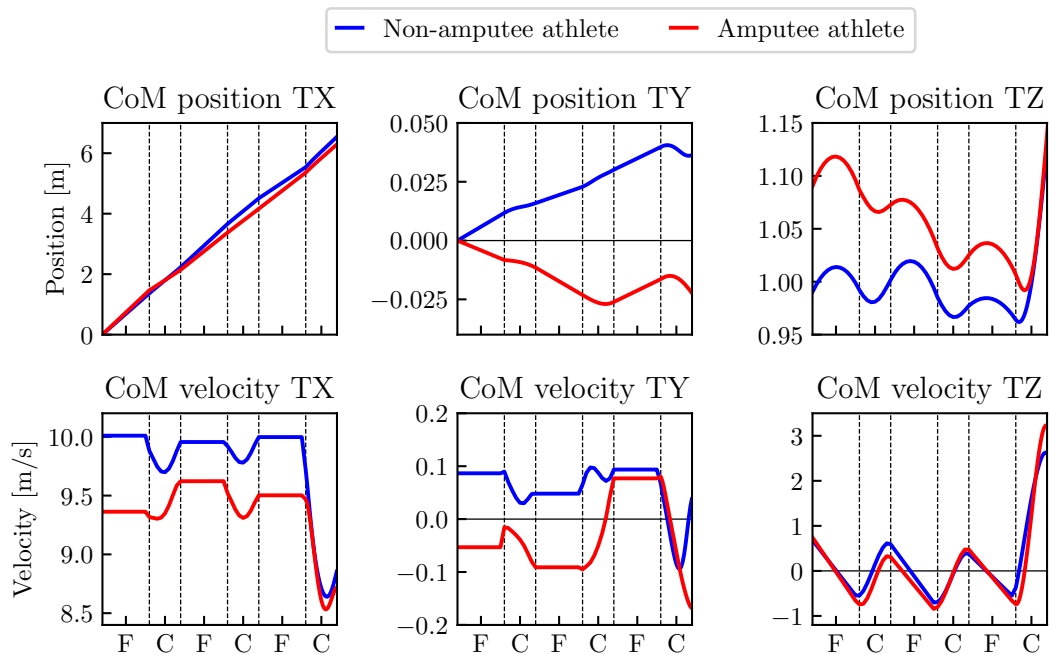


Figure 9.5: Center of mass (CoM) motion of the amputee and the non-amputee athlete for the reconstructed long jump motions. The abbreviations ‘F’ and ‘C’ on the x-axis stand for flight and contact phases, respectively. The phase order is as shown in Figure 8.1. Phase durations are scaled for comparability.

the distance covered by the amputee athlete after lift-off from the third-last contact phase is slightly shorter than that of the non-amputee athlete. This is probably because the forward velocity of the amputee athlete remains lower than that of the non-amputee athlete, despite the positive change in horizontal CoM velocity during the third-last contact phase. Thus, the non-amputee athlete achieves a higher overall approach velocity than the amputee athlete (greater by  $0.50 \text{ m s}^{-1}$  at the time of touchdown into the last contact phase). However, during the last contact phase, the non-amputee athlete loses significantly more horizontal CoM velocity, so that the difference between the horizontal CoM velocities is reduced (to a difference of  $0.14 \text{ m s}^{-1}$ ).

In the vertical CoM movement, it is noticeable that the amputee athlete starts the third-last step with a significantly higher CoM and his CoM is constantly above that of the non-amputee athlete up to the last contact phase. While the non-amputee athlete exhibits an approximately periodic vertical CoM movement during the third- and second-last steps, there is a significant drop in the amputee athlete toward the second-last step. Toward the last contact phase, there is another clear lowering for both athletes. At the touchdown into the last contact phase, the vertical CoM position of the non-amputee athlete is 2 cm to 3 cm below those at the touchdown into the second-last and third-last contact phases. For the amputee athlete, it is 2.5 cm lower than for touchdown into the second-last step and 8.0 cm lower than for touchdown into the third-last step. If we now compare the values of non-amputee and amputee athlete during the last contact phase, we see that at touchdown the vertical CoM position of the non-amputee athlete is 4.3 cm lower than that of the amputee athlete and that both take off with comparable heights (the CoM height of the non-amputee athlete is 1.2 cm higher than that of the amputee athlete at the jump). This is interesting because in absolute terms, the amputee athlete gains significantly more vertical velocity during the last contact phase than the non-amputee athlete ( $0.72 \text{ m s}^{-1}$  more). Remarkably, the amputee athlete has a larger gain in vertical velocity

Table 9.4: Measures related to the center of mass motion for the three contact phases of the reconstructed long jump motion of non-amputee and amputee athlete. The measures are computed as defined in Section 5.3.

	Non-amputee athlete	Amputee athlete
THIRD-LAST CONTACT PHASE		
Horizontal CoM velocity at touch-down	10.01 m s <sup>-1</sup>	9.36 m s <sup>-1</sup>
Horizontal CoM velocity at lift-off	9.96 m s <sup>-1</sup>	9.62 m s <sup>-1</sup>
Change in horizontal CoM velocity	-0.05 m s <sup>-1</sup>	0.26 m s <sup>-1</sup>
Vertical CoM velocity at touch-down	-0.54 m s <sup>-1</sup>	-0.66 m s <sup>-1</sup>
Vertical CoM velocity at lift-off	0.59 m s <sup>-1</sup>	0.31 m s <sup>-1</sup>
Change in vertical CoM velocity	1.13 m s <sup>-1</sup>	0.97 m s <sup>-1</sup>
SECOND-LAST CONTACT PHASE		
Horizontal CoM velocity at touch-down	9.96 m s <sup>-1</sup>	9.62 m s <sup>-1</sup>
Horizontal CoM velocity at lift-off	10.00 m s <sup>-1</sup>	9.50 m s <sup>-1</sup>
Change in horizontal CoM velocity	0.04 m s <sup>-1</sup>	-0.12 m s <sup>-1</sup>
Vertical CoM velocity at touch-down	-0.70 m s <sup>-1</sup>	-0.84 m s <sup>-1</sup>
Vertical CoM velocity at lift-off	0.38 m s <sup>-1</sup>	0.47 m s <sup>-1</sup>
Change in vertical CoM velocity	1.08 m s <sup>-1</sup>	1.31 m s <sup>-1</sup>
LAST CONTACT PHASE – TAKE-OFF PHASE		
Horizontal CoM velocity at touch-down	10.00 m s <sup>-1</sup>	9.50 m s <sup>-1</sup>
Horizontal CoM velocity at lift-off	8.86 m s <sup>-1</sup>	8.72 m s <sup>-1</sup>
Change in horizontal CoM velocity	-1.14 m s <sup>-1</sup>	-0.78 m s <sup>-1</sup>
Vertical CoM velocity at touch-down	-0.55 m s <sup>-1</sup>	-0.66 m s <sup>-1</sup>
Vertical CoM velocity at lift-off	2.61 m s <sup>-1</sup>	3.22 m s <sup>-1</sup>
Change in vertical CoM velocity	3.16 m s <sup>-1</sup>	3.88 m s <sup>-1</sup>

during the last two contact phases compared to the non-amputee athlete and a smaller gain in vertical velocity during the third-last contact phase compared to the non-amputee athlete. Hence, it seems that it is not (only) due to the RSP that the amputee athlete gains more vertical velocity during the take-off phase. This also becomes particularly evident once again when one considers that the non-amputee athlete has greater gains in vertical velocity in each of the contact phases with the take-off leg than in the contact phase with the other leg. This is probably due to the fact that the athletes use their ‘stronger’ leg for the take-off.

In summary, it can be seen that the amputee athlete starts the last step with a lower horizontal approach velocity and a lower vertical velocity of the CoM than the non-amputee athlete. In return, he has a more effective take-off technique because he can generate a larger gain in vertical velocity with a smaller loss in horizontal velocity compared to the non-amputee athlete. However, due to the worse starting position at touchdown into the last contact phase, this advantage is again somewhat limited. Nevertheless, the more effective take-off is probably one of the factors that makes the comparatively greater jumping distance possible. These observations are in compliance with the results described by Willwacher and colleagues [136].

### 9.2.4 Position and Joint Angles

Figure 9.6 shows the position of the pelvis segment in space and the joint angle curves of the non-amputee and the amputee athlete. The movement of the base segment (pelvis) in space roughly corresponds with the CoM movement, so there is no need to describe it again here. Unlike in sprinting movements, where we observed marked differences in the angular trajectories of athletes with and without below the knee amputation (BKA), fewer deviations are directly noticeable in long jump movements. In particular, the range of motion in each joint often appears comparable, albeit shifted along the y-axis for some of the DOFs (see e.g., the diagrams for Pelvis RY, Pelvis RX, Lumbar RY, Lumbar RX). Let us first consider the joints of the right leg, which in the case of the amputee athlete is the leg affected by the amputation: In the sagittal plane angles (RY), we find a lower range of motion for the amputee athlete for all joints (74 % of the hip joint motion range for the non-amputee athlete, 68 % of the knee joint motion range of the non-amputee athlete). It is particularly interesting to note that flexion in the knee of the amputee athlete differs significantly between the two contact phases: During the third-last contact phase, there is very little flexion; during the last contact phase (take-off step), flexion is clearly present, although less than in the non-amputee athlete. Here we see a clear difference between the running steps (both in the approach of the long jump and in the reconstructed sprinting movements studied before) and the take-off step, because in sprinting we described little knee flexion, which was also found in the literature, where stiffening of the knee is described as a locomotion strategy of amputee athletes [18]. For the left leg, the range of motion is comparable for both athletes. While the left leg joints in the sagittal plane (RY) show basically comparable curve shapes between the two athletes, the differences in the remaining two hip angles (RX and RZ) are clearly visible. In the sagittal plane, the movements of the trunk segments are significantly larger for the amputee athlete than for the non-amputee athlete. This is consistent with observations from sprinting motion reconstruction, where we identified larger movements in the trunk as a possible compensatory mechanism for inter-limb asymmetry. Unlike in sprinting, where we further described stronger arm movements of the amputee athlete as a compensatory mechanism for inter-limb asymmetry, the range of motion in the shoulder and elbow joints of the amputee athlete is comparable to that of the non-amputee athlete. However, in the joints of the left arm (which is located on the opposite side of the body to the amputation), there is a significantly greater movement during the third-last contact phase than in the non-amputee athlete, which may well be interpreted as compensation during contact with the RSP. It is interesting that such a movement is less pronounced during the last contact phase, which again occurs with the RSP. Looking specifically at the take-off step to examine the significance of the arm movements during the take-off, it is noticeable that the directions in which the two athletes perform their movements are the same for almost all angles, but the movements differ in intensity. The exception here are the RX DOFs in each case.

### 9.2.5 Joint Torques

Figure 9.7 shows the joint torques of the non-amputee and the amputee athletes, respectively. As the prosthetic device is a passive device, no active torque is generated. We computed the passive torque which is acting at the prosthetic ankle via Eq. (2.1) with the reconstructed values for the spring and damping constants. In addition, we computed measures related to energy efficiency based on the joint torques and joint torque derivatives as described in Section 5.3. They are given in Table 9.5.

Directly at first glance, it is noticeable that the torques of both legs of the amputee athlete are on average (significantly) smaller than those of the non-amputee athlete. Exceptions are

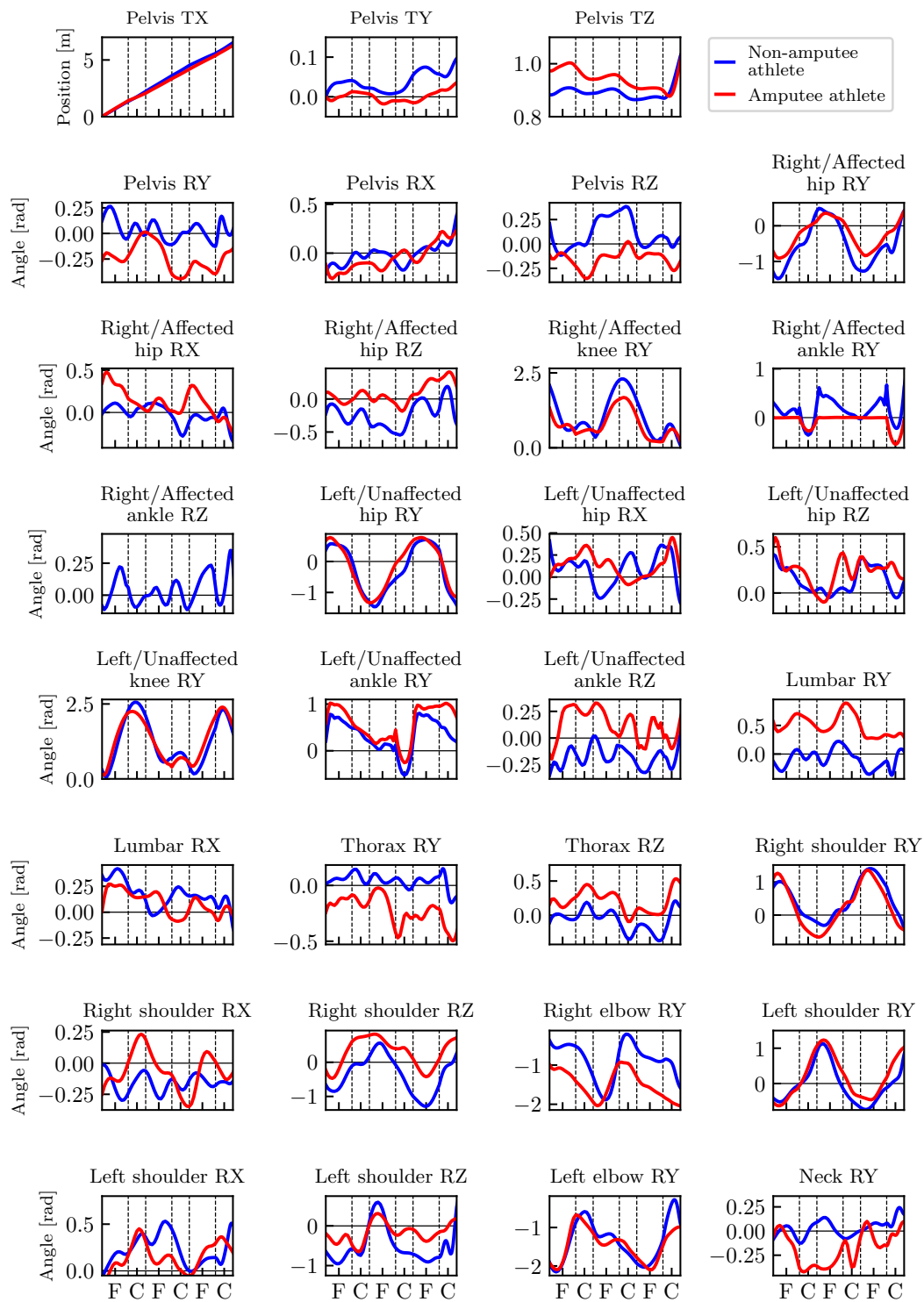


Figure 9.6: Generalized positions of the amputee and the non-amputee athlete for the reconstructed long jump motions. The abbreviations ‘F’ and ‘C’ on the x-axis denote flight and contact phases, respectively. The phase order is as shown in Figure 8.1. Phase durations are scaled for comparability. The directions of the angles are as in Figures 5.8 and 5.10, but they are omitted for reasons of clarity.

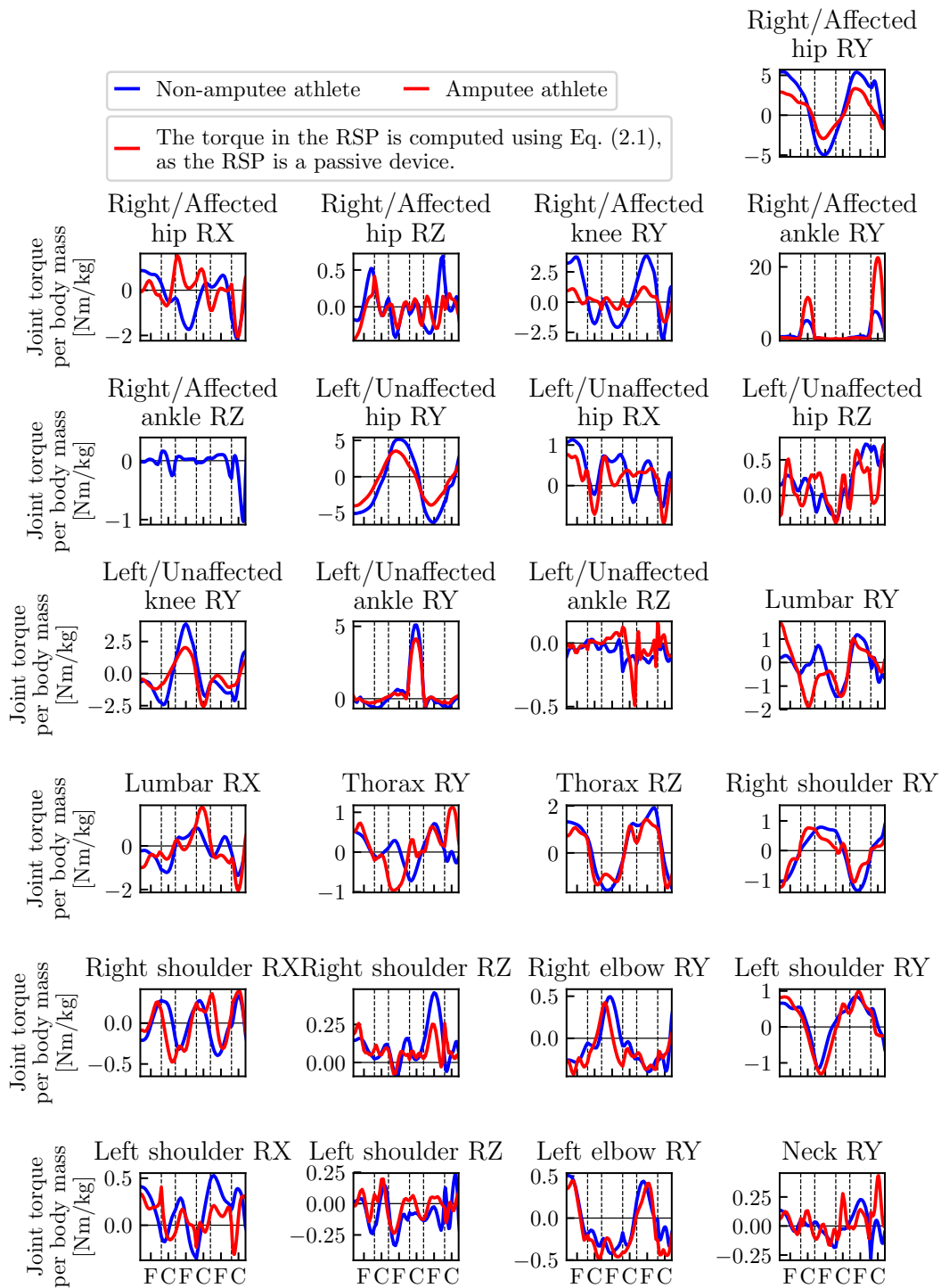


Figure 9.7: Joint torques of the amputee and the non-amputee athlete for the reconstructed long jump motions. The abbreviations ‘F’ and ‘C’ on the x-axis stand for flight and contact phases, respectively. The phase order is as shown in Figure 8.1. Phase durations are scaled for comparability and joint torque values are normalized by body mass.

the torques generated in the prosthetic ankle during the respective contact phases. However, a direct comparison of these torques with those generated in the biological leg is difficult due to the different geometry (in particular the long lever arm due to the significantly longer RSP

Table 9.5: Measures related to energy efficiency based on joint torques and joint torque derivatives for the long jump motions of the non-amputee and the amputee athlete. The computation of the measures is as described in Section 5.3. The abbreviations ‘NA’ and ‘A’ denote the non-amputee and the amputee athlete, respectively.

Joint	Absolute torques [N m kg <sup>-1</sup> ]		Squared torques [N <sup>2</sup> m <sup>2</sup> kg <sup>-2</sup> ]		Abs. torque derivatives [N m kg <sup>-1</sup> s <sup>-1</sup> ]		Sq. torque derivatives [N <sup>2</sup> m <sup>2</sup> kg <sup>-2</sup> s <sup>-2</sup> ]	
	NA	A	NA	A	NA	A	NA	A
Right Hip RY	3.417	1.806	14.136	4.171	45.19	26.47	2919.0	1092.1
Right Hip RX	0.799	0.520	0.952	0.537	15.59	21.55	424.4	857.7
Right Hip RZ	0.182	0.140	0.059	0.032	8.19	7.41	109.3	83.7
Right Knee RY	1.812	0.547	4.587	0.488	42.57	18.26	2751.3	549.5
Right Ankle RY	1.817	-	8.661	-	45.53	-	7021.8	-
Right Ankle RZ	0.119	-	0.056	-	5.62	-	91.3	-
Left Hip RY	3.438	2.262	14.957	6.656	45.30	30.70	3206.6	1242.4
Left Hip RX	0.513	0.387	0.361	0.206	10.78	12.10	183.9	289.9
Left Hip RZ	0.281	0.241	0.122	0.088	5.82	10.47	52.4	170.5
Left Knee RY	1.539	0.975	3.202	1.319	31.99	21.12	1471.5	817.0
Left Ankle RY	0.812	0.578	2.312	1.474	27.30	20.65	2672.6	1853.4
Left Ankle RZ	0.069	0.068	0.007	0.011	2.31	6.07	9.5	167.8
Lumbar RY	0.549	0.725	0.473	0.762	15.67	15.81	400.9	427.2
Lumbar RX	0.567	0.695	0.449	0.754	12.81	17.34	264.3	548.8
Thorax RY	0.276	0.471	0.120	0.332	7.94	11.01	88.7	188.1
Thorax RZ	1.056	0.935	1.322	0.985	15.12	16.97	362.5	534.2
Neck RY	0.076	0.097	0.010	0.017	3.25	5.69	23.7	57.0
Right Shoulder RY	0.606	0.448	0.486	0.302	9.13	8.95	143.0	142.4
Right Shoulder RX	0.191	0.214	0.047	0.060	5.34	6.65	39.5	69.3
Right Shoulder RZ	0.116	0.091	0.025	0.013	3.14	3.32	18.1	17.5
Right Elbow RY	0.228	0.244	0.068	0.070	4.57	5.28	37.7	44.7
Left Shoulder RY	0.492	0.583	0.320	0.448	8.81	9.54	118.0	141.8
Left Shoulder RX	0.248	0.152	0.078	0.032	5.33	5.90	38.8	91.8
Left Shoulder RZ	0.121	0.073	0.021	0.009	4.91	4.26	43.4	31.4
Left Elbow RY	0.264	0.311	0.086	0.112	5.72	6.19	52.2	61.0
Sum	19.59	12.56	52.92	18.88	387.9	291.7	22544	9479.2

compared to the human foot). However, if we compare the prosthetic ankle torque during the third-last step with the one generated during the corresponding phase of the sprinting reconstruction, they are of comparable magnitude and shape (see Figure A.10, in which we compare the two reconstructed sprinting steps with the third- and second-last steps of the long jump approach). In contrast to the sprinting motion, the amputee athlete applies less torque in his biological ankle indicating that he either relies more on the RSP for approaching the board and taking off efficiently or that he needs to adapt the torque in the second-last contact to achieve a proper take-off position. To determine if the latter idea affects the motion, it would be necessary to investigate further approach steps, at least the fourth-last contact phase. The torques in the right hip and knee of the amputee athlete have a 30 % to 62 % smaller range (by which we mean the difference between maximum and minimum torque throughout the movement) than those of the non-amputee athlete – except for the RX component of the hip joint torque where both athletes execute torques in a similar range. In particular, there is little torque inducing knee flexion for the amputee athlete. In the left leg of the amputee athlete, the torques are also lower on average than in the non-amputee athlete, although not as much as in the right leg. This is also reflected in the calculated measures for energy efficiency, which are based on joint torques and torque derivatives. The values of the amputee for all leg DOFs in the sagittal plane are (significantly) smaller than the values of the non-amputee athlete for

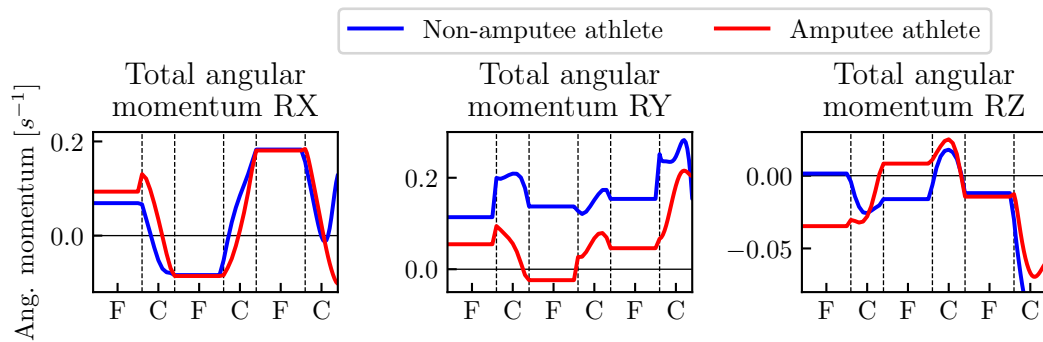


Figure 9.8: Angular momenta with respect to the center of mass of the amputee and the non-amputee athlete for the reconstructed long jump motions. The abbreviations ‘F’ and ‘C’ on the x-axis stand for flight and contact phases, respectively. The phase order is as shown in Figure 8.1. Phase durations are scaled for comparability and angular momentum values are normalized by body mass and body height squared.

all measures. This indicates that the amputee athlete has to spend less energy for the last three steps than the non-amputee athlete if energy is defined using torque curves as a measure. In the joints of the trunk and arms, the differences are not quite as pronounced; here, both the curves and the magnitudes of the torques are more comparable between the two athletes. Compared to the sprinting movement, we cannot determine that the amputee has to work harder in the upper body joints to compensate for the lower torques in the legs. Here, in direct comparison to the sprinting movement (Figure A.10), it is noticeable that the torques of the amputee athlete are of comparable magnitude for the two kinds of motion, thus indicating that he still has to apply a good amount of work in the upper body. However, on average the torques of the non-amputee are larger for the long jump compared to the sprinting motion. Since we only have one trial of a non-amputee athlete for comparison, it is not possible to say whether this behavior is generally observable or due to the specific athlete.

### 9.2.6 Angular momentum about the Center of Mass

Figure 9.8 shows the total angular momentum about the CoM for rotations in the frontal (RX), sagittal (RY) and transversal (RZ) planes. The total angular momenta of the two athletes are comparable for rotations in the frontal plane (RX). The most significant difference is that the directions at the end of the last contact phase are opposite: While the angular momentum of the non-amputee athletes has a positive sign, the one of the amputee athlete has a negative sign which means that they rotate in opposite directions (the non-amputee athlete to his right side and the amputee athlete to his left side). For the rotations in the remaining two planes (RY and RZ), both athletes have angular momentum values with identical sign at the end of the last contact phase which means that their overall rotations have the same direction. However, within the last three steps, some differences are visible also in the rotations in these planes. In fact, it appears that the amputee athlete has smaller angular momentum for rotations in the sagittal plane and larger angular momentum for rotations in the transversal plane than the non-amputee athlete. Similar to the sprinting movements, it is possible that the larger angular momentum for rotations in the transversal plane indicates that the overall running movement is more unstable due to the inter-limb asymmetry.

## 9.3 Summary

We successfully reconstructed the dynamics of the last three steps of the long jump approach of one amputee and one non-amputee athlete and analyzed relevant quantities. Some differences between the two athletes have become apparent, but also differences regarding the long jump approach steps compared to the reconstructed sprinting steps. Overall, it has been shown that the amputee athlete starts slower in direct comparison with the non-amputee athlete, but takes off more successfully and thus can achieve the greater jump distance. For this purpose, he definitely takes advantage of the RSP, although it cannot be conclusively clarified whether the inter-limb asymmetry may also have a downside effect, e.g., regarding the control of angular momentum in the non-sagittal planes.

However, we would like to clearly point out at this point that the comparison is very interesting, but at this point no general conclusions can be drawn from it in any way, as we are only comparing two individual athletes. Furthermore, we have no further information if and to what extent the training and performance level of the athletes are comparable. Instead, the main purpose of the dynamics reconstruction was to show that the approach can also provide meaningful results for long jump movements and that the employed models are useful for the description of long jump movements. Furthermore, the analysis of the motions provides valuable ideas which quantities can be meaningful for a comparison of long jump with and without RSP and which optimization criteria can be used for a synthesis. Based on the results of this chapter, we will generate and investigate long jump movements based on the two athletes in the following chapter. Then, in Chapter 11, we will also investigate what differences in the motions arise when the amputee athlete in the model is compared to himself without amputation.

Even though the consideration of the three-dimensional system provides interesting aspects for the movements in the frontal and transverse planes, in the following chapters we will restrict ourselves to the *2D+ model*, a model in the sagittal plane, which has three-dimensional shoulder joints as the only exception. This simplification is justified by the significant savings in computational time and complexity (see also the explanations in Section 5.4).



## 10 Synthesis of Long Jump Motions with and without Running-Specific Prostheses

For the prediction of long jump motions, we established two-dimensional rigid body models which, however, have three-dimensional shoulder joints. Compared to the previous chapter (dynamics reconstruction of long jump), we have reduced the number of degrees of freedom (DOFs) for complexity reasons. A detailed description of the used *2D+ model* is given in Section 2.2. The optimal control problem which we use to predict the long jump motions is the motion synthesis optimal control problem (OCP) described in Section 3.1.2.

**Constraints to the optimal control problem** In addition to the contact constraints (4.1)–(4.4), we formulate constraints introducing limits on the joint torques based on the Muscle Torque Generators described in Section 2.5. More specifically, we formulate two constraints for each joint torque, one for the maximum possible value and one for the minimum possible value:

$$\tau_i - \tau_{\text{EXT/FLEX}}^M(a, \theta_i, \dot{\theta}_i, \boldsymbol{\alpha}) \geq 0, \quad (10.1a)$$

$$-\tau_i + \tau_{\text{FLEX/EXT}}^M(a, \theta_i, \dot{\theta}_i, \boldsymbol{\alpha}) \geq 0. \quad (10.1b)$$

The maximum possible torques  $\tau_{\text{EXT/FLEX}}^M$  which can be generated by extension or flexion, respectively, are calculated using the Muscle Torque Generators (MTGs) via Eq. (2.9) (see Section 2.5). The indices “EXT” and “FLEX” denote extension and flexion torques, whereby the choice of the signs depends on the definition of the joint angles. Since we are interested in the calculation of the upper and lower limits for the torques, we set the activation of the muscles to the maximum value  $a = 1$ . We use the values calculated by means of the fitting routine described in Section 2.5 for the parameter  $\boldsymbol{\alpha}$ .

Different from the synthesis of sprinting movements, where the mere *2D model* was used, here, due to the three-dimensional shoulder joints, there is a possibility that the arms penetrate other parts of the body, since the model formulation does not formulate any borders of the segments. In reality, such overlapping or penetration is not possible; thus, it must be ruled out with the help of constraints. We proceed here analogously to the implementation of the segment distance computation in the HEIMAN model (see Chapter 4.6 in [38]): conceptually, cylinders of length  $l$  (convex hull of line segment) with hemispheres of radius  $r$  at both ends are assigned to each affected segment, which are called collision capsules. The measure of the distance  $d(C_1, C_2)$  between two capsules  $C_1$  and  $C_2$  is defined as the distance between the two closest points of the line segment minus the radii of each capsule. To prevent overlapping of two segments, the distance measure  $d$ , which depends on the current generalized positions  $\mathbf{q}$ , must be greater than zero, thus:

$$d(C_1, C_2, \mathbf{q}) > 0. \quad (10.2)$$

Finally, the landing at the end of the actual long jump is specified by introduction of constraints to the OCP. The landing conditions differ slightly between the non-amputee and the amputee athlete: For the non-amputee athlete, we require that the touchdown occurs with both heel

contact points. For the amputee athlete, we assume that the touchdown occurs with the heel contact point of the left foot as we assume that athletes with below the knee amputation (BKA) avoid the harshness of an inelastic impact with the affected leg. Furthermore, we use the constraints to limit the distances between the two feet, between the two hands and between the hands and feet in order to achieve a realistic landing position. This also ensures that the running-specific prosthesis (RSP) is sufficiently close to the ground on landing to resemble an actual long jump.

**Formulation of the objective function** For the mathematical description of a long jump including the last three steps before the jump we have identified three basic optimization criteria after analyzing real long jumps.

1. *Maximize Jump Distance:* (Main criterion) The jump distance  $d_{\text{jump}}$  is computed as the difference between the landing and the take-off positions. The take-off position is given by the hallux contact point of the right foot or the prosthetic device, respectively. We denote it by  $P^{RH}(h_{\text{take-off}})$ . As described before, the ‘landing’ situation at the end of the long jump is defined differently in the cases of the amputee and the non-amputee athlete. For the amputee athlete, we define it as the situation when the heel contact point of the left foot becomes zero and impose an additional constraint that the contact point of the prosthetic device is close to zero as well. Hence the landing position is determined by the heel contact point of the left foot which we denote by  $P^{lh}(h_{\text{landing}})$ . The jump distance is then computed as the horizontal difference between these two points:

$$d_{\text{jump}} = P_x^{lh}(h_{\text{landing}}) - P_x^{RH}(h_{\text{take-off}}). \quad (10.3a)$$

For the non-amputee athlete, we define landing as the situation when the heel contact points of both feet become zero. To compute the jump distance, we then take the position of the hind foot (denoted by  $P^{lh/rh}(h_{\text{landing}})$ ) as the distance in real long jumps is measured from the closest point to the board in the sand:

$$d_{\text{jump}} = P_x^{lh/rh}(h_{\text{landing}}) - P_x^{RH}(h_{\text{take-off}}). \quad (10.3b)$$

The objective function which maximizes this jump distance  $d_{\text{jump}}$  is formulated as a Mayer type objective function and evaluated at the end of the long jump flight phase:

$$\varphi_{M_1}(t_f, \mathbf{x}(t_f), \mathbf{p}) = -p_d = -d_{\text{jump}}. \quad (10.4)$$

2. *Minimize Torque Derivatives Squared:* (Minor criterion) The Lagrange-type objective function for torque derivatives minimization is added as a regularization term with a sufficiently small weighting factor to choose a unique solution:

$$\varphi_{L_2}(t, \mathbf{x}(t), \mathbf{u}(t), \mathbf{p}) = \|\dot{\boldsymbol{\tau}}(t)\|_2^2 = \|\mathbf{u}(t)\|_2^2. \quad (10.5)$$

3. *Head Stabilization:* (Minor criterion) Uncontrolled nodding and wobbling of the head is prevented by the formulation of an objective function of Lagrange-type:

$$\varphi_{L_3}(t, \mathbf{x}(t), \mathbf{u}(t), \mathbf{p}) = \|\theta_{\text{head,abs}}\|_2^2. \quad (10.6)$$

The three basic criteria are combined into one objective function of the form of Eq. (3.5) with  $n_M = 1$ ,  $n_L = 2$ ,  $\boldsymbol{\gamma} = (1, 2 \cdot 10^{-8}, 1)$ .

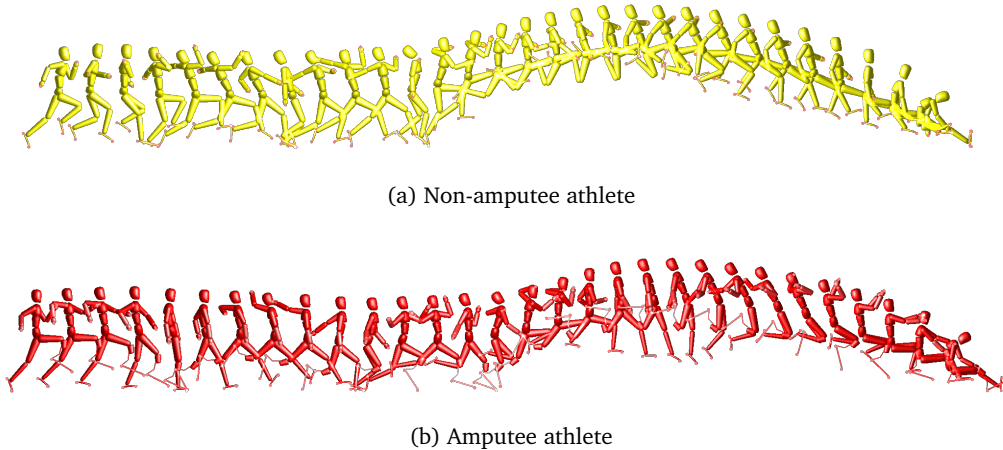


Figure 10.1: Animated sequences visualize the solutions of the long jump motion synthesis optimal control problem

## 10.1 Comparison of Reconstructed and Synthesized Long Jump Motions with and without Running-Specific Prostheses

Based on the above described problem formulation, we synthesized a long jump motion for the non-amputee and one for the amputee athlete. Again, when we refer to long jump motion, we mean the last three steps of the approach and the jump itself up to the landing (as shown in Figure 8.1).

Figure 10.1 shows visualizations of the computed long jump motions for both athletes from the sagittal plane view. Even though we will of course analyze the motions more closely in the following and also discuss differences in comparison to the respective reconstructed motions from Chapter 9 in detail, the animated motion sequences already show that the chosen problem formulation including the objective function is quite suitable for generating realistic-looking long jump motions. The first differences between the non-amputee and the amputee athlete can also already be seen from the sequences: The amputee athlete jumps slightly flatter and shorter than the non-amputee athlete. We will examine this in detail below.

The results from the long jump motion synthesis allow analyses from different perspectives: For each of the two athletes separately, the respective reconstructed and synthesized solution can be compared to find out where the long jump model and the motion synthesis formulation could be further improved. For each of the two athletes, we can also compare the three investigated contact phases to investigate if and how the take-off contact phase differs from the contact phases of the (final) approach steps. This allows us to determine information about the biomechanics of the long jump with and without BKA. Finally, the results can be used to compare the long jump movements of athletes with and without BKA. In this section (Section 10.1), we will first present differences and similarities between the reconstructed and synthesized solutions of both athletes (without comparing them to each other) and give possible reasons for the differences. In the following section (Section 10.2), we will then focus on the comparison of the biomechanical characteristics of the long jump movements of the two athletes.

Table 10.1 gives the individual phase durations of the synthesized long jump motions. Apart from the last contact phase and the flight phase before it, the phase durations for the non-amputee athlete are shorter in the synthesized solution than in the reconstructed solution. Compared with the reconstruction, the duration of the flight phases of the last three steps has become more uniform, varying only between 0.113 s and 0.119 s (whereas the range in the

Table 10.1: Phase durations of the amputee and the non-amputee athlete for the synthesized long jump motions. The numbering of the phases corresponds to the order shown in Figure 8.1: 1 - first flight phase, 2 - first right contact phase, 3 - second flight phase, 4 - left contact phase, 5 - third flight phase, 6 - second right contact phase (take-off), 7 - fourth flight phase. The abbreviations ‘NA’ and ‘A’ stand for the non-amputee and the amputee athlete, respectively.

phase	1	2	3	4	5	6	7
NA	0.113 s	0.080 s	0.119 s	0.110 s	0.117 s	0.084 s	0.887 s
A	0.203 s	0.079 s	0.195 s	0.110 s	0.101 s	0.106 s	0.781 s

reconstructed solution was 0.110 s to 0.144 s). In the case of the amputee athlete, the third-last and the second-last steps take significantly longer in the synthesized solution than in the reconstructed one; this is true for both the flight and contact phases. The last step is slightly shorter in the synthesized than in the reconstructed solution where the difference comes from the flight phase duration. If we look at the total duration for the last three steps, it is shorter for the synthesized solution of the non-amputee athlete and longer for the synthesized solution of the amputee athlete compared to the respective reconstructed solutions.

### 10.1.1 Estimated Jump Distance and Take-Off Angle

We compute the estimate of the jump distance and the take-off angle as described in Chapter 9 using (9.1)–(9.3). Based on these definitions, we compute the following values for the synthesized solutions:

- a jump distance of 9.22 m with a take-off angle of  $16.85^\circ$  for the amputee athlete and
- a jump distance of 9.86 m with a take-off angle of  $20.09^\circ$  for the non-amputee athlete.

For both athletes the estimated jump distance in the synthesized solution is larger than in the reconstructed solution: The non-amputee athlete jumps 2.02 m further, the amputee athlete jumps 0.96 m further. There are also clear differences in the take-off angle between reconstructed and synthesized solutions: for the non-amputee athlete, the take-off angle the synthesis is  $2.17^\circ$  larger than in the reconstruction, for the amputee athlete it is actually smaller (by  $-2.95^\circ$ ). This is interesting, because it shows that a larger take-off angle can lead to a larger jump distance, but is not the only decisive criterion for the jump distance.

The jump distances, which are after all significantly larger compared to those estimated for the actually measured motions, can be explained mainly by two observations: First, in the motion synthesis we consider a motion that is mainly restricted to the sagittal plane (compared to the three-dimensional reconstruction). Even though the main action takes place in this plane, we thereby prevent a movement of the whole athlete in the sideways direction, which would have a shortening influence on the total jump distance. Theoretically, such a sideways movement should also be excluded in the three-dimensional case by the optimization criterion of jump distance maximization; however, it is possible that the restriction to the sagittal plane allows a few centimeters of jump distance gain. The formulation of the motion synthesis as an OCP is the second main cause of the larger jump distances. In the solution of the OCP, all variables are known at each time point of the motion and accordingly all can be adjusted in such a way that the objective function can be fulfilled in an optimal way, i.e., the touch-down of the foot into the third last contact, for example, can already be adjusted exactly in such a way that the jump distance becomes maximal at the end. This is not the case in reality, with a human athlete. On the other hand, the larger jump distances also mean that there may still be potential for improvement in both athletes studied.

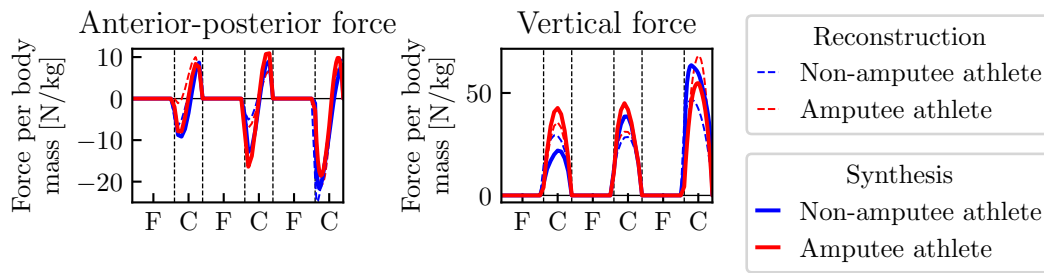


Figure 10.2: Ground reaction forces of the amputee athlete and the non-amputee athlete for the synthesized long jump motions. The abbreviations ‘F’ and ‘C’ on the x-axis stand for flight and contact phases, respectively. The phase order is as shown in Figure 8.1. Phase durations are scaled for comparability. Ground reaction forces are normalized by body mass.

### 10.1.2 Ground Reaction Forces

Figure 10.2 shows the ground reaction forces of the last three contact phases. For both athletes, in addition to the forces from the motion synthesis solution, we have included the reconstructed forces (with thinner dashed lines) to directly compare reconstructed and synthesized forces. It is immediately noticeable that there are differences between reconstructed and synthesized solutions in both athletes. This is particularly noticeable in the vertical force component. First for the non-amputee athlete: While the force curves of the third- and second-last step in the reconstruction are comparable in size and only the one of the take-off contact phase is significantly larger, the peak values of the vertical force in the synthesized solution increase with each contact phase. The synthesized force in the third-last contact phase is significantly smaller than the reconstructed force and in each of the last two contact phases a little larger than it. As in the reconstructed solution, the vertical force in the synthesized solution is again parabolic during the take-off contact phase – unlike in the force plate data. In the anterior-posterior force component, what is most striking is that in the synthesized solution of the non-amputee athlete, the braking force during the final contact phase, which was a bit overestimated in the reconstruction, becomes smaller and thus more realistic. Also in the case of the amputee athlete, the differences between the reconstructed and synthesized anterior-posterior force are mainly to be found in the fact that unexpected curves in the reconstructed solution were corrected, e.g., the hardly present braking force in the third-last contact phase. In the vertical forces it can be seen that the peak values of the third- and second-last contact are larger and the peak value in the last contact phase is significantly smaller than in the reconstructed solution. This is surprising because in sprinting movements we observed that the optimized solution exploited the RSP better than the real athlete and therefore larger vertical forces were generated.

### 10.1.3 Motion of the Center of Mass

Figure 10.3 compares the curves of the center of mass (CoM) motion for the reconstructed and synthesized solutions of the non-amputee and the amputee athlete. The two columns on the left give the horizontal (X; first column from left) and vertical (Z; second column from left) position (upper row) and velocity (lower row). The right column shows the evolution of the vertical CoM position depending on the CoM height at lift-off into the third-last step (upper row) and at touch-down into the take-off contact phase (lower row).

Again, we start with the comparison of the reconstructed and synthesized solutions of the non-amputee athlete. While the course of the horizontal CoM position and the vertical CoM motion

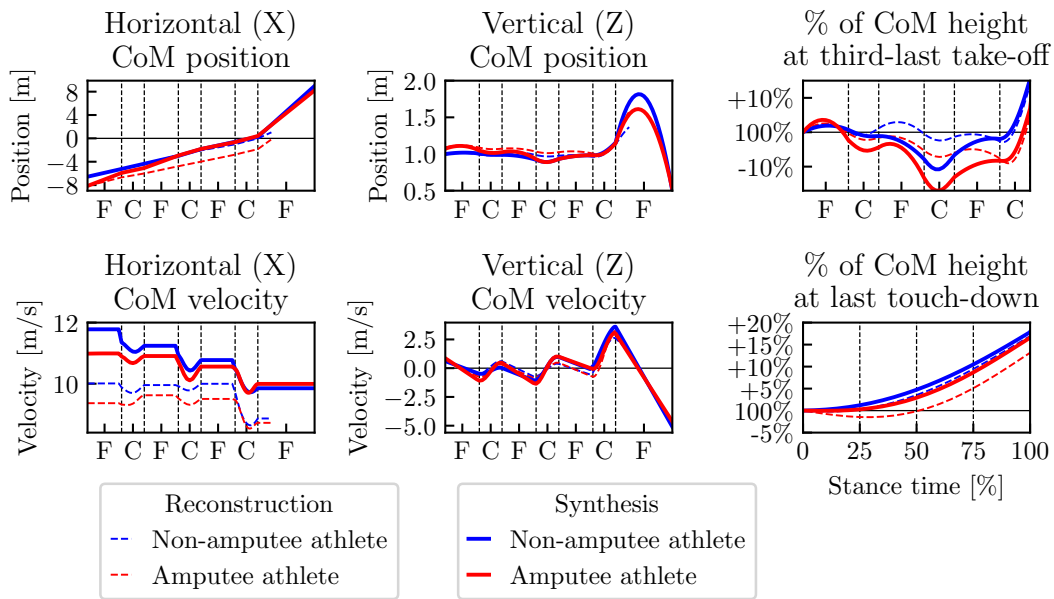


Figure 10.3: Center of mass motion of the amputee athlete and the non-amputee athlete for the synthesized long jump. The abbreviations ‘F’ and ‘C’ on the x-axis stand for flight and contact phases, respectively. The phase order is as shown in Figure 8.1. Phase durations are scaled for comparability.

look quite similar, the difference in horizontal CoM velocity is most striking. The non-amputee athlete has a significantly larger velocity in the synthesized solution than in the reconstructed solution over the entire steps examined. On average, he runs at a velocity that is  $1.16 \text{ m s}^{-1}$  larger. At the take-off, the velocity of the synthesized solution is  $0.99 \text{ m s}^{-1}$  greater than the reconstructed velocity. The second clear difference between reconstructed and synthesized solution in the non-amputee athlete is shown by the fact that he almost does not lower his CoM at all during the third-last contact, then reaches a very strong lowering during the second-last contact.

Also in the amputee athlete, the differences between reconstructed and synthesized solution are found mainly in the horizontal CoM velocity and the evolution of the vertical CoM position with respect to the CoM height at lift-off into the third-last step. The amputee athlete has also a significantly larger horizontal velocity in the synthesized solution; on average, he runs with a  $1.23 \text{ m s}^{-1}$  greater velocity. At take-off, the horizontal CoM velocity is  $1.27 \text{ m s}^{-1}$  higher than in the reconstructed solution. In addition, the synthesized solution lowers the CoM position significantly deeper compared to the reconstructed solution, so the amputee athlete gains more CoM height during the final contact phase.

#### 10.1.4 Joint Angles and Joint Torques

For comparing the joint angles and torques, we focus on the ones of the contact leg during the three contact phases as most relevant movement takes place in these joints. Figure 10.4 shows the hip (Figure 10.4a), knee (Figure 10.4b) and ankle (Figure 10.4c) angles and torques during the contact phases of the respective leg, i.e., the joints of the right leg for the third-last and last contact phase and the joints of the left leg for the second-last contact phase. We first consider the angle curves. Overall, there are only minor differences between the curves of the reconstructed and the synthesized angles of both athletes. For some angles, the curves seem to be “shifted” by an offset angle. Since we show the relative angles with respect to the

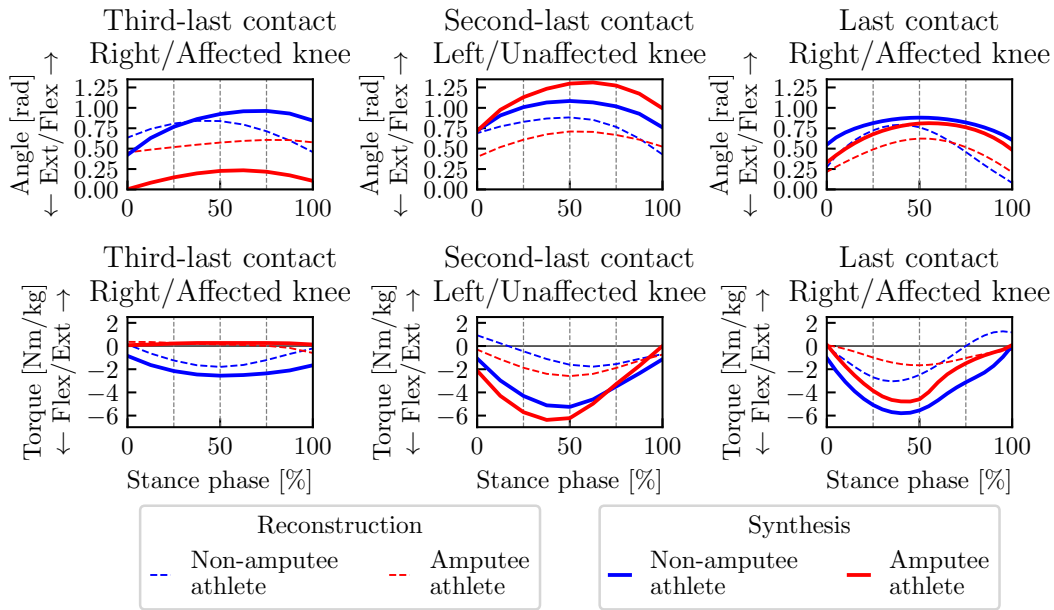
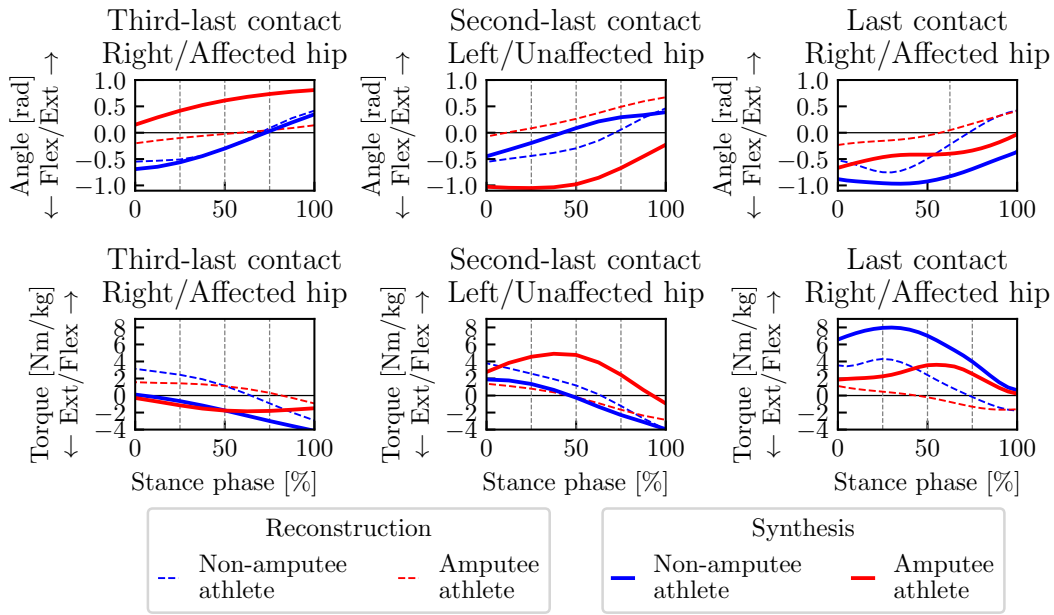
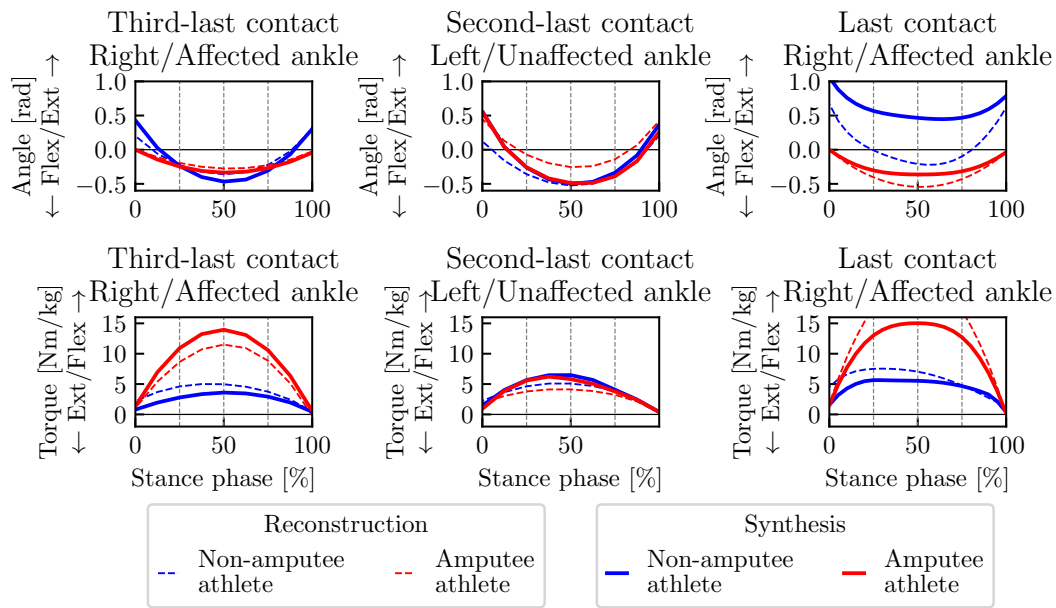


Figure 10.4: Contact leg joint angles and torques of the amputee athlete and the non-amputee athlete for the last three contact phases of the synthesized long jump. The phase order is as shown in Figure 8.1. Phase durations are scaled for comparability. Joint torque values are normalized by body mass.



(c) Ankle joint

Figure 10.4: Contact leg joint angles and torques of the amputee athlete and the non-amputee athlete for the last three contact phases of the synthesized long jump (cont.)

next higher joint in the kinematic chain, this shift might be explained by differences between the reconstructed and the synthesized solutions regarding higher angles along the kinematic chain. To evaluate the differences, we compare the range of motion of the hip, knee and ankle joints for the individual contact phases. For the non-amputee athlete, we see a clearly different range of motion between reconstructed and synthesized motions during the last contact phase in all three joints: The range of motion is significantly smaller for the synthesized solutions. It is half as large for the hip and the knee joint and about 50% smaller for the ankle joint. In the knee and ankle joints, we further see a smaller range of motion in the synthesized solution for the other two contact phases. Overall, it seems that the motions of the contact leg of the non-amputee athlete during the contact phases are less extensive in the synthesized solution when compared to the reconstructed one. In contrast, the motions of contact leg of the amputee athlete during the contact phases are on overall more extensive in the synthesized solution compared to the reconstructed solution. The exception to this is the last contact phase where the range of motion of hip and prosthetic ankle joint is larger (by 7.6% and 50.3%, respectively) and the range of motion in the knee joint is smaller by 15.2%.

For the joint torques, the differences between the reconstructed and synthesized solution are larger, especially in the take-off contact phase. For both athletes, we see that the hip and knee joint torques in the synthesized solution have similar curves, but significantly larger absolute values. Thus, our solution suggests that also amputee athletes should use their knees more to jump farther. The ankle torques of the reconstructed and synthesized solutions are roughly comparable in magnitude in all three phases. For the non-amputee athlete, in the right ankle cases, the synthesized torque is a little smaller in the right ankle cases, and a little larger in the left ankle case compared to the reconstructed solution. For the amputee athlete, the synthesized torque is larger during the third-last and second-last contact phases and significantly smaller during the last contact phase compared to the reconstructed torque. This is interesting because we expected that in the synthesis the amputee model would make a more extensive use of the RSP during the last contact phase (similar to the sprinting motion synthesis results where we

found larger torques in the RSP and lower torques in the biological ankle compared to the reconstruction).

### 10.1.5 Causes for Differences Between Reconstructed and Synthesized Motions

In contrast to the sprinting motion synthesis, we did not investigate different optimization criteria and objective functions for the synthesis of long jump motions, but used a concrete objective function as a basis for the computation of the motions. Therefore, it was natural to compare the generated motions with the reconstructed solutions to find out where differences could be found. While smaller deviations are always likely for numerical and practical reasons, more significant differences are certainly a reason to think about the causes. We have already briefly discussed this in the section on estimated jump distance and take-off angles (cf. Section 10.1.1, but would like to discuss it in a little more detail here.

There are three main directions of thought here: First, it is possible that the solution of the motion synthesis OCP will show opportunities for the individual athletes to improve their technique. We will also discuss this occasionally in the following section. The second, related reason for the differences between reconstructed and synthesized motion is the formulation of the predictive simulation as an OCP: The goal of solving an OCP is to determine the optimal parameters, state and control variables, i.e., exactly those that will optimize the objective function. In this sense, optimization solutions are always more perfect than reality, as they execute exactly the optimal solution without any perturbations. The motion is considered and solved as a whole, that is, at each shooting node all previous and future values of the variables are known, which allows the calculation of an ideal position at each time. On the one hand, this is not possible in reality for the human athlete, on the other hand, it may be that the athletes actually do not move ideally, but that at the same time the calculated ideal movement is not intuitive. Third, of course, there is also the possibility that the problem formulation is not yet ideal. The significant differences in torques during the third-last contact phase for the amputee athlete indicate that the OCP makes assumptions due to the start of the motion with the lift-off into the third-last step of the approach that do not correspond to reality and thus calculates different joint torques. Here it would be certainly interesting to calculate further steps of the approach<sup>1</sup>. Furthermore, in the context of problem formulation, there is also the possibility that the choice of optimization criteria is not yet complete or the weighting factors with which the criteria are combined in the objective function are not yet optimal. In the choice of optimization criteria, there would be, for example, the possibility of formulating further conditions on the take-off (e.g., striving for the optimal take-off angle or maximizing the take-off velocities) or the approach (e.g., maximizing the approach velocity). We chose to use jump distance maximization as the main criterion because it is the ultimate goal of a long jumper above anything else, and we wanted to avoid examining quantities to which we made explicit maximization demands. However, it would be interesting to investigate the influence of other criteria and other weight factors on the movement in subsequent studies. At this point, the calculation of an inverse optimal control problem (IOCP) for the long jump would then be of great interest, which would, however, face the challenge that the reference movement ends during the jump. Thus, it would be necessary to adjust the definition of jump distance in Eq.s (10.3a) and (10.3b) or to collect data for the flight phase.

All three directions of thought are related to each other and must be carefully weighed against each other in order to assess the quality of the movements. Even though we have described differences between reconstructed and synthesized solution in all variables for both athletes,

<sup>1</sup>In principle, it would be very intriguing to calculate the entire long jump movement including the complete approach from the standing position. Due to the size of the problem, especially the large number of phases, this is not possible at the moment.

we find them within an acceptable range to compare the synthesized movement of the athlete with BKA to the one of the athlete without BKA. Furthermore, since the models are based on different athletes and we are only comparing two individual athletes, it is in no way the goal of this chapter to make general statements about long jump with and without RSP<sup>2</sup>. Therefore, in the following section, we would like to compare the synthesized long jump motions with and without RSP.

## 10.2 Comparison of Synthesized Long Jump Motions with and without Running-Specific Prostheses

As we have already stated repeatedly, the ultimate goal of every long jumper is to achieve the greatest possible jump distance. The entire approach, the take-off as well as the flight and landing technique are oriented towards this goal. Thus, for a comparison of the amputee and non-amputee athlete, it is most obvious to compare the jump distances. The estimates of the jump distances show that the non-amputee athlete jumps 64 cm further than the amputee athlete in the synthesized solution. This result is in contrast to the estimated jump distances of the reconstructed solutions, in which the amputee athlete jumps significantly farther than the non-amputee athlete. This means that the studied non-amputee athlete has an even greater potential to improve his technique and thus his jump distance compared to the amputee athlete. However, since we are comparing two different athletes with different muscle parameters, it is not possible (and we would like to emphasize this explicitly) to conclude in general from this result that athletes without BKA could jump further. Instead, in this section we want to investigate which differences between the two athletes lead to the different jump distances: as a preparation for the envisioned simulator tool and in order to get hints about possible fundamental differences between long jump with and without RSP.

The take-off angle of the amputee athlete is significantly smaller than that of the non-amputee athlete (difference:  $3.24^\circ$ ). Since a connection between take-off angle and jump distance is indisputable, the smaller take-off angle is one of the reasons for the shorter jump distance of the amputee athlete. The take-off angle is related to the CoM velocities at take-off (see Eq. (9.3)), hence we expect to find differences in the behavior of the CoM as well. In addition to Figure 10.3 which shows the CoM-related curves, we listed the horizontal and vertical CoM velocities at touch-down and lift-off as well as the corresponding change in the velocities for all three contact phases in Table 10.2. It is immediately noticeable that the amputee athlete covers a greater distance during the third- and second-last step than the non-amputee athlete. This matches the significantly longer step durations, which are possible due to the longer flight phase durations. In addition, the amputee athlete lowers his CoM significantly more than the non-amputee athlete during these steps. However, his CoM height at the beginning of the three investigated steps is higher. At touch-down in the last contact phase and at the take-off, both athletes have similar CoM heights: At touch-down into the last contact phase, the amputee athlete's CoM is 2.9 cm higher than the one of the non-amputee athlete. At take-off into the actual jump, it is 0.9 cm lower than the one of the non-amputee athlete. Thus, in direct comparison, the non-amputee athlete gains more vertical height during the take-off contact phase.

When looking at the horizontal CoM velocity, it is notable that the non-amputee athlete slows down with each step, while the amputee athlete loses less velocity during the third-last and second-last contact phases. If we assume that both athletes have reached approximately their maximum approach velocity at lift-off into the third-last step, this implies that the non-amputee

---

<sup>2</sup>We present a first step towards possible generalizations in Chapter 11.

Table 10.2: Measures related to the center of mass motion for the three contact phases of the synthesized long jump motion of non-amputee and amputee athlete. The measures are computed as defined in Section 5.3.

	Non-amputee athlete	Amputee athlete
THIRD-LAST CONTACT PHASE		
Horizontal CoM velocity at touch-down	11.78 m s <sup>-1</sup>	10.99 m s <sup>-1</sup>
Horizontal CoM velocity at lift-off	11.24 m s <sup>-1</sup>	10.91 m s <sup>-1</sup>
Change in horizontal CoM velocity	-0.54 m s <sup>-1</sup>	-0.08 m s <sup>-1</sup>
Vertical CoM velocity at touch-down	-0.40 m s <sup>-1</sup>	-1.12 m s <sup>-1</sup>
Vertical CoM velocity at lift-off	0.02 m s <sup>-1</sup>	0.47 m s <sup>-1</sup>
Change in vertical CoM velocity	0.42 m s <sup>-1</sup>	1.59 m s <sup>-1</sup>
SECOND-LAST CONTACT PHASE		
Horizontal CoM velocity at touch-down	11.24 m s <sup>-1</sup>	10.91 m s <sup>-1</sup>
Horizontal CoM velocity at lift-off	10.77 m s <sup>-1</sup>	10.56 m s <sup>-1</sup>
Change in horizontal CoM velocity	-0.47 m s <sup>-1</sup>	-0.35 m s <sup>-1</sup>
Vertical CoM velocity at touch-down	-1.05 m s <sup>-1</sup>	-1.45 m s <sup>-1</sup>
Vertical CoM velocity at lift-off	0.97 m s <sup>-1</sup>	1.00 m s <sup>-1</sup>
Change in vertical CoM velocity	2.02 m s <sup>-1</sup>	2.45 m s <sup>-1</sup>
LAST CONTACT PHASE – TAKE-OFF PHASE		
Horizontal CoM velocity at touch-down	10.77 m s <sup>-1</sup>	10.56 m s <sup>-1</sup>
Horizontal CoM velocity at lift-off	9.85 m s <sup>-1</sup>	9.99 m s <sup>-1</sup>
Change in horizontal CoM velocity	-0.92 m s <sup>-1</sup>	-0.57 m s <sup>-1</sup>
Vertical CoM velocity at touch-down	-0.08 m s <sup>-1</sup>	-0.08 m s <sup>-1</sup>
Vertical CoM velocity at lift-off	3.60 m s <sup>-1</sup>	3.02 m s <sup>-1</sup>
Change in vertical CoM velocity	3.68 m s <sup>-1</sup>	3.10 m s <sup>-1</sup>

athlete achieves a greater approach velocity than the non-amputee athlete. However, the amputee athlete has the greater horizontal CoM velocity at lift-off.

The behavior regarding vertical velocity differs clearly between the third- and second-last step on the one hand and the last step on the other hand. During the third- and second-last step, the amputee athlete loses significantly more vertical velocity due to the longer flight durations, but can at the same time generate significantly more vertical velocity than the non-amputee athlete during the comparably long contact phases. Incidentally, this is true for both legs; in fact, the gain in vertical velocity is even greater for the biological leg during the second-last than for the prosthetic leg during the third-last contact phase. During the last contact phase, interestingly, this behavior reverses and the non-amputee athlete has the larger gain in vertical velocity (by 0.58 m s<sup>-1</sup>) and jumps off with a larger vertical velocity (by 0.58 m s<sup>-1</sup>).

In the literature, the ability to generate as much vertical velocity as possible during the take-off contact phase with as little loss of horizontal velocity as possible is described as one of the decisive criteria for a successful long jump[6, 53]. Thus, while the amputee athlete has the smaller loss of horizontal velocity compared to the non-amputee athlete, the non-amputee athlete has the greater gain in vertical velocity in return. Stupendously subtracting the loss in horizontal velocity from the gain in vertical velocity yields a value of 2.53 m s<sup>-1</sup> for the

Table 10.3: Measures related to the ground reaction forces for the three contact phases of the synthesized long jump motion of non-amputee and amputee athlete. The measures are computed as defined in Section 5.3.

	Non-amputee athlete	Amputee athlete
THIRD-LAST CONTACT PHASE		
Anterior-posterior change of momentum	$-0.192 \text{ N s kg}^{-1}$	$-0.042 \text{ N s kg}^{-1}$
Anterior-posterior mean force	$-1.84 \text{ N kg}^{-1}$	$-0.06 \text{ N kg}^{-1}$
Vertical change of momentum	$1.232 \text{ N s kg}^{-1}$	$2.200 \text{ N s kg}^{-1}$
Vertical mean force	$16.09 \text{ N kg}^{-1}$	$29.08 \text{ N kg}^{-1}$
Vertical peak force	$21.90 \text{ N kg}^{-1}$	$42.69 \text{ N kg}^{-1}$
SECOND-LAST CONTACT PHASE		
Anterior-posterior change of momentum	$-0.279 \text{ N s kg}^{-1}$	$-0.317 \text{ N s kg}^{-1}$
Anterior-posterior mean force	$-2.00 \text{ N kg}^{-1}$	$-2.14 \text{ N kg}^{-1}$
Vertical change of momentum	$2.990 \text{ N s kg}^{-1}$	$3.325 \text{ N s kg}^{-1}$
Vertical mean force	$28.17 \text{ N kg}^{-1}$	$31.06 \text{ N kg}^{-1}$
Vertical peak force	$38.55 \text{ N kg}^{-1}$	$45.02 \text{ N kg}^{-1}$
LAST CONTACT PHASE – TAKE-OFF PHASE		
Anterior-posterior change of momentum	$-0.625 \text{ N s kg}^{-1}$	$-0.505 \text{ N s kg}^{-1}$
Anterior-posterior mean force	$-7.44 \text{ N kg}^{-1}$	$-4.64 \text{ N kg}^{-1}$
Vertical change of momentum	$4.191 \text{ N s kg}^{-1}$	$4.053 \text{ N s kg}^{-1}$
Vertical mean force	$50.38 \text{ N kg}^{-1}$	$38.46 \text{ N kg}^{-1}$
Vertical peak force	$63.56 \text{ N kg}^{-1}$	$54.80 \text{ N kg}^{-1}$

amputee and of  $2.76 \text{ m s}^{-1}$  for the non-amputee athlete, which is consistent with the greater jump distance of the non-amputee athlete compared to the amputee athlete.

We have already addressed the differences in phase durations, which are primarily present in the flight phases. Since the contact times of the third- and second-last steps are comparable for the non-amputee and amputee athletes, these different phase durations must be primarily due to differences in ground reaction forces. In addition to the graphical representation of ground reaction forces in Figure 10.2, we calculated the change of momentum, mean, and peak forces for each of the three contact phases as in Chapter 9 for long jump dynamics reconstruction. Table 10.3 gives the resulting values for both athletes. The braking components of the anterior-posterior force are similar for non-amputee and amputee athlete during the third-last and second-last contact phases. In both phases, though, the amputee athlete generates larger propulsive components and larger vertical forces. As the contact phases are of comparable duration for both athletes, this explains the longer flight phase durations of the amputee athlete and also the larger step length which can be seen in the animated sequences of the computed long jump motions in Figure 10.1. While the amputee athlete has approximately equally large vertical peak force values in the third- and second-last contact phases (the peak value of the second-last contact phase is 105.46 % of the peak value of the third-last contact phase), the non-amputee athlete shows a significant increase over the steps (the peak value of the second-last contact phase is 176.03 % of the peak value of the third-last contact phase). Here, for the non-amputee athlete, the very small vertical force during the third-last contact is

unexpected. One possible explanation is the composition of the objective function: since we do not impose any other conditions on the approach, it is possible that the term ‘Minimize Torque Derivatives Squared’ (Eq. (10.5)) has a relatively strong influence, especially at the beginning of the motion, thereby finding the most energy-efficient way to accomplish the motion. Since (as described above) we also observed unexpected behavior in individual variables in the amputee athlete during the third-last contact phase, a more detailed investigation of the ideas described in Section 10.1.5 would be interesting.

Compared to the third- and second-last contact, both athletes have a significantly larger horizontal peak braking force value and a significantly larger vertical peak force value during the take-off phase. We find further differences between the amputee and the non-amputee athlete in the forces within the take-off contact phase: Regarding the anterior-posterior force, the amputee athlete performs better than the non-amputee athlete, as he generates less braking and more propulsive force during this phase. Therefore, he has a less negative horizontal change of momentum and a less negative horizontal mean force indicating that he loses less horizontal force during contact (which again corresponds with the larger horizontal CoM velocity). However, the non-amputee athlete applies a larger vertical ground reaction force in a shorter period of time resulting in a larger vertical change of momentum, a larger vertical mean force value and a larger peak force value. As already seen in the CoM movement, it is also evident in the force curves that the amputee athlete is able to maintain good horizontal movement, but this comes at the expense of vertical movement. Since the non-amputee athlete achieves the greater jump distance, vertical force appears to be critical.

Finally, we look at the joint angles and torques: Here, it is immediately noticeable that the curves of the third- and second-last contact phases are generally similar for the non-amputee athlete, even if they are not completely symmetrical. In particular, the knee torque is significantly larger in the second-last step than in the third-last step. The deviations between the motion of the right leg in the third-last step and that of the left leg in the second-last step are significantly greater in the amputee athlete. Here, it is not entirely clear whether the cause may reside in the problem formulation, so we do not want to infer too much into this deviation. Comparing non-amputee and amputee athletes, it is noticeable that the angle and torque curves of the second-last contact in the knee and ankle joints are very similar and very different in the hip joint. If we leave out the ankle joint, we observe a similar behavior during the take-off contact albeit with different magnitudes (here, ankle movements naturally differ more clearly from each other, simply because of the different geometries of RSP and biological leg). This is an interesting observation: if we consider only the last two contact phases, differences in joint angles and torques are found mainly in the hip, while similar movements happen in the knee. The intentional stiffening of the knee on the side affected by the amputation, which is described in the literature as a strategy to efficiently utilize the RSP, is not found in the optimized solution (in contrast to the reconstructed solution).

### 10.3 Summary

We were able to predict realistic long jump motions for the subject-specific models of one non-amputee and one amputee athlete based on a motion synthesis OCP formulation. The comparison of characteristic parameters and variables of the motions to the corresponding ones from the solutions of the dynamics reconstruction of motion capture recordings (Chapter 9) allows the conclusion that the problem formulation is valid for predicting long jump motions; minor deviations are still left and give ideas where the problem formulation could be improved. Especially in the case of the objective function, there is the possibility to try out further optimization criteria (however, it must always be weighed up which conditions dictate

the motion too strongly). As expected due to the formulation of an optimization problem, the estimated jump distances of the synthesized solutions outperform the ones for the dynamics reconstruction.

We summarize here the findings obtained from the comparison of the two athletes with and without BKA: Overall, the movements of the two athletes during the take-off contact phase are surprisingly similar, which was not necessarily expected based on the results of the reconstruction and also the fact that the geometry of the take-off legs differs significantly between the two athletes. What is most interesting is that the amputee athlete generates a similar torque in the knee joint during take-off compared to the non-amputee athlete instead of using a deliberate stiffening of the knee to exploit even more the spring-like properties of the RSP. The difference in jump distances appears to be primarily due to differences in horizontal and vertical CoM motion and forces. The literature describes athletes with BKA as having a slower approach velocity than athletes without BKA. This observation is confirmed when we consider the maximum forward velocity of the CoM during the last three steps. However, the amputee athlete still takes off with a greater horizontal CoM velocity because he loses less velocity during the contact phases due to the better ratio of propulsive and braking components of the force curve. Compared to the amputee athlete, the non-amputee athlete generates the greater vertical force during the final contact phase and gains more vertical CoM velocity. Together with the better ratio of gain in vertical to loss in horizontal velocity, which is also reflected in the larger take-off angle, this results in the greater jump distance.

From these observations, it can be assumed that in particular the vertical force during take-off and a good ratio of gain in vertical to loss in horizontal speed are more decisive overall than the pure approach velocity. However, since we are comparing two different athletes with different physiques, different muscle parameters, and possibly different performance levels, such generalizations are not tenable. Instead, we keep in mind the formulated hypothesis for the comparison of the amputee athlete to himself without amputation in the envisioned simulator tool (cf. Chapter 11).

## **Part IV**

# **Towards a Systematic Use of Optimization and Simulation for Performance Comparison Between Amputee and Non-Amputee Athletes**



# 11 Comparison of the Amputee Athlete to Himself without Amputation: The Idea of a Simulator Tool

In this chapter, we will discuss the vision of a simulator tool, which has already been mentioned in the introduction. We have pointed out several times in the discussion of the results of the sprinting and long jump studies in the previous parts that conclusions are difficult, among other reasons, because it is not possible to clearly determine which differences between the movements with and without running-specific prostheses (RSPs) are due to individual differences between the specific athletes and which are due to the use of RSPs. Thus, there are questions that cannot be answered by measurements, for instance, what the performance of the amputee athlete without amputation would be (i.e., if he had two biological legs). The simulator tool we propose is intended to address this issue and fill the gap in comparing the movements of athletes with and without below the knee amputation (BKA) with the help of realistic computer models of the athlete.

Computer models allow the amputee athlete to be compared to himself without amputation. To do this, we first create a model of the amputee athlete as a virtual twin (computer model). In our case, we use the model of the amputee athlete from the previous chapters. In addition, a modified version of this virtual twin is generated, which is intended to estimate, using all available knowledge, how the athlete would perform without amputation. We thus work with two model versions of the virtual twin of the real amputee athlete, which we will refer to as the ‘amputee version of the model’ (for the virtual twin of the real athlete) and ‘non-amputee version of the model’ in the following. In the case of an athlete with unilateral BKA, we can, for example, replace the prosthesis model with the corresponding segments of a biological leg and mirror the parameters of the biological leg to create a model without BKA. For both models, the simulator tool should be able to calculate realistic sprinting or long jump movements, which can then be further analyzed and compared. The requirement for this is that it is previously clear that the models are physically correct and reproduce the real movement at least well enough. Without this certainty, the conclusions drawn from the simulator tool would be worthless.

In this context, the results presented so far in Parts II and III serve as groundwork to test feasibility and to help in determining what features a simulator tool should have that can study motions with and without RSP. In particular, the results have shown which measurement data is required for the creation of realistic models.

## 11.1 Basic Structure of a Simulator Tool

In the following we will describe and explain the basic structure of the simulator tool in more detail. Figure 11.1 shows the three essential building blocks with the core features of creating subject-specific models, generating motions and comparing an amputee model version with the non-amputee model version.

The simulator tool should offer a graphical user interface (GUI) in which subject-specific models are created. As we intend to base the simulator tool on our previous work, the models

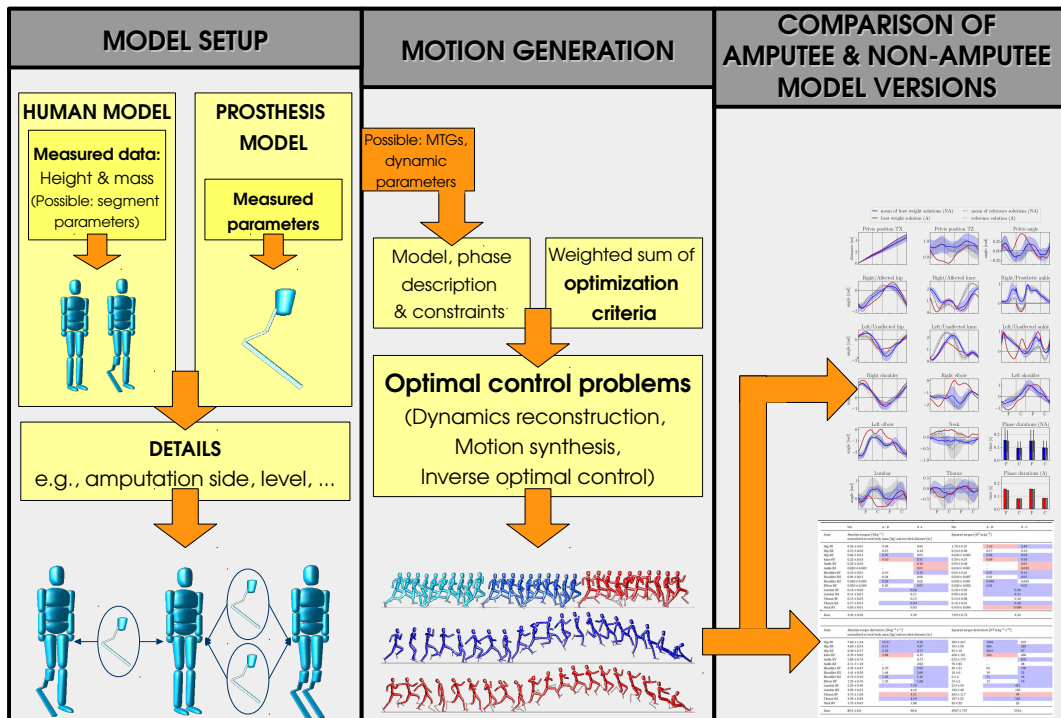


Figure 11.1: Basic structure of the simulator tool

would be created as lua models. The model setup is convenient since it is modular and the models are customizable with few parameters:

- For the creation of the human model, only the key parameters (total height and total mass) of the athletes are absolutely necessary since the segment parameters can be extrapolated using the de Leva data [26]. If there is additional measurement data for segment lengths, masses, centers, etc., it should be entered manually.
- A basic model of a RSP, more specifically the model which we used in the previous studies, should be available as well. It can be adapted to the specific RSP by entering the specific parameters from measurements of it. In particular, the knowledge of the length and the spring constant are relevant (the latter can also be determined by the dynamics reconstruction of the motion generation module, if motion capture recordings are available).
- To create the concrete non-amputee and amputee versions of the model, the human model and the prosthesis model are coupled based on information about amputation side and amputation level.

Furthermore, parameters like limits for angles, angular velocities, joint torques or even Muscle Torque Generators (MTGs) could be adjustable by a few tests (for example, measurements with Biodex systems) to fit the models to the particular athlete.

The basic feature of the motion generation module should be the predictive simulation of motions (here: sprinting and long jump motions) based on an optimal control problem (OCP) formulation in order to generate data for the comparison of the non-amputee and amputee versions of the model. For each motion (sprint/long jump), a model of the movement (i.e., the phases, their order, the respective equations of motion and all necessary constraints) and a set of optimization criteria with suitable weights are predefined. However, it should be also possible to modify the phases, add own constraints as well as optimization criteria and adjust the

weight factors. In addition to this main feature, the opportunity to solve a dynamics reconstruction problem for computing the dynamics of (purely kinematic) motion capture recordings and to solve the inverse optimal control problem (IOCP) for determining the underlying weights of a motion based on the predefined or custom optimization criteria should be included.

Finally, the motions of the model versions with and without BKA should be compared to each other. For this it is necessary that the motion generation problems output all necessary result variables, i.e., the joint angles, joint velocities, joint torques, control variables, ground reaction forces, center of mass (CoM) positions and velocities. Other characteristic variables such as angular momentum with respect to the CoM can be calculated from these using the model. The analysis should then on the one hand offer the possibility to analyze single movements, e.g., by creating the corresponding curve diagrams (see all result chapters in Parts II and III) or by calculating the measures related to effort or style (see Chapter 5) or by playing and exporting the animated motion sequences. On the other hand, it should also be possible to compare different athletes, be it athletes actually based on measurement data or also the model of an athlete, once with and once without RSP.

**Mandatory external data for the simulator tool** The minimum requirement is that the total height and total mass of the athlete under investigation is available. Furthermore, it is also necessary that the segment length of the remaining residual limb of the athlete with BKA and the parameters of the RSP are available. Basically, the more accurately the measurement data describe the anthropometric characteristics of the athlete, the more accurate and subject-specific the model and thus the results will be. In addition to segment parameters, realistic limits for joint torques as a function of joint position and velocity (as obtained, for example, from measurements with Biodex systems) are of particular importance in this context. For pure predictive simulation, no external data or measurements are required. For dynamics reconstruction and IOCP one needs reference data in the form of the overall position in space and joint angles fitting the respective model.

**Future options for extension** The above description of the simulator tool describes the basic features that we envision and which should already be implemented in the first version. A careful design of the tool is important, in order to be able to extend it as simply as possible. This can be done at various places, e.g., by improvements of the models or even completely new features. We name a number of possible directions for improvement in the following list (without any claim to completeness):

- A more accurate foot-contact model, which, for example, allows the foot to roll through a contact surface instead of contact with a fixed contact point, could possibly prevent undesirable effects that we have seen in previous solutions.
- Instead of using the MTGs only to calculate the boundaries, a complete muscle model including activation dynamics could actually be incorporated into the model. This would allow muscular effects to be studied. For this purpose, measurements of muscle parameters would also prove to be very helpful, if not necessary.
- The model of the RSP could be adapted: First, it would be possible to investigate whether a more detailed model (consisting of more segments or a flexible bendable segment) would more accurately reproduce the behavior of the RSP. Second, it would be possible that a description other than that of the RSP as a linear spring-damper system (e.g., a non-linear spring-damper system) would represent reality even better. Finally, different prosthetic shapes could be investigated by creating the respective models.

- The motion analysis module can be extended individually and in various ways in order to analyze further motion parameters (e.g., with regard to stability).
- More motion phases (e.g., sprint start and acceleration phases) or motion types (e.g., walking or high jump) could be included such that a comparison of these motions with and without RSP is possible. For this purpose, one would need to formulate a model of the motion (phase description and constraints) and a suitable cost function.

**Formulation for comparing the amputee athlete to himself without amputation** Even though the development and implementation of such a complex simulator tool is beyond the scope of this thesis, we want to use the final part of the thesis to describe the idea in more detail and demonstrate how a comparison of an athlete with BKA to himself without amputation could be done.

In all previous chapters, the amputee athlete was compared to different non-amputee athletes. For the following sections, we take the 2D model of the amputee athlete from the previous chapters (i.e., the virtual twin of the existing amputee athlete) as a basis and we compare it to the non-amputee version of himself. For the amputee model version, we simply copy the respective model. For the non-amputee model version, we replace the residual part of the shank and the prosthesis model with a model of the shank and foot, taking the (mirrored) parameters of the unaffected left leg for this purpose. All other segments are copied.

We proceed analogously with the fitted parameters for the MTGs: For the amputee version of the model, we adopt the previously used parameters. For the non-amputee version of the model, it depends on the specific movement: In the case of sprinting, we adopt the parameters of the amputee athlete, but all parameters of the right leg (affected by the amputation) are overwritten by the parameters of the left (unaffected) leg. This is necessary because in the fitted MTG model of the amputee athlete, the hip and knee joints also have weaker parameters. In the case of the long jump, we adopt the fitted parameters of the virtual twin of the existing non-amputee athlete for the right leg. This is necessary because the right leg is the take-off leg. However, during the jump step, much larger torques are generated in the leg joints than during the running steps. Data from the biological leg of the amputee athlete (as in the case of sprinting motions) can not be used since no take-off from this leg is observed (and it is not the strong jumping leg neither). If we simply mirrored the parameters of the left leg, we would make the non-amputee version of the model symmetric and thus probably weaken it.

We are aware that these assumptions represent a clear limitation of the results in terms of how they reflect reality. However, due to the lack of measured data of the muscle parameters or torque limits, the possibilities at this point are also limited. Nevertheless, this should be kept in mind when interpreting the following results. If the simulator tool described here were to be used to arrive at an actual legally valid statement regarding advantage and disadvantage due to the RSP, the way in which the limits or muscle parameters are determined for the non-amputee version of the model would have to be thoroughly reviewed again and possibly adjusted. For example, to get better parameters for the MTGs in long jump, special jump tests and a heuristic indicating how much stronger the take-off leg usually is could be developed. The modeling of the sprinting and long jump motions including phase order and constraints is adopted as explained in Chapters 4 and 8. The OCPs are formulated as described in Chapters 6 and 10. The concrete formulation of the objective functions is described in Section 11.2 for the sprinting motions and in Section 11.3 for the long jump motions. Finally we have to decide which parameters are used to determine differences in the motions of the two model versions which is a rather difficult decision. Differences in motions also exist when comparing two non-amputee athletes, since subtleties of motions are always individual. Even if we compare in the simulation one and the same basic athlete, once in the non-amputee and once in the

amputee model version, minor differences cannot be directly attributed to the RSP. For each movement, therefore, one must ask what constitutes the movement. There is certainly much room for discussion and widely differing opinions. Burkett and colleagues [19] discuss in their work regarding sprinting intensity with RSP that it is necessary to define what constitutes a running gait and where to draw the line in comparison to hopping, for example. Is it solely about covering the race distance as fast as possible in an upright posture and on two legs? Do energy efficiency, ground reaction forces, or the number of steps also play a role [19]? The present work cannot and does not want to give an answer to these fundamental and already philosophical questions. For the comparison of sprinting and long jump motions that follows here, we have therefore defined concrete comparison criteria that, in our opinion, characterize the respective motion.

## 11.2 Sprinting Motions of the Non-Amputee and Amputee Model Versions

We base our analysis of the sprinting motions of the amputee and non-amputee model versions on the OCP formulation which was already applied for the motion synthesis in Chapter 6 and for the IOCP in Chapter 7.

**Choice of objective function** For the comparison of the non-amputee and amputee model versions, we chose an objective function  $\Phi$  which has a focus on maximizing the average sprinting velocity. For this, we combine three optimization criteria defined in Chapter 6 as base functions into the objective function  $\Phi$  (i.e.,  $\varphi_{M_1}$  - Maximization of average velocity,  $\varphi_{L_6}$ : Minimization of torque derivatives squared,  $\varphi_{L_8}$ : Head stabilization). As the main criterion should be the maximization of the average velocity, we combine the base cost functions into the objective function as follows:

$$\Phi(\cdot) = \gamma_0^{\text{vel}} \varphi_{M_1}(\cdot) + \gamma_1^{\text{vel}} \varphi_{L_6}(\cdot) + \gamma_2^{\text{vel}} \varphi_{L_8}(\cdot) \quad \text{with} \quad \boldsymbol{\gamma}^{\text{vel}} = (1, 10^{-8}, 10). \quad (11.1)$$

Why did we choose this objective functions to make the comparison between the non-amputee and amputee model versions? As already described repeatedly, the goal of any sprinter is to finish the race in the shortest time possible. To do this, the athlete must accelerate out of the starting blocks to his maximum velocity as quickly as possible and maintain this maximum velocity for the remainder of the course. Since we are only considering the phase at maximum velocity here, an objective function that maximizes the average velocity seems to be a good description of this behavior. However, we keep in mind for the analysis that used in an OCP formulation, this objective function comes with the risk that the solution reaches unrealistically high velocities, since at each time point all variables can be chosen optimally (also anticipating the next time points), which in reality is not possible in this way.

Another possibility, which would also make sense from the course of this work, would be to use the best weights of the IOCP solutions to formulate an objective function. Indeed, the idea of the IOCP is to find the combination of base functions which underlie a measured motion with the corresponding weights. Accordingly, it is natural to assume that the best weights found for the amputee and non-amputee athletes are a good approximation to reality. Nevertheless, we decided not to use objective functions based on the best weights for this chapter because the IOCP results presented in Chapter 7 still leave important questions open. First, the results of the IOCP showed that there are differences in best weights between the three non-amputee athletes as well. Hence, a larger amount of data (i.e., more trials of non-amputee athletes) might be necessary to eliminate individual variations and to find reliable mean values for best

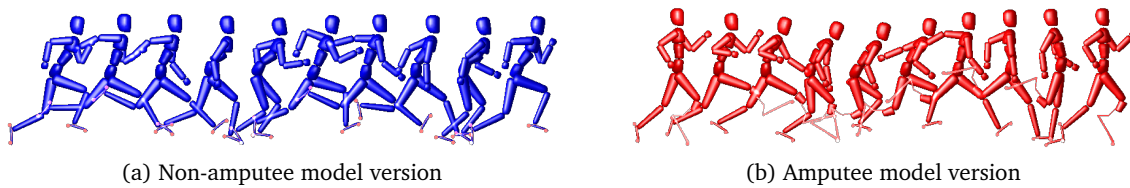


Figure 11.2: Animated sequences visualize the solutions of the sprinting motion synthesis optimal control problem for the comparison of the amputee athlete to himself without amputation in the simulator tool

weights for the non-amputee model version<sup>1</sup>. Second, the results of the IOCP yield cases where the average velocity was slower than the one from the reference data (e.g., non-amputee athlete 1) as well as cases where the average velocity was higher than the one from the reference data (e.g., amputee athlete). Hence, the best weights identified with the IOCP procedure do a good job in fitting the reference data overall, but some specific problems as the forward velocity estimate must be solved before applying the best weight objective functions for the comparison in the simulator.

Although the objective function  $\Phi$  does not account for the individual running styles of amputee and non-amputee athletes, this objective function can provide valuable insights for the comparison which we will now discuss. Figure 11.5 shows animated sequences of the resulting motions for the non-amputee and the amputee model versions.

**Comparison of the motions of the non-amputee and amputee model versions** The comparison of the average velocities is immediately very interesting: The non-amputee model version reaches an average velocity of  $14.08 \text{ m s}^{-1}$ , whereas the amputee model version reaches an average velocity of  $13.48 \text{ m s}^{-1}$ . Hence, the non-amputee version of the model reaches the higher velocity and the amputee version of the model is slower by  $0.60 \text{ m s}^{-1}$ . Since the objective functions are identical for both athletes, this difference cannot be attributed to individual variations in sprinting style or power level. Thus, it appears that there is indeed a ‘threshold velocity’ above which the RSP makes it more difficult to achieve higher velocities compared to the biological leg.

For a more detailed understanding, we consider in the next step joint angles (Figure 11.3), joint torques and ground reaction forces (both in Figure 11.4). The first thing to notice is that the objective function produces a very symmetric motion for the non-amputee athlete (which would be expected in principle due to the symmetry of the model and the objective function even without explicitly requiring single-step symmetry, but was not always clearly shown in the solutions in Chapter 6). When comparing the positions and joint angles with those of the amputee athlete, some differences are noticeable: The amputee athlete covers the greater distance after contact with the RSP, i.e., in the second step (Pelvis position TX). During contact with the RSP, he lets himself sink significantly into the RSP (Pelvis position TZ). Overall, the amputee athlete remains with the pelvis and thus the upper body significantly higher than the non-amputee athlete. The latter remains comparatively low during the flight phases and therefore takes rather flat steps. The differences in the knee joints are also striking: during contact with the RSP, the associated right knee shows comparable flexion to that present in the knees of the non-amputee athlete during the contact phases. In contrast, almost no flexion

<sup>1</sup>Since the purpose of the proposed simulator tool is to compare the amputee athlete with himself without amputation, this problem does not arise for the amputee version, as the best weights were determined precisely for this model. In a more general case, if for instance the aim was to examine another amputee athlete, one would have to think more carefully about which objective function to define.

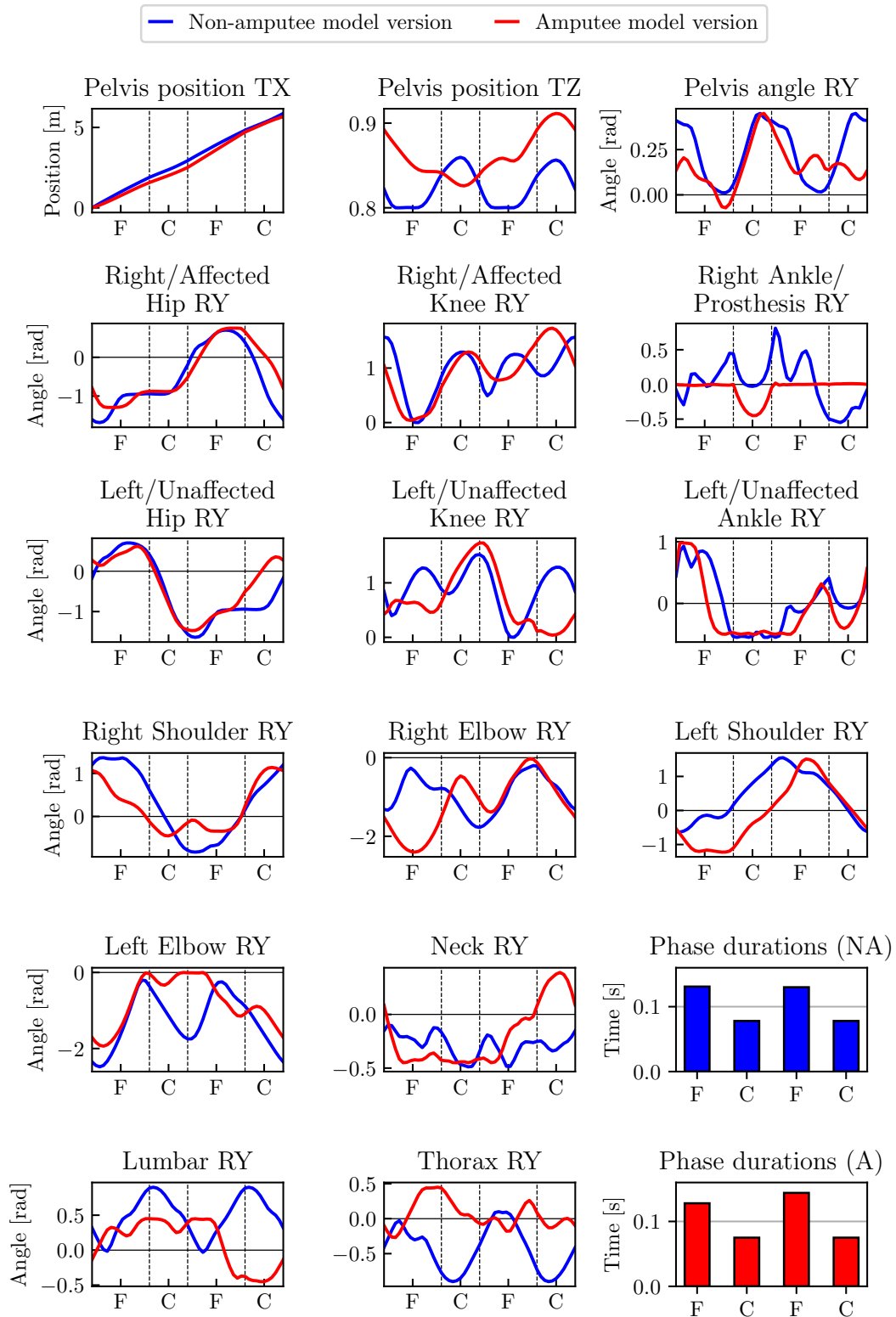


Figure 11.3: Positions, joint angles and phase durations of the synthesized sprinting motions for the non-amputee and amputee model versions

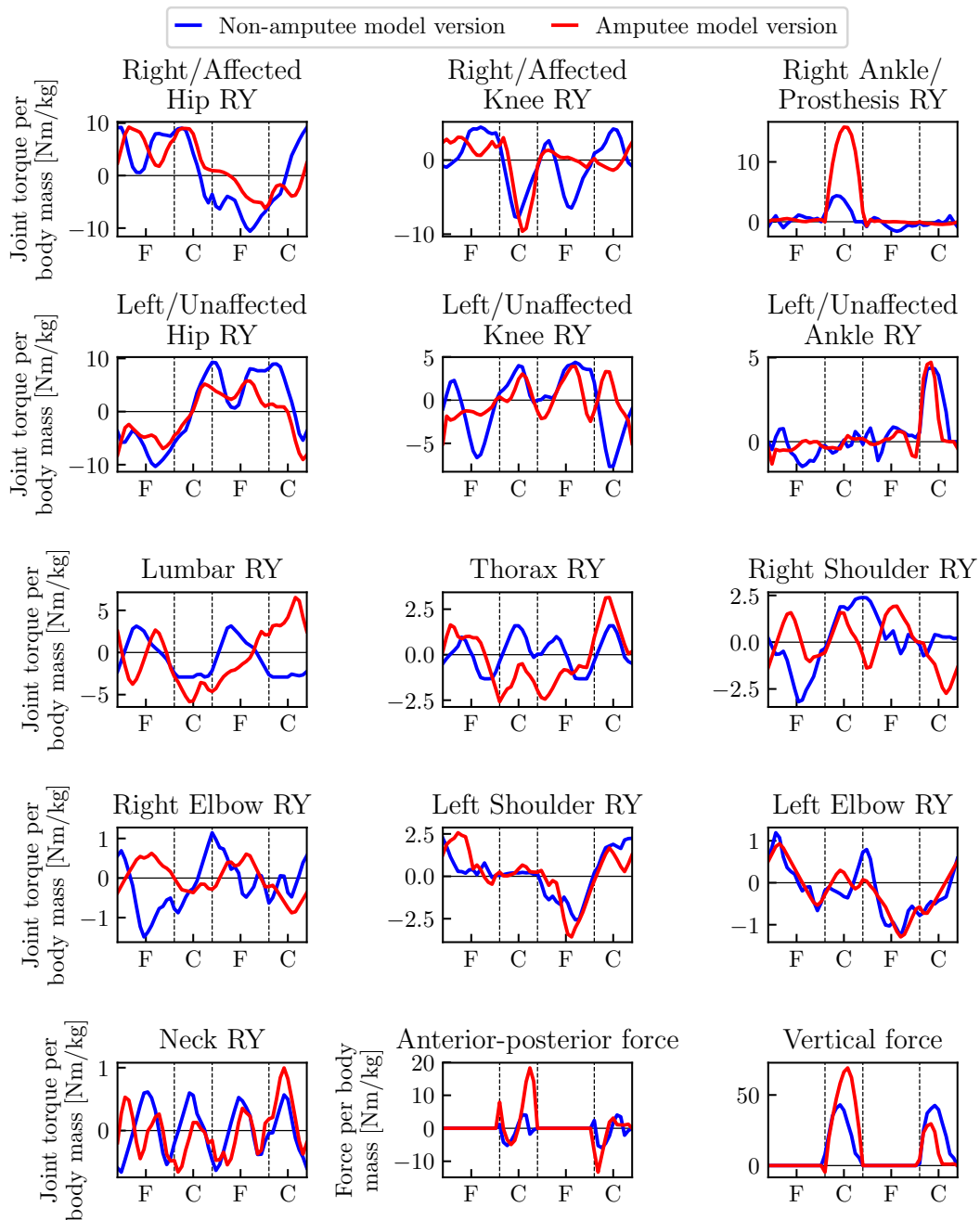


Figure 11.4: Joint torques and ground reaction forces of the synthesized sprinting motions for the non-amputee and amputee model versions

is found in the knee of the amputee model during contact with the other leg. Instead, the contact movement is predominantly performed by the hip and ankle. This is surprising, because in the reconstructed solutions from Chapter 5 we rather observed the opposite behavior – lower knee flexion in the knee of the affected side than in that of the unaffected side. As noted with the other synthesized movements, the optimal solution appears to utilize the RSP differently (possibly more) than the actual measured athlete. This is also evident in the ground reaction forces, as the vertical force is significantly greater in the amputee model during contact with the RSP than during contact with the biological leg (by a factor of 2.3 in the peak values). In

the non-amputee model, the peak values and curves of the vertical forces of the two contact phases are almost identical. Also for the horizontal force, the first contact phase (with the RSP) is the more helpful for the movement, since the driving component outweighs the braking one and thus generates a forward moment. The more zigzag shape of the force curves is justified by the fact that an objective function that mainly maximizes velocity does not necessarily favor smoother solutions. For the torques, the most crucial differences between non-amputee and amputee models are also found in the leg joints. Two observations in particular are interesting: First, that the torques of the left knee during the contact phase with the left leg differ more clearly than those of the right knee during the corresponding contact phase. While the torque of the amputee athlete in the right knee has a similar course and a slightly larger peak value in absolute terms than in the non-amputee athlete, the course in the left knee is completely different. As was the case for the joint angles, there is a clear difference here compared to the observations of the reconstructed motion (Chapter 5). Second, the torques in the left (biological) ankle of the two athletes are comparably large during the contact phase. Here, the strength of the simulator tool comparing the amputee athlete with a model of himself without amputation is evident, because in the motion synthesis solutions in Chapters 6 and 7, it was mostly the case that the torque of the amputee athlete in this leg was lower than that of the non-amputee athlete (whose model, however, was based on a measured non-amputee athlete and not on the amputee athlete).

**Concluding remarks** It is still difficult at this point to make a valid statement as to whether the RSP gives the athlete an advantage or disadvantage when sprinting. However, some observations can be noted that can assist in an assessment and demonstrate the capabilities of the simulator tool. The amputee athlete was able to achieve a greater vertical ground reaction force during contact with the RSP and a more advantageous propulsive to braking component ratio in the horizontal ground reaction force than the non-amputee version of the model. The results show that the amputee athlete cannot translate the larger forces during prosthetic contact into a higher average velocity such that the amputee athlete runs slower than the non-amputee athlete. Together with the results from Chapter 6 this suggests that there is some sort of threshold velocity above which the RSP actually has a detrimental effect on movement.

### 11.3 Long Jump Motions of the Non-Amputee and Amputee Model Versions

For predicting the long jump motions of the amputee and the non-amputee model versions, we apply exactly the same OCP formulation as in Chapter 10.

**Choice of objective function** Hence, the objective function consists of five optimization criteria (jump distance maximization, torque derivatives minimization and head stabilization criterion) and includes constraints to the dynamics, to the torque limits based on a MTG model, to colliding segments and to the landing posture.

**Comparison of the motions of the non-amputee and amputee model versions** Figure ?? Instead of comparing again all diagrams for joint angles, joint torques, ground reaction forces and CoM motion, we focus on the four criteria<sup>2</sup>. As described in the literature review

<sup>2</sup>However, as a small side note, the comparison of the corresponding diagrams from Chapter 10 with two models based on different athletes and the diagrams here with two models based on the anatomy of one athlete does not produce any significant differences. The corresponding diagrams for the comparison of the

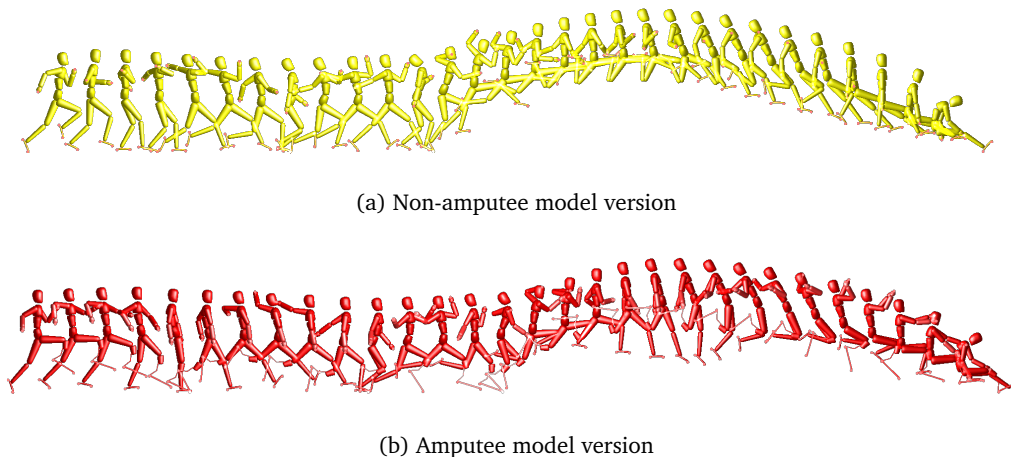


Figure 11.5: Animated sequences visualize the solutions of the long jump motion synthesis optimal control problem for the comparison of the amputee athlete to himself without amputation in the simulator tool

on long jump (cf. Chapter 8), performance in the long jump is determined by several factors: a high approach velocity as well as appropriate take-off, flight and landing techniques. Thus, to compare the amputee and non-amputee model versions, we consider:

- the horizontal CoM velocities of the three last contact phases as a measure of the approach velocity,
- the change in horizontal and vertical CoM velocity during the last contact phase (take-off step) as a measure of good take-off technique (as this is often described by maximum gain in vertical CoM velocity with minimum loss in horizontal CoM-velocity),
- the take-off angle as a measure for a good take-off and flight technique (since it decisively determines the trajectory) and
- the jump distance.

They are given in Table 11.1. The CoM velocities are directly taken from the result files. The changes in horizontal and vertical CoM velocities are computed by subtracting the respective CoM velocity at touch-down from the respective CoM velocity at take-off. The take-off angle and the estimated jump distance are defined and computed as described in Chapter 9 using Eq.s (9.3) and (9.2). To demonstrate the usefulness of the simulator tool, Table 11.1 further contains the respective results from the long jump synthesis (cf. Chapter 10) where the solutions using models of an existing non-amputee and an existing amputee athlete were used. In the following, we systematically go through the four comparison criteria to see the differences between the non-amputee and amputee versions of the model. We take the horizontal CoM velocities over the three contact phases to determine which athlete has the higher approach velocity. The largest horizontal CoM velocity is achieved at touch-down into the third-last contact phase for both model versions. At this time point, the velocity of the non-amputee model version is  $0.58 \text{ m s}^{-1}$  larger than the velocity of the amputee model version. Hence, if we assume that the velocity at touch-down into the third-last contact phase corresponds with the maximal velocity achieved during the approach run, the non-amputee model version approaches faster than the amputee model version. However, due to the smaller losses during the contact

---

amputee athlete with the non-amputee version of the model based on him can be found in the Appendix (Figures A.13 and A.14). We will return to this observation in the final discussion.

Table 11.1: Characteristic quantities for the comparison of the amputee athlete to himself without amputation (i.e., the non-amputee model version). For reference purposes, we further show again the results for the comparison of the long jump synthesis computations from Chapter 10. The columns for the amputee athlete coincide since we applied exactly the same optimal control problem formulation as in Chapter 10. The abbreviations ‘NA’ and ‘A’ denote the non-amputee and amputee models, respectively, and the abbreviations ‘TD’ and ‘LO’ stand for ‘touch-down’ and ‘lift-off’. The definition of the individual quantities is given in the main text.

	LONG JUMP SYNTHESIS from Chapter 10		SIMULATOR SYNTHESIS	
	NA	A	NA	A
THIRD-LAST CONTACT PHASE				
Horizontal CoM velocity (TD)	11.78 m s <sup>-1</sup>	10.99 m s <sup>-1</sup>	11.57 m s <sup>-1</sup>	10.99 m s <sup>-1</sup>
Horizontal CoM velocity (LO)	11.24 m s <sup>-1</sup>	10.91 m s <sup>-1</sup>	11.19 m s <sup>-1</sup>	10.91 m s <sup>-1</sup>
Change in horizontal CoM vel.	-0.54 m s <sup>-1</sup>	-0.08 m s <sup>-1</sup>	-0.38 m s <sup>-1</sup>	-0.08 m s <sup>-1</sup>
SECOND-LAST CONTACT PHASE				
Horizontal CoM velocity (TD)	11.24 m s <sup>-1</sup>	10.91 m s <sup>-1</sup>	11.19 m s <sup>-1</sup>	10.91 m s <sup>-1</sup>
Horizontal CoM velocity (LO)	10.77 m s <sup>-1</sup>	10.56 m s <sup>-1</sup>	10.84 m s <sup>-1</sup>	10.56 m s <sup>-1</sup>
Change in horizontal CoM vel.	-0.47 m s <sup>-1</sup>	-0.35 m s <sup>-1</sup>	-0.35 m s <sup>-1</sup>	-0.35 m s <sup>-1</sup>
LAST CONTACT PHASE (TAKE-OFF CONTACT PHASE)				
Horizontal CoM velocity (TD)	10.77 m s <sup>-1</sup>	10.56 m s <sup>-1</sup>	10.84 m s <sup>-1</sup>	10.56 m s <sup>-1</sup>
Horizontal CoM velocity (LO)	9.85 m s <sup>-1</sup>	9.99 m s <sup>-1</sup>	9.83 m s <sup>-1</sup>	9.99 m s <sup>-1</sup>
Change in horizontal CoM vel.	-0.92 m s <sup>-1</sup>	-0.57 m s <sup>-1</sup>	-1.01 m s <sup>-1</sup>	-0.57 m s <sup>-1</sup>
Vertical CoM velocity (TD)	-0.08 m s <sup>-1</sup>	-0.08 m s <sup>-1</sup>	-0.35 m s <sup>-1</sup>	-0.08 m s <sup>-1</sup>
Vertical CoM velocity (LO)	3.60 m s <sup>-1</sup>	3.02 m s <sup>-1</sup>	3.65 m s <sup>-1</sup>	3.02 m s <sup>-1</sup>
Change in vertical CoM vel.	3.68 m s <sup>-1</sup>	3.10 m s <sup>-1</sup>	4.00 m s <sup>-1</sup>	3.10 m s <sup>-1</sup>
Take-off angle	20.09°	16.85°	20.36°	16.85°
Jump distance	9.86 m	9.22 m	9.93 m	9.22 m

phases, the amputee model version can keep a larger amount of this approach velocity and finally takes-off at the end of the last contact phase with a velocity that is 0.16 m s<sup>-1</sup> higher than that of the non-amputee model version. This is an interesting observation, as there is an assumption that RSPs restrict force production and thus limit the maximum possible velocity [50]. In addition, Willwacher and colleagues [136] also observed slower approach velocities in amputee athletes in their study of the long jump with and without RSP. Both observations work well with our synthesized solutions, but only if one considers the maximally reached velocity. If one only takes into account the take-off contact phase (as it is often done in long jump studies), the amputee athlete actually has the larger horizontal velocities. At this point, it is worth looking at the differences from the movements in Chapter 10, which were calculated using two models based on different athletes: The above described findings are similar for the synthesized solutions of Chapter 10. We take the changes in horizontal and vertical CoM velocities during the last contact phase as a measure of ‘good’ take-off technique. In long jump literature, the strategy for take-off is commonly described as the ability to generate large vertical CoM velocity without losing too much horizontal CoM velocity. Let’s start by looking

at the horizontal CoM velocity: as described in the previous point, the amputee version of the model enters the final step with a slightly smaller horizontal velocity (by  $0.28 \text{ m s}^{-1}$ ). At the end of the contact phase, the amputee version of the model has a higher horizontal velocity (by  $0.16 \text{ m s}^{-1}$ ) since he loses less horizontal velocity (only 56.4% of the non-amputee model version's loss). The non-amputee model version succeeds more efficiently in generating vertical CoM velocity: The change in vertical CoM velocity is  $3.01 \text{ m s}^{-1}$  for the amputee version and  $4.00 \text{ m s}^{-1}$  for the non-amputee version which amounts to a difference of  $0.99 \text{ m s}^{-1}$ . However, since the amputee athlete starts the final contact with a less negative vertical CoM velocity, the difference in vertical velocities at take-off is less pronounced ( $0.63 \text{ m s}^{-1}$ ). Hence, we observe that the non-amputee model version takes off more efficiently as the gain in vertical velocity and the resulting vertical take-off velocity are much larger compared to the amputee model version. Although the loss in horizontal velocity is smaller and thereby the horizontal velocity at take-off larger for the amputee model version, this does not compensate the smaller gain in vertical velocity. The predictive simulation, therefore, seems to be in contrast to the observations of Willwacher et al. [136] which affirm the amputee athlete a more efficient take-off technique.

Since the take-off angle in combination with the height at take-off determines the parabola of the projectile motion, we take the take-off angle as a measure for a good take-off and flight technique. When comparing the amputee and non-amputee model versions, we find that the take-off angle of the amputee version is smaller by  $3.78^\circ$ . The angle of the non-amputee model version is closer to the optimal angle for distance maximization in the projectile motion. However, both take-off angles are within the range of take-off angles of successful long jumpers reported in the literature.

Finally, we take the jump distance as a measure of a successful jump in general. Looking only at the jump distance, the non-amputee model version is more successful because the jump distance is longer by 71 cm.

Since our aim in this chapter is also to illustrate why we think a simulator tool would be helpful, we will briefly compare the values of the two non-amputee models. For the horizontal velocities of the three contact phases, it is noticeable that the synthesis based on the model of the measured non-amputee athlete calculates larger velocities during the third-last and second-last steps. Thus, it appears that the muscular or body parameters of the amputee athlete actually only allow for lower approach velocities compared to the measured non-amputee athlete which would explain why Willwacher et al. [136], who by nature had to compare different athletes, found that amputee athletes started slower than non-amputee athletes). Since in the synthesized solutions, the jump distances of the non-amputee athletes are each greater than those of the amputee athlete, it appears that the approach velocity or horizontal velocity at take-off is less critical than the take-off angle and vertical velocity. For all three (jump distance, take-off angle, gain in vertical velocity during take-off contact phase), it can be seen that the non-amputee model version actually performs even better than the measured non-amputee athlete. These differences are also very clear: The improvement in jump distance is 7 cm, the improvement in take-off angle amounts for  $0.27^\circ$  and the improvement in gain in vertical velocity during the take-off contact phase is  $0.32 \text{ m s}^{-1}$ . A comparison of the amputee athlete with himself without amputation can indeed yield very different results (in both directions, of course).

**Concluding remarks** So, the overall picture is as follows: The comparison of the amputee athlete with a non-amputee model version of himself suggests that the RSP does not provide the amputee athlete an advantage since he would jump further without than with RSP. However, we remain careful in giving a conclusive assessment: on the one hand, the results contra-

dict the findings of Willwacher et al. [136]. Here, further studies that improve the modeling of the long jump even more (e.g., by testing out more optimization criteria or determining the weight factors by an IOCP), could be helpful to be sure that the results are valid. In addition, we are aware that the assumptions about the muscular parameters of the right leg of the non-amputee model version make the results vulnerable. Here, it would be useful to measure actual values for all joint torque limits and calculate the parameters of the right leg based on measurements of how much stronger the take-off leg is on average in non-amputee athletes. In addition, the restriction to four criteria certainly allows for discussions on how these have to be weighted and whether further or other criteria are necessary for a fair comparison. This discussion quickly takes us back to the question discussed in the introduction regarding what exactly characterizes the motion of the long jump. If this is a matter of comparable movements in terms of the curves of position, joint angles, and joint torques, the diagrams in Figures A.14 and A.13 show indeed minor differences in the magnitude and exact course of the respective variable between the two model versions during the take-off step, but not completely different curves. In a cautious interpretation, we would consider these differences small enough to classify the movements both as long jumps.

## 11.4 Summary

For both motions, we found characteristic differences in the solutions to the reconstructed motions (Chapters 5 and 9) and the previously synthesized movements (Chapters 6, 7 and 10). While the causes of the former would need further investigation to ensure that the simulator tool makes meaningful predictions, the latter highlight the power of the simulator tool to filter out differences based solely on comparing different athletes. Some of the differences in criteria crucial for sprinting or long jump performance are less or more pronounced when comparing the non-amputee and amputee model versions of the identical athlete instead of comparing models based on distinct athletes. Hence, some of the differences noted in Chapters 6, 7 and 10 are probably not due to the influence of the RSP on the movement, but rather can be attributed to individual differences between the different athletes. At this point, a simulator tool to compare an athlete to himself with altered parameters (e.g., without amputation) may provide helpful insights.

The comparisons in this chapter have relied on selected criteria due to space constraints, as the focus of the chapter was to show the importance of the simulator tool. However, a wide range of motion parameters is available from the result files which allows for more in-depth analyses (e.g., on the asymmetry of movements, which was only briefly addressed). This leads to an important concluding remark: The simulator tool cannot and does not want to stand on its own and provide quick and unambiguous answers, but is an auxiliary tool for a systematic and consistent approach to performance comparison of athletes with and without BKA. It always requires the reflected and critical evaluation of the user, e.g., in the selection of the objective function or the criteria on which the comparison is based.

Finally, we briefly summarize how we envision the work flow when using the simulator tool to compare an athlete with unilateral BKA to himself without amputation:

1. Measurement of the investigated athlete with BKA: At a minimum, total body height, total body mass and the critical parameters for modeling the RSP are measured. However, the simulator as a tool for comparing an amputee athlete with himself without amputation only becomes meaningful if very precise measurement data are available, including segment lengths, mass distribution, muscle parameters or limits for joint torques as a function of joint angle and joint velocity, and motion capture recordings.

2. **Model generation:** Based on the measurement data, a virtual twin of the athlete is created (= amputee version of the model). Furthermore, a non-amputee version of the model is established by mirroring the unaffected leg.
3. **Motion synthesis:** For both versions of the model, a motion is predicted based on the motion synthesis OCP formulation. If motion capture recordings are available, the objective function can be fitted to the athlete using an IOCP.
4. **Comparison of the investigated athlete with BKA to himself without amputation:** The results can be used to compare the athlete with BKA to himself without amputation.

## 12 Conclusions and Future Work

To conclude an extensive work such as this, it is certainly worthwhile to return to the introduction and to provide a connection that places the studies conducted in a larger context. The starting point for the work was the recurring and still ongoing discussions about athletes with below the knee amputation (BKA). The question of whether they might have an advantage or disadvantage over non-amputee athletes in sprinting and long jump competitions due to their running-specific prostheses (RSPs) and whether it should be possible for these athletes to participate in competitions of non-amputee athletes is not conclusively answered by the existing literature. Nevertheless, there are several studies that highlight differences and similarities between the movements of athletes with and without BKA (e.g., [18, 44, 45, 62, 63, 71, 125, 127, 131, 134, 136], cf. Chapters 1, 4 and 8 for reviews on the state of the art). What all studies have in common is that they compare the movements of the amputee athlete with those of non-amputee athletes, who are - naturally - other people with a different physique and level of performance. And even if preferably comparable non-amputee athletes are selected for the study, this point offers possibilities for doubt about the results and the evaluation of what influence the RSP has on the motions. The present work aims to fill this gap with the idea of a simulation tool that will allow the systematic comparison of the movements of the amputee athlete and the movements of a non-amputee version of the identical model. Specifically, we presented here the groundwork on the way to such a simulation tool and finally demonstrated the idea of the simulation tool using two example motions.

For the groundwork, we created subject-specific rigid multi-body system models as virtual twins of four non-amputee athletes (three for the sprinting motion and one for the long jump motion) and of one athlete with unilateral BKA as well as a detailed model of the prosthetic device. Based on these models of different athletes, we computed sprinting and long jump motions based on three different optimal control problem (OCP) formulations. Each of these formulations, either the dynamics reconstruction OCP, the motion synthesis OCP or the inverse optimal control problem (IOCP), has its justification, as the discussion in the individual chapters has demonstrated: The dynamics reconstruction serves on the one hand to check whether the modeling choices are valid, on the other hand it provides first results to compare the athletes. The good agreement of the joint angles, torques and forces with the measured data or literature values has also shown that the dynamics reconstruction approach is a good alternative to classical inverse dynamics approaches, especially if no measured data of the ground reaction forces is available. Motion synthesis offers a good method for predictive simulations. Two objectives are central: On the one hand, the influence of a certain optimization criterion on the motion can be investigated. On the other hand, movements calculated as solutions of the OCP with a fixed combination of optimization criteria for different athletes can be compared to find out differences. The IOCP aims to identify the combination of predefined optimization criteria underlying a measured motion capture movement of a particular athlete. We applied the IOCP formulation only for sprinting, since the long jump motion capture recordings end before landing. The goal was to find the weight factors for the sprinting movements of the amputee and non-amputee athletes, and to obtain a concrete objective function describing the running style for both groups. Although the results of the systematic IOCP approach indeed came closer to the measured movements than the hand-picked combinations of criteria, the

deviations are still too large for these specific objective functions to be used for the comparison of the two model versions when demonstrating the simulator tool. Hence, we have based the comparison of identical objective functions with a focus on maximizing the average velocity for both athletes.

For the demonstration of the simulator tool, we have kept the model of the athlete with BKA and established a corresponding non-amputee model version. For both sprinting and long jump movements, we have shown that comparing the athlete with BKA to the corresponding non-amputee model version yields significantly different results than comparing the athlete with BKA to other athletes without BKA. This was particularly evident in the long jump, where only one athlete without BKA was available for comparison. The demonstration of the simulator tool thus clearly showed why the comparison of amputee athletes with themselves without amputation is necessary for a fair assessment of the influence of the RSP on the motion. This is particularly the case when the comparison group of non-amputee athletes is small and/or there are significant differences in performance level or physique between athletes.

Based on this modeling and the three optimization problem formulations, we have examined in detail and compared the sprinting and long jump movements of athletes with and without BKA. As can be read in the individual chapters, we have observed differences between the motions with and without RSP in a large part of the variables. Whether these differences are now so decisive that the movement of the athlete with BKA can no longer be considered sprinting or long jumping, we do not want to discuss here. Instead, we would like to emphasize in summary three particular aspects, which are significant for the comparison in both investigated movements and, in our opinion, add new insights to the existing literature:

**Angular momentum control** We have computed angular momentum values for sprinting and long jumping with and without RSP. Proper angular momentum control is an important aspect for both sprinting and long jump motions. In our study on optimization criteria for synthesizing sprinting motions, we have seen that the criterion related to angular momentum control is among the best criteria in the sense that the synthesized motions come close to the reference data. This underlines its importance in sprinting. For the long jump movement, we restricted the study to one objective function with a main focus on maximizing the jump distance. However, based on the results of the sprinting synthesis, it is conceivable that adding an angular momentum-related optimization criterion could be useful and potentially improve some of the discrepancies still observed to the recorded motion. Furthermore, differences in the angular momentum courses of athletes with and without BKA suggest that angular momentum control is even more important for amputee sprinting than for non-amputee athletes. In particular, we have noted considerable differences between the angular momentum values for sprinting with and without RSP in the trunk and arm components for rotations in all three planes. The results of the IOCP furthermore have revealed larger weights for the angular momentum criterion for the athlete with BKA compared to the non-amputee control group. This means that indeed the importance of angular momentum control is greater for the movement of the amputee athlete. Without having investigated this further, we hypothesize that these stronger rotations might have an influence on the take-off and the subsequent flight phase and might have to be compensated during the flight phase.

**Asymmetry** The assumption that asymmetry plays a major role in the comparison of athletes with and without BKA (especially for sprinting) is directly plausible, since the athlete with BKA represents a clearly more asymmetric system compared to the athlete without BKA, and it has also been repeatedly mentioned in the course of this work. First of all, we would like to note that the sprinting movements of the non-amputee athletes also show a considerable amount

---

of asymmetry. Thus, it seems that an individual asymmetry is already present in each person due to physical conditions, even if the human body looks symmetrical “from a distance” and the models of the non-amputee athletes are symmetrical. On top of this, we observed stronger, additional asymmetries in the athlete with BKA. While one could certainly expect such to some degree due to inter-limb asymmetry, our calculations showed that in fact not only the legs, but the entire body and movement are affected by this asymmetry. For example, the athlete with BKA uses his arms and upper body to compensate for the inter-limb weight asymmetry. This results in more irregular movement and greater differences in the torques of the various joints, some of which are very large, potentially increasing the risk for fatigue and injury in the affected joints. In addition, the athlete with BKA must readjust his actuation pattern for each step, which makes the movement more complex and could have a destabilizing effect.

**Exploitation of the running-specific prosthesis** The need to answer the question of what influence the use of a RSP has on the overall motion arises, in addition to pure scientific interest, mainly from the assumption that athletes with BKA exploit their RSP in such a way that they might have an advantage over athletes without BKA. Therefore, it is particularly interesting to see how the model of the amputee athlete exploits the RSP in the optimal solutions of the motion synthesis OCPs. For the sprinting movements, we have observed that the synthesized torques in the prosthetic ankle (right leg) are larger than the reconstructed torques. In return, the synthesized torques in the biological ankle (left leg) are smaller than the reconstructed torques. Accordingly, the ground reaction forces of the synthesized solutions for the contact with the right leg are larger and for the contact with the left leg smaller than the reconstructed/measured ground reaction forces. So, for sprinting, it appears that the model utilizes the RSP more efficiently than the real athlete. For the long jump, the observation was more sophisticated. At the third-last (prosthetic leg) and second-last (biological leg) contact before takeoff, the ankle torques and ground reaction forces of the synthesized solution are larger than those of the reconstructed one. Here, the model seems to utilize the spring-like properties of the RSP more than the real athlete during contact, but not in favor of a reduced use of the biological leg. During the take-off (last contact), the model even uses the RSP less than the real athlete and the ankle torque and ground reaction force are smaller in the synthesized solution than in the reconstructed one. With the results obtained so far, these observations cannot be clearly explained yet. Questions remain as to why the real athlete does not use his RSP more efficiently during sprinting when, according to the optimized solution, this should be possible, and why the model does not use the RSP more efficiently during takeoff when, according to the reconstructed solution, this should be possible. Further investigation is needed to answer this. It is possible that the optimal solution calculated by the OCP is not executable for the real athlete (e.g., because the chosen optimization criteria do not yet describe the movement completely or because the real athlete, in contrast to the simulation, cannot choose every variable perfectly tuned at any time) or that the real athlete still has potential to improve his movement.

## Potential for follow-up studies

The fact that there are still unanswered questions at the end of this work is neither bad nor surprising. Albert Einstein is quoted as once saying, “The important thing is to never stop questioning.” In this sense, we complete this work with the presentation of selected new research questions that building on the results of this work open up. The present work provides a good basis for further studies. We first present individual aspects of the existing implementation that can be expanded or improved comparatively quickly and easily in smaller projects (1.–6.). We

will then conclude with an outlook on two possible larger applications of this work (7.–8.):

1. **Integration of a muscle model:** In this work, we have modeled the control of the joints by torque actuators, which are supposed to summarize the work of all muscles involved in a joint. Compared to the real human body with its complex muscle system, this represents a significant simplification. We have taken a first step towards integrating a muscle model by introducing the Muscle Torque Generator (MTG) model, which we use only for computing the torque limits, though. Using the muscle activation dynamics as control in the individual joints would bring the overall model even closer to the actual human body. In addition, the integration of a muscle model opens up further possibilities to compare the movements of athletes with and without BKA at a deeper level.
2. **Improvement of the contact modeling:** We have modeled ground contact by a rigid point-like contact of the hallux of the foot or the prosthetic device. The assumption that during sprinting the ground contact happens exclusively with the forefoot is certainly justified for the phase of sprinting at maximum velocity<sup>1</sup>. However, the point contact represents a simplification, since some rollover also occurs when contact is made with the forefoot or the front part of the RSP. It is not clear beforehand what influence the simplification we made actually has on the movement. We have seen that the reconstructions provide reasonable results, both in terms of kinematics and dynamics. However, we have also found that there are discrepancies, especially in the ground reaction forces, for which a possible explanation could also be found in the comparatively simple foot model. Therefore, it would be interesting to establish a more sophisticated foot-contact model, which describes the rolling of the foot more realistically, and to investigate whether a significant improvement of the result quality can be achieved by this. A possible implementation, which would be compatible with our foot models (and in an adapted form also with the RSP model) and the OCP, is described in [90] and replaces the single segment rigid foot with a two-segment rigid foot model.
3. **Extension of the model of the running-specific prosthesis:** We have modeled the RSP as a three-segment rigid body with one rotational degree of freedom (DOF) at the most posterior point of the RSP. Here, different directions for further investigations arise: On the one hand, it would be possible to keep using the existing model of the RSP, but to extend it to a three-dimensional rotational joint, i.e., to allow rotations about all three principal axes, and thus to reconstruct or calculate the corresponding torques (as, for example, in [45]). Second, it would be possible to change the modeling of the RSP. As described in the introduction, the real RSP is made of carbon fibers. As a result, it does not actually have a fixed rotational joint, but is flexible along the curvature due to the elastic material. Besides the possibility of making the modeling more detailed by subdividing it into more rigid segments to model the curvature, another starting point would be to model the RSP by one or more slender elastic beams. The starting points for such an attempt could be the work of Marinou et al. [85] on modeling an exoskeleton by slender beams and the work of Sandhu et al. [117] on modeling a golf club by slender beams. Finally, the models and OCP formulations presented in this work open the possibility to investigate the influence of small variations of the RSP, e.g., in terms of prosthetic alignment, prosthesis shape or stiffness, on the resulting motion.
4. **Investigation of other optimization criteria:** While we have conducted an extensive investigation of various optimization criteria in the sprinting motion synthesis, we have

---

<sup>1</sup>When modeling the acceleration phase as suggested below, one would have to adapt the ground contact model at least in a way that it consists of several phases as in the modeling of the human gait, compare for example [40].

---

limited our consideration of the long jump to one main criterion, maximizing the jump distance. Although this is the most obvious criterion for the specific movement, it is conceivable that additional optimization criteria could underlie the movement. In particular, we did not include optimization criteria that act directly on the approach steps, e.g., maximization of velocity. Moreover, we have seen in the IOCP solutions that although already close to the reference motion, they could still be improved. A possible starting point is also here the integration of further optimization criteria into the objective function.

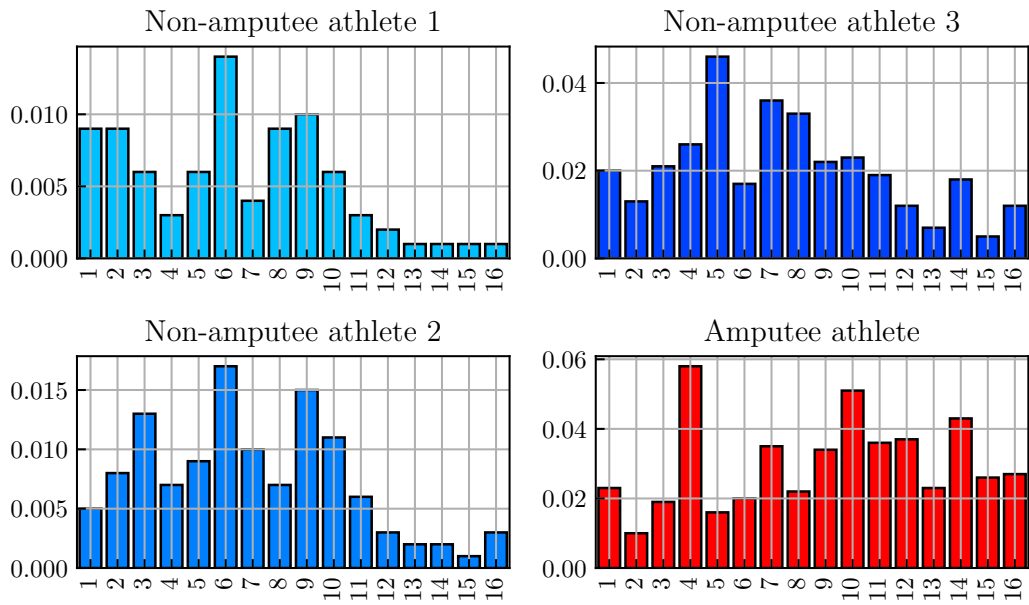
5. **Inverse optimal control of long jump motions:** We applied the IOCP formulation to sprinting motions in this work and identified weights for the four athletes studied that describe their individual running styles, at least to the extent that the solutions are closer to the measured motions than those obtained with hand-picked combinations of the optimization criteria. The IOCP formulation is also applicable in principle to the long jump movement. It would be interesting to identify the underlying combination of optimization criteria for this motion as well. One difficulty here is that the motion capture recordings used so far stop during the jump, but we compute the entire jump until landing, so only part of the reference motion would be included. New motion capture recordings, which record the jump until landing, would be helpful for this. Furthermore, it would be worth considering to include additional optimization criteria in the objective function for the long jump to find out if they characterize the motion (see the previous paragraph).
6. **Integration of further stages of the motions:** In this work, we have considered two sprinting steps at constant velocity (hence, we assume that the athlete has accelerated to his maximum velocity) as well as the last three steps of the long jump approach and the actual jump. However, a sprint race consists of several phases, i.e., the sprint start (possibly from a crouched position), an acceleration phase, a phase of constant maximum velocity and a deceleration phase after the finish line. A long jump consists of a start from a resting position, the approach run, the take-off, the flight and the landing. For a balanced complete comparison it is not enough to use only some of these phases, but the whole movement has to be investigated. Therefore, it would be very interesting to model further phases of the motions and examine them with regard to the differences and similarities between athletes with and without BKA. The modeling and simulation of an entire sprint race or an entire long jump consisting of all the phases mentioned above would of course be the optimum. However, it remains questionable whether the solution of such a large OCP would be computable in an acceptable amount of time (at least with the currently used multiple shooting code).
7. **Creation of a motion database:** The initial idea for the simulator tool was to provide a way to compare an amputee athlete with himself without amputation easily and without much required measurement data. We have shown in this work that such a comparison provides valuable information that is hidden when comparing to a control group of non-amputee athletes, and – once the simulator tool is fully in place – can be done easily and conveniently. Important requirements for a good prediction of the simulation are a suitable objective function and appropriate bounds for the joint torques (or in an extended version corresponding muscle parameters). Since the simulator tool is supposed to be about the concrete analysis of an athlete with BKA, it makes sense to perform accurate measurements of this athlete and to determine the torque limits as well as the objective function underlying his motion by means of an IOCP from them. For the non-amputee version of the model, however, it would be useful to have averages of a large number of athletes without BKA in terms of the bounds on the individual variables and

the modeling of the motion. As we saw in the discussion of the sprinting results, there were definitely still differences between the three non-amputee athletes studied, which were due to individual running styles and performance levels. Therefore, one goal, along with the simulator tool, would be to build a large database for sprinting and long jump movements. For the non-amputee version of the model, the parameters (scaled to the respective height and weight of the athlete under investigation with BKA) could then be adjusted using this database. In addition to the data of the athletes without BKA, data of the investigated athletes with BKA should of course also be included, so that in the longer term typical movement patterns can also be identified and, for example, it becomes clearer which observations are made based on the individual movement type.

8. **Use of the simulator tool for other purposes (e.g., performance improvement)** In addition to the use of the simulator tool presented in this work to compare an amputee athlete with himself without amputation, the simulator tool could also be used (through extensions) for a variety of other purposes. For example, it is possible to create a detailed model of an athlete and, based on predictive simulation of the movement, find the optimal movement for that particular athlete with respect to a particular combination of optimization criteria and compare it to the actual movement. Depending on the desired accuracy, a pure video recording of the real athlete is also sufficient to compare it with the calculated motion. Alternatively, a motion capture recording can be used to calculate the motion parameters to be compared by means of the dynamics reconstruction OCP. In this way, the simulator tool can be used to improve performance by allowing accurate statements on how the specific athlete needs to adjust his movement in order to optimize it. Furthermore, the envisaged structure of the simulator tool offers easy possibilities for extension, e.g., for the investigation of other prosthesis models, other degrees of amputation or other movements such as high jump.

# A Additional Figures

## A.1 Dynamics Reconstruction of Sprinting Motions



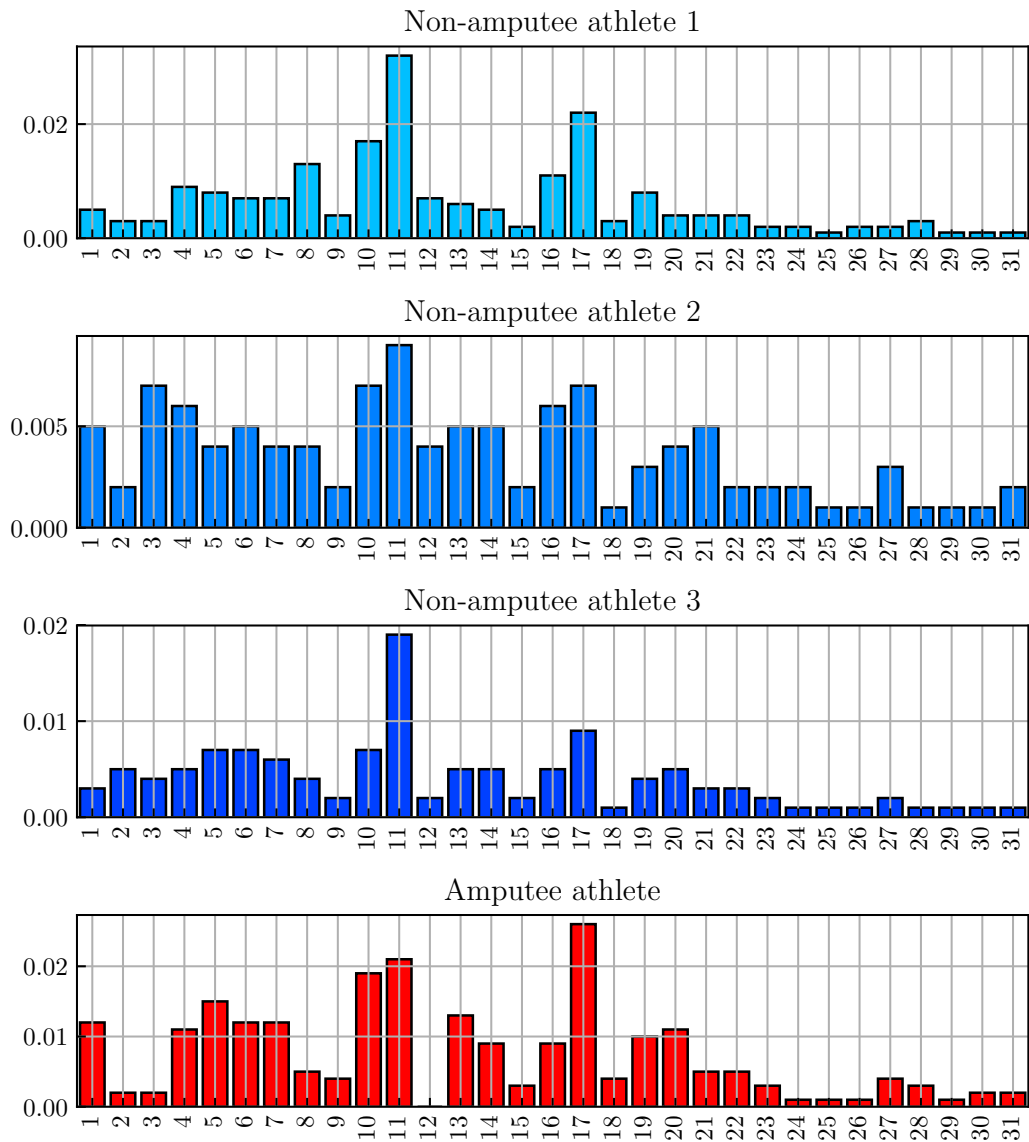

---

1	Pelvis TX [m]	6*	Prosthesis RY [rad]	12	Right shoulder RY [rad]
2	Pelvis TZ [m]	7	Left hip RY [rad]	13	Right elbow RY [rad]
3	Pelvis RY [rad]	8	Left knee RY [rad]	14	Left shoulder RY [rad]
4	Right hip RY [rad]	9	Left ankle RY [rad]	15	Left elbow RY [rad]
5	Right knee RY [rad]	10	Lumbar RY [rad]	16	Neck RY [rad]
6*	Right ankle RY [rad]	11	Thorax RY [rad]		

---

\* 'Right ankle' for the non-amputee athletes, 'Prosthesis' for the amputee athlete.

Figure A.1: Root-mean-square errors between the solutions of the dynamics reconstruction and the reference motions for the individual joints of the 2D models in sprinting. The meaning of the numbers on the x-axis is given in the table below the figure.

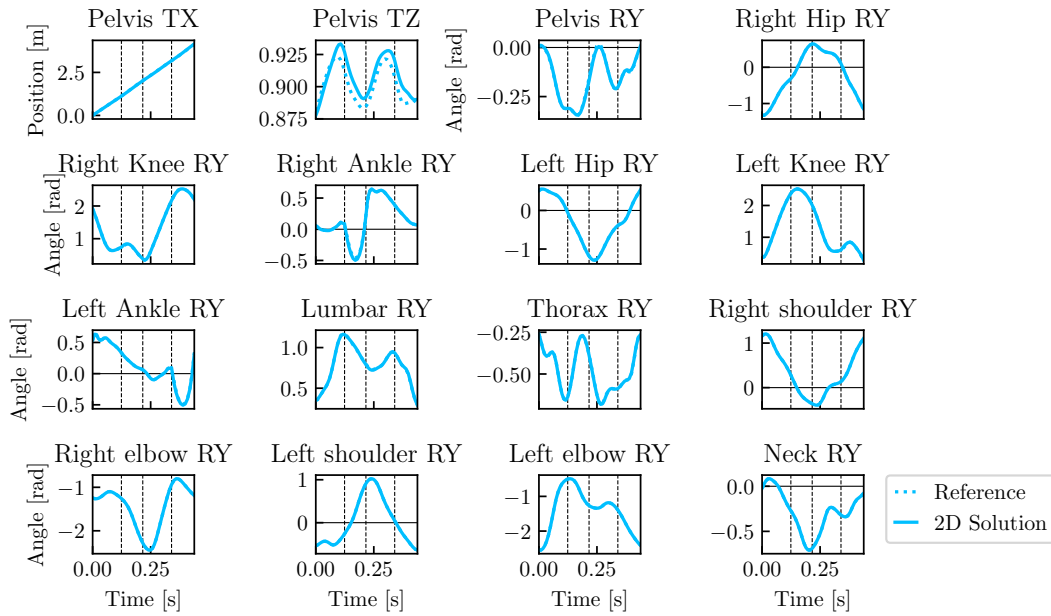


1	Pelvis TX [m]	11*	Prosthesis RY [rad]	22	Thorax RZ [rad]
2	Pelvis TY [m]	12 <sup>†</sup>	Right ankle RZ [rad]	23	Right shoulder RY [rad]
3	Pelvis TZ [m]	13	Left hip RY [rad]	24	Right shoulder RX [rad]
4	Pelvis RY [rad]	14	Left hip RX [rad]	25	Right shoulder RZ [rad]
5	Pelvis RX [rad]	15	Left hip RZ [rad]	26	Right elbow RY [rad]
6	Pelvis RZ [rad]	16	Left knee RY [rad]	27	Left shoulder RY [rad]
7	Right hip RY [rad]	17	Left ankle RY [rad]	28	Left shoulder RX [rad]
8	Right hip RX [rad]	18	Left ankle RZ [rad]	29	Left shoulder RZ [rad]
9	Right hip RZ [rad]	19	Lumbar RY [rad]	30	Left elbow RY [rad]
10	Right knee RY [rad]	20	Lumbar RX [rad]	31	Neck RY [rad]
11*	Right ankle RY [rad]	21	Thorax RY [rad]		

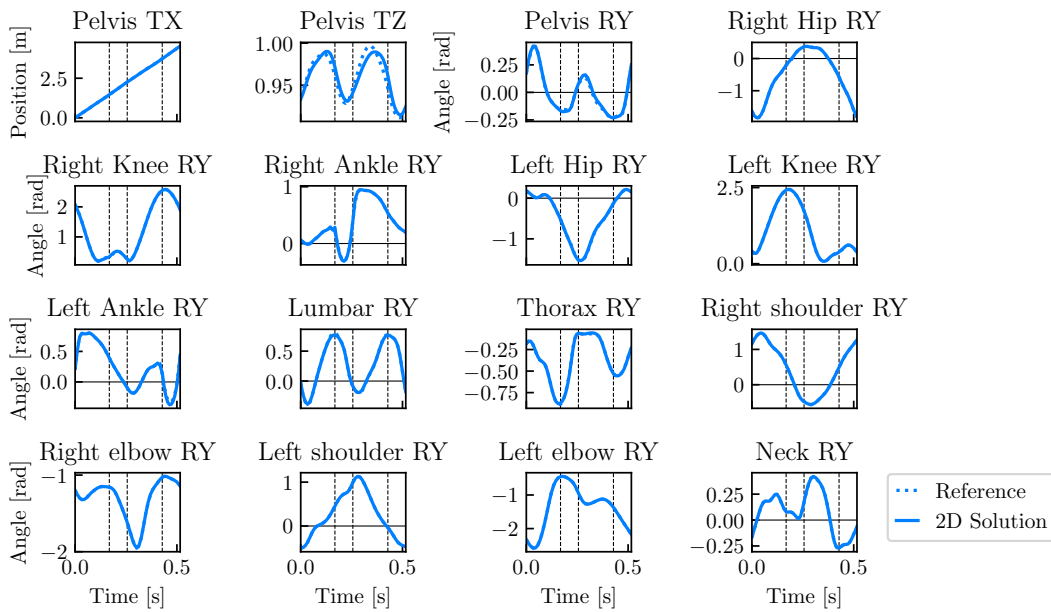
\* 'Right ankle' for the non-amputee athletes, 'Prosthesis' for the amputee athlete.

<sup>†</sup> Only applies for the non-amputee athletes.

Figure A.2: Root-mean-square errors between the solutions of the dynamics reconstruction and the reference motions for the individual joints of the 3D models in sprinting. The meaning of the numbers on the x-axis is given in the table below the figure.

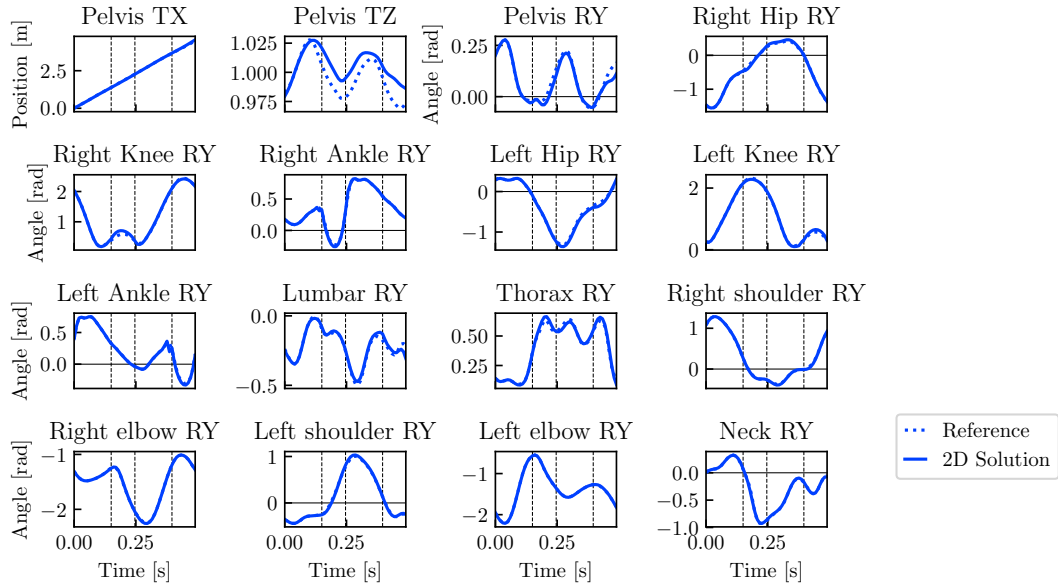


(a) Non-amputee athlete 1

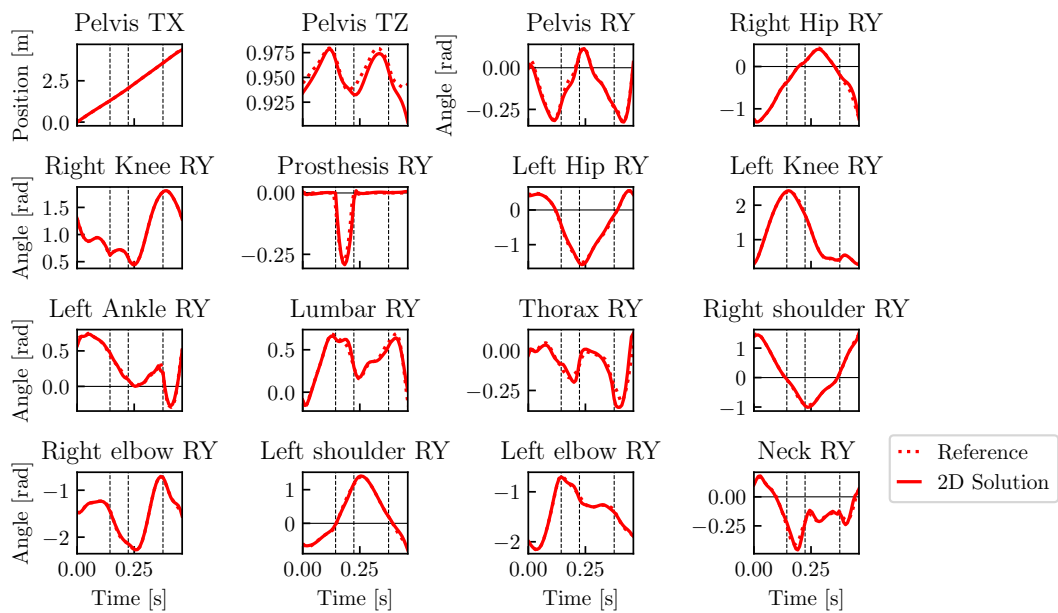


(b) Non-amputee athlete 2

Figure A.3: Two-dimensional generalized positions of the dynamics reconstruction and the reference motions of sprinting

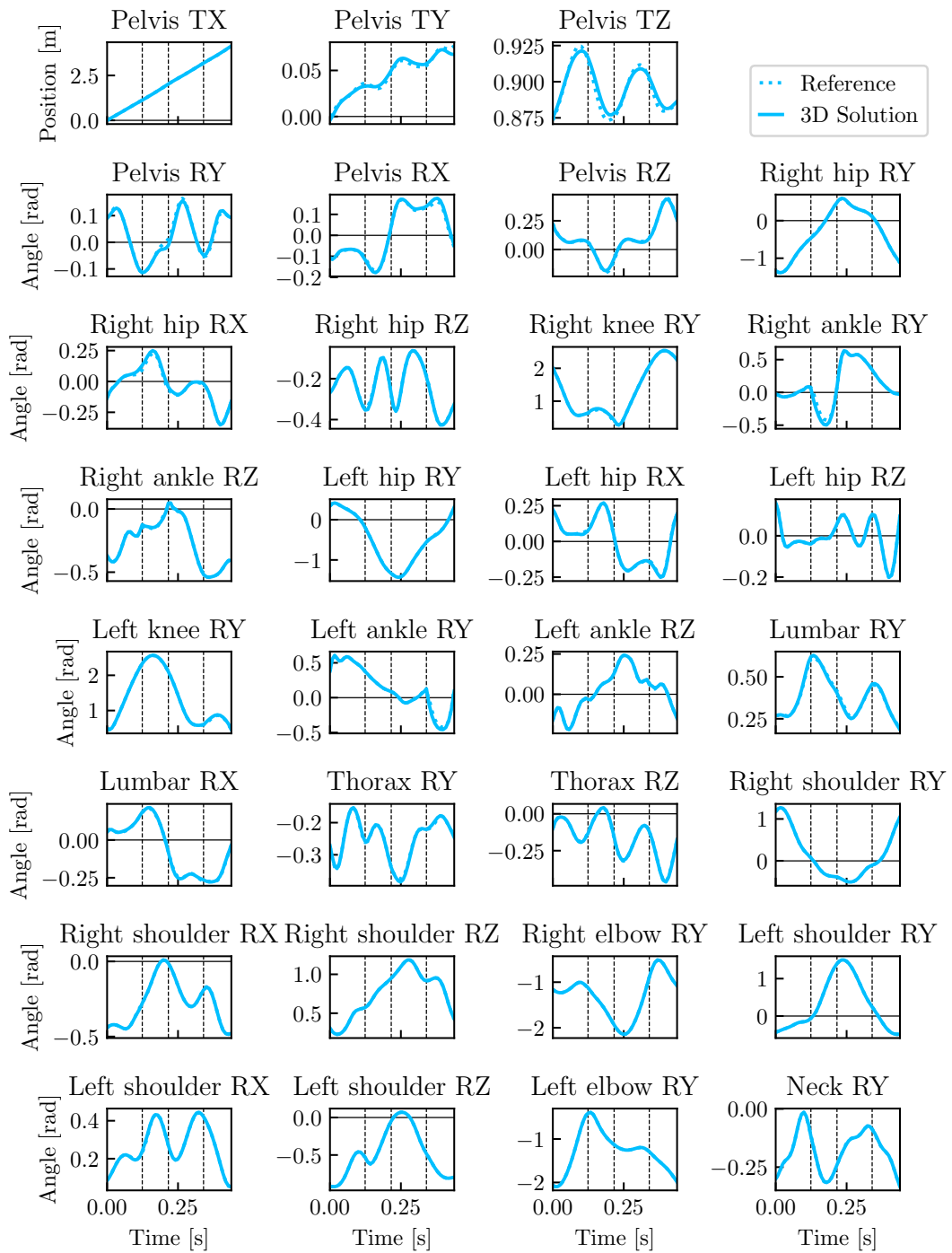


(c) Non-amputee athlete 3



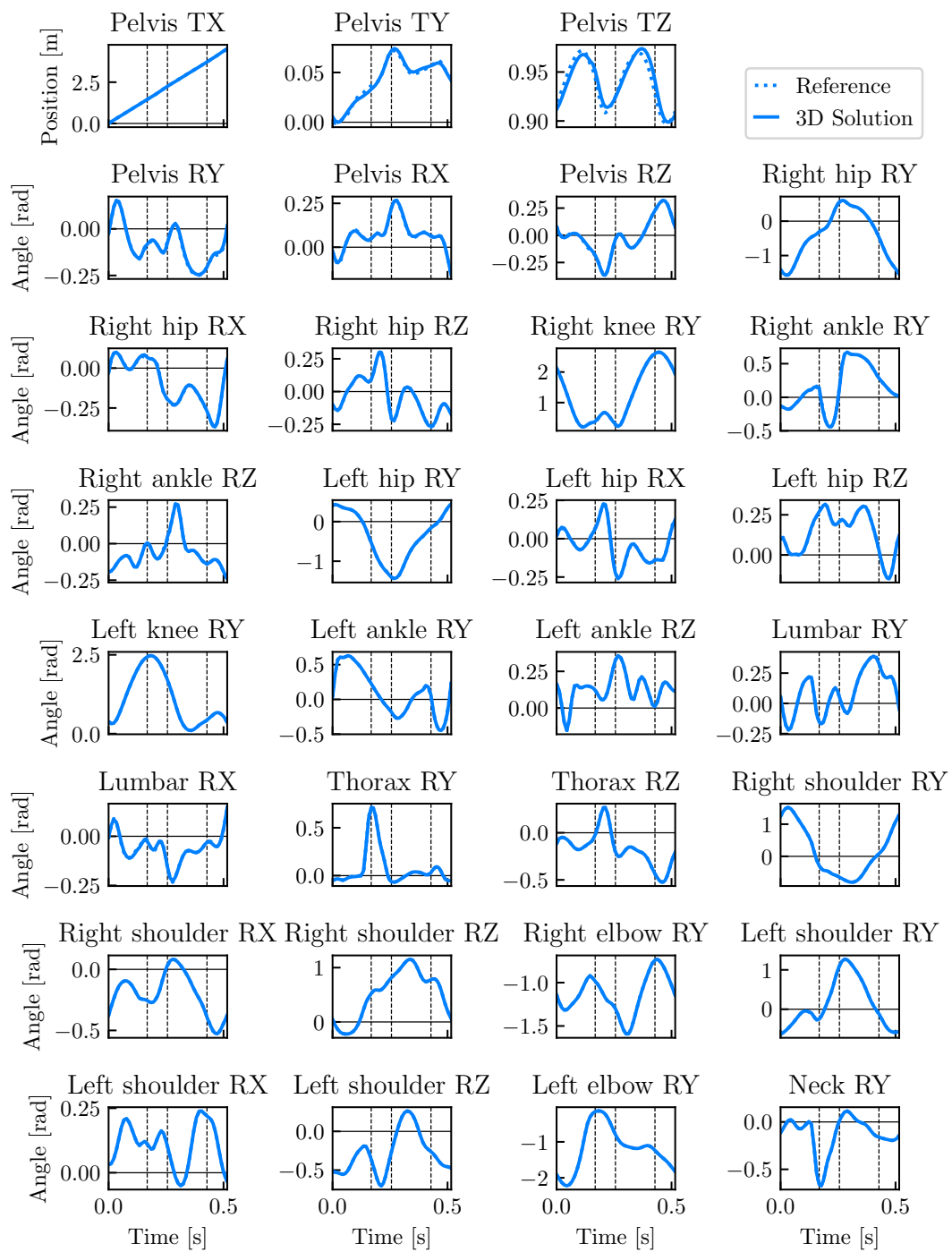
(d) Amputee athlete

Figure A.3: Two-dimensional generalized positions of the dynamics reconstruction and the reference motions of sprinting (cont.)



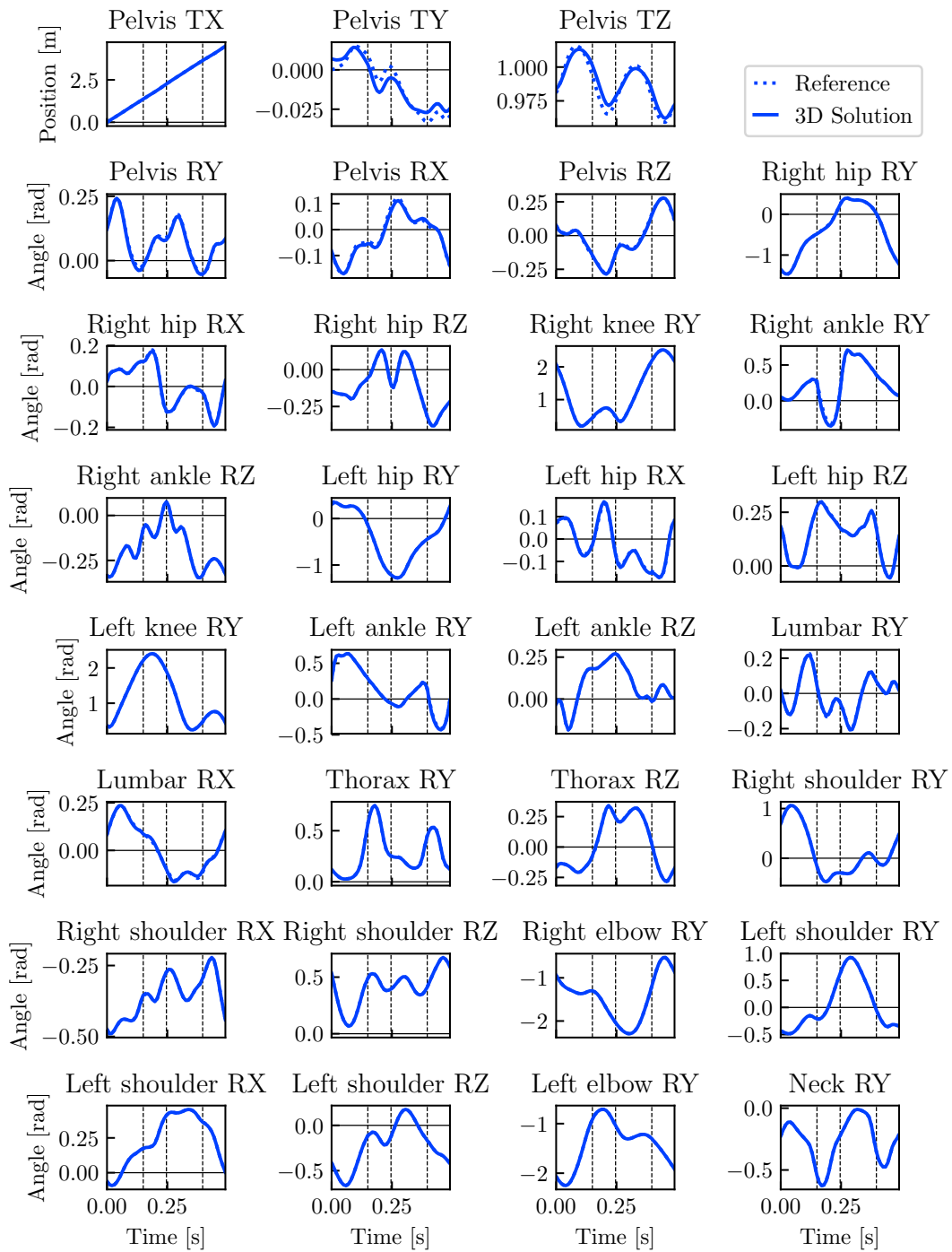
(a) Non-amputee athlete 1

Figure A.4: Three-dimensional generalized positions of the dynamics reconstruction and the reference motions of sprinting



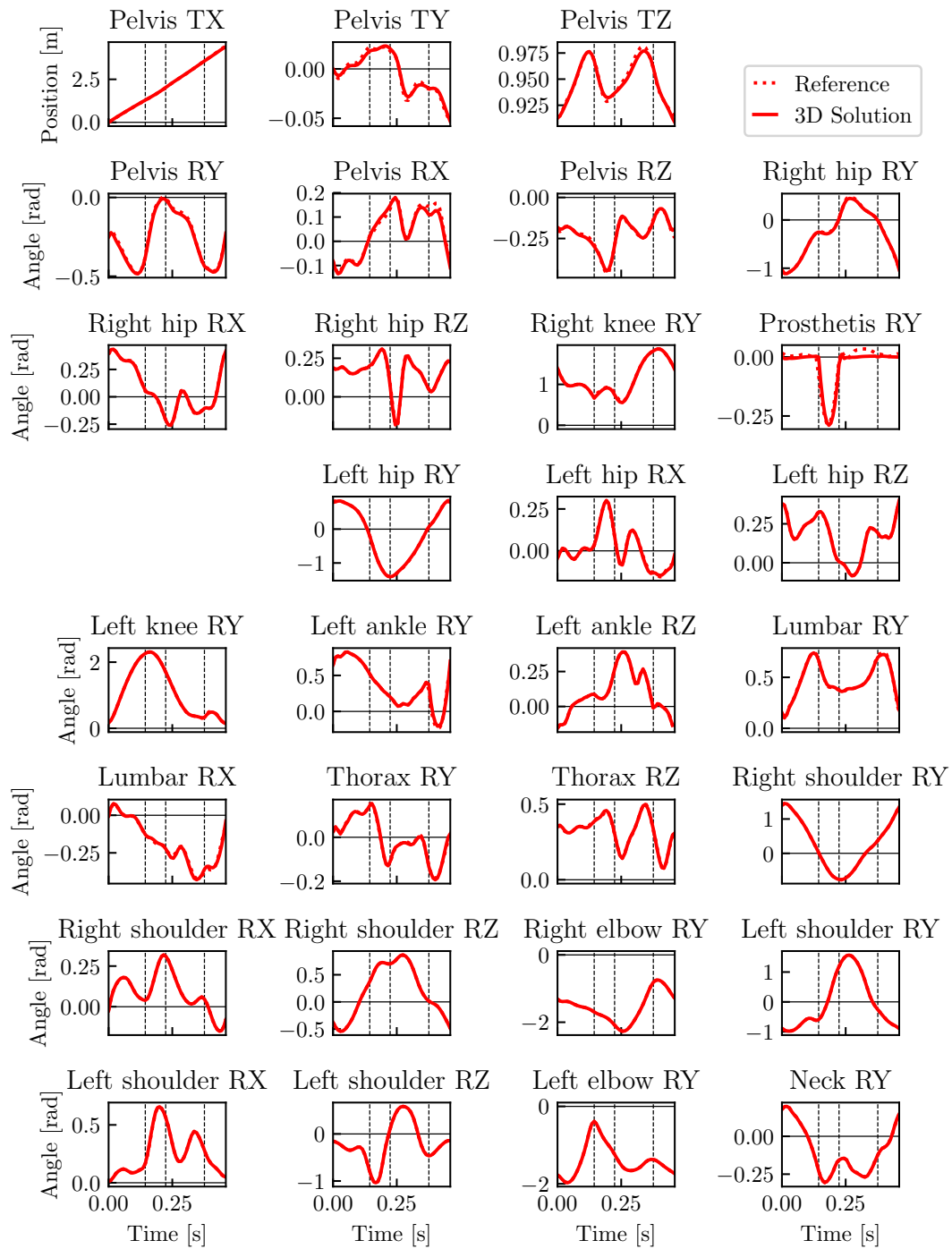
(b) Non-amputee athlete 2

Figure A.4: Three-dimensional generalized positions of the dynamics reconstruction and the reference motions of sprinting (cont.)



(c) Non-amputee athlete 3

Figure A.4: Three-dimensional generalized positions of the dynamics reconstruction and the reference motions of sprinting (cont.)



(d) Amputee athlete

Figure A.4: Three-dimensional generalized positions of the dynamics reconstruction and the reference motions of sprinting (cont.)

## A.2 Synthesis of Sprinting Motions

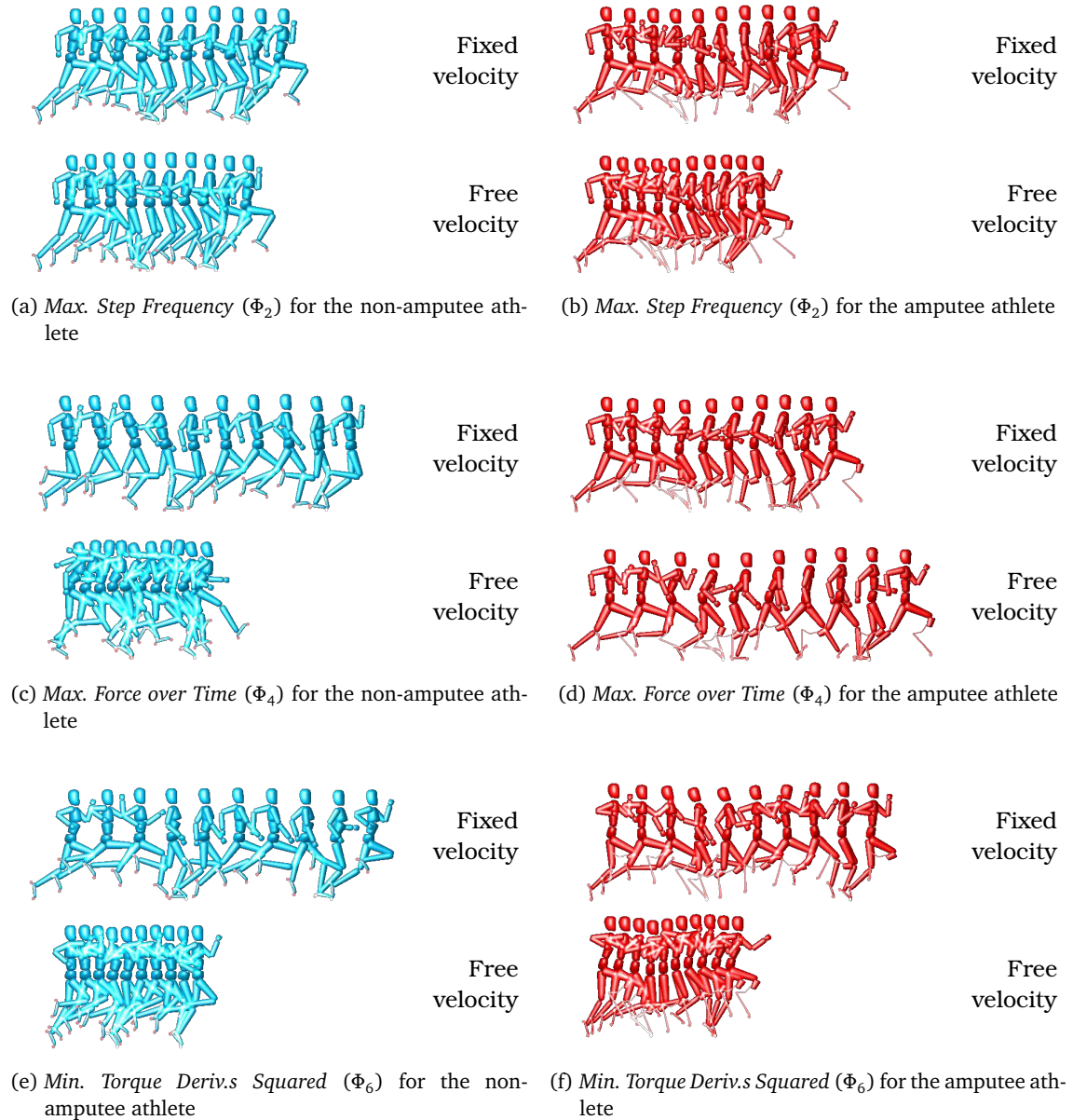


Figure A.5: Animated sequences of optimized sprinting motions for the amputee and the non-amputee athletes

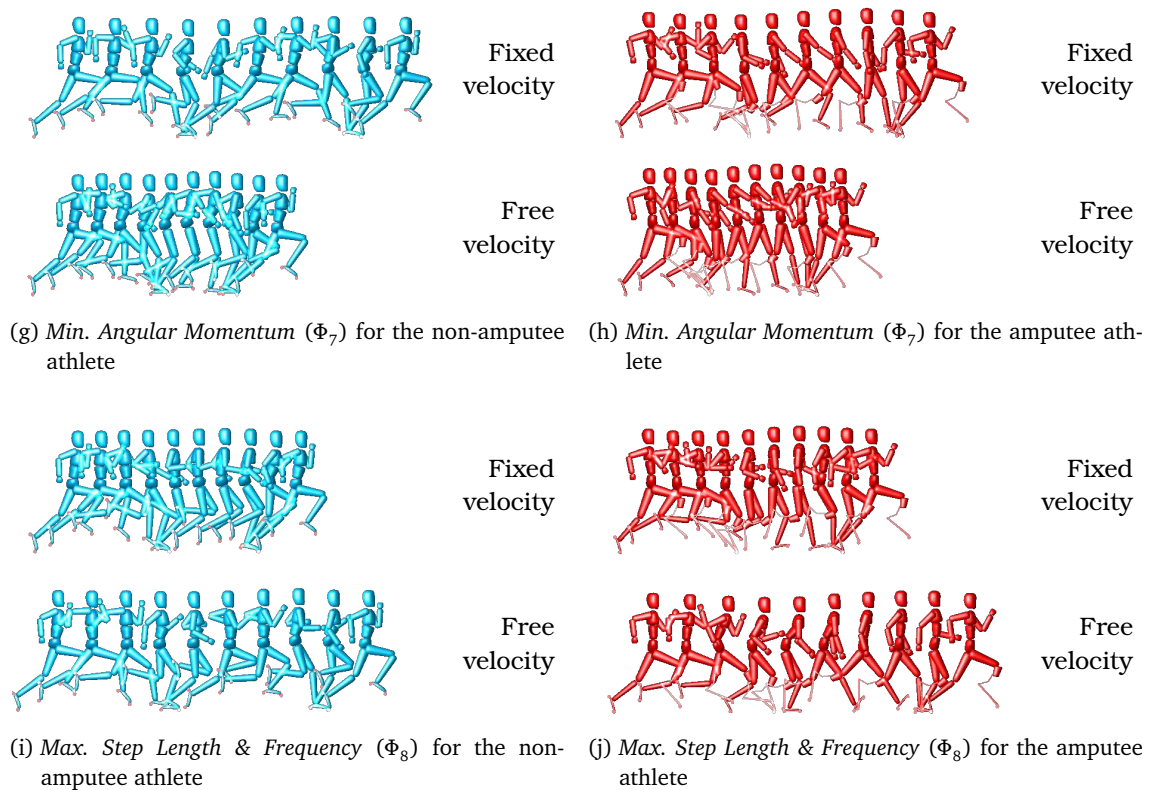


Figure A.5: Animated sequences of optimized sprinting motions for the amputee and the non-amputee athletes

### A.3 Inverse Optimal Control of Sprinting Motions

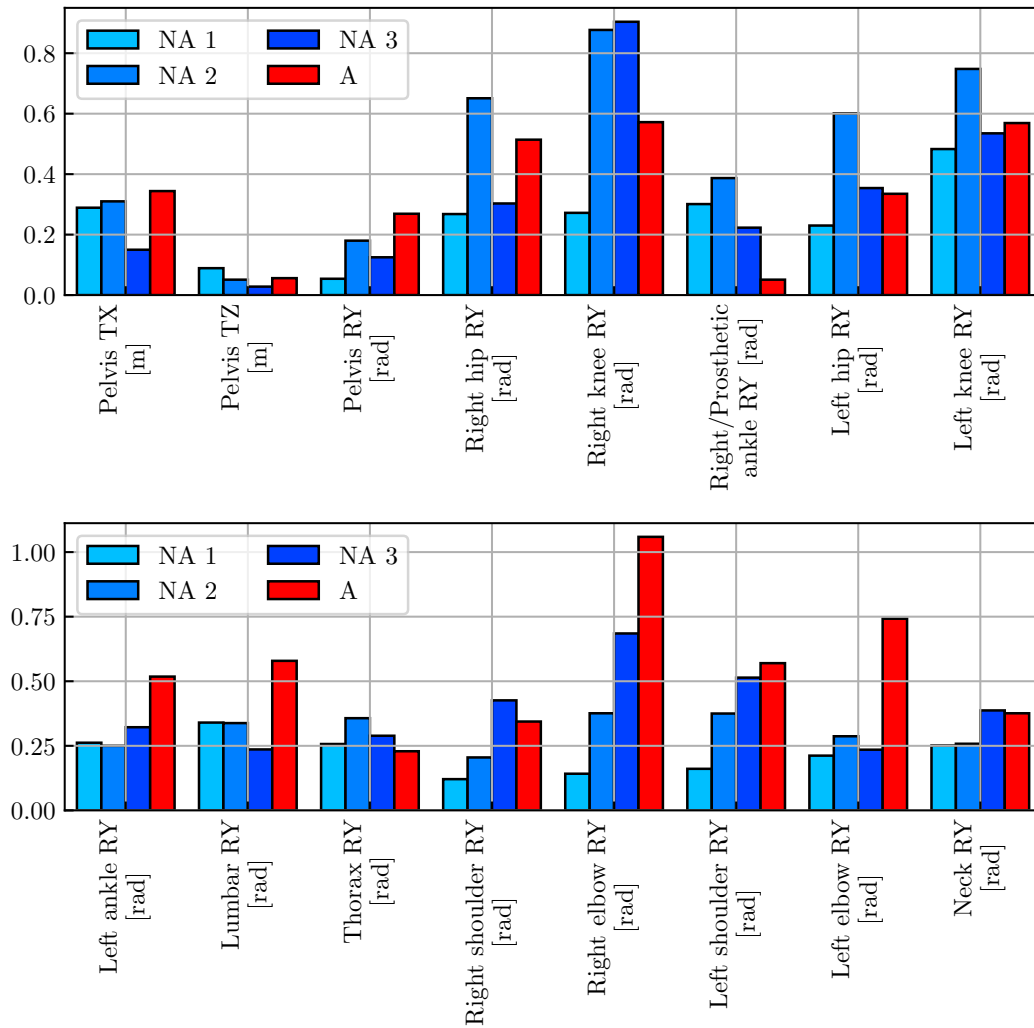
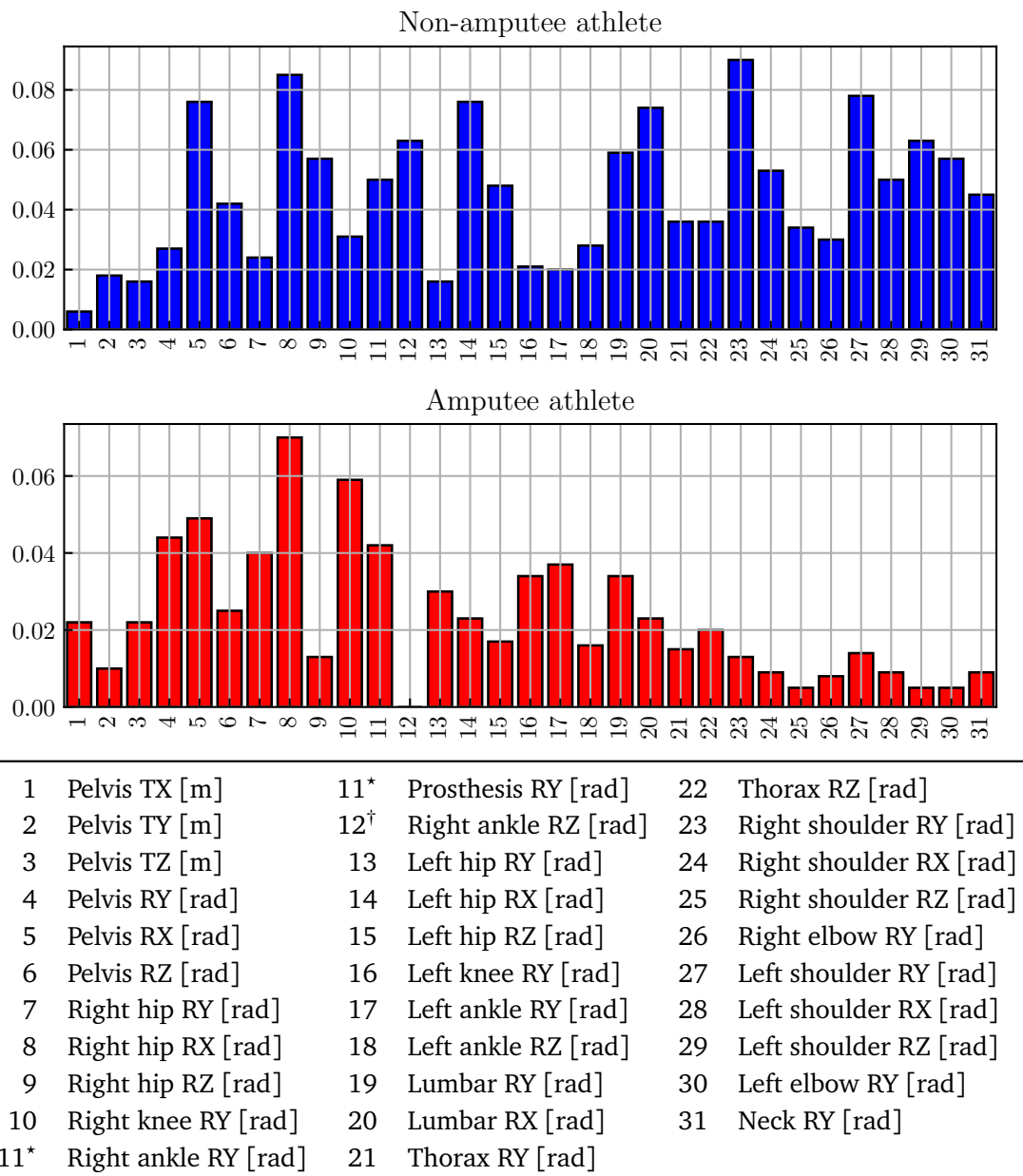


Figure A.6: Root-mean-square errors between the reference data and the best weight inverse optimal control problem solutions of the four athletes for the individual joints in sprinting

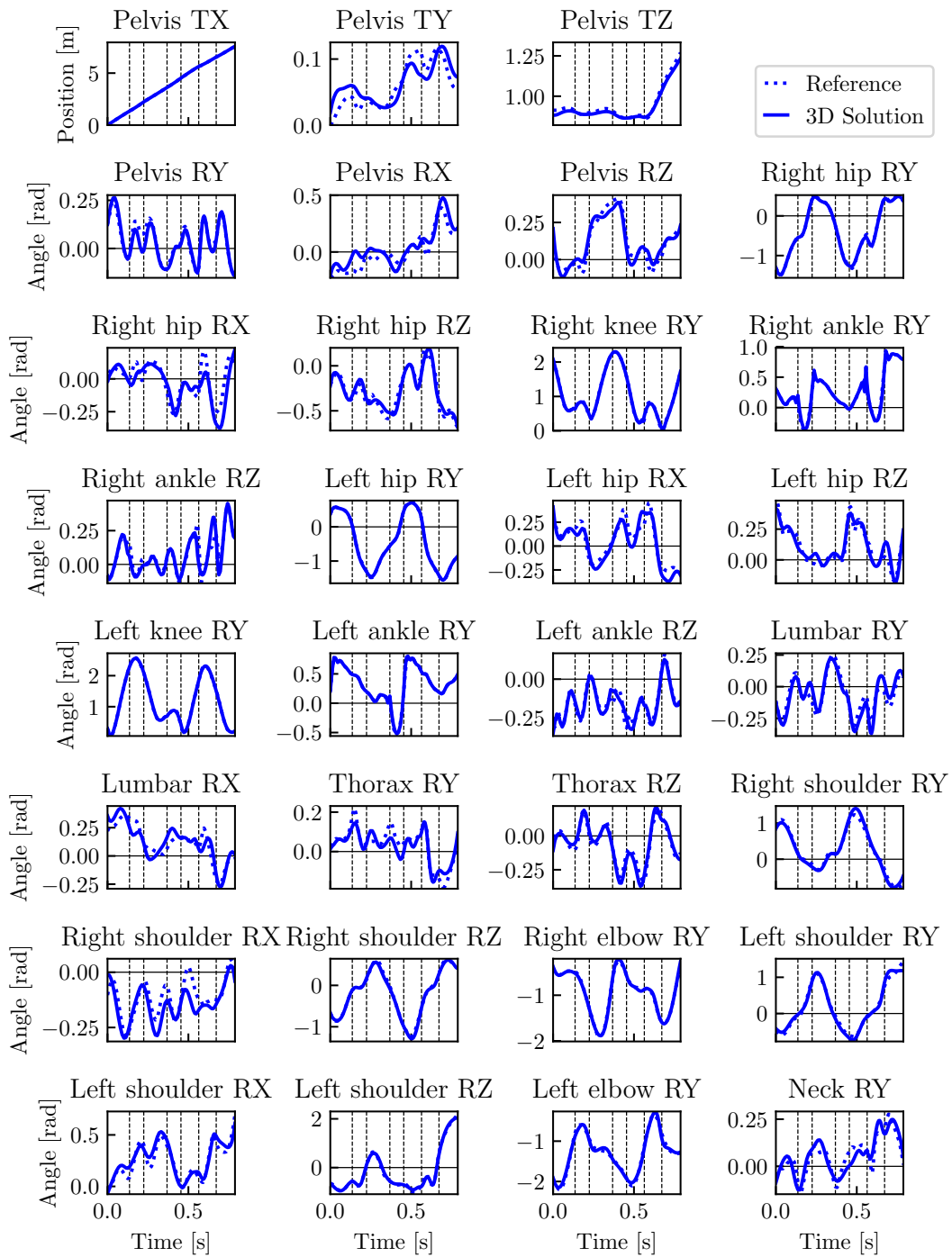
## A.4 Dynamics Reconstruction of Long Jump Motions



\* 'Right ankle' for the non-amputee athletes, 'Prosthesis' for the amputee athlete.

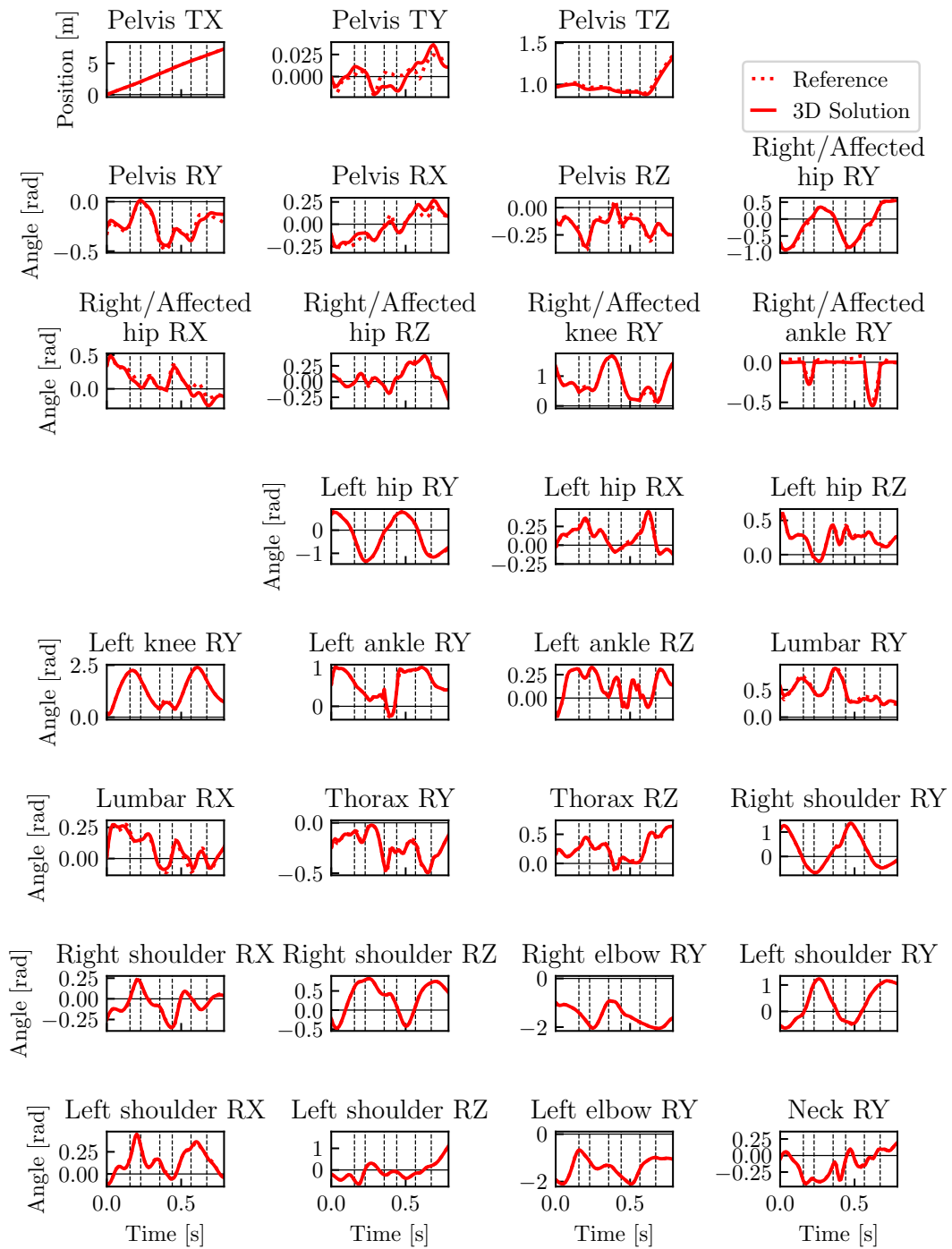
† Only applies for the non-amputee athletes.

Figure A.7: Root-mean-square errors between the solution of the dynamics reconstruction and the reference motion for the individual joints in long jump



(a) Non-amputee athlete

Figure A.8: Three-dimensional generalized positions of the dynamics reconstruction and the reference motions of long jump



(b) Amputee athlete

Figure A.8: Three-dimensional generalized positions of the dynamics reconstruction and the reference motions of long jump

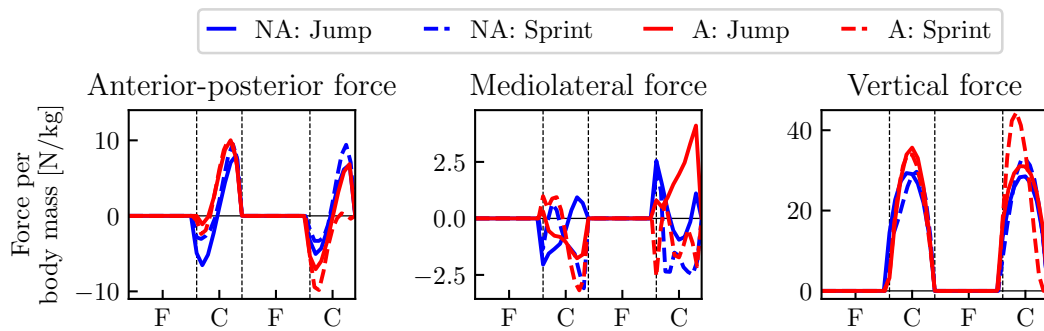


Figure A.9: Comparison of the ground reaction forces during the third-last and second-last steps of the long jump reconstruction and the two steps of the sprint reconstruction for the non-amputee ('NA') and the amputee athlete ('A'). For the sprint reconstruction, we show the curves of non-amputee athlete 1 and for the jump reconstruction the ones of non-amputee athlete 4. Forces are normalized by body mass and phase durations are scaled for comparability. The solid lines give the curves related to long jump and the dashed lines the curves related to sprint. The labels 'F' and 'C' on the x-axis indicate flight and contact phases, respectively.

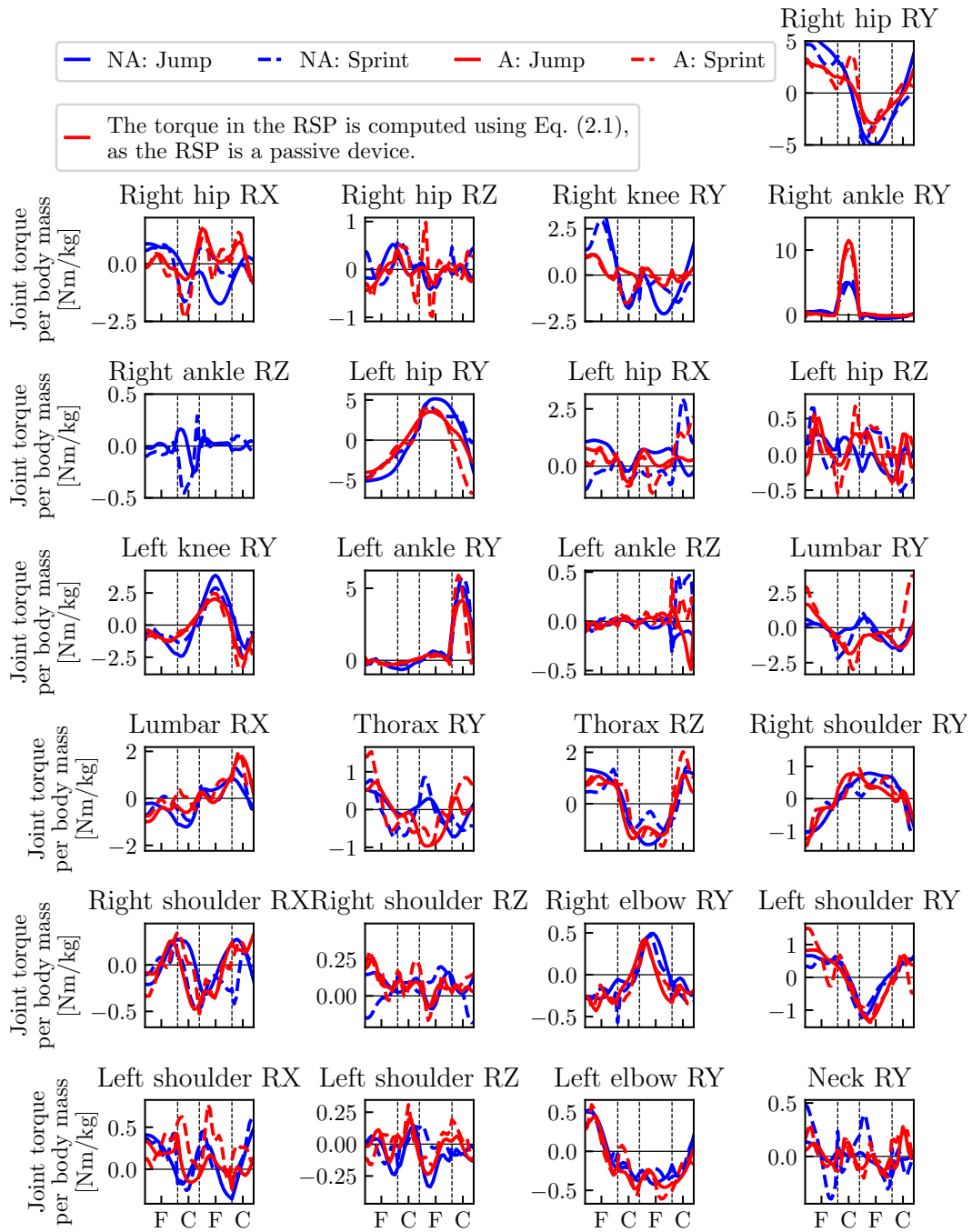


Figure A.10: Comparison of the joint torques during the third-last and second-last steps of the long jump reconstruction and the two steps of the sprint reconstruction for the non-amputee ('NA') and the amputee athlete ('A'). For the sprint reconstruction, we show the curves of non-amputee athlete 1 and for the jump reconstruction the ones of non-amputee athlete 4. Joint torques are normalized by body mass and phase durations are scaled for comparability. The solid lines give the curves related to long jump and the dashed lines the curves related to sprint. The labels 'F' and 'C' on the x-axis indicate flight and contact phases, respectively.

## A.5 Synthesis of Long Jump Motions

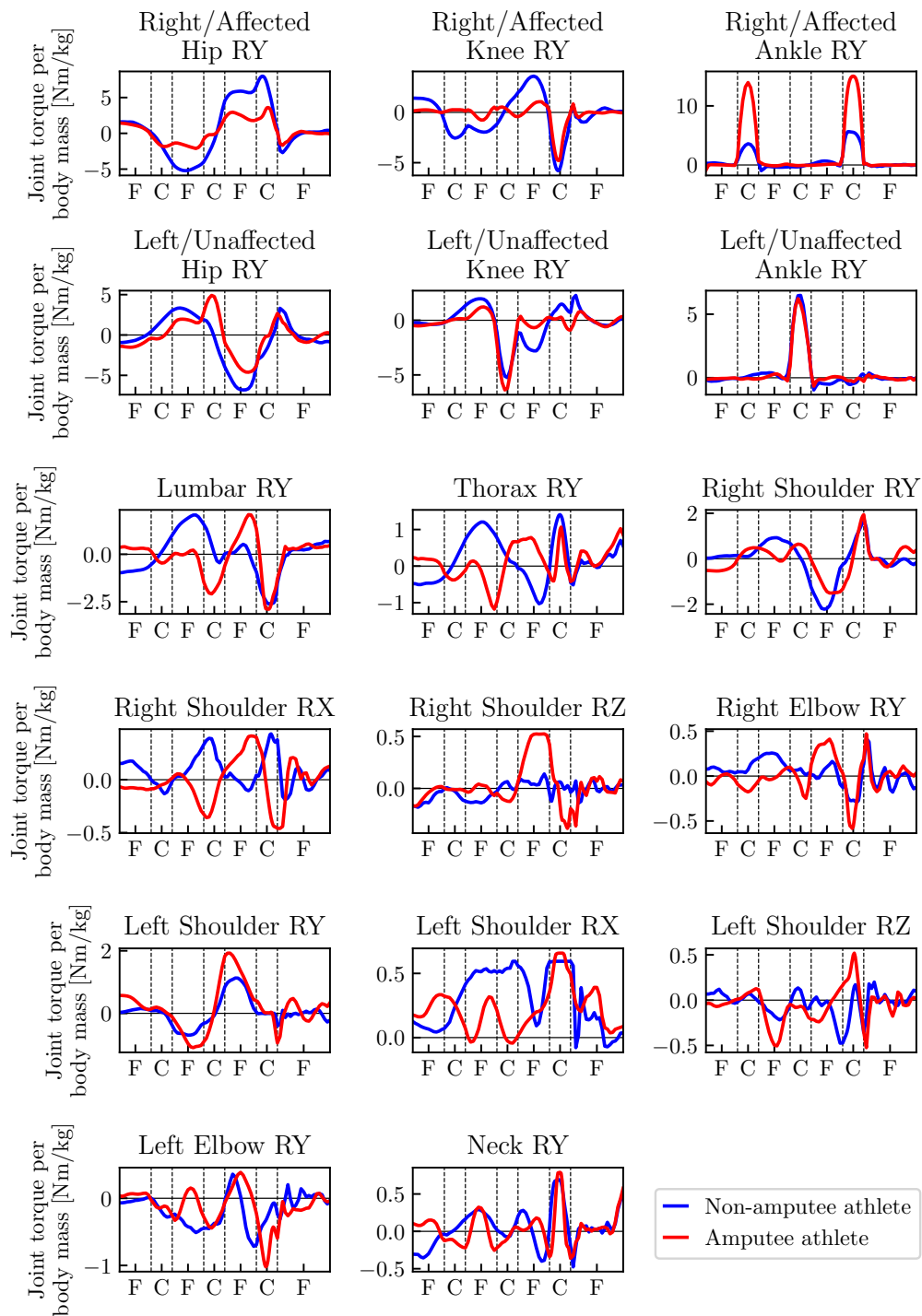


Figure A.11: Joint torques of the non-amputee and the amputee athlete for the synthesized long jump motions. The abbreviations ‘F’ and ‘C’ on the x-axis denote flight and contact phases, respectively, with the phase order as given in Figure 8.1. Phase durations are scaled for better comparability between the two athletes. Joint torques are normalized by body mass.

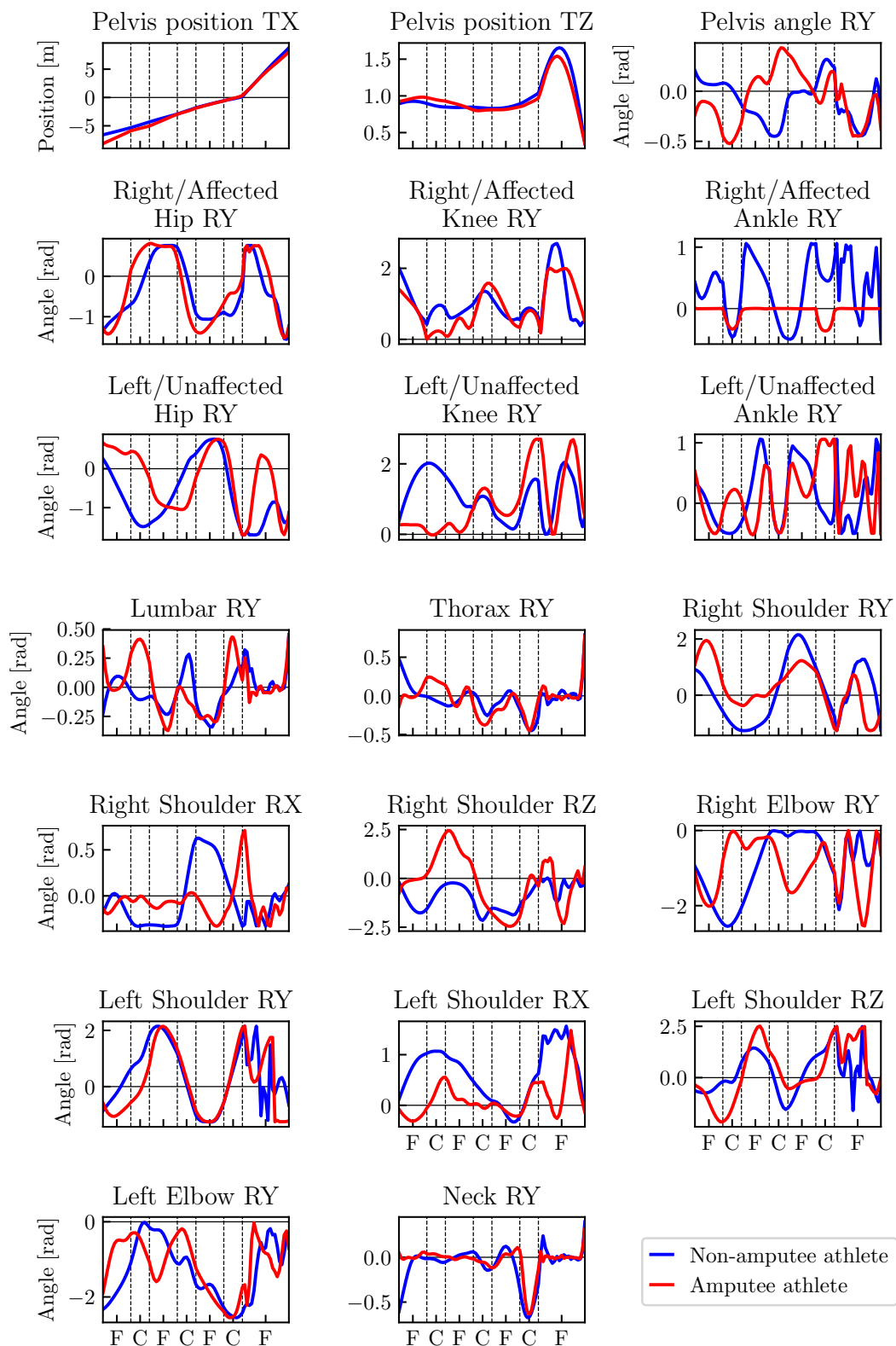
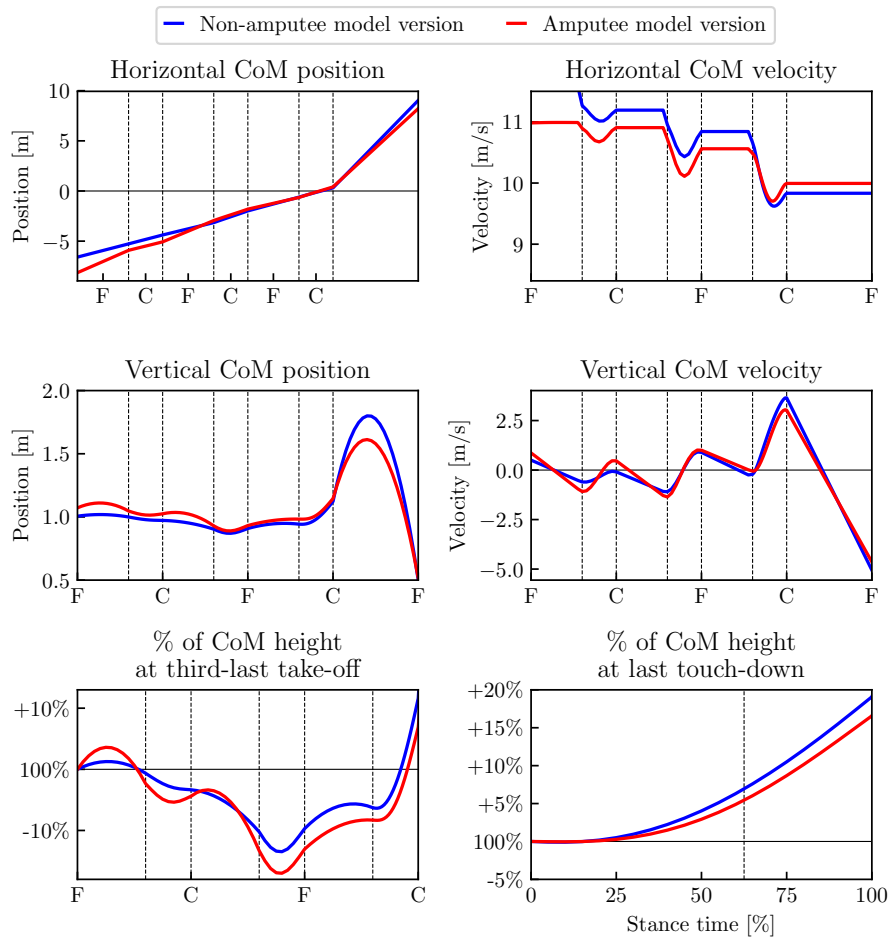
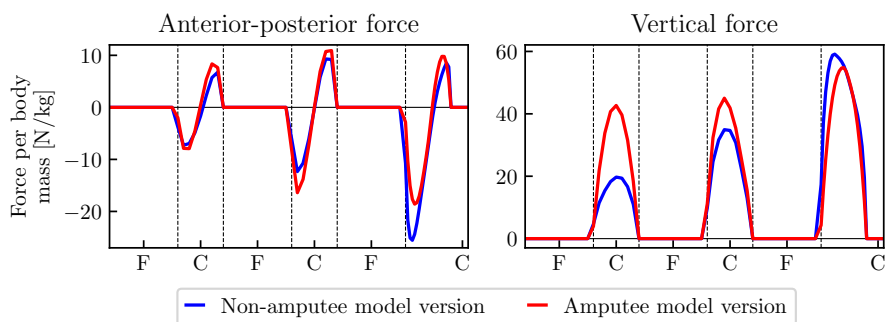


Figure A.12: Generalized positions of the non-amputee and the amputee athlete for the synthesized long jump motions. The abbreviations 'F' and 'C' on the x-axis denote flight and contact phases, respectively, with the phase order as given in Figure 8.1. Phase durations are scaled for better comparability between the two athletes.

## A.6 Towards a Simulator Tool: Long Jump

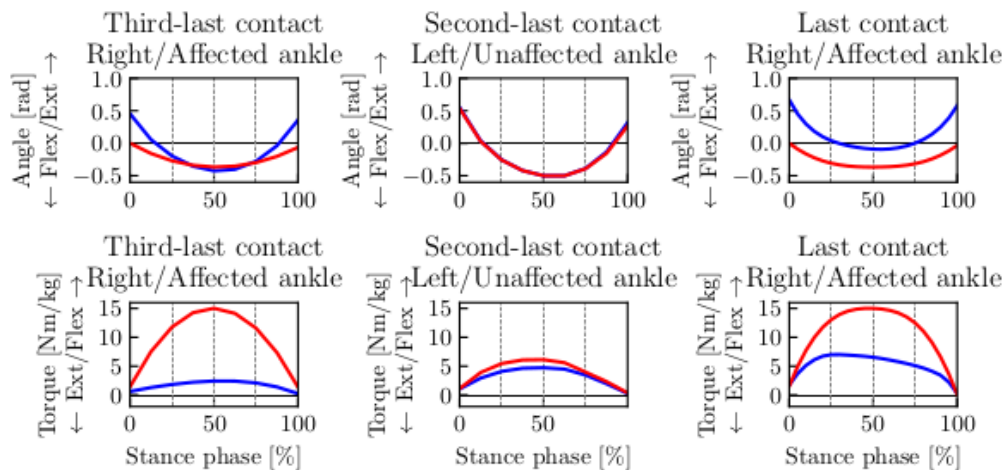


(a) CoM-related curves

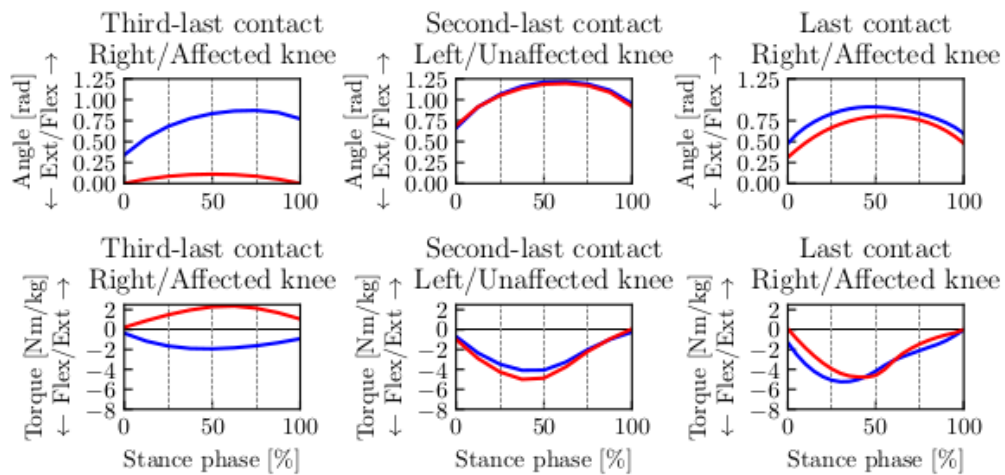


(b) Ground reaction forces

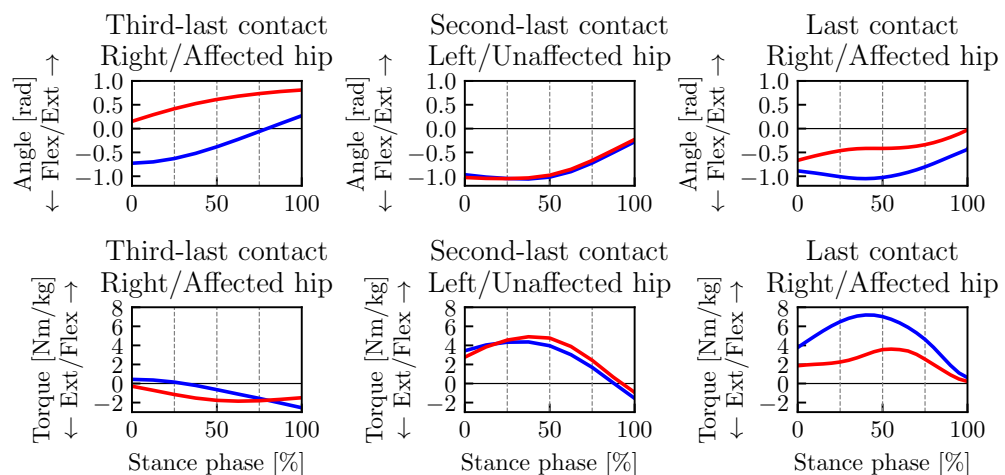
Figure A.13: Center of mass and ground reaction forces curves of the long jump motion for the comparison of the amputee and non-amputee model versions. The x-axis labels 'F' and 'C' denote flight and contact phases, respectively.



(a) Prosthetic/Biological ankle joints



(b) Knee joints



— Non-amputee model version    — Amputee model version

(c) Hip joints

Figure A.14: Leg joint angles and joint torques during the contact phases of the long jump motion for the comparison of the amputee and non-amputee model versions

# Bibliography

- [1] M. Ae, A. Ito, and M. Suzuki. The men's 100 metres. *New Studies in Athletics*, 7(1): 47–52, 1992.
- [2] S. Albrecht, P. Basili, S. Glasauer, M. Leibold, and M. Ulbrich. Modeling and analysis of human navigation with crossing interferer using inverse optimal control. In *7th Vienna International Conference on Mathematical Modelling*, volume 45 of *IFAC Proceedings Volumes*, pages 475–480, 2012.
- [3] S. Albrecht, M. Leibold, and M. Ulbrich. A bilevel optimization approach to obtain optimal cost functions for human arm movements. *Numerical Algebra, Control & Optimization*, 2(1):105–127, 2012. doi: 10.3934/naco.2012.2.105.
- [4] R. M. Alexander. The Gaits of Bipedal and Quadrupedal Animals. *The International Journal of Robotics Research*, 3(2):49–59, 1984. doi: 10.1177/027836498400300205.
- [5] R. M. Alexander. A minimum energy cost hypothesis for human arm trajectories. *Biological Cybernetics*, 76:97–105, 1997. doi: 10.1007/s004220050324.
- [6] R. M. Alexander and Q. Bone. Optimum take-off techniques for high and long jumps. *Philosophical Transactions of the Royal Society of London. Series B, Biological Sciences*, 329(1252):3–10, 1990. doi: 10.1098/rstb.1990.0144.
- [7] G. B. Allende and G. Still. Solving bilevel programs with the KKT-approach. *Mathematical Programming*, 138:309–332, 2013. doi: 10.1007/s10107-012-0535-x.
- [8] T. Alt, K. Heinrich, J. Funken, and W. Potthast. Lower extremity kinematics of athletics curve sprinting. *Journal of Sports Sciences*, 33(6):552–560, 2015. doi: 10.1080/02640414.2014.960881.
- [9] D. E. Anderson, M. L. Madigan, and M. A. Nussbaum. Maximum voluntary joint torque as a function of joint angle and angular velocity: Model development and application to the lower limb. *Journal of Biomechanics*, 40(14):3105–3113, 2007. doi: 10.1016/j.jbiomech.2007.03.022.
- [10] A. Arampatzis, G.-P. Brüggemann, and M. Walsch. Long jump. In G.-P. Brüggemann, D. Koszewski, and H. Müller, editors, *Biomechanical Research Project Athens 1997 Final Report*. Meyer & Meyer Sport, Oxford, 1999.
- [11] B. M. Ashby and S. L. Delp. Optimal control simulations reveal mechanisms by which arm movement improves standing long jump performance. *Journal of Biomechanics*, 39(9):1726–1734, 2006. doi: 10.1016/j.jbiomech.2005.04.017.
- [12] A. Baca. *Computer Science in Sport: Research and Practice*. Routledge, 1 edition, 2014. doi: 10.4324/9781315881782.
- [13] J. F. Bedi and J. M. Cooper. Take off in the long jump – Angular momentum considerations. *Journal of Biomechanics*, 10(9):541–548, 1977. doi: 10.1016/0021-9290(77)90034-3.

- [14] I. N. Bezodis, D. G. Kerwin, and A. I. T. Salo. Lower-Limb Mechanics during the Support Phase of Maximum-Velocity Sprint Running. *Medicine and Science in Sports and Exercise*, 40(4):707–715, 2008. doi: 10.1249/MSS.0b013e318162d162.
- [15] H. G. Bock and K. J. Plitt. A multiple shooting algorithm for direct solution of optimal control problems. *IFAC Proceedings Volumes*, 17(2):1603–1608, 1984. doi: 10.1016/S1474-6670(17)61205-9.
- [16] G. Bouchouras, D. Moscha, G. Papaiakevou, T. Nikodelis, and I. Kollias. Angular momentum and landing efficiency in the long jump. *European Journal of Sport Science*, 9(1):53–59, 2009. doi: 10.1080/17461390802594243.
- [17] M. Bragaru, R. Dekker, J. H. B. Geertzen, and P. U. Dijkstra. Amputees and sports. *Sports Medicine*, 41(9):721–740, 2011. doi: 10.2165/11590420-000000000-00000.
- [18] G.-P. Brüggemann, A. Arampatzis, F. Emrich, and W. Potthast. Biomechanics of double transtibial amputee sprinting using dedicated sprinting prostheses. *Sports Technology*, 1(4–5):220–227, 2008. doi: 10.1002/jst.63.
- [19] B. Burkett, M. McNamee, and W. Potthast. Shifting boundaries in sports technology and disability: equal rights or unfair advantage in the case of oscar pistoriu? *Disability and Society*, 26(5):643–654, 2011. doi: 10.1080/09687599.2011.589197.
- [20] J. Campos, J. Gàmez, A. Encarnación, M. Gutiérrez-Dávila, J. Rojas, and E. S. Wallace. Three-Dimensional Kinematics during the Take-Off Phase in Competitive Long Jumping. *International Journal of Sports Science & Coaching*, 8(2):395–406, 2013. doi: 10.1260/1747-9541.8.2.395.
- [21] J. W. Chow and J. G. Hay. Computer Simulation of the Last Support Phase of the Long Jump. *Medicine and Science in Sports and Exercise*, 37(1):115–123, 2005. doi: 10.1249/01.MSS.0000150086.13664.32.
- [22] K. P. Clark, L. J. Ryan, and P. G. Weyand. A general relationship links gait mechanics and running ground reaction forces. *Journal of Experimental Biology*, 220(2):247–258, 2017. doi: 10.1242/jeb.138057.
- [23] D. Clever and K. Mombaur. An Inverse Optimal Control Approach for the Transfer of Human Walking Motions in Constrained Environment to Humanoid Robots. In *Proceedings of Robotics: Science and Systems*, 2016. doi: 10.15607/RSS.2016.XII.005.
- [24] D. Clever, Y. Hu, and K. Mombaur. Humanoid gait generation in complex environments based on template models and optimality principles learned from human beings. *The International Journal of Robotics Research*, 37(10):1184–1204, 2018. doi: 10.1177/0278364918765620.
- [25] I. P. Committee. International Paralympic Committee: IPC Policy on Sport Equipment. [https://www.paralympic.org/sites/default/files/document/120203164107739\\_Sec\\_ii\\_Chapter\\_3.10\\_IPC\\_Sport\\_Equipment\\_Policy.pdf](https://www.paralympic.org/sites/default/files/document/120203164107739_Sec_ii_Chapter_3.10_IPC_Sport_Equipment_Policy.pdf), April 2011. Last accessed: 2021-06-28.
- [26] P. de Leva. Adjustments to Zatsiorsky-Seluyanov’s segment inertia parameters. *Journal of Biomechanics*, 29(9):1223–1230, 1996. doi: 0021-9290(95)00178-6.

- [27] S. Debaere, I. Jonkers, and C. Delecluse. The Contribution of Step Characteristics to Sprint Running Performance in High-Level Male and Female Athletes. *J. Strength Cond. Res.*, 27(1):116–124, 2013. doi: 10.1519/JSC.0b013e31825183ef.
- [28] S. L. Delp, F. C. Anderson, A. S. Arnold, P. Loan, A. Habib, C. T. John, E. Guendelman, and D. G. Thelen. OpenSim: Open-Source Software to Create and Analyze Dynamic Simulations of Movement. *IEEE Transactions on Biomedical Engineering*, 54(11):1940–1950, 2007. doi: 10.1109/TBME.2007.901024.
- [29] W. Demtröder. *Experimentalphysik 1*. Springer-Lehrbuch. Springer Spektrum, Berlin ; [Heidelberg], 8 edition, 2018. doi: 10.1007/978-3-662-54847-9.
- [30] P. Dolan, A. F. Mannion, and M. A. Adams. Passive tissues help the back muscles to generate extensor moments during lifting. *Journal of Biomechanics*, 27(8):1077–1085, 1994. doi: 10.1016/0021-9290(94)90224-0.
- [31] A. L. Emonds and K. Mombaur. Inverse Optimal Control Based Enhancement of Sprinting Motion Analysis with and without Running-Specific Prostheses. In *2018 7th IEEE International Conference on Biomedical Robotics and Biomechatronics*, pages 556–562, 2018. doi: 10.1109/BIOROB.2018.8488779.
- [32] A. L. Emonds and K. Mombaur. Optimality Studies of Human Sprinting Motions with and Without Running-Specific Prostheses. *International Journal of Humanoid Robotics*, 16(03):1940003, 2019. doi: 10.1142/S0219843619400036.
- [33] A. L. Emonds and K. Mombaur. Asymmetry in Three-Dimensional Sprinting with and without Running-Specific Prostheses. *Symmetry*, 13(4):580, 2021. doi: 10.3390/sym13040580.
- [34] A. L. Emonds and K. Mombaur. Using Subject-Specific Models to Find Differences in Underlying Optimization Criteria of Sprinting with and without Prostheses. In *2020 IEEE-RAS International Conference on Humanoid Robots*, pages 283–290, 2021.
- [35] A. L. Emonds, J. Funken, W. Potthast, and K. Mombaur. Comparison of sprinting with and without running-specific prostheses using optimal control techniques. *Robotica*, 37(12):2176–2194, 2019. doi: 10.1017/S0263574719000936.
- [36] C. T. Farley and O. González. Leg stiffness and stride frequency in human running. *Journal of Biomechanics*, 29(2):181–186, 1996. doi: 10.1016/0021-9290(95)00029-1.
- [37] R. Featherstone. *Rigid Body Dynamics Algorithms*. Springer US, Berlin, Heidelberg, 2008. doi: 10.1007/978-1-4899-7560-7.
- [38] M. L. Felis. *Modeling Emotional Aspects in Human Locomotion*. Phd thesis, Heidelberg University, 2015. URL <http://katalog.ub.uni-heidelberg.de/titel/67881412>.
- [39] M. L. Felis. RBDL: an efficient rigid-body dynamics library using recursive algorithms. *Autonomous Robots*, 41(2):495–511, 2017. doi: 10.1007/s10514-016-9574-0.
- [40] M. L. Felis and K. Mombaur. Synthesis of full-body 3-d human gait using optimal control methods. In *2016 IEEE International Conference on Robotics and Automation*, pages 1560–1566, 2016. doi: 10.1109/ICRA.2016.7487294.

- [41] M. L. Felis, K. Mombaur, and A. Berthoz. An optimal control approach to reconstruct human gait dynamics from kinematic data. In *2015 IEEE-RAS 15th International Conference on Humanoid Robotics*, pages 1044–1051, 2015. doi: 10.1109/HUMANOIDS.2015.7363490.
- [42] J. Funken. The biomechanics of the long jump with a below the knee prosthesis : recent insights. *Japanese journal of biomechanics in sports & exercise*, 23(3):145–150, 2019.
- [43] J. Funken, K. Heinrich, S. Willwacher, R. Müller, and W. Potthast. Amputation side and site determine the performance capacity in paralympic curve sprinting. In *Proceedings of the 34th International Conference on Biomechanics in Sports*, volume 34, pages 589–592, 2016.
- [44] J. Funken, S. Willwacher, K. Heinrich, R. Müller, H. Hobara, A. M. Grabowski, and W. Potthast. Long jumpers with and without a transtibial amputation have different three-dimensional centre of mass and joint take-off step kinematics. *Royal Society Open Science*, 6(4):190107, 2019. doi: 10.1098/rsos.190107.
- [45] J. Funken, S. Willwacher, K. Heinrich, R. Müller, H. Hobara, A. M. Grabowski, and W. Potthast. Three-Dimensional Takeoff Step Kinetics of Long Jumpers with and without a Transtibial Amputation. *Medicine and Science in Sports and Exercise*, 51(4):716–725, 2019. doi: 10.1249/MSS.0000000000001853.
- [46] H. Geyer, A. Seyfarth, and R. Blickhan. Compliant leg behaviour explains basic dynamics of walking and running. *Proceedings of the Royal Society B: Biological Sciences*, 273(1603):2861–2867, 2006. doi: 10.1098/rspb.2006.3637.
- [47] P. E. Gill, W. Murray, and M. H. Wright. *Practical optimization*. Academic Press, London [u.a.], 1981.
- [48] P. E. Gill, W. Murray, and M. A. Saunders. User’s guide for QPOPT 1.0: A Fortran package for Quadratic programming. Technical report, 1995.
- [49] A. M. Gordon, A. F. Huxley, and F. J. Julian. The variation in isometric tension with sarcomere length in vertebrate muscle fibres. *The Journal of Physiology*, 184(1):170–192, 1966. doi: 10.1113/jphysiol.1966.sp007909.
- [50] A. M. Grabowski, C. P. McGowan, W. J. McDermott, M. T. Beale, R. Kram, and H. M. Herr. Running-specific prostheses limit ground-force during sprinting. *Biology Letters*, 6(2):201–204, 2010. doi: 10.1098/rsbl.2009.0729.
- [51] M. Günther, V. A. Sholukha, D. Kessler, V. Wank, and R. Blickhan. Dealing with skin motion and wobbling masses in inverse dynamics. *Journal of Mechanics in Medicine and Biology*, 3(3–4):309–335, 2003. doi: 10.1142/S0219519403000831.
- [52] K. Hatz, J. Schlöder, and H.-G. Bock. Estimating Parameters in Optimal Control Problems. *SIAM Journal on Scientific Computing*, 34(3):A1707–A1728, 2012. doi: 10.1137/110823390.
- [53] J. G. Hay. The Biomechanics of the Long Jump. *Exercise and Sport Sciences Reviews*, 14: 401–416, 1986.
- [54] J. G. Hay. Approach strategies in the long jump. *Journal of Applied Biomechanics*, 4(2): 114–129, 1988. doi: 10.1123/ijbs.4.2.114.

- [55] J. G. Hay. Citius, altius, longius (faster, higher, longer): The biomechanics of jumping for distance. *Journal of Biomechanics*, 26(Suppl 1):7–21, 1993.
- [56] J. G. Hay and H. Nohara. Techniques used by elite long jumpers in preparation for takeoff. *Journal of Biomechanics*, 23(3):229 – 239, 1990. doi: 10.1016/0021-9290(90)90014-T.
- [57] W. Herzog. Maintenance of body orientation in the flight phase of long jumping. *Medicine & Science in Sports & Exercise*, 18(2):231–241, 1986.
- [58] A. V. Hill. The Heat of Shortening and the Dynamic Constants of Muscle. *Proceedings of the Royal Society B: Biological Sciences*, 126(843):136–195, 1938. doi: 10.1098/rspb.1938.0050.
- [59] R. N. Hinrichs. Upper Extremity Function in Running. II: Angular Momentum Considerations. *International Journal of Sport Biomechanics*, 3(3):242–263, 1987. doi: 10.1123/ijsb.3.3.242.
- [60] R. N. Hinrichs, B. A. Munkasy, and S. A. Chinworth. Analysis of angular momentum during the run-up and takeoff in long jumping. *Journal of Biomechanics*, 22(10):1023, 1989. doi: 10.1016/0021-9290(89)90278-9.
- [61] H. Hobara. Running-specific prostheses: The history, mechanics, and controversy. *Journal of the Society of Biomechanisms*, 38(2):105–110, 2014. doi: 10.3951/sobim.38.105.
- [62] H. Hobara, B. S. Baum, H.-J. Kwon, R. H. Miller, T. Ogata, Y. H. Kim, and J. K. Shim. Amputee locomotion: Spring-like leg behavior and stiffness regulation using running-specific prostheses. *Journal of Biomechanics*, 46(14):2483–2489, 2013. doi: 10.1016/j.jbiomech.2013.07.009.
- [63] H. Hobara, Y. Kobayashi, and M. Mochimaru. Spatiotemporal Variables of Able-bodied and Amputee Sprint in Men’s 100-m Sprint. *International Journal of Sports Medicine*, 36(6):494–497, 2015. doi: 10.1055/s-0034-1387794.
- [64] A. F. Huxley. Muscle structure and theories of contraction. *Progress in Biophysics and Biophysical Chemistry*, 7:255–318, 1957. doi: 10.1016/S0096-4174(18)30128-8.
- [65] M. I. Jackson. *The mechanics of the Table Contact Phase of Gymnastics Vaulting*. PhD thesis, Loughborough University, 2010.
- [66] S. G. Johnson. The NLOpt nonlinear-optimization package. 2015. URL <http://ab-initio.mit.edu/nlopt>.
- [67] B. B. Kentel, M. A. King, and S. R. Mitchell. Evaluation of a subject-specific torque-driven computer simulation model of one-handed tennis backhand ground strokes. *Journal of Applied Biomechanics*, 27(4):345–354, 2011. doi: 10.1123/jab.27.4.345.
- [68] A. L. Kleesattel, D. Clever, J. Funken, W. Potthast, and K. Mombaur. Modeling and Optimal Control of Able-Bodied and Unilateral Amputee Running. In *Proceedings of the 35th International Conference on Biomechanics in Sports*, volume 35, pages 164–167, 2017.
- [69] A. L. Kleesattel, W. Potthast, and K. Mombaur. Towards a Better Understanding of Human Sprinting Motions With and Without Prostheses. In *2017 IEEE-RAS International Conference on Humanoid Robots*, pages 158–164, 2017. doi: 10.1109/HUMANOIDS.2017.8239551.

- [70] J. Koschorreck and K. Mombaur. Modeling and optimal control of human platform diving with somersaults and twists. *Optim. Eng.*, 13(1):29–56, 2012. doi: 10.1007/s11081-011-9169-8.
- [71] R. Kram, A. M. Grabowski, C. P. McGowan, M. B. Brown, and H. M. Herr. Counterpoint: Artificial legs do not make artificially fast running speeds possible. *Journal of Applied Physiology*, 108(4):1012–1014, 2010. doi: 10.1152/jappphysiol.01238.2009a.
- [72] M. Krzysztow and A. Mero. A Kinematic Analysis Of Three Best 100 M Performances Ever. *Journal of Human Kinetics*, 36(1):149–160, 2013. doi: 10.2478/hukin-2013-0015.
- [73] F. Kugler and L. Janshen. Body position determines propulsive forces in accelerated running. *Journal of Biomechanics*, 43(2):343–348, 2010. doi: 10.1016/j.jbiomech.2009.07.041.
- [74] D. N. Lee, J. R. Lishman, and J. A. Thomson. Regulation of gait in long jumping. *Journal of Experimental Psychology: Human Perception and Performance*, 8(3):448, 1982. doi: 10.1037/0096-1523.8.3.448.
- [75] A. Lees, N. Fowler, and D. Derby. A biomechanical analysis of the last stride, touch-down and take-off characteristics of the women’s long jump. *Journal of Sports Sciences*, 11(4):303–314, 1993. doi: 10.1080/02640419308730000.
- [76] A. Lees, P. Graham-Smith, and N. Fowler. A Biomechanical Analysis of the Last Stride, Touchdown, and Takeoff Characteristics of the Men’s Long Jump. *Journal of Applied Biomechanics*, 10(1):61 – 78, 1994. doi: 10.1080/02640419308730000.
- [77] D. B. Leineweber, I. Bauer, H. G. Bock, and J. P. Schlöder. An efficient multiple shooting based reduced SQP strategy for large-scale dynamic process optimization (Parts 1 and 2). *Computers and Chemical Engineering*, 27(2):157–174, 2003. doi: 10.1016/S0098-1354(02)00158-8. doi: 10.1016/S0098-1354(02)00195-3.
- [78] Y.-C. Lin and M. G. Pandy. Three-dimensional data-tracking dynamic optimization simulations of human locomotion generated by direct collocation. *Journal of Biomechanics*, 59:1–8, 2017. doi: 10.1016/j.jbiomech.2017.04.038.
- [79] N. P. Linthorne. Biomechanics of the long jump. In Y. Hong and R. Bartlett, editors, *Routledge Handbook of Biomechanics and Human Movement Science*, pages 340–353. Taylor & Francis, 2008.
- [80] N. P. Linthorne, M. S. Guyman, and L. A. Bridgett. Optimum take-off angle in the long jump. *Journal of Sports Sciences*, 23(7):703–712, 2005. doi: 10.1080/02640410400022011.
- [81] J. Longman. An amputee sprinter: Is he disabled or too-abled? *The New York Times*, 2007. URL <https://www.nytimes.com/2007/05/15/sports/othersports/15runner.html>. Published online: 2007-05-15, last accessed: 2021-06-17.
- [82] J. Mainprice, R. Hayne, and D. Berenson. Predicting human reaching motion in collaborative tasks using Inverse Optimal Control and iterative re-planning. In *2015 IEEE International Conference on Robotics and Automation*, pages 885–892, 2015. doi: 10.1109/ICRA.2015.7139282.

- [83] A. S. Majumdar and R. A. Robergs. The Science of Speed: Determinants of Performance in the 100 m Sprint. *International Journal of Sport Science & Coaching*, 6(3):479–493, 2011. doi: 10.1260/1747-9541.6.3.479.
- [84] E. Marey. *Animal Mechanism: A Treatise on Terrestrial and Aerial Locomotion*. Henry S. King & Co., London, 1874.
- [85] G. Marinou, M. Millard, N. Šarabon, and K. Mombaur. Comparing the risk of low-back injury using model-based optimization: Improved technique versus exoskeleton assistance. *Wearable Technologies*, 2:e13, 2021. doi: 10.1017/wtc.2021.12.
- [86] C. P. McGowan, A. M. Grabowski, W. J. McDermott, H. M. Herr, and R. Kram. Leg stiffness of sprinters using running-specific prostheses. *Journal of The Royal Society Interface*, 9(73):1975–1982, 2012. doi: 10.1098/rsif.2011.0877.
- [87] A. Menache. *Understanding Motion Capture for Computer Animation*. Elsevier, Amsterdam, 2nd edition, 2011.
- [88] A. A. Mero, P. V. Komi, and R. J. Gregor. Biomechanics of Sprint Running: A Review. *Sports Medicine*, 13(6):376–392, 1992. doi: 10.2165/00007256-199213060-00002.
- [89] P. Merriault, Y. Dupuis, R. Boutteau, P. Vasseur, and X. Savatier. A Study of Vicon System Positioning Performance. *Sensors*, 17(7):1591, 2017. doi: 10.3390/s17071591.
- [90] M. Millard and K. Mombaur. A quick turn of foot: Rigid foot-ground contact models for human motion prediction. *Frontiers in Neurorobotics*, 13, 2019. doi: 10.3389/fnbot.2019.00062.
- [91] M. Millard, A. L. Emonds, M. Harant, and K. Mombaur. A reduced muscle model and planar musculoskeletal model fit for the simulation of whole-body movements. *Journal of Biomechanics*, 89:11–20, 2019. doi: 10.1016/j.jbiomech.2019.04.004.
- [92] R. H. Miller, B. R. Umberger, J. Hamill, and G. E. Caldwell. Evaluation of the minimum energy hypothesis and other potential optimality criteria for human running. *Proceedings of the Royal Society B: Biological Sciences*, 279(1733):1498–1505, 2011. doi: 10.1098/rspb.2011.2015.
- [93] R. H. Miller, B. R. Umberger, and G. E. Caldwell. Limitations to maximum sprinting speed imposed by muscle mechanical properties. *Journal of Biomechanics*, 45(6):1092–1097, 2012. doi: 10.1016/j.jbiomech.2011.04.040.
- [94] K. Mombaur. A Mathematical Study of Sprinting on Artificial Legs. In H. G. Bock, X. Hoang, R. Rannacher, and J. Schlöder, editors, *Modeling, Simulation and Optimization of Complex Processes - HPSC 2012*, pages 157–168. Springer, Cham, 2014. doi: 10.1007/978-3-319-09063-4\_13.
- [95] K. Mombaur. Optimization as guiding principle of locomotion. In M. Sharbafi and A. Seyfarth, editors, *Bioinspired Legged Locomotion: Models, Concepts, Control & Applications*, pages 164–195. Elsevier, 2017. doi: 10.1016/B978-0-12-803766-9.00006-3.
- [96] K. Mombaur, A. Truong, and J.-P. Laumond. From human to humanoid locomotion – an inverse optimal control approach. *Auton. Robots*, 28(3):369–383, 2010. doi: 10.1007/s10514-009-9170-7.

- [97] K. Mombaur, A. H. Olivier, and A. Crétual. Forward and inverse optimal control of bipedal running. In K. Mombaur and K. Berns, editors, *Modeling, Simulation and Optimization of Bipedal Walking*, volume 18 of *Cognitive Systems Monographs*, pages 165–179. Springer, Berlin, Heidelberg, 2013. doi: 10.1007/978-3-642-36368-9\_13.
- [98] J. B. Morin, P. Samozino, K. Zameziati, and A. Belli. Effects of altered stride frequency and contact time on leg-spring behavior in human running. *Journal of Biomechanics*, 40(15):3341–3348, 2007. doi: 10.1016/j.jbiomech.2007.05.001.
- [99] Y. Muraki, M. Ae, H. Koyama, and T. Yokozawa. Joint torque and power of the takeoff leg in the long jump. *International Journal of Sport and Health Science*, 6:21–32, 2008. doi: 10.5432/ijshs.6.21.
- [100] E. Muybridge. *Animal locomotion*. J. B. Lippincott Company, Philadelphia, 1874.
- [101] E. Nixdorf and G.-P. Brüggemann. Biomechanical analysis of the long jump. In G.-P. Brüggemann and B. Glad, editors, *Scientific Research Project at the Games of the XXIVth Olympiad — Seoul 1988 Final Report*. International Athletic Foundation, Monaco, 1990.
- [102] J. Nocedal and S. Wright. *Numerical Optimization*. Springer Science and Business Media, Berlin Heidelberg, 2nd edition, 2006.
- [103] L. Nolan. Carbon fibre prostheses and running in amputees: A review. *Foot and Ankle Surgery*, 14(3):125–129, 2008. doi: 10.1016/j.fas.2008.05.007.
- [104] L. Nolan and A. Lees. Touch-down and take-off characteristics of the long jump performance of world level above- and below-knee amputee athletes. *Ergonomics*, 43(10):1637–1650, 2000. doi: 10.1080/001401300750004050.
- [105] L. Nolan and A. Lees. Prosthetic limb versus intact limb take-off in the amputee long jump. In *Proceedings of the 23rd International Symposium on Biomechanics in Sports*, volume 23, pages 305–308, 2005.
- [106] L. Nolan, B. L. Patrilli, and K. J. Simpson. A Biomechanical Analysis of the Long-Jump Technique of Elite Female Amputee Athletes. *Medicine and Science in Sports and Exercise*, 38(10):1829–1835, 2006. doi: 10.1080/02640410600717931.
- [107] L. Nolan, B. L. Patrilli, and K. J. Simpson. Effect of take-off from prosthetic versus intact limb on transtibial amputee long jump technique. *Prosthetics and Orthotics International*, 36(3):297–305, 2012. doi: 10.1177/0309364612448877.
- [108] K. M. Norton. A brief history of prosthetics. *Motion Magazine*, 17(7), 2007.
- [109] T. Park and S. Levine. Inverse optimal control for humanoid locomotion. In *Robotics: Science and systems – Workshop on inverse optimal control and robotic learning from demonstration*, 2013.
- [110] M. J. D. Powell. A Direct Search Optimization Method That Models the Objective and Constraint Functions by Linear Interpolation. In S. Gomez and J. P. Hennart, editors, *Advances in Optimization and Numerical Analysis*, Mathematics and Its Applications, pages 51–67. Springer, Dordrecht, 1994. doi: 10.1007/978-94-015-8330-5\_4.
- [111] G. Rabita, S. Dorel, J. Slawinski, E. Sàez-de-Villarreal, A. Couturier, P. Samozino, and J.-B. Morin. Sprint mechanics in world-class athletes: a new insight into the limits of human locomotion. *Scandinavian Journal of Medicine and Science in Sports*, 25(5):583–594, 2015. doi: 10.1111/sms.12389.

- [112] M. R. Ramey. Significance of angular momentum in long jumping. *Research Quarterly. American Association for Health, Physical Education and Recreation*, 44(4):488–497, 1973. doi: 10.1080/10671188.1973.10615229.
- [113] M. R. Ramey. The use of angular momentum in the study of long-jump take-offs. In *Biomechanics IV*, pages 144–148. Springer, 1974. doi: 10.1007/978-1-349-02612-8\_20.
- [114] U. Raschke and D. B. Chaffin. Support for a linear length-tension relation of the torso extensor muscles: an investigation of the length and velocity emg-force relationships. *Journal of Biomechanics*, 29(12):1597–1604, 1996. doi: 10.1016/S0021-9290(96)80011-X.
- [115] R. Riener. The Cybathlon promotes the development of assistive technology for people with physical disabilities. *Journal of NeuroEngineering and Rehabilitation*, 13:49, 2016. doi: 10.1186/s12984-016-0157-2.
- [116] A. I. T. Salo, I. N. Bezodis, A. M. Batterham, and D. G. Kerwin. Elite Sprinting: Are Athletes Individually Step-Frequency or Step-Length Reliant? *Medicine and Science in Sports and Exercise*, 43(6):1055–1062, 2011. doi: 10.1249/MSS.0b013e318201f6f8.
- [117] S. Sandhu, M. Millard, J. McPhee, and D. Brekke. 3d dynamic modelling and simulation of a golf drive. *Procedia Engineering*, 2(2):3243–3248, 2010. doi: 10.1016/j.proeng.2010.04.139.
- [118] A. G. Schache, P. D. Blanch, T. W. Dorn, N. A. T. Brown, D. Rosemond, and M. G. Pandy. Effect of Running Speed on Lower Limb Joint Kinetics. *Medicine and Science in Sports and Exercise*, 43(7):1260–1271, 2011. doi: 10.1249/MSS.0b013e3182084929.
- [119] A. G. Schache, T. W. Dorn, P. D. Blanch, N. A. T. Brown, and M. G. Pandy. Mechanics of the Human Hamstring Muscles during Sprinting. *Medicine and Science in Sports and Exercise*, 44(4):647–658, 2012. doi: 10.1249/MSS.0b013e318236a3d2.
- [120] M.-S. Scholz, J. P. Blanchfield, L. D. Bloom, B. H. Coburn, M. Elkington, J. D. Fuller, M. E. Gilbert, S. A. Muflahi, M. F. Pernice, S. I. Rae, J. A. Trevarthen, S. C. White, P. M. Weaver, and I. P. Bond. The use of composite materials in modern orthopaedic medicine and prosthetic devices: A review. *Composites Science and Technology*, 71(16):1791–1803, 2011. doi: 10.1016/j.compscitech.2011.08.017.
- [121] G. Schultz and K. Mombaur. Modeling and Optimal Control of Human-Like Running. *IEEE/ASME Transactions on Mechatronics*, 15(5):783–792, 2010. doi: 10.1109/TMECH.2009.2035112.
- [122] A. Seyfarth, A. Friedrichs, V. Wank, and R. Blickhan. Dynamics of the long jump. *Journal of Biomechanics*, 32(12):1259–1267, 1999. doi: 10.1016/S0021-9290(99)00137-2.
- [123] Y. Shimizu and M. Ae. Three-dimensional analysis of the takeoff motion in the long jump. In *Proceedings of the 31st International Conference on Biomechanics in Sports*, volume 31, 2013.
- [124] S. Stafilidis and A. Arampatzis. Track compliance does not affect sprinting performance. *Journal of Sports Sciences*, 25(13):1479–1490, 2007. doi: 10.1080/02640410601150462.

- [125] G. Strutzenberger, A. Brazil, H. von Lieres und Wilkau, J. D. Davies, J. Funken, R. Müller, T. Exell, C. Willson, S. Willwacher, W. Potthast, H. Schwameder, and G. Irwin. 1st and 2nd step characteristics preceding the sprint start in amputee sprinting. In *Proceedings of the 34th International Conference on Biomechanics in Sports*, volume 34, 2016.
- [126] T. Sugihara. Solvability-Unconcerned Inverse Kinematics by the Levenberg–Marquardt Method. *IEEE Transactions on Robotics*, 27(5):984–991, 2011. doi: 10.1109/TRO.2011.2148230.
- [127] P. Taboga, A. M. Grabowski, P. E. di Prampero, and R. Kram. Optimal Starting Block Configuration in Sprint Running: A Comparison of Biological and Prosthetic Legs. *Journal of Applied Biomechanics*, 30(3):381–389, 2014. doi: 10.1123/jab.2013-0113.
- [128] E. van der Kruk and M. M. Reijne. Accuracy of human motion capture systems for sport applications; state-of-the-art review. *European Journal of Sport Science*, 18(6):806–819, 2018. doi: 10.1080/17461391.2018.1463397.
- [129] A. J. K. van Soest, L. J. R. Casius, and K. K. Lemaire. Huxley-type cross-bridge models in largeish-scale musculoskeletal models; an evaluation of computational cost. *Journal of Biomechanics*, 83:43–48, 2019. doi: 10.1016/j.jbiomech.2018.11.021.
- [130] V. Wank and V. Keppler. Vor- und Nachteile von Sportlern mit Hochleistungsprothesen im Vergleich zu nichtbehinderten Athleten. *Deutsche Zeitschrift für Sportmedizin*, 66(11):287–293, 2015. doi: 10.5960/dzsm.2015.204.
- [131] P. G. Weyand and M. W. Bundle. Point: Artificial limbs do make artificially fast running speeds possible. *Journal of Applied Physiology*, 108(4):1011–1012, 2010. doi: 10.1152/japphysiol.01238.2009.
- [132] P. G. Weyand, D. B. Sternlight, M. J. Bellizzi, and S. Wright. Faster top running speeds are achieved with greater ground forces not more rapid leg movements. *Journal of Applied Physiology*, 89(5):1991–1999, 2000. doi: 10.1152/jappl.2000.89.5.1991.
- [133] P. G. Weyand, M. W. Bundle, C. P. McGowan, A. Grabowski, M. B. Brown, R. Kram, and H. Herr. The fastest runner on artificial legs: different limbs, similar function? *Journal of Applied Physiology*, 107(3):903–911, 2009. doi: 10.1152/japphysiol.00174.2009.
- [134] S. Willwacher, V. Herrmann, K. Heinrich, J. Funken, G. Strutzenberger, J.-P. Goldmann, B. Braunstein, A. Brazil, G. Irwin, W. Potthast, and G.-P. Brüggemann. Sprint Start Kinetics of Amputee and Non-Amputee Sprinters. *PLOS ONE*, 11(11):e0166219, 2016. doi: 10.1371/journal.pone.0166219.
- [135] S. Willwacher, J. Funken, K. Heinrich, T. Alt, R. Müller, and W. Potthast. Free moment application by athletes with and without amputations in linear and curved sprinting. In *Proceedings of the 35th International Conference on Biomechanics in Sports*, volume 35, pages 847–850, 2017.
- [136] S. Willwacher, J. Funken, K. Heinrich, R. Müller, H. Hobara, A. M. Grabowski, G.-P. Brüggemann, and W. Potthast. Elite long jumpers with below the knee prostheses approach the board slower, but take-off more effectively than non-amputee athletes. *Scientific Reports*, 7(1):16058, 2017. doi: 10.1038/s41598-017-16383-5.
- [137] J. M. Winters. Hill-based muscle models: a system engineering perspective. In J. M. Winters and S. L.-Y. Woo, editors, *Multiple Muscle Systems*, pages 69–93. Springer Verlag, 1990.

- [138] A. Wächter and L. T. Biegler. On the implementation of an interior-point filter line-search algorithm for large-scale nonlinear programming. *Mathematical Programming*, 106(1):25–57, 2006. doi: 10.1007/s10107-004-0559-y.
- [139] D. C. Young. *A brief history of the Olympic games*. Blackwell, 2004.
- [140] F. E. Zajac. Muscle and Tendon: properties, models, scaling, and application to biomechanics and motor control. *CRC Critical Reviews in Biomedical Engineering*, 19(4):359–411, 1989.

# List of Figures

I	Schematic overview of the structure of this thesis . . . . .	5
<b>1</b>	<b>Overview on Analyzing Motions with and without Running-Specific Prostheses</b>	<b>13</b>
1.1	Sketch of the setup for the sprinting and long jump motion capture experiments	13
<b>2</b>	<b>Modeling of Human Motions with and without Below the Knee Amputation</b>	<b>16</b>
2.1	Anatomical planes and axes as defined for this thesis . . . . .	16
2.2	Rigid multi-body system models of amputee and non-amputee athletes . . . . .	16
2.3	Model of the running-specific prosthesis consisting of three rigid segments . . .	18
<b>4</b>	<b>Biomechanics and Modeling of Sprinting Motions with and without Running-Specific Prostheses</b>	<b>34</b>
4.1	Phase description of the sprinting model . . . . .	34
<b>5</b>	<b>Dynamics Reconstruction of Sprinting Motions with and without Running-Specific Prostheses</b>	<b>37</b>
5.1	Animated sequences of the reconstructed sprinting movements . . . . .	37
5.2	Ground reaction forces of the reconstructed two-dimensional and three-dimensional sprinting motions . . . . .	39
5.3	Sagittal plane joint torques of the amputee athlete and the non-amputee reference group for the reconstructed sprinting motions . . . . .	41
5.4	Frontal and transversal plane joint torques of the amputee athlete and the non-amputee reference group for the reconstructed sprinting motions . . . . .	42
5.5	Amount of asymmetry in the generalized positions between the two steps of the amputee athlete and the non-amputee reference group . . . . .	44
5.6	Amount of asymmetry in the joint torques between the two steps of the amputee athlete and the non-amputee reference group . . . . .	45
5.7	Ground reaction forces, center of mass positions and velocities of the amputee athlete and the non-amputee reference group for the reconstructed sprinting motions . . . . .	47
5.8	Sagittal plane generalized positions of the amputee athlete and the non-amputee reference group for the reconstructed sprinting motions . . . . .	48
5.9	Sagittal plane angular momentum about center of mass of the amputee athlete and the non-amputee reference group for the reconstructed sprinting motions	50
5.10	Frontal and transversal plane generalized positions of the amputee athlete and the non-amputee reference group for the reconstructed sprinting motions . . .	52
5.11	Angular momentum about center of mass of the amputee athlete and the non-amputee reference group for the reconstructed sprinting motions . . . . .	54
<b>6</b>	<b>Synthesis of Sprinting Motions with and without Running-Specific Prostheses</b>	<b>62</b>
6.1	Visualization of the friction cone condition . . . . .	62
6.2	Animated sequences of some exemplary optimized sprinting motions for the amputee and the non-amputee athletes . . . . .	66

6.3	Similarity measures computed for the solutions of the sprinting motion synthesis optimal control problems with fixed and free average velocity . . . . .	67
6.4	Overall position and leg joint angles of the non-amputee and amputee athletes for eight synthesized motions with free average velocity . . . . .	71
6.5	Leg joint torques of the non-amputee and amputee athletes for eight synthesized motions with free average velocity . . . . .	72
6.6	Ground reaction forces of the non-amputee and amputee athletes for eight synthesized motions with free average velocity . . . . .	73
<b>7</b>	<b>Inverse Optimal Control of Sprinting Motions with and without Running-Specific Prostheses</b>	<b>79</b>
7.1	Similarity measures comparing the best weight inverse optimal control problem solutions with the solutions by hand-picked combinations of weights for three non-amputee athletes and one amputee athlete . . . . .	79
7.2	Animated sequences of the best weight inverse optimal control problem solutions and the reference motions . . . . .	80
7.3	Generalized positions of the best weight inverse optimal control problem solutions and the reconstructed reference motions for the non-amputee reference group and the amputee athlete . . . . .	85
7.4	Joint torques of the best weight inverse optimal control problem solutions and the reconstructed reference motions for the non-amputee reference group and the amputee athlete . . . . .	86
<b>8</b>	<b>Biomechanics and Modeling of Long Jump Motions with and without Running-Specific Prostheses</b>	<b>93</b>
8.1	Phase description of the long jump model . . . . .	93
<b>9</b>	<b>Dynamics Reconstruction of Long Jump Motions with and without Running-Specific Prostheses</b>	<b>96</b>
9.1	Ground reaction forces of the amputee and the non-amputee athlete for the reconstructed three-dimensional long jump motions . . . . .	96
9.2	Stance leg joint torques of the non-amputee and the amputee athlete during the last contact phase of the reconstructed three-dimensional long jump motions. . . . .	98
9.3	Animated sequences of the reconstructed long jump movements . . . . .	99
9.4	Ground reaction forces of the amputee and the non-amputee athlete for the reconstructed long jump motions . . . . .	101
9.5	Center of mass motion of the amputee and the non-amputee athlete for the reconstructed long jump motions . . . . .	104
9.6	Generalized positions of the amputee and the non-amputee athlete for the reconstructed long jump motions . . . . .	107
9.7	Joint torques of the amputee and the non-amputee athlete for the reconstructed long jump motions . . . . .	108
9.8	Angular momenta with respect to the center of mass of the amputee and the non-amputee athlete for the reconstructed long jump motions . . . . .	110
<b>10</b>	<b>Synthesis of Long Jump Motions with and without Running-Specific Prostheses</b>	<b>115</b>
10.1	Animated sequences visualize the solutions of the long jump motion synthesis optimal control problem . . . . .	115
10.2	Ground reaction forces of the amputee athlete and the non-amputee athlete for the synthesized long jump motions . . . . .	117

10.3	Center of mass motion of the amputee athlete and the non-amputee athlete for the synthesized long jump . . . . .	118
10.4	Contact leg joint angles and torques of the amputee athlete and the non-amputee athlete for the last three contact phases of the synthesized long jump . . . . .	119
<b>11</b>	<b>Comparison of the Amputee Athlete to Himself without Amputation: The Idea of a Simulator Tool</b>	<b>130</b>
11.1	Basic structure of the simulator tool . . . . .	130
11.2	Animated sequences visualize the solutions of the sprinting motion synthesis optimal control problem for the comparison of the amputee athlete to himself without amputation in the simulator tool . . . . .	134
11.3	Positions, joint angles and phase durations of the synthesized sprinting motions for the non-amputee and amputee model versions . . . . .	135
11.4	Joint torques and ground reaction forces of the synthesized sprinting motions for the non-amputee and amputee model versions . . . . .	136
11.5	Animated sequences visualize the solutions of the long jump motion synthesis optimal control problem for the comparison of the amputee athlete to himself without amputation in the simulator tool . . . . .	138
<b>A</b>	<b>Additional Figures</b>	<b>149</b>
A.1	Root-mean-square errors between the solutions of the dynamics reconstruction and the reference motions for the individual joints of the 2D models in sprinting	149
A.2	Root-mean-square errors between the solutions of the dynamics reconstruction and the reference motions for the individual joints of the 3D models in sprinting	150
A.3	Two-dimensional generalized positions of the dynamics reconstruction and the reference motions of sprinting . . . . .	151
A.4	Three-dimensional generalized positions of the dynamics reconstruction and the reference motions of sprinting . . . . .	153
A.5	Animated sequences of optimized sprinting motions for the amputee and the non-amputee athletes . . . . .	157
A.6	Root-mean-square errors between the reference data and the best weight inverse optimal control problem solutions of the four athletes for the individual joints in sprinting . . . . .	159
A.7	Root-mean-square errors between the solution of the dynamics reconstruction and the reference motion for the individual joints in long jump . . . . .	160
A.8	Three-dimensional generalized positions of the dynamics reconstruction and the reference motions of long jump . . . . .	161
A.9	Comparison of the forces during the third-last and second-last steps of the long jump reconstruction and the two steps of the sprint reconstruction . . . . .	163
A.10	Comparison of the joint torques during the third-last and second-last steps of the long jump reconstruction and the two steps of the sprint reconstruction . . . . .	164
A.11	Joint torques of the non-amputee and the amputee athlete for the synthesized long jump motions . . . . .	165
A.12	Generalized positions of the non-amputee and the amputee athlete for the synthesized long jump motions . . . . .	166
A.13	Center of mass and ground reaction forces curves of the long jump motion for the comparison of the amputee and non-amputee model versions . . . . .	167
A.14	Leg joint angles and joint torques during the contact phases of the long jump motion (Simulator tool) . . . . .	168

# List of Tables

<b>1</b>	<b>Overview on Analyzing Motions with and without Running-Specific Prostheses</b>	<b>12</b>
1.1	Anthropometric data of the athletes with and without below the knee amputation as used in this work . . . . .	12
<b>2</b>	<b>Modeling of Human Motions with and without Below the Knee Amputation</b>	<b>17</b>
2.1	Degrees of freedom for the different models established in this work . . . . .	17
<b>5</b>	<b>Dynamics Reconstruction of Sprinting Motions with and without Running-Specific Prostheses</b>	<b>38</b>
5.1	Rotational and translational root-mean-square errors between reconstructed and reference motions for the reconstructed sprinting motions . . . . .	38
5.2	Phase durations of the modeled phases for the amputee athlete and the non-amputee reference group for the reconstructed sprinting motions . . . . .	43
5.3	Measures of sprinting with and without running-specific prosthesis applied to the results of the sprinting dynamics reconstruction . . . . .	57
<b>6</b>	<b>Synthesis of Sprinting Motions with and without Running-Specific Prostheses</b>	<b>65</b>
6.1	Weight factors for the formulation of objective functions for sprinting from basic optimization criteria . . . . .	65
6.2	Average velocities of the solutions of the different sprinting motion synthesis optimal control problems . . . . .	70
<b>7</b>	<b>Inverse Optimal Control of Sprinting Motions with and without Running-Specific Prostheses</b>	<b>81</b>
7.1	Scaling factors, initial and optimal weight factors for the base optimization criteria of the inverse optimal control problem . . . . .	81
7.2	Asymmetry values computed for the individual joints of the best weight solutions for the three non-amputee athletes and the amputee athlete . . . . .	83
7.3	Comparison of the reference data and the best weight inverse optimal control problem solution for the four athletes regarding selected criteria . . . . .	84
<b>9</b>	<b>Dynamics Reconstruction of Long Jump Motions with and without Running-Specific Prostheses</b>	<b>95</b>
9.1	Rotational and translational root-mean-square errors between reconstructed and reference motions for the reconstructed long jump . . . . .	95
9.2	Phase durations of the modeled phases for the amputee and the non-amputee athlete for the reconstructed long jump . . . . .	100
9.3	Measures related to the ground reaction forces for the reconstructed long jump	102
9.4	Measures related to the center of mass motion for the reconstructed long jump	105
9.5	Measures related to energy efficiency for the reconstructed long jump . . . . .	109
<b>10</b>	<b>Synthesis of Long Jump Motions with and without Running-Specific Prostheses</b>	<b>116</b>
10.1	Phase durations of the amputee and the non-amputee athlete for the synthesized long jump . . . . .	116

10.2 Measures related to the center of mass motion for the synthesized long jump .	123
10.3 Measures related to the ground reaction forces for the synthesized long jump .	124
<b>11 Comparison of the Amputee Athlete to Himself without Amputation: The Idea of a Simulator Tool</b>	<b>139</b>
11.1 Characteristic quantities for the comparison of the amputee athlete to himself without amputation for the long jump motions in the simulator tool . . . . .	139

## List of Acronyms

<b>BKA</b>	below the knee amputation
<b>BFGS</b>	Broyden-Fletcher-Goldfarb-Shenno
<b>CFRP</b>	carbon fiber reinforced polymer
<b>CoM</b>	center of mass
<b>DAE</b>	differential algebraic equation
<b>DOF</b>	degree of freedom
<b>GUI</b>	graphical user interface
<b>IOCP</b>	inverse optimal control problem
<b>IPC</b>	International Paralympic Committee
<b>KKT</b>	KARUSH-KUHN-TUCKER
<b>MTG</b>	Muscle Torque Generator
<b>NLP</b>	non-linear programming problem
<b>OCP</b>	optimal control problem
<b>ODE</b>	ordinary differential equation
<b>OSP</b>	Optimalsteuerungsproblem
<b>QP</b>	quadratic programming problem
<b>RMSE</b>	root-mean-square error
<b>RSP</b>	running-specific prosthesis
<b>SQP</b>	Sequential Quadratic Programming